A Study of Amidoamines as Inhibitors For Mild Steel Corrosion in Saline Media Saturated with Carbon Dioxide

BY

M. Wadah Saleh Jawich

A Thesis Presented to the

DEANSHIP OF GRADUATE STUDIES

KING FAHD UNIVERSITY OF PETROLEUM & MINERALS

DHAHRAN, SAUDI ARABIA

In Partial Fulfillment of the
Requirements for the Degree of

MASTER OF SCIENCE

In

CHEMISTRY

MAY 2011

KING FAHD UNIVERSITY OF PETROLEUM & MINERALS

DHAHRAN, SAUDI ARABIA

DEANSHIP OF GRADUATE STUDIES

This thesis, written by M. Wadah Saleh Jawich under the direction of his thesis advisor and approved by his thesis committee, has been presented to and accepted by the Dean of Graduate Studies, in partial fulfilment of the requirements for the degree of MASTER OF SCIENCE in Chemistry.

Thesis Committee

G. A. Oweimreen

Thesis Advisor
Dr. Ghassan Owiemreen

Sk. Asrof Ali

Co-advisor/Member
Dr. Sheik Asrof Ali

Member
Dr. Abdullah Abu Al-Kibash

Department Chairman
Dr. Abdullah J. Al-Hamdan

Member
Dr. Mohammad Wazeer

Dean of Graduate Studies
Dr. Salam A. Zummo

18/7/2011

Date

Member
Dr. Abdel-Nasser Kawde

DEDICATION

To The Holy Person Who Taught Me

Determination, Patience and Constancy

Prophet Muhammad (PBUH)

And To My Parent

Family

And Friends

ACKNOWLEDGMENT

Acknowledgment is due to the King Fahd University of Petroleum & Minerals for supporting this research. I wish to express my appreciation to

I am heartily thankful to my supervisors, Dr. Ghassan Oweimreen and Dr. Sheik Asrof Ali, whose encouragement, guidance and support from the initial to the final level enabled me to develop an understanding of the subject.

I also wish to thank the other members of my thesis committee: Dr. Abdullah Abu Al-Kibash , Dr. Mohammad Wazeer and Dr. Abdel-Nasser Kawde .

I am indebted to my family and many of my colleagues to support me during this work, and I also wish to give special thanks to all the KFUPM staff for providing their best effort to me.

There are many other people to thank, all of whom are important and again thank them all for their support.

TABLE OF CONTENTS

LIST OF TABELS

LIST OF FIGURES

مخلص الرسالة

الاسم: **محمد وضاح صالح جاويش**

عنوان الرسالة : دراسة أمين الاميدات كمضادات لتآكل الفولاذ في محلول ملحي مشبع بغاز ثنائي اكسيد الكربون.

التخصص: **الكيمياء**

تاريخ التخرج: **أيار – مايو 2011**

تعتبر كلفة التآكل الداخلي للانابيب من أهم الامور في صناعة النفط والغاز لأن أغلب مرافقها عرضة للتآكل الناجم عن تماسها مع الماء، والذي يزداد بوجود ثنائي اكسيد الكربون وكبريتيد الهيدروجين مع الغاز المرافق. ينفق جزء كبير من كلفة التآكل على شراء مضادات التآكل. مضادات التآكل الشائعة والتي تعتمد على تشكيل غشاء رقيق هي إما من الايميدازولينات او من أمينات الاميد والتي تصنع منها الايميدازولينات.

في هذه الرسالة تم تصنيع تسعة من امينات الاميد وثلاثة مركبات ايميدازولينية عبر تفاعل متعددات الامين مع الحموض الدسمة والنتريلات ذات سلاسل كربونية باطوال مختلفة. تم التأكد من بنية هذه المركبات عبر مطيافية الرنين المغناطيسي للهيدروجيني ^{1}H والكربوني ^{13}C ومطيافية الاشعة تحت الحمراء. وتم تحديد قدرتها على منع التآكل عبر تقنية مقاومة الاستقطاب الخطية و مخططات استقطاب تافل. تميزت مركبات الايميدازولين بممانعة تآكل أعلى من مقابلاتها الامينو اميدية. كما أن قيمة انثالبية الامتزاز بينت ان الامتزاز فيزيائي ، وهذا يفسر بكون املاح كربونات الايميدازولين ضعيفة التأين وان الامتزاز يترافق مع استبدال جزيئات الايميدازولين بجزيئات الماء وغاز ثنائي اكسيد الكربون الممتزة على سطح المعدن. دراسة التوتر السطحي لمحاليل المركبات بينت ان بينة المركبات تلعب دورا في تشكل الميسيلات وفي ذوبانيتها وبالتالي في امتزازها وفي كفائتها كممانعات تآكل.

THESIS ABSTRACT

NAME OF STUDENT: M. WADAH SALEH JAWICH

TITLE OF STUDY: A Study of Amidoamines as Inhibitors For Mild Steel Corrosion in Saline Media Saturated with Carbon Dioxide

MAJOR FIELD: CHEMISTRY

DATE OF DEGREE: MAY 2011

The internal corrosion of pipelines is a major cost for the oil and gas industry, because most of the production facilities are subject to corrosion by water, which is enhanced by the presence of CO_2 and H_2S in the gas phase. A large portion of the cost for internal pipelines corrosion is for corrosion inhibitors. The commonly used film-forming corrosion inhibitors are imidazolines and their amidoamines precursors.

In this thesis, nine different amidoamines and three of their corresponding imidazolines were successfully synthesized by the reaction of polyamines with fatty acids or fatty nitriles of different chain lengths. The structures of these compounds were confirmed by their NMR and IR spectra. The corrosion inhibition efficiencies of the inhibitors were determined by polarization resistance and Tafel plots. The imidazolines showed very good inhibition as compared to their corresponding amidoamine precursors. The value of the enthalpy of adsorption, ΔH_{ads}, suggests that the adsorption of the imidazolines is of the physisorption type. This was attributed to the weak counter anion CO_3^{2-} and the nature of the adsorption process which involves the desorption of CO_2 and water molecules from the metal surface. Surface tension studies showed that the structure of the inhibitor affects its solubility and micellization, which in turn affects its adsorption and inhibition efficiency.

CHAPTER 1

INTRODUCTION

1.1. CORROSION AND CORROSION COST

Corrosion is defined as the destruction or deterioration of a material because of its reaction with its environment [1]. It is mostly referred to the process that damages a metal due to a chemical reaction with its environment [2]. Air, water and soil and their slat constituents are the environments that corrode metals.

In 2003 [3], Saudi Aramco initiated a study to define the cost of corrosion throughout core operations with the objective of focusing on plant engineering, and research investment in corrosion control to the areas that had the largest economic impact on corporate performance. For Saudi Aramco's five domestic refineries, 36% of the maintenance budget was allocated to corrosion. For gas sweetening plants, it was found that 25% of the maintenance budget was committed to corrosion control. For gas fractionation plants, 17% of the maintenance budget was due to corrosion.

For production operations onshore, corrosion was responsible for 28% of maintenance costs, while on offshore facilities, corrosion accounts for 60% to 70% of maintenance costs. Specific sectors of onshore oil operations, notably those handling seawater injections, report that approximately 60% of their maintenance budget is due to

corrosion. Onshore and offshore operational costs attributed to corrosion are about the same, in the region of 21%.

Production in Saudi Arabia is different from most other operating areas of the world in that the generally very low associated water content results in some of the lowest corrosion control costs in the industry. Due to the dynamic nature of crude oil production in the gas and oil separation plants, these costs will increase as oil fields age. Corrosion in oil and gas production varies from location to location. Corrosion can be classified into three general categories: Internal corrosion caused by the produced fluids and gases, external corrosion caused by exposure to groundwater or seawater, and atmospheric corrosion caused by salt spray and weathering offshore. Of these, internal corrosion is the most costly since internal mitigation methods cannot be easily maintained and inspected.

In 2002, the American federal highway administration (FHWA) released a study [4] on the direct costs associated with metallic corrosion in nearly every American industry sector. According to this study, downhole tubing, surface pipelines, pressure vessels, and storage tanks in oil and gas production are subject to internal corrosion by water, which is enhanced by the presence of CO_2 and H_2S in the gas phase. Internal corrosion control is the major cost item. The total annual cost of corrosion in the oil and gas production industry is estimated to be $1.372 billion, broken down into $589 million in surface pipeline and facility costs, $463 million annually in downhole tubing expenses, and another $320 million in capital expenditures related to corrosion.

A large portion of the costs for internal pipelines is for corrosion inhibitors. Optimization of inhibitor use could be accomplished through the use of more advanced inhibitor treatment schemes, such as active monitoring systems connected to inhibitor pumps to increase or decrease dosage as the corrosivity increases or decreases. Even passive systems could be developed that couple inspection and monitoring data with treatment schemes more accurately. The total consumption of corrosion inhibitors in the United States has doubled from approximately $600 million in 1982 to nearly $1.1 billion in 1998 [4].

Carbon dioxide corrosion in the oilfield is called *Sweet Corrosion*, while hydrogen sulfide corrosion is often called *Sour Corrosion*. Carbon dioxide corrosion is characterized by the presence of smooth edged pits that are closely grouped. Unlike homogeneous corrosion, pipeline failures caused by pitting corrosion are not associated with the removal of large amount of metal, and thus the time required to develop a failure is shorter, which justifies the attention localized corrosion has received in the last three decades.

Many strategies have been investigated to minimize the cost of localized corrosion, such as corrosion resistant alloys (CRA), coatings, non-metallic pipelines, ceramics and rubber lining of reactors and vessels used for the industry. However, the use of chemical corrosion inhibitors is the most cost-effective method.

1.2. FORMS OF CORROSION IN OILFIELD SYSTEMS

The process of corrosion manifests itself in differing forms of attack and metallurgical examination may reveal the specific form of attack on an individual specimen. This can be helpful for identifying better strategies for corrosion control [5].

1. General corrosion is the uniform thinning of a surface by corrosion. When general corrosion occurs, the anodic and cathodic areas are able to change which causes all areas to be evenly corroded.

2. Localized Corrosion is a term that is used to describe all non-uniform corrosion. Pitting may occur as a consequence of a non-homogeneous surface becoming exposed under layers of foreign matter or at breaks in surface coatings.

3. Stress corrosion cracking (SSC) where dissolved sulfide causes a corrosion cell to develop, which produces FeS and hydrogen that penetrates the metal, creating high internal pressures at metal imperfections.

4. Galvanic corrosion is the result of immersing dissimilar metals in electrolytes. At the junction of the two metals there will be a flow of electrons, which leads to electrochemical pitting.

5. Erosion corrosion is attack accelerated by high fluid velocity that can either physically remove protective films or mechanically disturb the surface itself.

1.3. CURRENT STATUS OF THE RESEARCH

1.3.1. SYNTHESIS OF AMIDOAMINES AND IMIDAZOLINES

There are two types of organic corrosion inhibitors that are used in the oilfield industry: Neutralizing corrosion inhibitors and film forming corrosion inhibitors.

Neutralizing corrosion inhibitors work in pipelines by reacting with corrosive gases in the fluid stream. Consequently, there is no need to maintain a constant concentration all along the line in a closed transportation system like that of an oil pipeline. However, their use in the oil and gas pipes is limited to refineries because of their high consumption and consequently their cost if used in the oil and gas production facilities.

Film forming corrosion inhibitors retard the corrosion reaction by adsorbing on the inner surface of the pipeline and reducing the surface area vulnerable to corrosion. They can be oil soluble, oil soluble/water dispersible, water soluble /oil dispersible or water soluble based on the water to oil ratio in the stream. In high oil/water systems they should be dispersible in the water phase to attain a constant concentration that is high enough to form and maintain a tenacious film all along the pipeline. When the water ratio increases these inhibitors are designed to be more water soluble. The dispersiblility / solubility of the inhibitor should increase proportionately with the water percentage in the fluid stream.

This can be achieved by the selection or design of an inhibitor molecule that exhibits both the proper surface activity and the necessary water solubility.

In the wet crude production facilities, the film formed by the inhibitors consists partially of the oil itself. The ability of the corrosion inhibitor to emulsify a part of the oil and transfer it to the metal surface in contact with the associated water enhances its performance because the oil decreases the water wettability of the surface and thus retards the corrosion reaction.

Two of the commonly used film-forming corrosion inhibitors are amidoamines and imidazolines. Fatty amidoamines and imidazolines film forming inhibitors are industrially synthesized by the reaction of fatty acids and polyamines (H_2N-C_2H_4-(NH-C_2H_4)$_n$-NH_2). The reaction gives amidoamines at temperatures not exceeding 160 ^oC and depending on the fatty acid and the polyamine used lower temperatures may be used. For fatty acids with shorter alkyl chain lengths in the range C_8-C_{12} reaction temperatures as low as 120 ^oC were reported [6]. Prolonged heating of amidoamines under vacuum removes a water molecule and initiates the ring closure reaction which results in the formation of the imidazoline ring (Scheme 1.1). The cheapest source of fatty acids is a by-product from the paper industry called tall oil fatty acid (TOFA) which is a mixture of saturated and unsaturated fatty acids with chain lengths in the range C_{12}-C_{22}. The chain-length distribution of TOFA depends on the source of the raw materials used in the paper industry.

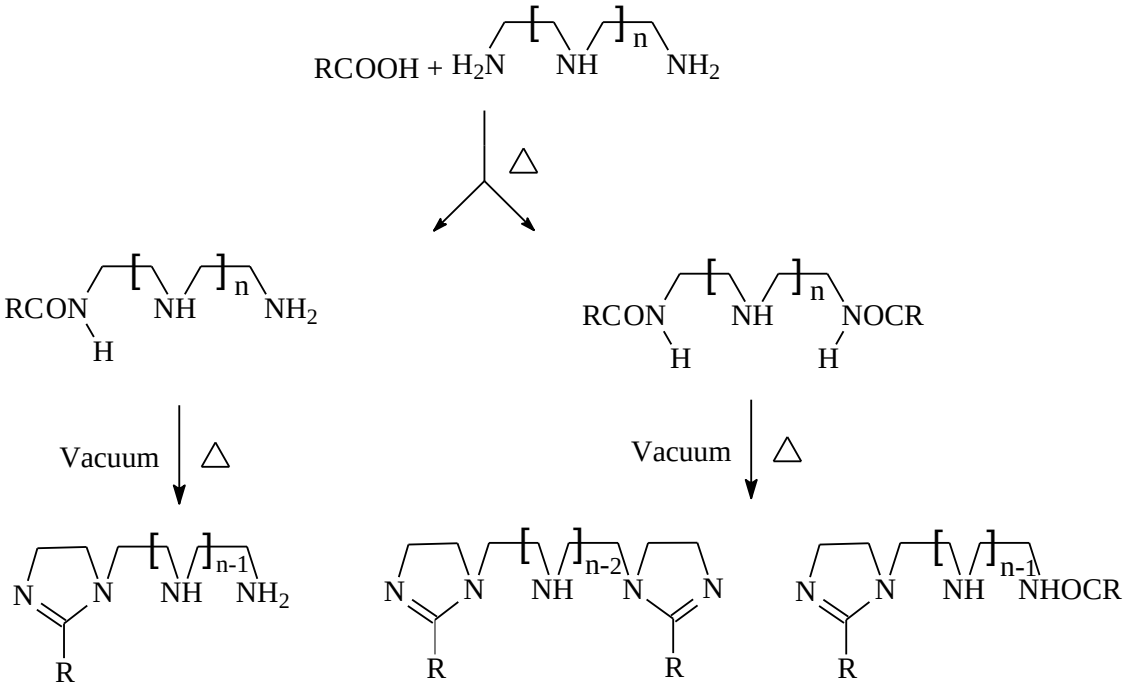

Scheme 1.1

Linfield and co-workers [7] prepared imidazoline by the addition of diethylene triamine DETA to stearic acid at 90 ^{o}C where the reaction mixture turned into a gel as a result of amine soap formation. This was overcome by warming above 125 ^{o}C. Heating at 150 ^{o}C was continued for 6 h. At this stage formation of diamidoamine takes place. Heating was continued at 150 ^{o}C for 2 h under 0.3 mm Hg. In this step cyclization of diamidoamine takes place by removal of one water molecule and imidazoline is formed.

Linfield and coworkers [7] also studied the reaction rate of fatty acid and DETA (reaction Scheme 1.2). A series of fatty acid: DETA reactions were carried out at 125 ^{o}C, 150 ^{o}C, 175 ^{o}C and 200 ^{o}C and the distillates were collected for analysis.

Result showed that excessive amounts of DETA co-distilled with the water formed from the reaction at 175 ^{o}C and 200 ^{o}C, only small amounts of DETA were found in the distillate from the 150 ^{o}C reaction. It was concluded that 150 ^{o}C was the optimum temperature for the reaction.

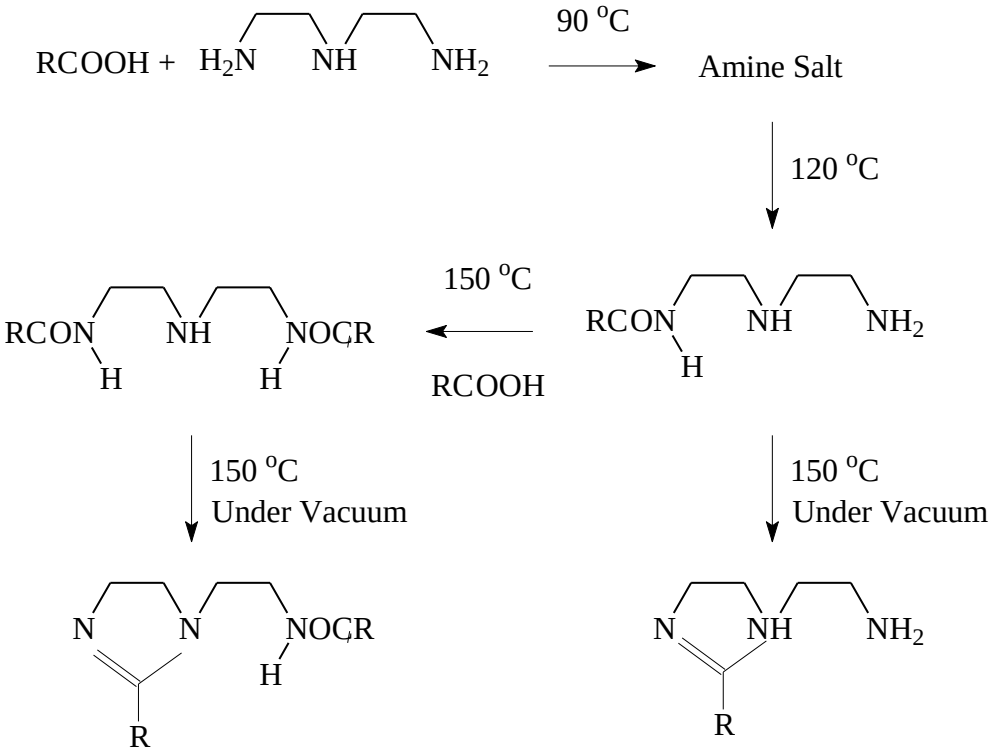

Scheme 1.2

The reaction was conducted at 150 ^{o}C under atmospheric pressure, using 2 mol tallow fatty acids and 1 mol DETA. Initially and at 2 h intervals, samples were withdrawn for analysis of free fatty acid, primary, secondary, and tertiary amine. Within the first 2 h period, the amount of available fatty acid decreased to 1/3 of the original value. This

indicated that DETA and the fatty acid do not react in a 1: 1 molar ratio. However, during the same period, the meq/gr of secondary amine dropped to an insignificant amount, whereas only a 1/3 reduction was detected for primary amine. This indicated clearly that in a non-aqueous system the secondary amino group was more reactive than the primary one as has been reported in aqueous systems. After the reaction had proceeded for 6 h at 150^{o}C, the free fatty acid content was less than 5%and the meq/g of primary amine reached a constant value roughly equivalent to one free amino group. Thus, the structure of the intermediate is RCON($CH_2CH_2NH_2$) CH_2CH_2NHCOR

The reaction of DETA with tallow and methyl tallowate [7] were similarly investigated which gave amidoamines and the cyclization to the imidazoline was completed after heating 2 h at 150^{O}C under 0.2 mm Hg pressure in a 9.2% yield. Imidazoline are also prepared by the reaction of triglycerides or fatty acids with DETA. Earl G.W. *et al*.[8] prepared imidazoline by the reaction of triglycerides with DETA. In the same manner, the diamidoamine formed in the first step is subjected to elevated temperature and vacuum resulting in loss of molecule of water to get imidazoline molecule. Warner and co-workers [9] also prepared imidazoline based on the reaction of fatty acid with DITA. Hofmann first prepared the 2-alkyl 2-imidazoline the homologous series from the fatty acid and ethylene diamine. Butler and coworkers [10] described the synthesis of long chain dialkyldiamido imidazolines by the reaction of diethylenetriamine and several fatty acids under non-solvent microwave irradiation using calcium oxide as support. Amine salt formation was observed, which were dehydrated at 130^{o}C to a

diamide fatty acid complex and finally at 180^{o}C. The continued heating of the liberated diamide, identified as $(C_{17}H_{35}CONHCH_2CH_2)_2NH$, for 48 h at 240-260^{o}C yielded imidazoline. Yue *et al* [11] prepared an imidazoline cationic surfactant from oleic acid. Welley *et al*[12] used stearic acid as fatty material and hydroxy diethylene amine to make hydroxy imidazoline. Bajpai *et al* [13] synthesized imidazolines by the reaction of fatty acids and diethylenetriamine under non-solvent microwave irradiation using calcium oxide as a support. Baltork *et al* [14] synthesized imidazolines under non-solvent microwave irradiation using elemental sulfur as a catalyst.

1.3.2. CORROSION INHIBITION OF AMIDOAMINES AND IMIDAZOLINES

Most of the fatty saturated amidoamines and imidazolines are solids, while the unsaturated fatty imidazoline are either solids or liquids with high melting points. They have a yellow to brown color with a characteristic smell. Their solubility in water depends on the substituent types, the monoamidoamine and the amino or hydroxy imidazolines C_{8-14} are easily water soluble, while compounds with higher chain length are less soluble, the ones with very long hydrocarbon chain are only soluble in non-polar solvents. Amidoamines are very stable thermally, while imidazolines can undergo hydrolysis giving the corresponding amidoamines. Their corrosion inhibition efficiency is still a matter of discussion. Jovanicevic *et al* [15] have found that alkyl imidazolines are less efficient corrosion inhibitors than their alkylamidic precursors.

Recently, the alkyl imidazolines were found to be more efficient than their alkylamidic precursors [16]. Martin *et al* [17] studied several amides and imidazolines and found that imidazoline compounds rapidly convert into their amide precursor, and expected that the performance of imidazoline or its amidoamine precursor would be similar. Desimone *et al* [18] found that amidoamines made from oleic acid and DETA exhibited high corrosion inhibition efficiency as a mixed-type inhibitor with a predominant influence on the anodic process. The organic inhibitor acts by blocking surface sites at low concentrations and by modifying the adsorption mechanism forming a protective barrier against corrosive ions at high concentrations.

Butler *et al*. [10] reported a high conversion rate (upto80%) from imidazoline to amide within a period of 2–9 days under atmospheric conditions because of the low stability of the imidazoline cycle. Jovancicevic *et al*. [15] studied the effect of hydrolysis of imidazoline on corrosion inhibition by using the Linear Polarization Resistance (LPR) method with the Rotating Cylinder Electrode (RCE) assembly in CO_2 containing brines. They found that the hydrolysis of saturated straight chain imidazolines plays an important role in their inhibition. Thus, under those test conditions, stearic imidazoline hydrolyzes fairly rapidly to a product equivalent in performance to stearic amide.

Duda *et al* [20] synthesized amidoamines and imidazolines using fatty acids of different chain length and studied their efficiency as corrosion inhibitors, and tried to suggest a simple model for the relationship of their structure to their efficiency. They

found that the 1-(2-alkylaminoethyl)-2-alkylimidazolines are better corrosion inhibitors than their amidic derivatives ; therefore, the inhibition efficiency is highly modulated by the electronic factors present in the molecular structure. For compounds of type 1-(2-alkylaminoethyl)-2-alkylimidazolines, at 25 ppm or lower concentration values, the hydrocarbon tail length and hence the partition coefficient are the main variables that control the inhibition efficiency. Based on the molecular modeling and experimental evidence, it was established that imidazolines, which possess an iminic nitrogen atom, form stronger coordination bonds with the surface, instead of the weaker bonds present with the amidic precursors, which gives it better corrosion inhibition properties.

Nowadays, there is no conclusive answer about the stability (hydrolysis) of imidazolines and imidazoline formulated products and the activity of the hydrolyzed products. The hydrolysis of imidazoline-based corrosion inhibitors is considered negligible under most conditions, but the presence of significant amounts of water and high temperatures can hydrolyze them to form their amide precursor. There are controversial results in literature about the performance of imidazoline and amide based products.

It is expected that changing the chain length of the alkyl tails ($R=C_{12}$-C_{18}), the length of the of the polyamine (n = 2 - 4) and the molar ratio of the fatty acid to polyamine will change the surface active properties of the resulting inhibitor, such as the critical micelle concentration (CMC), emulsification, the partitioning factor and the wetting

ability which determine its adsorption behavior. Usually the molar ratio of the fatty acid to polyamine is 2:1 for oil soluble inhibitors and a portion of the fatty acid is replaced by glacial acetic acid to make the inhibitor oil soluble/ water dispersible. The higher the water content in the fluid passing through the pipeline is, the higher is the percentage of glacial acetic acid needed. Since we will study an aqueous system, only water soluble or water dispersible inhibitor will be used. The magnitude and sign of the effect of the length of the aliphatic chain on the efficiency of the inhibitor depends on the percentage of water in the pipeline fluid. If the water content is high then adsorption is the main factor in inhibition, while if the water content is less than a certain value, the wetting process will play a role in minimizing the corrosion by introducing more oil molecules to the surface, thus the higher the wettability caused by the inhibitor is, the higher is its efficiency. However, if an emulsion is formed by the inhibitor, it will consume a considerable portion of the inhibitor and the efficiency will decrease, which gives an impression that the effectiveness of the inhibitor decreased. A proper design of the inhibitor, which requires a proper selection of the TOFA oil, is needed to guarantee the highest efficiency of the inhibitor.

The dispersiblility in water of the different amidoamines prepared by the reaction of a polyamine with a fatty acid will be determined by measuring the change in surface tension with concentration. Only inhibitors that are soluble or dispersible in water will be considered for corrosion inhibition studies.

The values of the surface tension of aqueous solutions at 40 °C of each of the selected inhibitors at different concentrations were determined using du Nouy ring method. For each inhibitor, the surface tension decreased as the inhibitor concentration increased until the CMC is approached, where a bend is observed, beyond which the interfacial tension is practically independent of concentration. Usually the actual critical micelle concentration is taken at the point where extrapolations of these two regions of the curve intersect. The influence of both the hydrocarbon chain length and the length of the polyamine on the CMC value will be discussed. The relevance of the CMC value on the inhibitor performance lies in two possible opposing effects. When an inhibitor reaches it critical micelle concentration, it emulsifies some of the oil and introduces it to the metal surface, which enhances the surface coverage, in turn the inhibition efficiency. On the other hand, micellization reduces the concentration of single molecules of the inhibitor and in turn decreases inhibition efficiency which depends on surface coverage by single molecules [15].

The inhibition efficiencies of the dispersible amidoamine inhibitors (within a matrix of fatty acids and polyamines of different chain lengths) will be studied at room temperature and a one atmosphere CO_2 pressure. These are the conditions at which corrosion is usually encountered. A screening test for the inhibitor efficiency against its concentration in the water phase will be conducted, and only the inhibitors that have a considerable stable efficiency will be included in the study.

Adsorption is a spontaneous process thus ΔG_{ads} is negative. Usually ΔS_{ads} is negative because the translational freedom of the adsorbate is reduced upon adsorption. Therefore for ΔG_{ads} (= $\Delta H_{ads} - T\ \Delta S_{ads}$) to be negative ΔH_{ads} must be negative, i.e., the adsorption is usually exothermic, whether the adsorption is of the chemisorptions type or the physisorption type. Because chemisorption involves forces comparable to bond energies while physisorption involves forces of the van der Waals type the magnitude of ΔH_{ads} is larger in the former type of adsorption. In rare cases where dissociation occurs upon adsorption, entropy increases as a result of dissociation. If in addition the decrease in translational energy upon adsorption is too small to counterbalance this increase in entropy, because the moieties formed move freely on the surface of adsorbent, then ΔS_{ads} is positive, $-T\ \Delta S_{ads}$ is negative and ΔH_{ads} may be positive [19]. The entropy change ΔS_{ads} indicates whether the overall system becomes more structured (ΔS_{ads} negative) or more random (ΔS_{ads} positive). It is expected that these parameters will change as the chemical structure of the inhibitor and the temperature of the solution in which it is dissolved changes. An attempt was made to relate the thermodynamic parameters of adsorption of an inhibitor to its chemical structure and its inhibition efficiency as well as the experiment parameters.

1.4. BRIEF DESCRIPTIONS OF THE CONTENTS OF SUCCEEDING CHAPTERS

Chapter 2 reviews the literature on CO_2 corrosion mechanism, the effects of environmental factors on the rate and mechanism of this corrosion, the methods used for

monitoring CO_2 corrosion in the lab and in the field and the corrosion inhibitors used to protect mild steel against pitting corrosion. The chapter also covers the mechanism of inhibition and the behavior of organic corrosion inhibitors as a surface active agents and their adsorption on metal surfaces.

Chapter 3 describes the methods used to synthesize amidoamines and imidazolines. Also, the electrochemical methods for analyzing CO_2 corrosion are described and the inhibition efficiency is discussed. Finally the methods to study the surface activity of the inhibitors and their adsorption isotherms are considered.

Chapter 4 presents and discusses the results obtained from this research. This includes the analysis of the FTIR and NMR spectra of the synthesized molecules, and the corrosion inhibition efficiencies of these molecules obtained using Linear Polarization Resistance (LPR) and Tafel Plots. Chapter 4 also summarizes the conclusions and recommendations for the use of amidoamines and imidazolines as CO_2 corrosion inhibitors. Finally directions for future research are recommended.

1.5. OBJECTIVES OF THE STUDY

Following are the objectives of the proposed study:

A. Synthesis of several amidoamines and diamidoamines (Scheme 1.3).

B. Synthesis of several imidazolines and diimidazolines (Scheme 1.4).

C. Measurements of inhibition efficiency of the abovementioned inhibitors (in various concentrations) against mild steel corrosion in brine solution saturated with CO_2 at several temperatures by electrochemical methods.

D. Measurements of surface tension of some of the synthesized inhibitors.

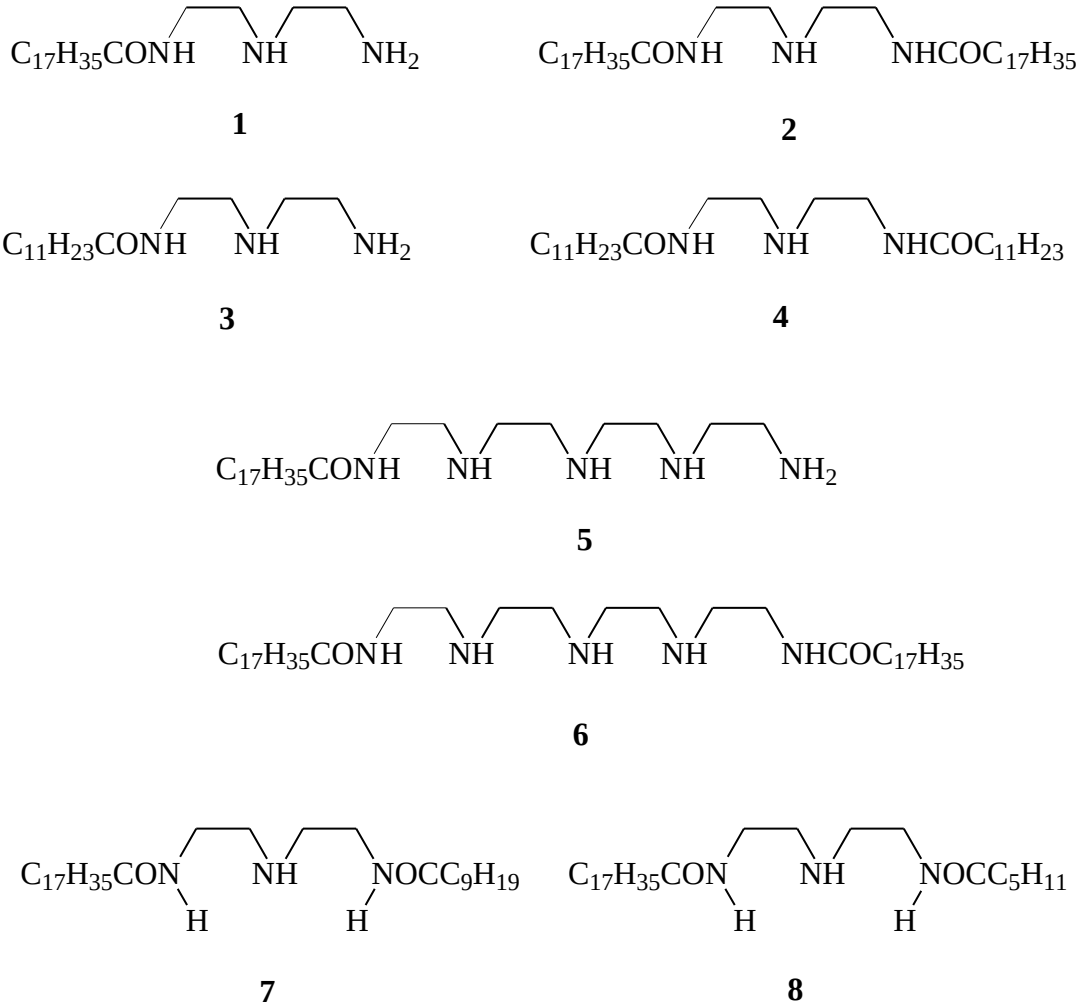

Scheme 1.3

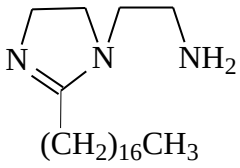

9

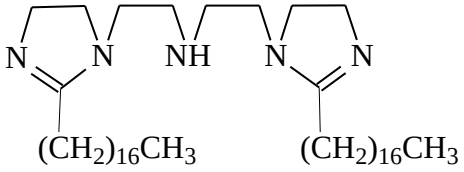

10

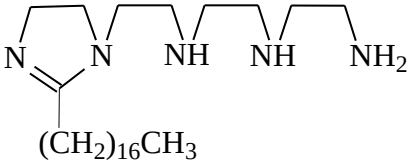

11

Scheme 1.4

CHAPTER 2

LITERATURE REVIEW

2.1. CARBON DIOXIDE CORROSION

Carbon dioxide corrosion in the oilfield is called *Sweet Corrosion*. Carbon dioxide causes corrosion for two reasons. Firstly, the dissolved carbon dioxide lowers the pH of water and this increases the corrosion rate. However, when the gas flows from an upstream high pressure pipelines to a low pressure downstream, the pH of the water increases due to the evolution of CO_2. Secondly, Carbon dioxide dissolves in water to form H_2CO_3 which reacts directly with iron to form Iron (II) carbonate. The overall reaction is:

$$H_2CO_3\,(aq) + Fe\,(s) \rightleftharpoons FeCO_3\,(s) + H_2\,(g) \qquad (2.1)$$

Iron (II) carbonate is soluble in water at low temperatures, however, at high temperature it might form a protective layer that minimizes the speed of the reaction, or might dissolve at lower pH leaving the pipeline surface beneath it vulnerable to further attack by the dissolved CO_2. Carbon dioxide corrosion is characterized by the presence of smooth edged pits that are closely grouped.

It is widely known that solutions containing H_2CO_3 are more corrosive to mild steel than solutions of strong acids, such as hydrochloric acid (HCl) or sulfuric acid (H_2SO_4), at the same pH. This was a topic of debate and speculation in the past few decades. De Waard and Milliams [21] suggested that this is due to the reduction of the undissociated H_2CO_3 molecule, which occurs after it is adsorbed onto the metal surface. According to them, this is the dominant and rate-determining step in the CO_2 corrosion process, so the corrosion rate of the mild steel surface is directly related to the concentration of the undissociated H_2CO_3 in solution and to the CO_2 partial pressure. However, there are two possible cathodic reactions that can occur in the process of mild steel CO_2 corrosion: the above-mentioned "direct" reduction of H_2CO_3 but also reduction of hydrogen ions:

$$2H_2CO_3 + e^- \rightleftharpoons H_2 + 2HCO_3^- \qquad (2.2)$$

$$2H^+ + 2e^- \rightleftharpoons H_2\,(g) \qquad (2.3)$$

While the rate of the former process is determined by the amount of CO_2 in the system, the rate of the latter process is strongly pH-dependent. The electrons required to keep the process going are provided by a single anodic reaction; iron dissolution:

$$Fe\,(s) \rightleftharpoons Fe^{2+} + 2e^- \qquad (2.4)$$

Whether or not the direct reduction of H_2CO_3 actually occurs on the metal surface was and still is a topic of debate, since it could be argued that undissociated H_2CO_3 is merely a

source of hydrogen ions and would dissociate to give a hydrogen ion faster than it (carbonic acid) could diffuse to the surface of the steel. In this way H_2CO_3 would act as an additional source of hydrogen ions and lead to higher corrosion rates. Both pathways release hydrogen gas as a product from water and, nowadays, it is accepted that direct reduction of H_2CO_3 dominates at high partial pressures of CO_2 and high pH, while the reduction of hydrogen ions dominates at low CO_2 partial pressures and low pH.

2.1.1. CARBON DIOXIDE INTERFACIAL REACTION AND THE IRON CARBONATE LAYER.

The mechanisms of CO_2 corrosion and the formation and removal of protective iron carbonate films are not fully understood due to the complex reaction mechanisms and the presence of many critical environmental factors such as pH, temperature, dissolved species concentration and hydrodynamics that can appreciably change the corrosion rate. In addition, CO_2 corrosion products can also form protective iron carbonate ($FeCO_3$) films on the surface under certain conditions and can prevent the metal from further corrosion by acting as a diffusion barrier [22-26]. The protective nature of these iron carbonate films depends on the environmental factors as well. When steel corrodes in CO_2-saturated water, the solubility of iron carbonate salt ($FeCO_3$) may be exceeded and precipitation sets in, which increases rapidly with the degree of supersaturation and increase in temperature. The precipitate of iron carbonate may form a protective film depending on the solution composition, pressure, and temperature of the system. Other solid corrosion products may

form in the presence of chlorides, sulfides, and oxygen [21].

Dugstad [27] found that the super saturation level of iron carbonate and the pH are dependent on the water to steel volume ratio and temperature. Protective films are not easily formed as the precipitation rate of iron carbonate is temperature dependent and slow. It takes a supersaturated solution of iron carbonate 20 to 40 hours to cover the metal surface with the protective iron carbonate layer.

Understanding the properties of surface films and the rate at which they form on pipelines due to the presence of carbon dioxide will help in achieving better protection of oil tube steels. It will also help to increase the efficacy of corrosion mitigation techniques.

2.1.2. CARBON DIOXIDE CORROSION RATE

The prediction of corrosion in carbon dioxide environments of oil and gas production has attracted much attention over many years and extensive researches have been done to investigate corrosion mechanism of carbon steel due to carbon dioxide, but adequate models still do not exist because most models are based on experiments carried out in stirred beakers, rotating cylinder electrodes and small diameter pipes. Correction factors determined for such systems cannot be relied on in other environments and the need for basing models on experimental results from large diameter flow loops is imperative. Study of sweet corrosion in multiphase flow requires the prediction of the effects of oil/water composition, flow regimes, and flow characteristics, such as phase distribution and holdup at different pressures and temperatures, on corrosion rates [28].

Several models for predicting corrosion rates have been forwarded over the years. De Waard and Milliams [21] studied carbon dioxide corrosion of carbon steel under various conditions of pH, temperature, and pressure and suggested mechanisms for such corrosion. Nesic *et al*.[29] proposed a model for carbon dioxide corrosion based on electrochemical reactions occurring in water-carbon dioxide systems. Dayalan *et al.* [30] proposed a mechanistic model for the carbon dioxide corrosion of steel in pipe flow. They suggested that the overall corrosion process occurs in four steps. The first step is the dissolution of carbon dioxide in the aqueous solution to form the reactive species which undergo the corrosion reaction either by the reduction of H^+ at pH < 4 and CO_2 pressure < 1 bar, or by the direct reduction of H_2CO_3 at pH >5 and CO_2 pressure > 1 bar. The second step is the transport of these reactive species to the metal surface. The third step involves the electrochemical reactions (anodic and cathodic) taking place at the surface. The final step is the transportation of the corrosion products to the bulk of the solution. If corrosion products can form a passive layer and then this layer is cracked or disrupted, the type of the pit formed depends mainly on the adhesion of this layer on metal surface. If this layer is strongly attached to the surface, a pine pit will develop when the layer is disrupted like in H_2S corrosion; otherwise a shallow homogenous pit will develop when the layer is not strongly attached to the metal.

Herce *et al*. [31] showed that the combined effects of CO_2 partial pressure and ionic strength, temperature, and initial bicarbonate ion concentration of the solution may be described by a single variable; namely pH. They combined the effects of fluid flow with

pH to define a hydrogen ion flux which they related to corrosion rate under a variety of conditions.

Nesic *et al*. [32] developed an integrated CO_2 corrosion – multiphase flow model which takes into account the effect of the most important variables such as the kinetics of electrochemical reactions at the steel surface, transient one-dimensional transport of species between the bulk solution and the steel surface, the kinetics of chemical reactions including precipitation, the effect of traces of H_2S and the effect of inhibition by crude oil and/or corrosion inhibitors.

2.1.3. FACTORS AFFECTING CORROSION RATE

2.1.3.1. Acidity or pH : The effect of pH on corrosion can be classified as follows: At pH 7.0 and above significant corrosion is unlikely. In the pH range of 6.5 to 7 slight corrosion is possible. In the pH range of 6.0 to 6.5 moderate corrosion with possible pitting occurs. At pH 6.0 and below there is significant corrosion with probable pitting. Between pH 6.0 and pH 4.0, the corrosion rate decreases due to the depletion of H+ in the electrolyte which is required for one of the cathodic reactions in CO_2 corrosion. In addition, another significant cathodic reaction takes place: the direct reduction of H_2CO_3 . At pH less than 4, the available H+ ions makes H^+ reduction the dominating cathodic reaction. Also the corrosion rate is found to be flow sensitive at this low pH [33, 34].

Fajardo *et al*. [35] found that formic, acetic and propionic acids increase the corrosion rate due to an additional cathodic reaction; namely the direct reduction of the undissociated organic acid. They found that this reaction is very sensitive to temperature changes and may be limited by diffusion of the acid molecules. The presence of organic acids makes it harder for protective iron carbonate scales to form a "scale undermining" effect.

2.1.3.2. Temperature and Pressure: Increased temperature (in general) and pressure (stress related failures) increase corrosion; Sweet corrosion can be accompanied by hydrogen-induced failures, where hydrogen gas forms at the cathode [36].

Although high temperatures reduce the solubility of corrosive gases, the extent of corrosion may not necessarily decrease because the rate of corrosion increases as temperature increases. Salts present in oilfield waters and the dissolved carbon dioxide, together, bring about buffer action that prevents low pH [33] values that give rise to corrosion. Calcium carbonate and calcium sulfate scales may reduce corrosion if they are tight, uniform and nonporous. A break in the scale surface may increase corrosion below the scale.

2.1.3.3. Composition of the Brine: If the associated water has high salinity, a scale layer might deposited and prevent the corrosion. However, high porosity of the scale layer and low strength might induce localized corrosion (pitting corrosion) [37]. The rates of corrosion reactions are affected by the ion strength of the media and the mass

transfer of the corrosion ions to the surface of the metal.

Pisigan and Singley [38] developed several models for mild steel corrosion rate prediction from a combination of static and dynamic laboratory test data. They found that corrosion rates observed in their tests could be correlated to chloride and sulfate, calcium, alkalinity, buffer capacity, dissolved oxygen levels, and exposure. Ferguson [39] found that corrosion rate correlates with sulfate and chloride content, water alkalinity, Calcium content, time of exposure, and corrosion inhibitor level.

2.1.4. CO_2 -BICARBONATE BUFFER

The presence of bicarbonate or carbonate ion in the solution creates a buffer that stabilizes the pH. The reaction of CO_2 gas with water has two steps:

$$CO_2\,(g) \rightleftharpoons CO_2\,(aq) \qquad (2.5)$$

$$CO_2\,(aq) + H_2O \rightleftharpoons H_2CO_3\,(aq) \qquad (2.6)$$

The last reaction is kinetically slow. At equilibrium, only a small fraction (0.2 - 1%) of the dissolved CO_2 is actually converted to H_2CO_3. Most of the CO_2 remains as solvated molecular CO_2 .

Carbonic acid is a weak acid that dissociates in two steps [40].

$$H_2CO_3\,(aq) + 2H_2O \rightleftharpoons HCO_3^-\,(aq) + H_3O^+ \quad pK_{a1}\,(25\,^oC) = 6.37 \qquad (2.7)$$

$$HCO_3^-\,(aq) + H_2O \rightleftharpoons CO_3^{2-}\,(aq) + H_3O^+ \quad pK_{a2}\,(25\,^oC) = 10.25 \qquad (2.8)$$

If we assume CO_2 is a simple gas we can apply Henry's law that relates its equilibrium vapor pressure, p_{CO2}, to its equilibrium mole fraction, x_{CO2}, in the liquid phase by,

$$p_{CO2} = K \cdot x_{CO2} \qquad \text{(Eq2.1)}$$

where K is the Henry's law constant.

As Table 2.1 shows the solubility of CO_2 is decreases with temperature [41]

TABLE 2.1. Solubility of CO_2 at different temperatures and a partial pressure of 1 bar.

Temperature (^oC)	0	10	20	30	40	50	80	100
Solubility (cm^3 CO_2/g water)	1.8	1.3	0.88	0.65	0.52	0.43	0.29	0.26

Form the partial pressure of CO_2 and the experimental Henry's constant for CO_2 in water at the system temperature, the equilibrium mole fraction of CO_2 in liquid phase (x_{CO2}) can be determined. The molar concentration of the dissolved CO_2 is calculated by multiplying equilibrium mole fraction of CO_2 by the molar density of water at the system temperature.

$$[CO_2\,(aq)] = x_{CO2} \times d_m \qquad \text{(Eq 2.2)}$$

The molar density of water is given by the following equation:

$$d_m = \frac{d_T}{MM_{H2O}}\, d_m \qquad \text{(Eq 2.3)}$$

Where d_T is water density at the temperature (T) and MM_{H2O} is the molar mass of water 18.02 g / mol. To calculate the pH of the CO_2- saturated water we proceed as follows. The carbonic acid undergoes two reactions:

$$H_2CO_3 + e^- \overset{K_a}{\rightleftharpoons} H^+ + HCO_3^- \qquad (2.9)$$

$$H_2CO_3\,(aq) \overset{K_2}{\rightleftharpoons} CO_2\,(aq) + H_2O \qquad (2.10)$$

The equilibrium constant, K_a, for the acid-base reaction (2.9) is:

$$K_a = \frac{[H^+][HCO_3^-]}{[H_2CO_3]} \qquad \text{(Eq 2.4)}$$

The equilibrium constant, K_2, for reaction (2.10) is:

$$K_2 = \frac{[CO_2(aq)]}{[H_2CO_3(aq)]} \qquad \text{(Eq 2.5)}$$

Because the two equilibrium reactions (2.9 and 2.10) occur simultaneously, Equations 2.4 and 2.5 are simultaneous equations. Solving for the equilibrium concentration of carbonic acid gives

$$[H_2CO_3] = \frac{[H^+][HCO_3^-]}{K_a} = \frac{[CO_{2(l)}]}{K_2} \qquad \text{(Eq 2.6)}$$

Rearranging equation 2.6 allows us to solve for the equilibrium proton concentration in terms of the two equilibrium constants and the concentrations of the other species:

$$[H^+] = \left(\frac{K_2}{K_a}\right)\left(\frac{\left[CO_{2(l)}\right]}{[HCO_3{}^-]}\right) \qquad \text{(Eq 2.7)}$$

Equation 2.7 can be rewritten as:

$$pH = pK - log\left(\frac{\left[CO_{2(l)}\right]}{[HCO_3{}^-]}\right) \qquad \text{(Eq 2.8)}$$

where $K = \frac{K_2}{K_a}$.

In a real life situation, the calculation of [CO_2 (aq)] from equation 2.2 is found to be inaccurate due to many factors that affect the dissolution of CO_2 in water. These factors include salinity and the inhomogeneous mechanical distribution of CO_2 in the water during the fluid flow through the pipeline.

From an analysis of the temperature dependence of the solubility of CO_2 and the dissociation constants of H_2CO_3, De Waard, Lotz and Dugstad [42] showed that in the temperature range between 10 and 80 ^oC the pH due to CO_2 dissolution is approximately given by:

$$pH = 3.82 + .00384 - 0.5 \log(pCO_2) \qquad \text{(Eq 2.9)}$$

They further correlated corrosion rate as a function of pH, thereby suggesting a linear relation between corrosion rate and H^+ concentration at high mass transport rates. However, at lower flow rates, the overall dependence on pH will be less.

2.3. CORROSION MONITORING

2.3.1. WEIGHT LOSS METHOD

The simplest, and longest-established, method of estimating corrosion losses in plant and equipment is weight loss analysis. Weight loss method can be used onsite as well as in the lab.

2.3.1.1. CORROSION COUPONS –FIELD MONITORING

A weighed sample (coupon) of the metal or alloy under consideration is introduced into the process, and removed after a reasonable time interval. The coupon is then cleaned of all corrosion products and reweighed (Figure 2.3). The weight loss is converted to a total thickness loss or to an average corrosion rate using an appropriate conversion equation.

2.3.1.2. CORROSION IMMERSION TESTS (LABORATORY METHOD)

2.3.1.2.1. Static Weight Loss Test (ASTM G31 steel coupon).

In the case of oil soluble inhibitors the test involves exposure of the steel coupon installed on a coupon holder to an inhibited solution of oil for a short period of time, followed by immersion in non-inhibited brine for the remainder of the test. In the case of water soluble inhibitors, the brine is inhibited. The test period is usually 7 days.

Temperature can be varied by immersion in a suitable bath. Care must be taken in the preparation and cleaning of the test coupons. At the end of the test the coupons are cleaned, the weight loss is calculated and the inhibitor efficiency reported. The test provides a reasonable estimate of corrosivity in very severe brine conditions. The main shortcoming of this method is the lack of dynamic conditions (no shear effects).

2.3.1.2.2. Dynamic Weight Loss Test (NACE 1D182 Wheel Test)

NACE 1D182 test method proposed by the National Association of Corrosion Engineers is used to evaluate film-persistent corrosion inhibitors for oilfield applications. The test method is not uniformly accepted throughout the oil industry because of its inaccuracy especially in estimating the performance of CO_2 and H_2S corrosion inhibitors. In this method a weighed metal coupon is placed in a glass jar or cell and filled with the required ratio of deoxygenated (nitrogen/carbon dioxide saturated) brine and crude. The jar is then allowed to overflow slightly to eliminate all gas space from the bottle. The desired chemical inhibitor dosage is then injected into the lower liquid level and the bottle capped tightly. This is repeated until the required numbers of jars have been prepared. The jars are rotated for specified times. It is normal to conduct each test for a particular time in triplicate to take statistical variations into account. Since the coupon is alternately immersed in the crude oil and then the brine due to the rotational effect of the wheel, the partitioning tendencies of the inhibitors tend to be more realistic and compare better with those from the field. The test period is usually 2-3 days. Temperature can be controlled by

putting the wheel in a suitable oven. At the end of the test the coupons are cleaned, the weight loss is measured and the inhibitor efficiency is reported.

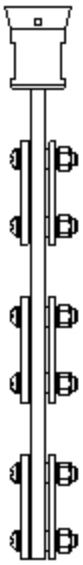

FIGURE 2.3. Ladder Strip Coupon Holder.

2.3.2. ELECTROCHEMICAL METHODS

Electrochemical methods provide a faster way to monitor corrosion, and usually the results can be read simultaneously in the field, or, within hours, in the lab. However, not all the electrochemical methods can be used for monitoring corrosion in the field. A severe limitation of electrochemical methods is the requirement for a conducting corrosive environment. This makes them inaccurate or even not applicable in gas system or in oil systems where the water content is less than 30% of the fluids. However, the rapidity of measurement makes these techniques useful in characterizing inhibitor performance. The electrochemical methods that found applications in the field are linear polarization resistance (LPR), electrical resistance (ER), electrochemical impedance spectroscopy (EIS) and recently electrical noise (EN). Of these methods, LPR will be discussed in detail.

2.3.2.1. THE ELECTRICAL RESISTANCE METHOD

This technique [46] operates by measuring the change in electrical resistance of a metallic element immersed in a product media relative to a reference element sealed within the probe body. Since temperature changes affect the resistance of both the exposed element and the protected element equally, measuring the resistance ratio minimizes the influence of changes in the ambient temperature. Therefore, any net change

in the resistance ratio is solely attributable to metal loss from the exposed element once temperature equilibrium is established.

The ER method is uniquely suited to corrosive environments having either poor or non-continuous electrolytes such as vapors, gases, soils, "wet" hydro-carbons, and non aqueous liquids.

2.3.2.2. ELECTROCHEMICAL IMPEDANCE SPECTROSCOPY (EIS)

Electrochemical Impedance Spectroscopy (EIS) [47-48] is an experimental method for characterizing electrochemical systems. In this technique a small amplitude sinusoidal excitation signal is applied to the system under investigation and the response (current or voltage) or the impedance of a system over a range of frequencies is determined, and therefore the frequency response of the system, including the energy storage and dissipation properties, is revealed. The frequency responses versus frequencies obtained by EIS are expressed graphically in a Bode plot (the log of impedance magnitude in ohms versus the log of frequency in hertz of the signal) or in a Nyquist plot (The plot of the real part of impedance against the imaginary part in a complex plan where impedance is given by the equation $Z(\omega) = Z_r(\omega) + j\, Z_j(\omega)$).

In the EIS experiment, a small amplitude signal, usually a voltage between 5 to 50 mV, is applied to a specimen over frequencies from 0.001 Hz to 100,000 Hz. The EIS instrument records the real resistance and imaginary capacitance components of the impedance response of the system. Depending upon the shape of the EIS spectrum, a

circuit model or circuit description code and initial circuit parameters are assumed and fed to the program by the operator. The program then fits the best frequency response of the given EIS spectrum, to obtain fitting parameters. The quality of the fitting is judged by how well the fitting curve overlaps the original spectrum. By fitting the EIS data it is possible obtain a set of parameters which can be correlated with the inhibitor coverage condition and the corrosion of the steel substrate.

2.3.2.3. ELECTROCHEMICAL NOISE (EN)

The EN [49] method is a non-intrusive method for corrosion monitoring especially for sensitive equipment such as aircraft parts and gas scrubbing towers. During localized corrosion an electrical noise occurs. This noise is believed to be generated by a combination of stochastic processes, such as passivation breakdown and repassivation events, and deterministic processes which can be caused by film formation or pit propagation processes. The EN method studies the fluctuations of potential or current of a corroding metallic specimen in the system to monitor the onset of events characterizing localized corrosion such as pitting or stress corrosion cracking (SCC), exfoliation, erosion-corrosion either in the laboratory or in diverse and complex industrial environments.

2.3.2.4. LINEAR POLARIZATION RESISTANCE METHOD (LPR)

The electrochemical technique, commonly referred to as Linear Polarization Resistance (LPR) [5], is the only corrosion monitoring method that allows corrosion rates to be measured directly, in real time. Although its application is limited to conducting media, the response time and data quality of this technique make it clearly superior, where applicable, to all other forms of corrosion monitoring.

The corrosion current (I_{corr}), generated by the flow of electrons from anodic to cathodic sites, can be used to compute the corrosion rate. However, anodic and cathodic sites continually shift position, and they exist within a continuously conductive surface, making direct measurement of I_{corr} impossible. To find I_{corr}, small, externally-imposed, potential shifts (E) - usually 10–30 mV- will produce a measurable current flow (I) at the corroding electrode (Figure 2.4) . The behavior of the externally imposed current is governed, as is that of I_{corr}, by the degree of difficulty with which the anodic and cathodic corrosion processes take place. The greater the difficulty, the smaller the value of $\boldsymbol{I_{corr}}$, and the smaller the value of I for a given potential shift. In fact, at small values of E, I is directly proportional to $\boldsymbol{I_{corr}}$, and hence to the corrosion rate. This relationship is embodied in the theoretically derived **Stern-Geary equation**:

$$\frac{\Delta E}{\Delta I} = \frac{\beta_a \beta}{2.3\, I_{corr}\, (\beta_a + \beta_c)} \qquad \text{(Eq 2.26)}$$

The numbers β_a and β_c are empirical rate constants (called Tafel constants) of the anodic and cathodic reactions respectively. The relationship can be expressed more simply as:

$$I_{corr} = \frac{I}{E} \times constant \qquad \text{(Eq 2.27)}$$

The value E/I is known as the Polarization Resistance. In principle it is most easily measured by placing a second (auxiliary) electrode in the liquid, and connecting it to the corroding (test) electrode through an external power supply.

The applied potential, in this simple type of two-electrode measurement, is required to overcome the solution resistance as well as the polarization resistance of the corrosion reactions. Consequently, the polarization resistance will be overestimated, and the corrosion rate will be underestimated.

The solution resistance error makes a two-electrode measurement valid only in metal/environment systems having a low corrosion rate, and low solution resistance, which is a rare combination. To overcome the problem of solution resistance error, a three-electrode measurement is used. This uses separate circuits for the measurement of I and E. The circuit in which the E measurement is made has extremely high input impedance; consequently solution resistance has a negligible effect on the value of the potential shift applied to the coupon electrode.

For the field monitoring, the accurate value of E_{corr} is not required, since the monitoring depends on relative corrosion rates, thus to simplify the setup of the

monitoring probe, a three-element setup is used: two identical metal bars of a mild steel alloy are used for the working and auxiliary electrodes, and a third bar made of a corrosion resistance alloy is considered as a reference electrode. The three bars are installed in a nonconductive epoxy holder.

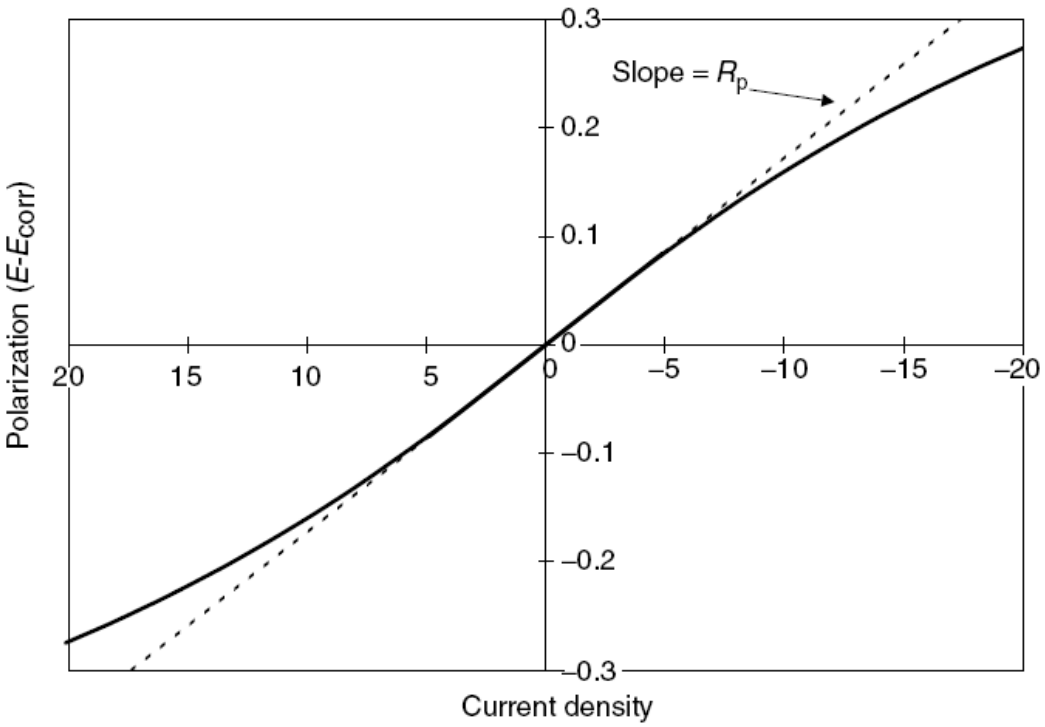

FIGURE. 2.4**.** Hypothetical Linear Polarization Plot.

Figure 2.5 shows commercial sensor elements to carry out linear polarization resistance (LPR) measurements in the field made by Metal Samples Company.

FIGURE 2.5. Linear Polarization Resistance Sensors

2.4. ORGANIC CORROSION INHIBITORS

2.4.1. CORROSION INHIBITORS.

The International Standards Organization (ISO) defines an inhibitor as a "chemical substance which decreases the corrosion rate when present in the corrosion system at suitable concentrations without significantly changing the concentration of any other corrosive agent" [50].

Corrosion inhibitors can be classified into three types: 1) anodic, 2) cathodic and 3) film forming inhibitors. The first two types affect the corresponding electrochemical reaction either by forming a complex with the metal ions on the protected surface or by stabilizing the corrosion product layer which decreases the diffusion of the corrosion product away from the metal surface. The third type involves the developing of an insoluble protective layer (film) which restricts the diffusion of dissolved corrosive species to the metal. If this film is non-conductive to electrons, the corrosion reaction becomes retarded [51].

Inhibitors can be inorganic, organic, polymeric, simple or complex formulations. **Passivating inhibitors** such as chromates, molybdates, silicates and phosphates form a strong non-corrosive oxide film with steels which causes the surface to be cathodic. They are not used to protect internal surfaces in the oil production industry as corrosion control by passivating inhibitors is only possible if the surface is 100% covered.

In some cases, the adsorbed corrosion inhibitor may react, usually by electrochemical reduction, to form a product that may also be inhibitive. Inhibition due to the added substance has been termed ***primary inhibition*** and that due to the reaction product, ***secondary inhibition***. In such cases, the inhibitive efficiency may increase or decrease with time according to whether the secondary inhibition is more or less effective than the primary inhibition

2.4.2. ORGANIC INHIBITORS.

Organic Corrosion inhibitors can be classified in two different categories depending on their protection mechanism. The two main types are (i) adsorption inhibitors and (ii) film-forming inhibitors.

2.4.2.1. Adsorption Inhibitors. [52]

Adsorption inhibitors form a chemisorptive bond with the metal surface and impede ongoing electrochemical dissolution reactions. Most organic inhibitors are chemisorption-type inhibitors. For example; aliphatic organic amines have an electron pair on the nitrogen atom which is available for donation to the metal surface. In addition, the hydrocarbon tails of the molecule are oriented away from the interface toward the solution so that further protection is provided by the formation of an array of hydrophobic hydrocarbon tails located on adjacently adsorbed amines. This hydrophobic network serves to keep water molecules and aggressive anions, such as Cl^-, away from the metal surface.

Chemisorption involves an actual charge transfer or charge sharing between the inhibitor molecule and the metal surface. By interacting with metal surface atoms, the chemisorbed inhibitor interferes with metallic dissolution. The simplest picture is one of a blockage of active surface sites, but this view is not quite complete. Like all adsorbed species, chemisorbed molecules have a certain residence time at the surface and thus play a dynamic role by participating in a number of adsorption–desorption steps.

Chemisorption-type inhibitors usually contain N, S, or O atoms; and chemisorption occurs through the donation of electrons from these atoms to the metal surface. The efficiency of the corrosion inhibition is indirectly proportional to the electronegativity of these atoms. [53]

The chemisorption of organic molecules, and accordingly their effectiveness as corrosion inhibitors, is influenced by three principal chemical factors [52]. These are (i) the electron donor ability of the molecule, (ii) the size of the molecule, and (iii) its solubility

A first estimate of the ability of a molecule to act as an electron donor is given by its base strength. Stronger bases are better electron donors than are weak bases

A second factor in determining the effectiveness of a chemisorbed organic inhibitor is the molecular size. In general, the larger the molecular area, the better the inhibitor (other factors being equal). However, with very large molecules (such as polymers), there may be steric hindrance problems when a large molecule attempts to fit onto a surface already partially occupied with previously adsorbed molecules. Thus,

complete coverage of the surface by large molecules may sometimes be difficult to achieve.

The third factor affecting chemisorption, and thus inhibition, is the solubility of the organic molecule. Less soluble molecules have a greater tendency to be adsorbed than soluble molecules.

2.4.2.2. FILM-FORMING AMINE INHIBITORS.

Organic corrosion inhibitors require two functionalities: one nucleophilic and the other hydrophobic. The nucleophilic functionality gives rise to chemisorptions, by means of coordinating with the acidic surface of iron atoms, while the hydrophobic functionality shields the metal surface for aqueous corrosive media. Nitrogenous inhibitors are the main active constituent in most oilfield inhibitor compositions. The terminal amines groups are protonated, i.e., are cationic at use concentrations. The cationic polar part of the molecule is attracted and chemisorbed to the negatively charged sites on the steel surface and the fatty (hydrocarbon) part of the molecule is exposed to the crude oil and acts as a barrier to water. The inhibitor will displace any pre-existing water molecules on the steel surface (lower interaction energy) [54].

Film forming inhibitors are mainly amines which have one or more long-chain hydrophobic alkyl groups attached to one or more hydrophilic nitrogen functionalities. The nitrogen group may be protonated, alkylated or ethoxylated.

Film forming inhibitors can be classified into the following broad groupings:

A- Amides and imidazolines

B- Salts of nitrogenous molecules with carboxylic acids (fatty acids, naphthenic acids)

C- Nitrogen quaternaries

D- Polyoxylated amines, amides, and imidazolines

E- Nitrogen heterocyclics

Amides are formed by the condensation of polyamines, usually diethylene triamine DETA, with fatty acids. Imidazolines are formed from the same ingredients but under different reaction conditions. Fatty acids that are used include low cost tall oil (C_{18} + minor rosins) and oleic (C_{18} unsaturated) acid. Amides and Imidazolines are widely used in oil dispersible inhibitor formulations. To prepare water dispersible versions, imidazolines and fatty amines are reacted with acetic or propionic acids. Imidazolines and primary amines generally become more efficient as the chain length is increased.

2.4.3. MECHANISM OF CORROSION INHIBITION BY ORGANIC INHIBITORS

As earlier discussed, inhibitors reduce corrosion rates by either slowing the corrosion rate determining step; or by introducing a new rate determining step. In another word inhibitors increase the anodic or cathodic polarization behavior (Tafel slopes) or

reduce the movement or diffusion of ions to the metallic surface, or increase the electrical resistance of the metallic surface.

Whatever the mechanism might be, effective corrosion inhibitors involve developing an inter-phase system with a three dimensional protective layer between the corroded substrate and the electrolyte [55]. Such layer generally consists of weakly soluble compounds such as film forming inhibitors, thus inhibition efficiency depends mainly on the mechanical, chemical and structural properties of the layer, which in turn are related to the chemical and physical properties of the inhibitor.

Inhibitor efficiency increases with concentration until the surface is saturated, i.e, it has adsorbed inhibitor molecules on all available site. Organic inhibitors form films that are water repellent. Hydrocarbons are sometimes added to inhibitor formulations that will wet the adsorbed inhibitor forming a secondary barrier. By replacing and repelling water away from the metal surfaces, the oil films are able to stifle corrosion much like other physical barriers such as paints. Certain hydrocarbon components of the crude will also co-adsorb with the inhibitor to improve the barrier effect.

2.4.4. FACTORS AFFECTING THE PERFORMANCE OF ORGANIC INHIBITORS

Studies showed that the first step in the mechanism of most inhibitors is the formation of a protective hydrophobic film on the metal surface by adsorption [56]. For many physically adsorbed organic compounds, the inhibition properties are exhibited or

enhanced above the critical micelle concentration (CMC), whereas for many organic chelating compounds, inhibition starts with the onset of the formation of an insoluble chemisorbed complex [57]. In the absence of a corrosion product layer (oxide, carbonate etc) the factors affecting inhibitor adsorption on a metal surface include [5]:

A- **The nature and surface charge of the metal:** Adsorption may be due to electrostatic attractive forces between ionic charges or dipoles on the adsorbed species and the electric charge on the metal at the metal-solution interface.

B- **The functional groups and structure of the inhibitor compound:** Inhibitors can also bond to metal surfaces by electron transfer to the metal to form a coordinate type of link. This process is favored by the presence of vacant electron orbitals of low energy in the metal, and by the presence of relatively loosely bound electrons in the adsorbed species, such as may be found in anions, and neutral organic molecules containing a lone pair of electrons or a π-electron systems associated with multiple (especially triple) bonds or aromatic rings.

C- **Interactions between the adsorbed species**: Adsorption of inhibitor molecules involves the removal of adsorbed water molecules from the surface. During adsorption, an inhibitor molecule changes from a state in which it is dissolved to one in which it is adsorbed. This change in interaction energy with water molecules changes the free energy of adsorption, and increases the energy of solvation of the adsorbing species, which in turn increases with increasing size of the hydrocarbon portion of the organic inhibitor molecule. Increasing the size of the molecule leads to

decreasing its solubility and increasing its adsorbability. This is consistent with the increasing inhibitive efficiency observed at constant concentrations with increasing molecular size in a series of related compounds.

By increasing the molecular size or increasing the concentration of the inhibitor, lateral interactions between adsorbed inhibitor species may become significant as the surface coverage, and hence the proximity, of the adsorbed species increases. These lateral interactions may be either attractive or repulsive. Attractive interactions occur between molecules containing large hydrocarbon components (e.g., n-alkyl chains). As the chain length increases, the increasing Van der Waals attractive force between adjacent molecules leads to stronger adsorption at high coverage. Repulsive interactions occur between ions or molecules containing dipoles and lead to weaker adsorption at high coverage. In the case of ions, the repulsive interaction can be altered to an attractive interaction if an ion of opposite charge is simultaneously adsorbed. In a solution containing inhibitive anions and cations the adsorption of both ions may be enhanced and the inhibitive efficiency greatly increased compared to solutions of the individual ions. Thus, synergistic inhibitive effects occur in such mixtures of anionic and cationic inhibitors.

The mass transfer coefficient of the pipeline corrosion inhibitor determines its migration to the metallic surface and in turn its effect on corrosion rate. The higher the mass transfer, the faster the migration and the faster the formation of the protective film. The solubility of the corrosion inhibitor in the oil phase should be selected in a way to

allow the fastest migration rate, but at the same time maintain the protective film thickness at a certain limit.

The salinity of the water will affect the dispersiblility of the corrosion inhibitor as well as the formed film strength. The desired dispersion characteristics of the inhibitor will vary from field to field. When testing the dispersion characteristics of a proposed blend, a sample of the field brine should be used.

2.4.5. ORGANIC INHIBITORS EFFICIENCY

A corrosion inhibitor is a chemical substance which, when added in small concentrations to an environment, effectively decreases the corrosion rate. The efficiency of an inhibitor is a measure of this improvement [58]

$$\text{Inhibitor Efficiency}(\%) = 100 \times \frac{(CR_{unin\ hibited} - CR_{in hibited}}{CR_{unin\ hibited}} \qquad \text{(Eq 2.20)}$$

Where $CR_{uninhibited}$ is the corrosion rate of the uninhibited system and $CR_{inhibited}$ is corrosion rate of the inhibited system.

The inhibitor efficiency is a measure of θ, the surface coverage of the metal surface by adsorbed inhibitor molecules, where 100% efficiency is attained when θ = 1. Gravimetric or weight loss methods are used most for inhibitor testing although electrochemical methods are faster and give mechanistic information. Corrosion rates can be determined electrochemically in minutes while weight loss methods can take days. With the near instantaneousness of electrochemical methods, changes of inhibitor performance with time are readily measurable.

2.4.6. AMIDOAMINES AND IMIDAZOLINES.

The main inhibitor families used for the oil and gas production are fatty imidazolines and fatty amides. They are also used widely as surface-active compounds or as precursors for surface-active compounds [59].

Chemically, imidazoline compounds belong to the heterocyclic compounds having a five-membered ring with two nitrogen atoms in the ring. Industrially, amidoamines are prepared by the reaction of polyamines -such as diethylenetriamine (DETA) - with fatty acids, triglycerides, or methyl esters of fatty acids [6-60]. The temperature of the reaction should be carefully controlled; otherwise imidazoline will be formed by the cyclization reaction of the resulting amidoamine [61]. Changing the length of the alkyl group R of the fatty acid and the polyamine used changes the performance of the resulting amidoamine as a corrosion inhibitor in several ways, as it determines its solubility, dispersiblility and surface activity.

2.5. ADSORPTION OF CORROSION INHIBITOR

2.5.1. THE EFFECT OF ADSORPTION ON INHIBITION EFFICIENCY

The inhibitive efficiency is usually proportional to the fraction of the surface θ covered with adsorbed inhibitor. However, it is not the only factor that determines the efficiency. In some cases the effectiveness of adsorbed inhibitor species in retarding the corrosion reactions may be greater at low surface coverage ($\theta < 0.1$) than at high surface coverage. In other cases, adsorption of inhibitors, such as thiourea and amines, from diluted solutions, may stimulate corrosion. The information on inhibitor adsorption derived from direct measurements and from inhibitive efficiency measurements indicates that inhibitor adsorption on metals is also influenced by the surface charge on the metal, the functional group and structure of the inhibitor, and interaction of the inhibitor with water molecules and with other adsorbed inhibitor species. These factors individually or in combination can be responsible for the high inhibition at low surface coverage [5].

Species that are physically absorbed interact rapidly with the metal but are easy to remove. Chemisorption takes place more slowly and involves a higher heat of adsorption and it is not completely reversible. So for a corrosion inhibitor to be efficient, its surface activity should involve chemisorption. The adsorption of an organic molecule on a metal surface is actually a displacement reaction involving competition with an adsorbed water molecule, and in the case of CO_2 saturated brine, many other species such as CO_2 (aq) and H_2CO_3 might adsorb as well. The function of the hydrophilic, positively charged nitrogen

part of the inhibitor is to displace adsorbed molecules on the metal and attach the inhibitor molecule to the negatively charged metal surface, while the hydrophobic part gives the molecule a degree of oil solubility and attracts crude oil molecules thereby forming a protective ‘film’ barrier between the corrosive water phase and the metal surface. When using these surfactants, it is important to adopt a concentration that fills all sites on the metal surface and gives the best possible protection, thus to form a protective layer the inhibitor has to be present at or above a critical concentration in the aqueous phase. The differences between physisorption and chemisorption are summarized in the table 2.2.

Studying the effect of corrosion inhibitors is not a straight forward task. There is a plethora of approaches in the literature, varying from the use of simple inhibitor factors and inhibition efficiencies to the application of complicated molecular modeling techniques to describe inhibitor interactions with the steel surface and iron carbonate film. Nevertheless, studies are generally based on the assumption that corrosion protection is achieved by surface coverage, i.e. that the inhibitor is adsorbed onto the steel surface and prevents the electrochemical reactions from occurring on it. The degree of protection is assumed to be directly proportional to the fraction of the steel surface covered by the inhibitor

TABEL 2.2. Comparison between Physisorption and Chemisorption

Properties	Physisorption	Chemisorption
Forces of attraction	vander Waals' forces	chemical bond forces
Adsorption enthalpy	Heat of liquifaction (5- 40 k.J/mole)	High enthalpy of adsorption (40 - 800 k.J/mole)
Adsorption temperature	Low temperature , near or below T_{bp} of adsorbate	High temperatures, unlimited
Specificity	It is not specific	It is highly specific
Saturation	Multi-molecular layers may be formed	Generally, monomolecular layer is formed
Adsorption kinetic	Fast, non-activated process	Activated process
Nature of adsorption	non-dissociative and reversible	often dissociative and irreversible

The Tafel Equation can be written as:

$$\eta = \pm\beta \, log \frac{i}{i_0} \qquad \text{(Eq2.28)}$$

Where η is over voltage (in volts), i is the current density (in A m^{-2}), β is the Tafel slope (in volts), i_0 is the exchange current density (A m^{-2}), and the "+" sign applies for anodic reactions while the "–" sign applies for cathodic reactions.

When the surface coverage is taken into account, the equation becomes.

$$i = i_o \, . 10^{\mp\frac{\eta}{\beta}} . \prod_{s=1}^{n_s} (1 - \theta_s) \qquad \text{(Eq2.29)}$$

Where θ_s is the fraction of the steel surface where a given electrochemical reaction does not occur because the surface is covered by a species which could be an adsorbed inhibitor or a protective film. The product sign Π accounts for a compounding (additive) effect by more than one surface species.

The study of inhibition efficiency should establish a relationship between the surface coverage θ and the inhibitor concentration in the solution c_{inh}. This can be done by the use of a proper adsorption equation for a binary, isothermal system that relates the surface excess of inhibitor (mol/cm^2) –which is related to surface coverage -with the solution concentration of the inhibitor (M). This relation is called adsorption isotherm.

2.5.2. ADSORPTION ISOTHERMS

According to IUPAC, an adsorption isotherm is an isotherm describing adsorption of the sample component on the surface of the stationary phase from the mobile phase. There are many well established isotherms that can be used to describe the adsorption of corrosion inhibitors on a metal surface.

2.5.2.1. THE LANGMUIR ADSORPTION ISOTHERM

The Langmuir adsorption isotherm describes quantitatively the build-up of a layer of molecules on an adsorbent surface as a function of the concentration of the adsorbed material in the liquid in which it is in contact. It was theoretically derived assuming that the adsorption takes place on fixed homogenous absorption sites of equal energy forming a monolayer surface coverage, with no interactions between molecules adsorbed.

The rate of adsorption ν_a will be proportional to the molar concentration of gas or liquid (c) above the surface and the fraction of the surface that is not covered (1-θ), yielding a rate equation

$$\upsilon_a = k_a c(1-\theta) \qquad \text{(Eq2.30)}$$

where k_a is the rate constant for adsorption. The rate of desorption is simply proportional to the fraction of the surface that is already occupied, so the rate equation is

$$\upsilon_d = k_d c(\theta) \qquad \text{(Eq2.31)}$$

and k_d is the rate constant for desorption. At equilibrium, the two equations are equal , which yields an equilibrium statement that can be written as

$$\frac{\theta}{1-\theta} = \frac{k_a}{k_d} c \qquad \text{(Eq2.32)}$$

The ratio of rate constants is equal to equilibrium constant which represents the affinity between adsorbate and adsorbent. The final isotherm can be written as:

$$\frac{\theta}{1-\theta} = k_{ads}\, c \qquad \text{(Eq2.33)}$$

Langmuir isotherm shows that at low concentrations of the adsorbate, the extent of adsorption is linear and at high concentrations the extent of adsorption is a constant.

The shape of the isotherm (assuming the (x) axis represents the concentration of adsorbing material in the contacting liquid) is a gradual positive curve that flattens to a constant value.

2.5.2.2 . FREUNDLICH ADSORPTION EQUATION:

The Freundlich adsorption equation may be considered as a special case of the Langmuir equation where no monolayer formation (complete coverage) occurs. The extent of adsorption varies directly with concentration until the saturation concentration is reached. Beyond that point the rate of adsorption becomes independent of concentration even at high concentrations, thus the Freundlich Adsorption Isotherm fails at higher concentrations. It often represents an initial surface adsorption followed by a

condensation effect resulting from extremely strong solute-solute interaction. The Freundlich Adsorption Isotherm is mathematically expressed as:

$$\theta = k_{ads}\, c^{n} \qquad \text{(Eq2.27)}$$

where n is the Freundlich power constant. It also can be written as,

$$\log \theta = log\, k_{ads} + n \log c_{inh} \qquad \text{(Eq2.28)}$$

The Freundlich isotherm curve is exponential in form. It does not become linear at low concentrations, but remains convex to the concentrations axis. An isotherm is recognized as being of the Freundlich type if the plot of log θ versus log c_{inh} yields is a straight line. From the intercept, the parameter k_{ads} is obtained, while the slope is equal to n.

The Freundlich adsorption isotherm has a limited application; it is an empirical isotherm with no theoretical basis. Its application is limited to low concentrations, and shows deviation at higher concentrations, and the values of constants k and n change with temperature. It was found by Halsey [62, 63] that the Freundlich isotherm holds for the heterogenous surface when adsorption energy is inversely proportional to log θ. The enthalpy of adsorption [64] is assumed to vary logarithmically with fractional coverage for θ values in the range 0.2–0.8.

2.5.2.3. TEMKIN ISOTHERM

The surface of a solid electrode is not homogeneous; even an apparently smooth surface as observed in an optical microscope contains corners and edges of the crystal

structure of the metal and dislocations, i.e. sites where the regular crystal structure is disordered. Adsorption on a physically heterogeneous surface differs from that on a physically homogeneous surface. The heat of adsorption and Gibbs energy of adsorption differ from one site to another, and the sites with the lowest Gibbs energy of adsorption are occupied first. M. Temkin derived an adsorption isotherm that takes into account the heterogeneity of the surface [44]. It has been developed considering the chemisorption of an adsorbate onto the adsorbent.

This empirical adsorption isotherm [64] is useful for the chemisorption experiments where a monolayer forms, and it considers that all sites are not energetically equivalent. The enthalpy of adsorption is assumed to vary linearly with the fractional coverage. Temkin's adsorption isotherm is written as,

$$K_{ads}C = e^{f\theta} \qquad \text{(Eq2.29)}$$

It also can be written in a logarithmic way:

$$\theta = {}^{1}/_{f}\ \ln(C_{inh}) + {}^{1}/_{f}\ ln(k_{ads}) \qquad \text{(Eq2.30)}$$

where f is the molecular interaction constant. This isotherm is useful for fitting the middle region of chemisorption isotherms. The plot of Θ versus log C_{inh} will generate a straight line. The Temkin constants $(1/f)$ and $(1/f)$ K_{ads} can be calculated from the slope and intercept of the linear plot.

2.5.2.4. FRUMKIN ISOTHERM

Frumkin [65, 66] assumed that there is some interaction between the adsorbed species. Typically the adsorption isotherm suggested by him is written as:

$$\frac{\theta}{1-\theta} e^{-2a\theta} = K_{ads} C_{inh} \qquad \text{(Eq2.31)}$$

Where $K_{ads} = e^{-\frac{\Delta G^o}{RT}}$, $\Delta G_{ads}{}^o$ is the standard Gibbs energy of adsorption, C_{inh} is the adsorbed species equilibrium concentration, and "***a***" is a constant representing the interaction between adsorbed species. A positive value of "***a***" means attraction between the adsorbed molecules, and a negative value, repulsion between the adsorbed molecules. When the parameter "**a**" is equal to zero (i.e., there is no interaction between the adsorbed molecules), the Frumkin isotherm reduces to the Langmuir isotherm, which means Langmuir isotherm is a special case of the Frumkin adsorption isotherm for a = 0. Fig 2.6 shows adsorption isotherms of Langmuir, Temkin and Frumkin [67] type.

2.5.3. THERMODYNAMIC PARAMETERS OF ADSORPTION

Since the adsorption isotherm relates the inhibitor concentration in the solution to the surface coverage of the inhibitor θ, experimental data collected from inhibitor testing can be used to identify adsorption isotherm that fits the data best, and thus the K_{ads} of the adsorption process and the changes in the free Gibbs energy of adsorption, ΔG_{ads}

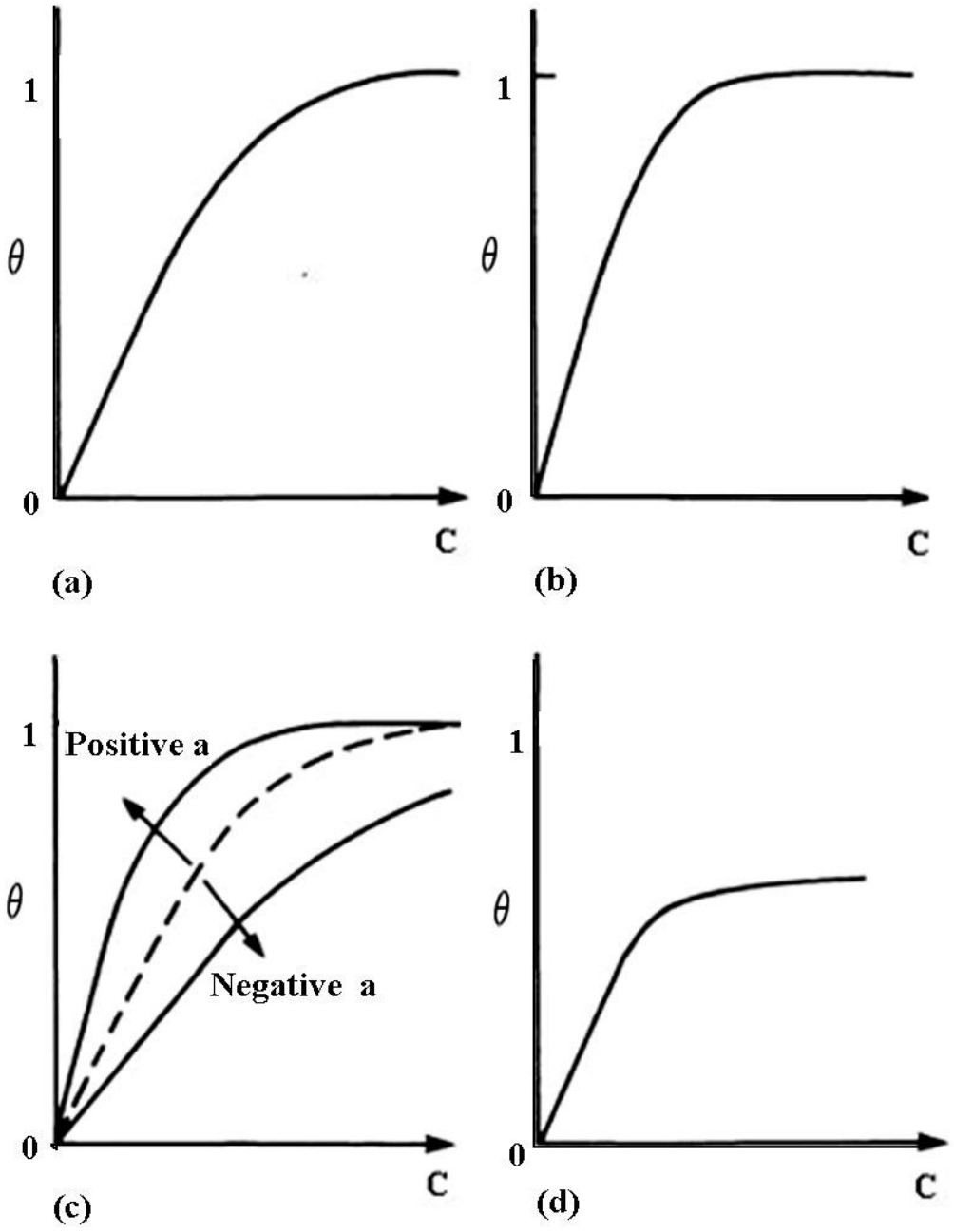

FIGURE 2.6 Adsorption isotherms: (a) Langmuir; (b) Temkin; (c) Frumkin; (d) Freundlich .

Adsorption is generally accompanied by release of energy, that is, most adsorption processes are exothermic in nature. Adsorption is a spontaneous process; therefore its free energy change is negative ($\Delta G_{ads}<0$). However, the entropy change associated with adsorption is generally negative because the adsorbate molecules lose their translation freedom when they get attached to the surface of the adsorbent.

Therefore, in order for ΔG_{ads} to be negative, the enthalpy change (ΔH_{ads}) must be sufficiently negative, such that, ($\Delta G_{ads} = \Delta H_{ads} - T\ \Delta S_{ads})<0$. This explanation accounts for exothermic adsorption processes. In cases, where endothermic adsorption occurs as in the case of hydrogen adsorption on glass, the entropy change ΔS_{ads} is sufficiently positive such that ΔG_{ads} remains negative. The positive entropy is attributed to the fact that hydrogen dissociates when adsorbing on the glass surface which increases the number of atoms in the system upon adsorption, another reason is the fact that hydrogen atoms have a very high mobility on the glass surface compared to the hydrogen H_2 molecules.

Enthalpy of adsorption, which is the enthalpy change for the adsorption of one mole of an adsorbate on an adsorbent surface, is usually in the range of 20 kJ/mole to 40kJ/mole while for chemisorption, the values are an order of magnitude high, that is, 200 kJ/mole to 400 kJ/mole [19, 68-69].

2.6. SURFACE TENSION OF CORROSION INHIBITOR

The adsorption of surface active compounds like inhibitors on solids can be classified on the basis of type of surface, type of the surface active compound and on the concentration of the surface active compound [70]. Broadly speaking, two types of solids and two types of surface active compounds can be distinguished: the surface is hydrophilic or hydrophobic and the surfactant is ionic or nonionic. Depending on the water content of the crude steam the surface of the pipeline can be hydrophilic (when it is covered with water molecules) or hydrophobic (when it is wetted by oil).

Amphiphilic molecules consist of a hydrophobic (non-polar) end and a hydrophilic (polar) end. Amphiphilic molecules interact with water in two different ways. They can arrange themselves such that their polar ends lie on the surface of water while their non-polar ends are held above the surface of water either in the air or in contact with another non-polar liquid. Such surface active molecules or 'surfactants' disrupt the cohesive energy between the water molecules on the surface and lower the surface tension. Another arrangement of these molecules allows each of its two components to interact with the environment it favors. Thus such molecules can form aggregates such that the hydrophobic portions orient themselves within a cluster and the hydrophilic portions are exposed to the polar solvent; usually water. Such aggregates ar called micelles. At low concentrations the surfactant prefers the surface arrangement. As the surface becomes saturated with surfactant molecules any more added surfactant molecules will form

micelles. The concentration at which the onset of micelle occurs is called the critical micelle concentration (CMC). Accordingly one expects the surface tension of the polar solvent to be constant prior to the addition of any surfactant, to decrease in a more or less linear fashion with the concentration of the added surfactant during the stage at which the surfactant molecules are solely at the surface of the solvent and to remain constant beyond the critical micelle concentrations.

In this study we are concerned with the adsorption of the surfactant on the interface between a solid surface and the solution it is in. The critical micelle concentration (CMC)[71] of an ionic surfactant is related to its chemical structure. The longer the hydrophobic portion of the surfactant is, the lower the CMC value. This relation is described by the so-called Klevens constant as:

$$log(CMC) = A - B\, n_C$$

where A is a constant that correlates with the contribution of the head group, B is a constant that correlates with the hydrophobic forces driving the surfactant to aggregation. n_c is the number of carbon atoms in the hydrocarbon part of the molecule.

In general, adsorption of surfactants at various interfaces starts at concentrations much below the CMC value and it reaches a pseudosaturation value at the CMC value. A pseudo-saturation value rather than a typical surface saturation value is reached, because the concentration of the free surfactant is nearly constant above the CMC. Provided the

surfactant solution remains dilute, the 'driving force' on the surfactant to go to the interface remains the same above the CMC [72].

The adsorption of the inhibitor on the surface of the metal is affected by the CMC value, because it can involve the adsorption of single molecule or a surface micelle on the charged surface. The change in the surface free energy due to the adsorption of a micelle is more complicated than that due to a single molecule. The surface of the metal can be water wetted or oil-wetted, and thus it can be hydrophilic or hydrophobic, which will affect the adsorption behavior of the inhibitor and its efficiency. When the CMC is reached, problems like emulsification and foaming start to appear, thus the efficiency of the inhibitor starts to decrease due to the migration of the inhibitor to the liquid/liquid or the gas/liquid interface. Figure 2.7 shows the various types of adsorption of surface active molecules on metal surface.

The emulsification tendency of the inhibitor can play a double role: when the water content is low, a slug flow regime develops water in oil emulsion. This emulsion protects the pipeline and reduces corrosion rate, but at the same time some corrosion inhibitor forms a film on the water/oil interface minimizing the free surfactant concentration and decreasing the apparent inhibitor efficiency.

Another factor that affects the efficiency of the inhibitor is the change in the wetability of the surface by oil due to the surface activity of the inhibitor. If the inhibitor

tends to make the surface hydrophobic, the oil molecules will play a role in forming the inhibiting film, which increases the inhibitor efficiency.

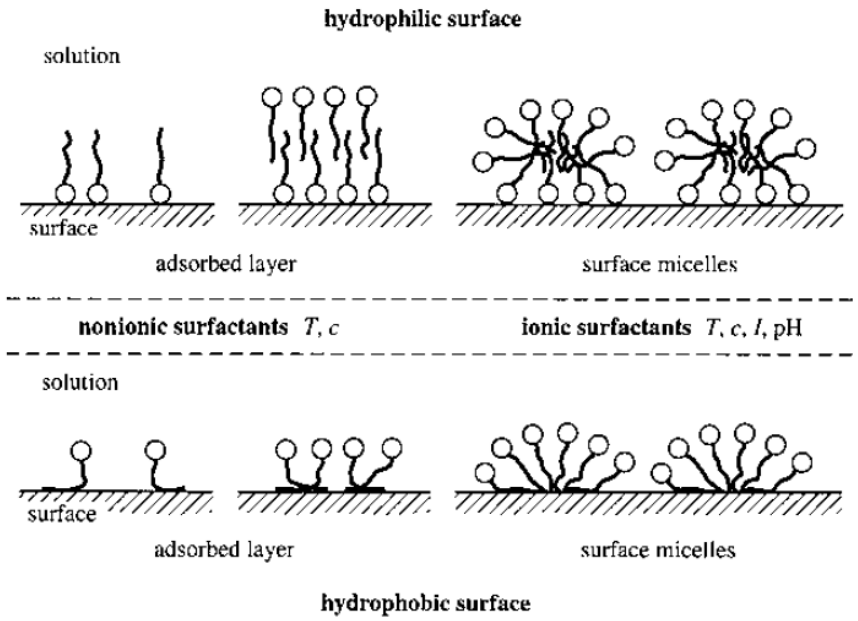

FIGURE 2.7. Adsorption of Surface Active Agents on Metal Surfaces.

CHAPTER 3

EXPERIMENTAL PART

3.1. REAGENTS

All the reagents used in the synthesis of the corrosion inhibitors were of laboratory grade purity. The polyamines used are N-(2-aminoethyl)-1,2-ethanediamine and diethylene triamine (DETA) and N-(2-aminoethyl)-N´-{2-{(2-aminoethyl) amino}ethyl}-1,2-ethane diamine) or tetraethylenepentamine (TEPA).

The laboatory grade TEPA is a mixture of four polyethyleneamines. These are:

1- TEPA : N-(2-aminoethyl)-N´-{2-{(2-aminoethyl)amino}ethyl}-1,2-ethanediamine.

2- AETETA : 4-(2-aminoethyl)-N-(2-aminoethyl)-N´-{2-{(2-aminoethyl)amino}ethyl}-1,2-ethanediamine .

3- APEEDA: 1-(2-aminoethyl)-4-[(2-aminoethyl)amino]ethyl]-piperazine.

4- PEDETA : 1-[2-[[2-[(2-aminoethyl)amino]ethyl]-amino]ethyl]-piperazine.

The TEPA used for this work was purified to get a pure N-(2-aminoethyl)-N´-{2-{(2-aminoethyl)amino}ethyl}-1,2-ethanediamine. The structures of the synthesized compounds were determined using infrared spectroscopy and ^{1}H and ^{13}C nuclear magnetic resonance (NMR) spectroscopy.

3.2. INFRARED ANALYSIS (IR)

The IR instrument used for the analysis of the synthesized amidoamines and imidazoline is NICOLET 6700 IR spectrometer (THERMO ELECTRON CORPORATION) with a wave number range from 400 to 4000 cm^{-1}.

3.3. NUCLEAR MAGNETIC RESONANCE (NMR)

^{1}H and ^{13}C NMR spectroscopy were used to characterize synthesized compounds. The NMR measurements were conducted using a JEOL LA 500 MHz spectrometer. ^{1}H NMR spectra were obtained using deuterated chloroform $CDCl_3$ as solvent. Tetramethylsilane (TMS) was used as internal standard.

3.4. CORROSION RATE MEASUREMENTS

The evaluation of corrosion inhibition of the synthesized compounds was carried out in a 3% NaCl solution saturated with CO_2 gas. Corrosion inhibition evaluation was carried out using electrochemical methods only (LPR and Tafel Plot), because the gravimetric method (The Standard NACE 1D182 Wheel Test Method) does not usually give reproducible readings with pitting corrosion and requires much longer duration.

The cell used is a 200 ml EuroCell made by Gamry shown in Figure 3.1. This cell has five ports: a 24/40 ground-glass joint, two #7 Ace-Threads, and two 14/20 ground-glass joints. The central 24/40 ground glass joint supports the cylindrical Working

Electrode (the corrosion sample) in the Sample Holder. The Reference Electrode Bridge Tube and the Counter Electrode and the Bubbler are all mounted in the Ace-Threads, which allow them to be adjusted vertically to accommodate a wide range of sample volumes. The vertical adjustment is also handy to make sure that the Reference Electrode Bridge Tube is placed close to the surface of the corrosion sample. The Bubbler is contained in the 14/20 joint and has one position for de-aeration and another for blanketing. The standard Counter Electrode is a graphite rod. The last 14/20 port is for a thermometer. The reference electrode is a standard calomel electrode.

The working electrode is a standard AISI C1018 carbon steel cylindrical electrode (model **EL410** supplied by METAL SAMPLES® shown in Figure 3.2) with a surface area of 4.5 cm^2. The composition of this alloy is given in Table 3.1.

TABLE 3.1. Chemical Composition of CI 1018 Mild Steel Alloy Used in the EL410 Electrode

Element	**% Fe**	**% C**	**% Mn**	**% P_{max}**	**% S_{max}**
Percentage	98.1-98.5	0.15-0.20	0.60 -0.90	0.040	0.050

The reference electrode should not be immersed directly in the test solution; it is connected to the cell using a special salt bridge called Luggin-Haber capillary shown in Figure 3.3. The Luggin-Haber capillary is a cell made of glass and has a capillary tube at the bottom end that is sealed with a special porous glass called Vycore™. The Luggin capillary allows sensing of the solution potential close to the working electrode without

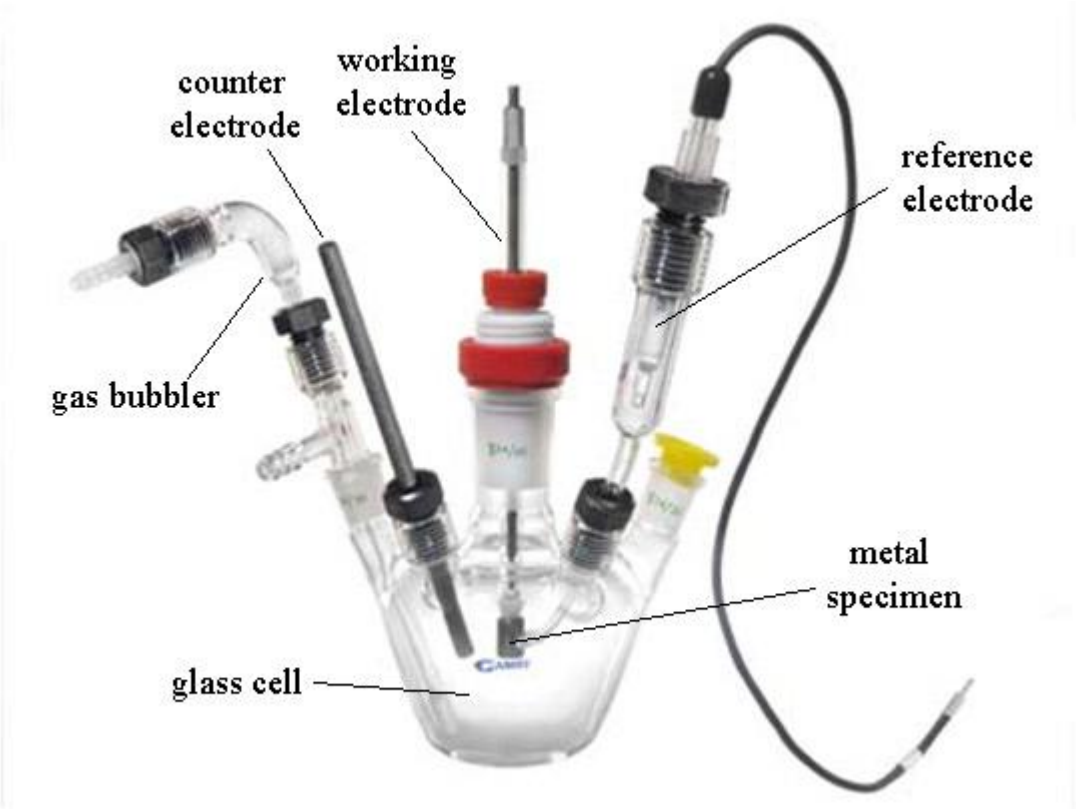

FIGURE 3.1. The Eurocell

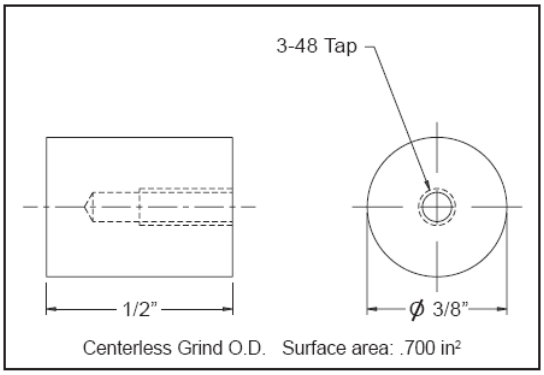

FIGURE 3.2. The Cylindrical Electrode Model EL410

the adverse effects that occur when the large reference electrode is placed near the working electrode.

The use of this bridge prevents the contamination of the reference electrode with the corrosion products that accumulate in the cell and minimizes the solution resistance error, which can be estimated from the product of the applied current density, the solution resistivity and the perpendicular distance from the Luggin-Haber capillary to the specimen surface [73]. Therefore, when installing the working electrode, the distanced between the Luggin-Haber probe end and the surface of the working electrode should be no more than 2mm.

Since linear polarization and Tafel plots correlate the surface coverage of the metal by the corrosion inhibitor- which is estimated by measuring the current generated by the electrochemical reaction of iron with CO_2 - with the corrosion rate; all the other electro active species in the solution- especially oxygen - should be removed. To avoid the corrosion caused by oxygen, the purity of CO_2 gas was 99.999%.

Since the concentration of the dissolved CO_2 is related to the flow rate, the partial pressure, the contact area at the gas/solution interface and temperature, the solution pH is likely to change during the experiment and in turn reduce the linearity of the polarization line. The studies on CO_2 [74] show that the corrosion at $pH < 4$ is mainly by the reaction of H^+, while the active specie in less acidic solutions is the adsorbed CO_2 gas or the adsorbed H_2CO_3 molecule. To avoid possible changes in the mechanism of corrosion

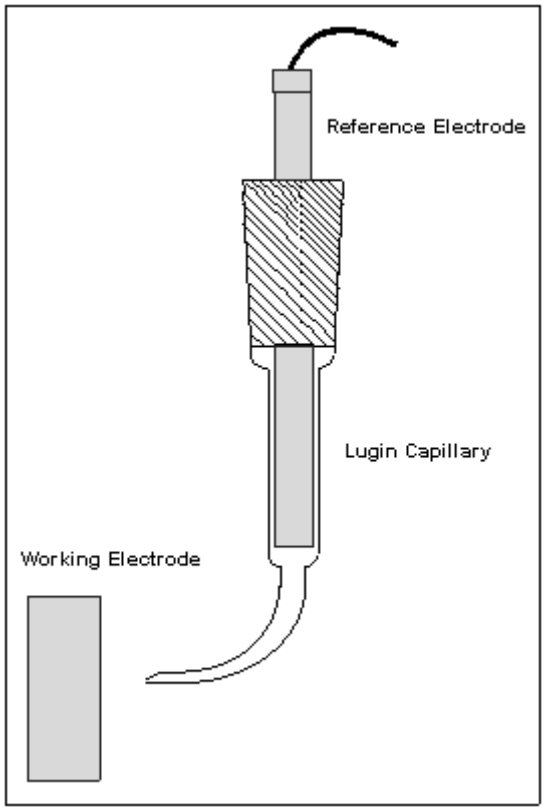

FIGURE 3.3. The Luggin-Haber Probe

reaction, a 100 mg/L solution of $NaHCO_3$ was added to maintain a pH between 5.0 and 5.5 limits. The pH was regularly measured experimentally using a pH meter (HANNA Instrument, Model pH210) to ensure that it remained within these limits.

3.4.1. CONDITIONING OF THE SOLUTION.

A 200mL 3%NaCl solution was added to the cell and the lid fitted. The gas sparge lines were inserted and the outlet ports were sealed except for one outlet line that passes through a bubbler to ensure that the system is sealed. A magnetic bar was placed inside the cell which was placed in a water bath heated by a thermally controlled hot plate (YellowLine MSC Basic C). The magnetic bar was stirred at a constant speed (around 300 rpm). Baseline rates increase by about 30% as the speed is raised from 0 to 100 rpm. Above this speed there is little influence of stirring on corrosion rate.

The solution is de-aerated with a 99.999% nitrogen gas for 30 minutes. This facilitates the removal of oxygen to below 10ppb. After the total removal of oxygen, the solution is saturated with CO_2 (99.999 % pure) at room temperature by passing it a rate of 70 ml/min.

3.4.2. PREPARATION OF THE WORKING ELECTRODE.

The mild steel electrode is abraided with a 600 grade silicon carbide paper then with 800 grade silicon carbide paper. After this the electrode is washed with distilled water,

degreased with acetone and then placed in an ultra sonic bath for 5 minutes. The electrode is then washed again with distilled water and directly used.

3.4.3. CONDITIONING OF THE WORKING ELECTRODE.

The working electrode is pre-corroded in the solution until a stable open circuit potential is obtained; this might take 30-60 minutes depending on the solution condition, temperature and pH. The equilibrium potential assumed by the metal in the absence of electrical connections to the metal is called the Open Circuit Potential, and denoted by the symbol E_{oc}

A stable E_{oc} indicates that the system being studied has reached a "steady state", i.e., the various corrosion reactions have assumed a constant rate. Some corrosion reactions reach steady state in a few minutes, while others may take several hours. Regardless of the time required, a computer-controlled system can monitor the E_{oc} and begin the experiment after it has stabilized.

The electrode is mounted in the cell and the solution is heated to the desired temperature while E_{oc} is being monitored. The quality of the (Open Circuit Potential) baseline determines the quality of all the other lines obtained by this experiment. At the end of the conditioning period, the surface of the electrode should be completely covered with a homogenous corrosion layer and exhibit a constant polarization resistance. If this layer doesn’t form homogenously, further corrosion during the experiment shall give

erroneous inhibition efficiency that may be mistakenly attributed to the corrosion inhibitor.

This can be checked by running the OCP until a stable reading that is not affected by stirring or the flow rate of the bubbling gas is obtained. E_{oc} is considered stable if the fluctuation in its value is ±1mV.

In case no stable reading is achieved, the electrode should be re-cleaned with 800 grade silicon carbide papers, immersed in 1M HCl solution for 30 seconds, and then rinsed with distilled water.

3.4.4. CORROSION RATE DETERMINATION BY THE MEASUREMENT OF THE LINEAR POLARIZATION RESISTANCE (LPR)

The corrosion rates are generally monitored using the Linear Polarization Resistance (LPR) method, via a computer controlled interface system. LPR data are collected by measuring the current density at the applied potential, with a scan rate of 10 mV/min and current interrupt 10 mV either side of E_{oc}. These measurements are recorded automatically at regular intervals over a certain period of time. To provide a baseline, the corrosion rate is measured by LPR prior to the addition of inhibitor, to assess the corrosivness of the environment being tested.

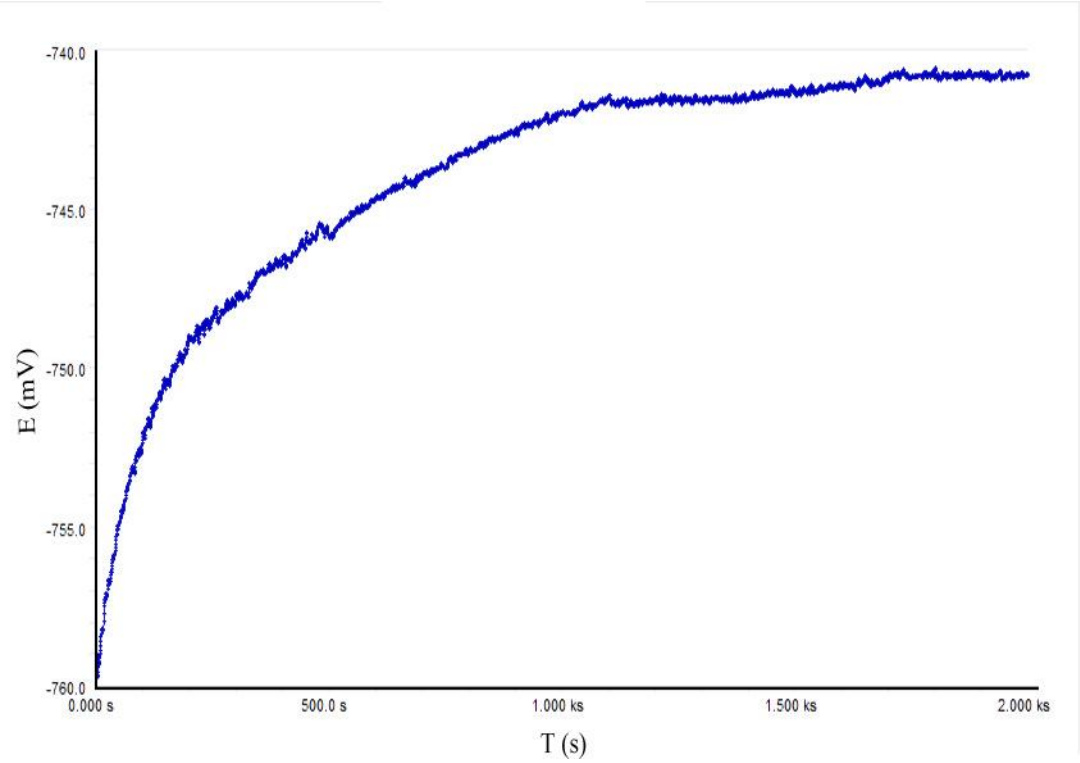

FIGURE 3.4. E_{oc} versus time for a preconditioned 3% NaCl solution at 40 ^{o}C

Experimental Parameters and Equipment Used

Tafel constants $\beta_a=\beta_c$ = 120 mV/decade

Scan rate = 0.166 mV/second

Scan Range = ±10 mV vs. E_{oc}

Initial E = - 10 mV vs. E_{oc}

Final E = +10 mV vs. E_{oc}

Sample period = 1 seconds

Sample Area = The total surface area of the cylindrical sample carefully measured and calculated utilizing a caliper, excluding the top surface covered by the Teflon washer.

Density = (7.87 g/cm^3)

Reference electrode = Standard Calomel

Auxiliary electrode = Graphite

Working electrode = Cylindrical Electrode made of AISI 1018 standard alloy.

Potentiostat= G 750 Potentiostat –Gamry (Hardware).

DC105 (Software)

Gamry Echem Analyst™ (Software)

3.4.5. CALCULATING CORROSION CURRENT.

The polarization resistance value is approximated from the stepwise potentiostatic polarization using a single small potential step, ΔE , 10 mV to − 10 mV. In this case, the specimen current, ΔI is measured after steady state is obtained, and then used to calculate ΔE/ΔI. The DC105 software converts the current (I) to current density (i_{corr}) automatically and the resulting plot is of i_{corr} versus E, where E is the applied potential. In the vicinity of i_{corr} = 0 (ΔE→0), the E vs. i_{corr} curve becomes linear, hence the polarization resistance can be considered as the slope of the best fit for the E vs. i_{corr} plot at i_{corr} = 0. In another word, the polarization resistance is:

$$R_p = \frac{\Delta E}{\Delta i}_{\Delta E \to 0} = \frac{\beta}{i_{corr}} \qquad \text{(Eq 3.1)}$$

The Stern-Geary constant β in volt units must be estimated or calculated to convert polarization resistance values to corrosion current density. Stern-Geary constant can be calculated from the corresponding Tafel slopes β_a and β_c.

$$\beta = \frac{\beta_a \beta_c}{2.303\,(\beta_a + \beta_c)} \qquad \text{(Eq 3.2)}$$

Where β_a is slope of the anodic Tafel reaction (V/decade) and β_c is slope of the cathodic Tafel reaction (V/decade). In the vicinity of I_{corr} = 0, βa and β_c are estimated to be 0.12 V/decade. The corrosion current then can be calculated as follows:

$$I_{corr} = \frac{\beta}{R_p} \qquad \text{(Eq 3.3)}$$

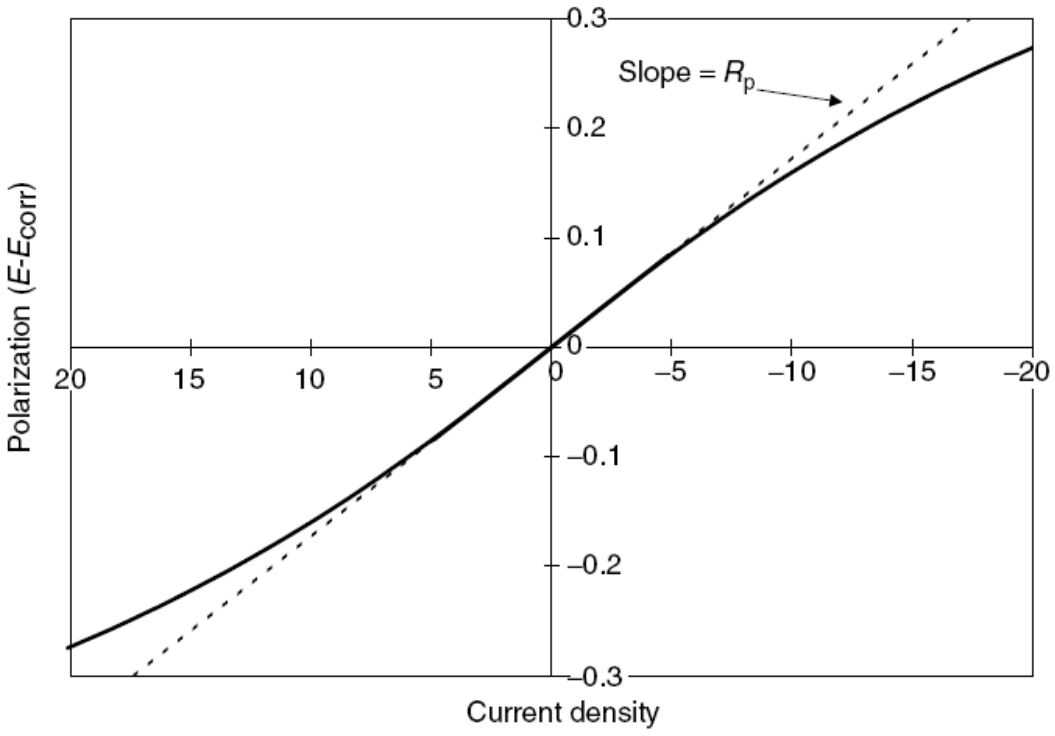

FIGURE 3.5. LPR plot for the C1018 electrode in brine saturated with CO_2

3.4.6. CALCULATING CORROSION RATE.

The corrosion rate is defined by IUPAC as the amount of substance S transferred per unit time at a specified surface. Faraday's law is: Q = n . F . M where n is the number of electrons involved in the electrochemical reaction, F is Faraday's constant 96486.7, and M is the number of moles of the substance involved in the reaction. By introducing the concept of equivalent weight, which is the mass of species S that will react with one Faraday of charge. For an atomic species, EW = AW/n (where AW is the atomic weight of the species). The number of moles of the substance M equals the weight of the reacted substance divided by the atomic weight M= W/AW. Faraday's law can be written as:

$$W = \frac{EW \times Q}{F} \qquad \text{(Eq 3.4)}$$

Where Q is the current passing though the reaction time: Q = I_{corr} .t

$$W = \frac{EW \times t}{F} I_{corr} \qquad \text{(Eq 3.5)}$$

The equation 3.5 can be used to calculate the corrosion rate, either in terms of penetration rate (CR) or mass loss rate (MR) depending on corrosion current.

$$CR = K_1 \frac{i_{corr}}{\rho} EW \qquad \text{(Eq 3.6)}$$

$$MR = K_2 i_{corr} EW \qquad \text{(Eq 3.7)}$$

CR is given as a thickness decrement per time unit, and its unit is determined by the choice of K_1, ρ and i_{corr} (see table 3.2). ρ is the density of the alloys used in corrosion testing. i_{corr} is the current density (the measured current , I_{corr} , divided by sample's area)

MR is the weight loss per surface area unit during time unit. K_2 is a constant (see table 3.2). EW is the mass of a given electrode alloy that will supply or react with one mole of electrons in the corrosion reaction.

If the corrosion rate is measured by (g/m^2 d), Eq 3.5 is divided by the expose area (m^2) and the time is determined by second per day (60second ×60 minute×24 hours). Substituting t and F values in Eq 3.5 and dividing by the sample's area A gives

$$MR\left({}^{g}/_{m^2.\,d}\right) = \frac{86400}{96486.7}.\ \frac{I_{corr}}{A} EW = \frac{86400}{96486.7}\ .\ i_{corr}\ EW \Rightarrow K_2 = 0.8953\ {}^{g}/_{A.\,d}$$

All the values of K_1 and K_2 can be calculated similarly. Table 3.2 shows the values of K_1 and K_2 for the different units of corrosion rate.

TABLE 3.2. Values of Constants for Use in Faraday's Equation Rate

A				
Penetration Rate Unit (CR)	**i_{corr} Unit**	**ρ Unit**	**K_1**	**Units of K_1[A]**
mpy	µA/cm^2	g/cm^3	0.1288	mpy g/ µA cm
mm/yr [B]	µA/m^2 [B]	kg/m^3 [B]	327.2	mm kg/A m y
mm/yr [B]	µA/cm^2	g/cm^3	3.27 ×10^{-3}	mm g/ µA cm y
B				
Mass Loss Rate Unit (MR)	**i_{corr} Unit**	**K_2**	**Units of K_2[A]**	
g/m^2 d[B]	A/m^{2B}	0.8953	g/Ad	
mg/dm^{2}d (mdd)	µA/cm^2	0.0895	mg cm^2/ µA dm^2 d	
mg/dm^{2}d (mdd)	A/m^{2B}	8.953 ×10^{-3}	mg m^2/ A dm^2 d	

[A]*EW is assumed to be dimensionless.*

[B]*SI unit.*

3.4.7. CALCULATING INHIBITION EFFICIENCY

The corrosion rate of the solution should first be determined in the absence of the inhibitor. The electrode is cleaned as previously described and conditioned as described in section 3.4.3. A calculated amount of the inhibitor is added to the cell to achieve the required concentration, and the open circuit potential is monitored until a steady-state is reached (a fluctuation of ±1mV in the E_{oc} value is considered as stable). A potentiostatic polarization scan is conducted in the range ±10 mV compared to the open circuit potential E_{oc}.

The inhibitor efficiency (%Protection) at a certain inhibitor concentration and under certain conditions (Salinity, temperature and CO_2 partial pressure) is calculated from the following general relation:

$$\text{Inhibitor Efficiency } \% = 100 \times \frac{(CR_{\text{uninhibited}} - CR_{\text{Inhibited}})}{CR_{\text{uninhibited}}} \qquad \text{(Eq 3.8)}$$

Where

$CR_{\text{uninhibited}}$ is the corrosion rate of the blank solution

$CR_{\text{inhibited}}$ is the corrosion rate after the addition of the inhibitor at a certain concentration.

For the Linear polarization resistance, CR is directly proportional to i_{corr} according to Eq 3.3, replacing the value of i_{corr} in Eq 3.6 gives and using CR value in Eq 3.8 gives:

$$\text{Inhibitor Efficiency \%} = 100 \times \frac{(Rp_{\text{inhibited}} - Rp_{\text{Uninhibited}})}{Rp_{\text{inhibited}}} \qquad \text{(Eq 3.9)}$$

Where $R_{p,\ \text{inhibited}}$ is the average reading of polarization resistance of the solution after the addition of the inhibitor and reaching a steady state (when the R_p readings stabilize). $R_{p,\ \text{uninhibited}}$ is the average reading of polarization resistance of the blank solution after reaching the steady state.

3.4.8. THE ADSORPTION ISOTHERM.

The protection efficiency is directly related to the surface coverage of the electrode by the corrosion inhibitor. The plot of protection efficiency against concentration of the corrosion inhibitor at a certain temperature and gas composition is called Adsorption Isotherm. This plot shows how effective the corrosion inhibitor is at that concentration (Figure 3.6).

Usually the performance of the corrosion inhibitor is defined by concentration and protection efficiency, or concentration against corrosion rate. (e.g 25 ppm to achieve 95% protection or to achieve 5 mpy)

There are two areas of interest in the isotherm, the range of protection at low concentrations where the packing of adsorption layer is expected to be monolayer and the range at high concentration where the packing of adsorption layer is expected to me multilayer. Usually the recommended dosage is the concentration at which the corrosion inhibition reaches 95 % protection.

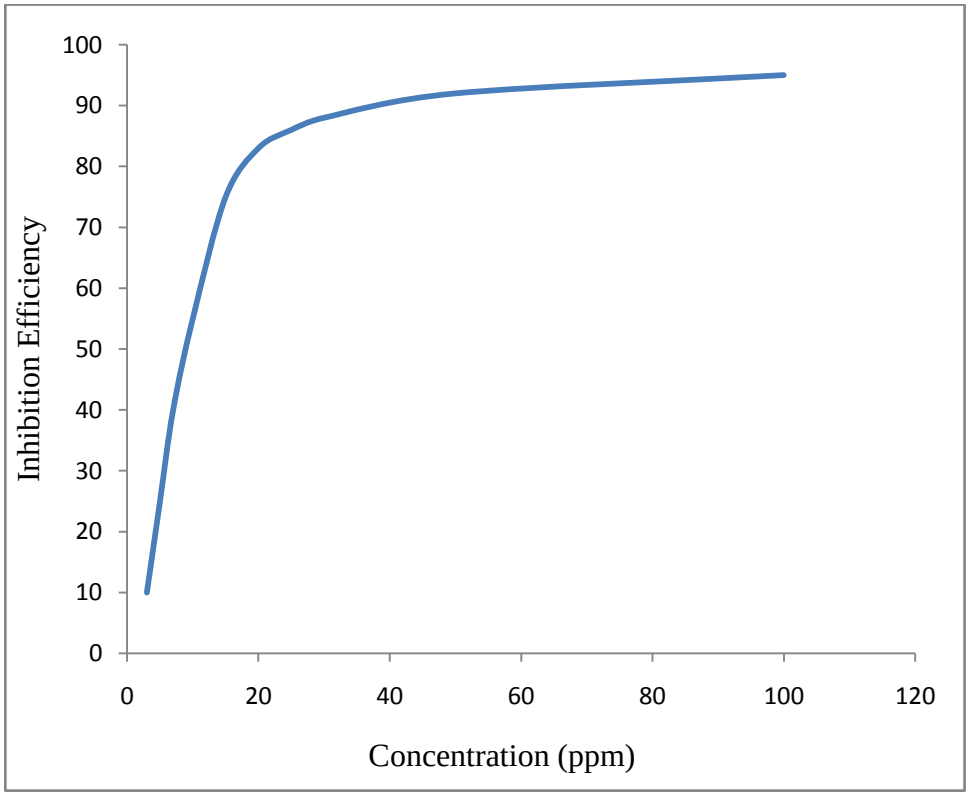

FIGURE 3.6. Inhibition Efficiency Versus Concentration.

3.5. POTENTIOSTATIC POLARIZATION - TAFEL PLOTS

The value of either the anodic or cathodic current at E_{oc} is called the Corrosion Current, I_{corr} which is used to calculate the corrosion rate of the metal. Unfortunately, I_{corr} cannot be measured directly. However, it can be estimated using electrochemical techniques. In any real system, I_{corr} and Corrosion Rate are a function of many system variables including the type of metal, the solution composition, temperature, the solution movement, and the metal history.

Potentiostatic polarization is an electrochemical technique used to measure the corrosion current I_{corr} and Tafel Constants β_a and β_c. Tafel constants can be used with polarization resistant (Rp) and electrical impedance spectroscopy to calculate the corrosion current density (i_{corr}).

A potentiostatic polarization -Tafel Plot is obtained for a specimen by sweeping the polarization potential in the range from −300 mV to +300 mV from the corrosion potential, E_{corr}.

An E versus log I plot is called a Tafel plot (Figure 3.7). The y-axis is potential and the *x*-axis is the logarithm of absolute current or the current density. The theoretical currents for the anodic and cathodic reactions are shown as straight lines. The curved line is the total current (i.e the sum of the anodic and cathodic currents). This is the measured current during the sweeping of the potential of the metal with the potentiostat. The use of

a log axis is necessary because of the wide range of current values obtained during a corrosion experiment.

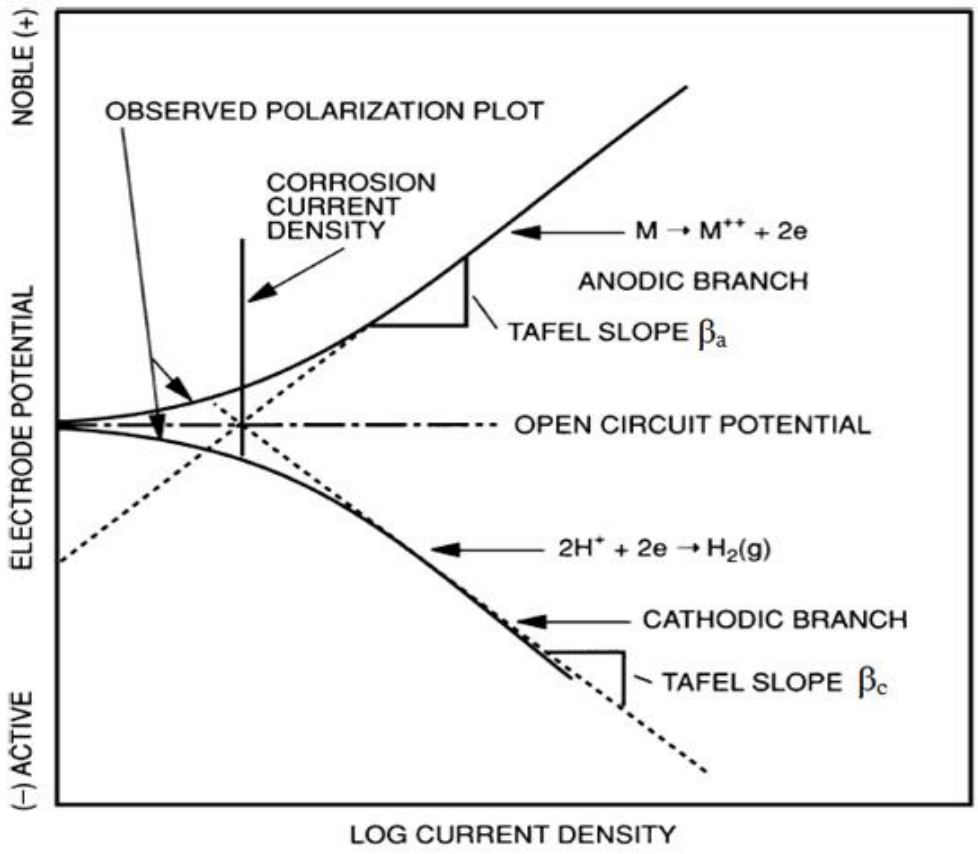

FIGURE 3.7. Tafel plot

A classic Tafel analysis involves extrapolating the linear portions of the potential versus log current plots back to their intersection. The value of either the anodic or the cathodic current at the intersection is I_{corr}. Unfortunately, many real world corrosion

systems do not provide regions where the plots are sufficiently linear to permit accurate extrapolation. Gamry Instruments DC105 DC Corrosion Techniques software performs a more sophisticated numerical fit to the Butler-Volmer equation.

$$I = I_a + I_c = I_{corr}(e^{(2.3(E-Eoc)/\beta_a)} - e^{(-2.3(E-Eoc)/\beta_c)}) \qquad \text{(Eq 3.10)}$$

The measured data are fitted to Butler-Volmer equation and the values of E_{corr}, I_{corr}, βa, and βc are obtained from the fit. The curve fitting method does not require a fully developed linear portion for the curves.

The cell used for this experiment is same as that used for the linear polarization resistance measurements.

Experiment Parameters.

Scan rate = 0.166 mV/second

Scan Range = ±250 mV vs. E_{oc}

Initial E = - 250 mV vs. E_{oc}

Final E = +250 mV vs. E_{oc}

Sample interval = 2 seconds (this is the time interval between two successive readings)

Sample Area = the total surface are of the cylindrical sample carefully

measured and calculated utilizing a caliper excluding the surface covered by the Teflon washer.

Density = 7.87 g/cm^3

Reference electrode = Standard Calomel

Auxiliary electrode = Graphite

Working electrode = AISI 1018

Potentiostat: G 750 Potentiostat –Gamry (Hardware).

DC105 (Software)

Gamry Echem Analyst™ (Software)

3.5.1. CALCULATING CORROSION CURRENT.

The corrosion current, I_{corr} is calculated from the empirical relation found by Stern–Geary [5].

$$I_{corr} = \frac{\beta_a \beta_c}{2.3\ R_p (\beta_a + \beta_c)} \qquad \text{(Eq 3.11)}$$

Where:

I_{corr} =corrosion current in µA

R_p = Polarization resistance

β_a, β_c = Tafel Constants

3.5.2. CALCULATING CORROSION RATE

The corrosion rate is calculated according to Eq 3.6 or Eq 3.7.

3.5.3. CALCULATING THE INHIBITOION EFFICIENCY

The corrosion rate of the solution in the absence of the inhibitor should be first determined. The electrode is cleaned as previously described and conditioned as described in section 3.4.3. A calculated amount of the inhibitor is added to the cell to achieve the desired concentration; the open circuit potential is monitored until a steady-state is reached (a fluctuation of ±1mV in the E_{oc} value is considered as stable). A potentiostatic polarization scan is conducted in the range ±250 mV compared to the open circuit potential E_{oc}

The inhibitor efficiency at a certain inhibitor concentration and under a certain conditions (Salinity, temperature and CO_2 partial pressure) is calculated from the relation,

$$\text{Inhibitor Efficiency } \% = 100 \times \frac{(CR_{\text{uninhibited}} - CR_{\text{Inhibited}})}{CR_{\text{uninhibited}}} \qquad \text{(Eq 3.12)}$$

Where

$CR_{uninhibited}$ is the corrosion rate of the blank solution

$CR_{inhibited}$ is the corrosion rate after the addition of the inhibitor.

3.6. DETERMINATION OF SURFACE TENSION.

The purpose of measuring the surface tension of the synthesized compounds at different concentrations is to find their critical micelle concentration in order to see if they are adsorbed on the surfaces of the mild steel electrode used in the electrochemical study as micelles or as single molecules. The measurements were carried out using a Fisher Scientific Manual Model 20 Surface Tensiometer.

The FISHER surface tensiometer, Model 20, is used to determine the apparent surface tension and interfacial surface tension of liquids. Its mode of operation is based on the du Nouy ring method that is described in the ASTM standards D 1331 (surface tension of detergents) and D971 (interfacial tension between two immiscible liquids). In this method, a thin platinum-iridium ring of precisely known diameter is suspended from a counter-balanced lever arm. The arm is held horizontally by torsion applied to a taut stainless steel wire, to which is clamped. Increasing the torsion in the wire raises the arm and the ring, which carries with it a film of the liquid in which it is immersed. The force necessary to pull the test ring free from this surface film is measured. The tensiometer shows this apparent surface tension on a calibrated dial. The dial reading can be use directly for comparative studies or converted to the “true” values by using a correction factor chart.

3.6.1. INSTRUMENT AND SAMPLE PREPARATION

In the determination of surface tension experiment, a careful preparation of the sample and the surface tensiometer must precede the actual handling of the instrument. The sample should be placed in a glass beaker or cylindrical vessel with a diameter of at least 45 millimeters. The glassware is immersed in a hot cleaning solution of chromic acid, and then it is rinsed thoroughly with tap water, then with distilled water. It should be drained in an inverted position over a clean cloth, unless it is to be used immediately

The platinum -iridium ring should be cleaned by rinsing it in petroleum naphtha or benzene, then by rinsing in methyl ethyl ketone. The ring should then be heated in the oxidizing portion of a gas flame.

Surface tension depends on temperature which must be specified whenever surface tension values are reported. In this study all measurements were done on solutions at 40 ^{o}C.

For measurements on 3% NaCl solutions saturated with CO_2 the following steps were carried out. The 3% NaCl solution was pre-saturated with CO_2 in a closed cell then heated using to and thermostated at the test temperature a thermostate-controlled hotplate before a calculated volume of the saturated surfactant solution was added to avoid foaming during the gas sparging. After the addition of the surfactant, the cell was purged with CO_2 to maintain the solution saturation. A 50 mL of the solution is transferred to a

100mL beaker previously warmed to 40 ^{o}C using a pipette, and the surface tension was determined immediately to ensure that the measurement is as close as possible to 40 ^{o}C.

3.6.2. MEASURING SURFACE TENSION

The cleaned platinum -iridium ring should first be attached to the hook at the end of the lever arm. The arrest mechanism should be holding the arm at this time. The liquid to be measured is transferred to the clean glass vessel and placed on the sample table. The sample table is moved around until it is directly beneath the platinum-iridium ring.

The sample table is raised until the ring is about 1/8 inch below the surface of the test liquid. The torsion arm is now released and the instrument adjusted to a zero reading. The knob on the right side of the instrument case is adjusted until the index and its image are exactly in line with the reference mark on the mirror. The sample table may be raised or lowered if necessary be means of the knob adjustment underneath the table but one must ensure that the ring remains immersed in the liquid.

Then the knob beneath the main dial on the front of the instrument's case is turned until the vernier reads zero on the outer scale of the dial. The sample table is lowered until the ring is on the surface of the liquid. The knob on the right side of the instrument's case is used to keep the index lined up with the reference mark on the mirror. As the sample table is lowered and the surface of the liquid will becomes distended the index must be kept on the reference. The two nearly simultaneous steps of carefully lowering the sample table and ensuring that the index is kept on the reference are continued until the distended

film at the surface of the liquid breaks. The scale reading at the breaking point of the distended film is the apparent surface tension.

3.6.3. SYNTHESIS OF THE AMIDOAMINES AND IMIDAZOLINES

N-[2-(2-aminoethylamino)-ethyl]-octadecanamide (1).

A mixture of octadecanoic acid (100 mmol) and N-(2-aminoethyl)-1,2-ethanediamine (diethylenetriamine DETA) (200 mmol) was heated to 120 ^{o}C for 30 minutes, then heated to 160 ^{o}C for 90 minutes. The reaction mixture was cooled and recrystallized from methanol (50 mL). The white solid precipitate is a mixture of mono and diamide. The filtrate was frozen and recrystallized in methanol. The final precipitate (amidoamine **1**) is a white solid (4.92 g). The product (**1**) is a white wax with a melting point of 105 ^{o}C. It dissolves in hot methanol and gives a hazy solution when added to water even at low concentrations (200 ppm)

Yield: 13% M.P.= 105 °C

ν_{max} (Neat): 3296, 3081, 2915, 2847, 2015, 1637, 1550, 1465, 1277, 1127, 895 and 722 cm^{-1}.

δ_H ($CDCl_3$): 0.86 (3H, t, *J* 6.7 Hz), 1.25 (28H, m), 1.60 (2H, m), 2.10 (3H, NHs), 2.15 (2H, t, *J* 7.5 Hz), 2.65 (2H, t, *J* 5.8 Hz), 2.74 (2H, t, *J* 5.7 Hz), 2.79 (2H, t, *J* 5.6 Hz), 3.3 (2H, m), 6.28 (1H, CONH).

δ_C ($CDCl_3$): 14.13, 22.70, 25.81, 29.38 (2C), 29.55, 29.71 (7C), 31.93, 36.82, 38.83, 41.10, 48.43, 51.39, 173.51.

N-[2-(2-octadecanoylamino-ethylamino)-ethyl]octadecanamide (2)

A mixture of octadecanoic acid (25 mmol) and N-(2-aminoethyl)-1,2-ethanediamine (DETA) (12.5 mmol) was heated to 160 ^oC for three hours. The reaction mixture was cooled and recrystallized from methanol (50 mL). The white solid precipitate (**2**) is a pure diamide (5.8 g). The filtrate was discarded.

The product (**2**) is a white solid with a melting point of 102-103 ^oC. It is insoluble in water, hot methanol, isopropanol and acetone, and in aromatic solvents toluene and xylene. It is partially soluble in hot xylene.

Yield: 73%. M.P. =102-103 ^oC;

$\nu_{max.}$ (Neat) 3289, 3090, 2956, 2846, 2051, 1635, 1560, 1461, 1381, 1263, 1200, 1128 and 721 cm^{-1}.

δ_H ($CDCl_3$): 0.88 (6H, t, *J* 7.0 Hz), 1.26 (56H, m), 1.51 (1H,br, s), 1.63 (4H, quint, *J* 7.0 Hz), 2.19 (4H, t, *J* 7.6 Hz), 2.76 (4H, t, *J* 5.8 Hz), 3.34 (4H, apparent q , *J* 5.8 Hz), 5.90 (2H, br s).

δ_C ($CDCl_3$): 14.12, 22.69, 25.80, 29.39 (2 times), 29.71 (10 times), 31.93, 36.83, 39.10, 48.56, 173.61.

N-[2-(2-aminoethylamino)-ethyl]-dodecanamide (3)

A mixture of dodecanoic acid (25 mmol) and N-(2-aminoethyl)-1,2-ethanediamine (DETA) (12.5 mmol) was heated to 160 ^{o}C for two hours. The reaction mixture was cooled recrystallized from methanol (50 mL). The white solid precipitate is a diamide. The filtrate was evaporated to remove methanol and the resulting white solid was dissolved in water then extracted using methylene chloride to remove any remaining DETA. The extract was dried using anhydrous sodium sulfate. The residual solvent was removed by evaporation. The solid product was dissolved in ethyl ether and extracted using hexane. The filtrate was recrystallized from hexane giving amidoamine (**3**).

The product (**3**) is a white solid with a melting point of 91 ^{o}C. It is partially soluble in water, and is soluble in methanol at room temperature. The product mass is 1.55 g.

Yield: 22 %. M.P. = 91-92 ^{o}C

ν_{max} (Neat) 3290, 3079, 2915, 2847, 2176, 2051, 1636, 1550, 1465, 1334, 1277, 1128, 1065, 895 and 722 cm^{-1}.

δ_H ($CDCl_3$): 0.88 (3H, t, *J* 6.7 Hz), 1.25 (16H, m), 1.60 (2H, m), 2.18 (2H, t, *J* 7.6 Hz), 2.70 (2H, t, *J* 5.0 Hz), 2.76 (2H, t, *J* 5.8 Hz), 2.83 (2H, t, *J* 5.5 Hz), 3.28 (3H, br, NHs), 3.34 (2H, apparent q, J 5.8 Hz), 6.46 (1H, CONH).

δ_C ($CDCl_3$): 14.13, 22.69, 25.84, 29.37, 29.39, 29.43, 29.56, 29.65 (2C), 31.92, 36.84, 39.04, 41.28, 48.55, 51.31, 173.67.

N-[2-(2-dodecanoylamino-ethylamino)-ethyl]dodecanamide (4)

A mixture of dodecanoic acid (50 mmol) and N-(2-aminoethyl)-1,2-ethanediamine (DETA) (25 mmol) was heated to 160 ^{o}C for three hours. The reaction mixture was cooled and recrystallized from methanol (50 mL). The white solid precipitate (**4**) is a diamide. The filtrate was discarded

The product (**4**) had a melting point of 101 ^{o}C. It is insoluble in water and partially soluble in hot methanol. The product mass is 7.8 g.

Yield: 67 %. M.P. = 101 ^{o}C

$\nu_{max.}$ (Neat) 3285, 3095, 2956, 2917, 2875, 2846, 2177, 2051, 1947, 1637, 1565, 1458, 1382, 1250, 1167, 1128, 939 and 722 cm^{-1}.

δ_H ($CDCl_3$): 0.88 (6H, t, *J* 7.0 Hz), 1.26 (33H, m), 1.63 (4H, quint, *J* 7.0 Hz), 2.19 (4H, t, *J* 7.6 Hz), 2.77 (4H, t, *J* 5.7 Hz), 3.34 (4H, apparent q , *J* 5.7 Hz), 5.95 (2H, br s).

δ_C ($CDCl_3$): 14.10, 22.68, 25.82, 29.40 (3C), 29.55, 29.63 (2C), 31.91, 36.81, 39.09, 48.55, 173.66.

2-[2-{2-(2-Aminoethylamino)-ethylamino}ethylaminoethyl]-octadecanamide (5)

A mixture of octadecanoic acid (25 mmol) and (tetraethylenepentaamine TEPA) (35 mmol) was heated to 160 ^{o}C for two hours. The disappearance of TEPA peaks from the ^{1}H NMR spectra of the reaction solution indicated the completion of the reaction. The

reaction mixture was cooled and recrystallized from methanol (50 mL). The yellowish-to-white waxy solid precipitate (**5**) is a monoamide. ^{1}H NMR spectrum revealed the presence of minor impurities (3-5%). The product (**5**) had a melting point of 63-64 ^{o}C. It is soluble in water and methanol at room temperature. The product mass is 4.2 g.

Yield: 54 %. M.P. = 63-64 ^{o}C

ν_{max} (Neat): 3294, 3077, 2915, 2846, 2051, 1636, 1550, 1464, 1278, 1123 and 722 cm^{-1}.

δ_H ($CDCl_3$): 0.88 (3H, t, *J* 6.7 Hz), 1.25 (28H, m), 1.60 (2H, m), 2.18 (2H, m), 2.23 (5H, br, NHs), 2.68 (2H, m), 2.75 (10H, s), 2.86 (2H, m), 3.36 (2H, m), 6.60 ((1H, br).

δ_C ($CDCl_3$): 14.14, 22.70, 25.84, 29.37, 29.42, 29.56, 29.71 (9C), 31.93, 36.78, 38.02, 38.94, 41.47, 48.69, 48.81, 48.94, 49.05, 51.97, 173.5.

2-[2-{2-(2-octadecanoylaminoethylamino)-ethylamino}ethylaminoethyl]-octadecan amide (6)

A mixture of octadecanoic acid (25 mmol) and (tetraethylenepentaamine TEPA) (12.5 mmol) was heated to 160 ^{o}C for two hours. The disappearance of TEPA peaks from the ^{1}H NMR spectra of the reaction solution indicated the completion of the reaction. The reaction mixture was cooled and recrystallized from methanol (50 mL). The white solid precipitate (**6**) formed is a diamide. The filtrate was discarded. ^{1}H NMR spectrum revealed the presence of minor impurities (3-5%). The product weight is 6.6 g.

The amidoamine (**6**) is soluble in cold methanol. It has a melting point range between 84 and 85 ^{o}C. It gives a cloudy solution in fresh water.

Yield: 73 %. M.P. =84-85 ^{o}C

ν_{max} (Neat): 3297, 2914, 2847, 2050, 1638, 1550, 1465, 1264, 1121 and 720 cm^{-1}.

δ_H ($CDCl_3$): 0.88 (6H, t, *J* 6.7 Hz), 1.25 (56H, m), 1.62 (4H, m), 2.18 (4H, t, *J* 7.5 Hz), 2.80 (15 H, m), 3.41 (4H, m), 6.75 (2H, br).

δ_C ($CDCl_3$): 14.13, 22.70, 25.81, 29.38, 29.46, 29.59, 29.73 (9 times), 31.64, 36.74, 38.27, 47.77, 48.23, 48.60, 173.74.

N-[2-(2-decanoylamino-ethylamino)-ethyl]octadecanamide (7)

A solution of decanoic acid (10 mmol) and amidoamine (**1**) (10 mmol) were heated to 160 ^{o}C for 80 minutes. It was difficult to determine the end of the reaction. Samples of the reaction solution were taken periodically and their ^{1}H NMR spectra were taken. The disappearance of the carboxylic hydrogen peak of decanoic acid was considered as an indication of the completion of the reaction. The reaction mixture was cooled and recrystallized from methanol (50 cm^{3}). The white solid precipitate formed was a mixture of N-[2-(2-octadecanoylamino-ethylamino)-ethyl]octadecanamide (amidoamine **2**) and N-[2-(2-decanamidoethylamino)ethyl] octadicanamide **(7)**. The filtrate was recrystallized in

methanol giving amidoamine **(7)**. The ^{1}H NMR spectrum revealed the presence of minor impurities (3-5%). The product mass is 0.97 gr

The product (**7**) is white wax which has a melting point in the range 86 to 87 ^{o}C. It is soluble in hot methanol and gives a cloudy and very foamy solution in water. Its solubility in water is limited

Yield: 18.5 %. M.P. =86-87 ^{o}C .

ν_{max} (Neat): 3298, 3055, 2915, 2848, 2051, 1945, 1638, 1550, 1465, 1268, 1164, 1123, 857 and 719 cm^{-1}.

δ_H ($CDCl_3$): 0.88 (6H, t, *J* 7.0 Hz), 1.26 (40H, m), 1.62 (5H, m), 2.19 (4H, t, *J* 7.6 Hz), 2.79 (4H, t, *J* 5.5 Hz), 3.36 (4H, apparent q, *J* 5.6 Hz), 6.47 (2H, amide NHs, br).

δ_C ($CDCl_3$): 14.13 (2C), 22.70 (2C), 25.83 (2C), 29.32, 29.39, 29.43 (2C), 29.52, 29.59, 29.73 (10C), 31.89, 31.94, 36.75 (2C), 38.75 (2C), 48.48 (2C), 173.86 (2C).

N-[2-(2-hexanoylamino-ethylamino)-ethyl]octadecanamide (8)

A mixture of hexanoic acid (10 mmol) and amidoamine **1** (10 mmol) were heated to 160 ^{o}C for 1 hour. It was difficult to determine the end of the reaction. Samples of the reaction solution were taken periodically and their ^{1}H NMR spectra were taken. The disappearance of the carboxylic hydrogen peak of hexanoic acid was considered as an indication of the completion of the reaction. The reaction mixture was cooled and

recrystallized from methanol (50 mL). The white solid precipitate formed was pure amidoamine (**2**). The filtrate was recrystallized from methanol giving amidoamine (**8**) which is N-[2-(2-decanamidoethylamino)ethyl] octadicanamide. ^{1}H NMR spectrum revealed the presence of minor impurities (3-5%). The product (**8**) is white wax with a melting point of 83-84 ^{o}C. It is soluble in hot methanol and gives a cloudy and very foamy solution in water. Its solubility in water is limited. The product mass was 0.82 g.

Yield: 17.5%., M.P. =83-84 ^{o}C

ν_{max} (Neat): 3296, 2916, 2848, 2177, 2051, 2639, 1551, 1464, 1381, 1264, 1122, 1034 and 719 cm^{-1}.

δ_H ($CDCl_3$): 0.88 (6H, overlapping t, *J* 7.0 Hz), 1.26 (33H, m), 1.62 (4H, quint, J 6.7 Hz), 2.19 (4H, t, *J* 7.6 Hz), 2.78 (4H, t, *J* 5.8 Hz), 3.36 (4H, apparent q, *J* 5.5 Hz), 6.29 (2H, amide NHs, br).

δ_C ($CDCl_3$): 13.98, 14.13, 22.44, 22.70, 25.47, 25.82, 29.38, 29.41, 29.57, 29.72 (9C), 31.53, 31.94, 36.69, 36.75, 38.80 (2C), 48.51 (2C), 173.95 (2C).

1-(2-aminoethyl)-2-heptadecanyl-2-imidazoline (9)

A mixture of octadecanenitrile (38.08 mmol) and diethylenetrimine (DETA) (76.16 mmol) were heated to 150 ^{o}C. When the reactants reached the required temperature 112 mg of elemental sulfur were added and the heating was continued for 40 minutes. Thereafter, another portion of sulfur (72 mg) was added and the heating of the reaction

mixture was continued at 150 ^{o}C for an additional 1 h. A third portion of sulfur (62mg) was added and the heating of the reaction mixture was continued at 150 ^{o}C for another 20 minutes. The reaction solution turned dark blue indicating the presence of sulfur radicals. Evolution of NH_3 gas was observed as it bubbled through the connected U-tube containing mineral oil. The completion of the reaction was indicating by the stopping of the evolution of NH_3 gas. The reaction mixture was cooled and dissolved in methylene chloride (50 mL). The organic layer was carefully washed with water (4×750 cm^3) to remove the unreacted DETA. The organic layer was dried with anhydrous Na_2SO_4 and concentrated to obtain the imidazoline mixture as a yellowish solid; which was recrystallized from ethyl ether. The filtrate was concentrated giving 7g of compound (**9**). The product is a yellow wax, with a melting point of 69-70 ^{o}C. It is partially soluble in water and polar solvents like methanol at room temperature.

Yield: 60 % M.P. =69-70 °C.

ν_{max} (Neat): 3288, 3243, 2915, 2847, 1661, 1605, 1551, 1466, 1249, 1090, 1022, and 719 cm^{-1}.

δ_H ($CDCl_3$) 0.87 (3H, t, *J* 7.0 Hz), 1.25 (30 H, m), 1.62 (2H, quint, *J* 7.4 Hz), 2.20 (2H, t, *J* 7.8 Hz), 2.84 (2H, t, *J* 6.1 Hz), 3.12 (2H, t, *J* 6.1 Hz), 3.26 (2H, t, *J* 9.7 Hz), 3.69 (2H, t, *J* 9.5 Hz).

δ_C ($CDCl_3$): 14.03, 22.59, 26.40, 27.93, 29.29 (2C), 29.44, 29.60 (9C), 31.83, 40.49, 50.15, 50.22, 51.92, 168.00.

N,N'-Di-2,2'-[2-heptadecanyl-2-imidazolinyl]diethylamine (10)

A mixture of octadecanenitrile (15 mmol) and tetraethylenepentamine (TEPA) (23 mmol) was heated to 150 ^{o}C. When the reactants reached the required temperature, 100 mg of elemental sulfur were added and the heating was continued for 25 minutes. Thereafter, another portion of sulfur (50 mg) was added and the heating was continued at 150 ^{o}C for an additional period of 25 minutes. A third portion of sulfur (50mg) was added and the heating was continued at 150 ^{o}C for another 10 minutes. The reaction solution turned dark blue indicating the presence of sulfur radicals. Evolution of NH_3 gas was observed as it bubbled through the connected U-tube containing mineral oil. The completion of the reaction was indicating by the stopping of the evolution of NH_3 gas. The reaction mixture was cooled and dissolved in methylene chloride (50 cm^3). The organic layer was carefully washed with water (5×750 cm^3) to remove the unreacted TEPA. The organic layer was dried with anhydrous Na_2SO_4 and concentrated, and then it was recrystallized from pentane. The final product **10** is a yellowish solid and its final mass was (1.76 g). ^{1}H NMR spectrum revealed the presence of minor impurities (3-5%). The imidazoline **10** were not purified further and used as such for the corrosion inhibition study. Because of its impure nature, the elemental analysis of compound 10 was not carried out.

The imidazoline **10** is dark yellow soft wax, with a melting point of 39-40 ^{o}C. The product is partially soluble in water and polar solvents like methanol at room temperature.

Yield: 34% M.P. =39-40 °C.

$\nu_{max.}$ **(Neat)** 3290, 2915, 2847, 1636, 1550, 1467, 1277, 1127, 895, and 721 cm^{-1}.

δ_H **($CDCl_3$)** 0.88 (6 H, t, *J* 7.0 Hz), 1.26 (57 H, m), 1.63 (4 H, m), 2.12 (4H, t, *J* 7.7 Hz), 2.78 (4H, m), 3.21 (4H, t, *J* 6.2 Hz), 3.28 (4H, t, *J* 9.7 Hz), 3.68 (4H, t, *J* 9.6 Hz).

δ_C **($CDCl_3$)** 13.97, 22.54, 26.33, 27.84, 29.21, 29.27, 29.40, 29.49, 29.50 (2C), 29.55 (6C), 31.78, 47.24, 48.16, 50.37, 51.85, 167.83. The compound is symmetric as such it has 42/2 carbon signals.

1-[2-{2-(2-Aminoethylamino)-ethylamino}ethyl]-2-heptadecanyl-2-imidazoline (11)

A mixture of octadecanenitrile (7.5 mmol) and tetraethylenepentamine (TEPA) (24.8 mmol) was heated to 150 ^oC. When the reactants reached the required temperature 75 mg of elemental sulfur were added and heating of the reaction mixture was continued for 25 minutes. Thereafter, another portion of sulfur (60 mg) was added and the heating of the reaction mixture was continued at 150 ^oC for an additional period of 25 minutes. A third portion of sulfur (50mg) was added and the heating of the reaction mixture was continued at 150 ^oC for another 10 minutes. The reaction solution turned dark blue indicating the presence of sulfur radicals. Evolution of NH_3 gas was observed as it bubbled through the connected U-tube containing mineral oil. The completion of the reaction was indicating by the stopping of the evolution of NH_3 gas. The reaction mixture was cooled and dissolved in methylene chloride (50 mL). The organic layer was carefully

washed with water (4×250 cm^3) to remove the unreacted TEPA. The organic layer was dried with anhydrous Na_2SO_4 and concentrated to obtain the imidazoline (**11**) as a yellowish solid with a mass of (2.02 g) . ^1H NMR spectrum revealed the presence of minor impurities (3-5%). The imidazoline **11** was not purified further and used as such for the corrosion inhibition study. Because of its impure nature the elemental analyses of the imidazoline **11** were not carried out.

The product is yellow soft wax with a melting point of 40-41 ^oC. It is partially soluble in water and polar solvents like methanol at room temperature.

Yield 61%, M.P. =40-41 °C.

$\nu_{max.}$ (Neat) 3301, 3244, 2245, 2050, 1606, 1551, 1464, 1248, 1122 ,1007, 783 and 721 cm^{-1}.

δ_H ($CDCl_3$) 0.88 (3H, t, *J* 7.0 Hz), 1.25 (30H, m), 1.52 (2H, m), 1.63 (2H, m), 2.19 (2H, t, *J* 7.9 Hz), 2.68 (2H, t, *J* 6.0 Hz), 2.75 (6H, m), 2.81 (2H, t, *J* 5.8 Hz), 3.19 (2H, t, *J* 6.2 Hz), 3.27 (2H, t, *J* 9.6 Hz), 3.67 (2H, t, *J* 9.6 Hz).

It was difficult to remove minor impurities from the compound. An approximate analysis if the ^{13}C NMR spectrum is as follows:

δ_C ($CDCl_3$): 13.76, 22.32, 26.15, 27.64, 29.05 (2C), 29.33 (10C), 31.57, 41.43, 47.07, 47.84, 48.64, 48.92, 50.21, 51.62, 52.03, 167.49.

CHAPTER 4

RESULTS AND DISCUSSION

4.1. SYNTHESIS

In this work, thus, 11 polyamine derivates were synthesized by the reaction of polyamines with fatty acids of different chain lengths to obtain the corresponding amido-amines and imidazolines. The polyamines used were N-(2-amino ethyl)-1,2-ethanediamine or and N-(2 amino ethyl)-N´-{2-{(2-aminoethyl)amino}ethyl}-1,2-ethanediamine) or tetra ethylene penta amine (TEPA). The TEPA used for this work was purified to get a pure N-(2-amino -ethyl)-N´-{2-{(2-aminoethyl)amino}ethyl}-1,2-ethanediamine.

4.1.1. PREPARATION OF AMIDES OF THE SAME FATTY ACID.

The synthesized amido-amines have the following general structures

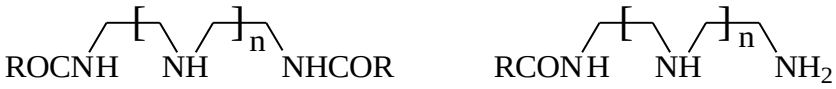

The fatty acids used for the synthesis were octadecanoic acid and dodecanoic acid. The compounds were prepared by heating a polyamine and a fatty acid mixture in the ratio mentioned in chapter 3 to 160 ^{o}C for around 1 hour, and then the reaction mixture

was cooled and re-crystallized in hot methanol to remove the remaining acid and polyamine (Scheme 4.1).

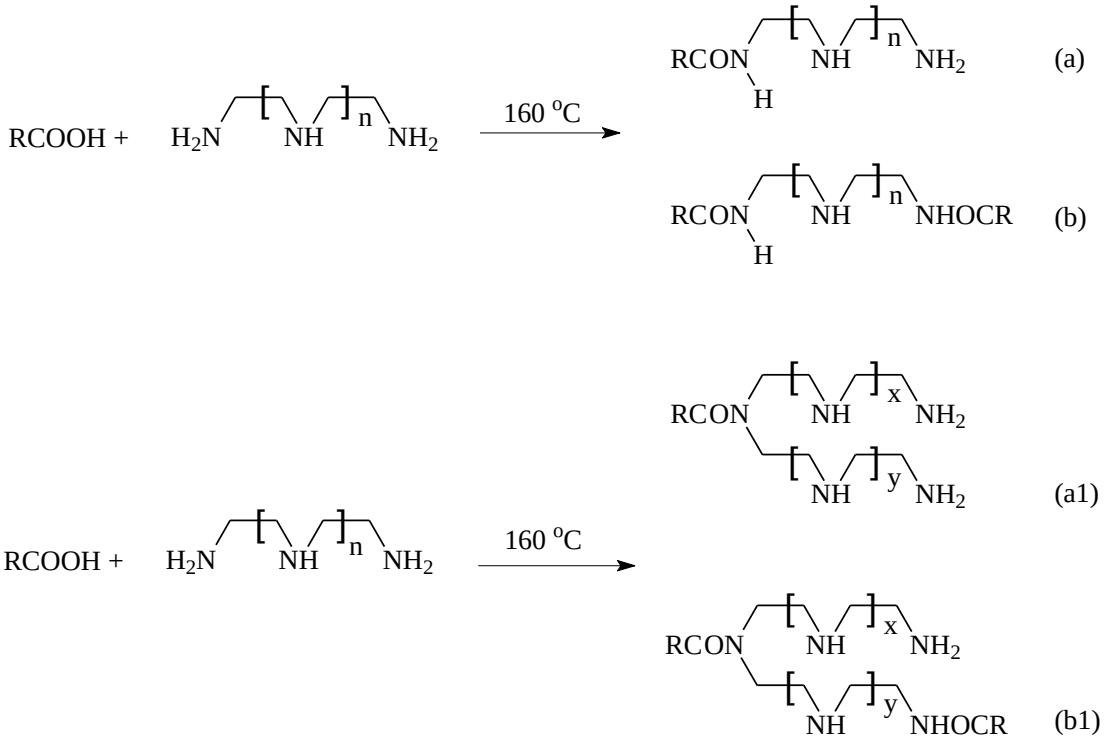

Scheme 4.1

The reaction product is a mixture of mono and diamides. The monoamide could have the structure **a** or $\mathbf{a_1}$ depending on which amine will the acid attack, the primary amine or the secondary amine, consequently the diamide will have the structure **b** or $\mathbf{b_1}$**.**

The use of different polyamines and different polyamine to acid ratios was intended to vary the solubility in water and the adsorption behavior and in turn the corrosion inhibition efficiency of the amide molecules. It also shows which functional group, the

amide group or the terminal amine group, is responsible for corrosion inhibition as compounds of structure (**b**) do not have a terminal amine.

The monoamides have a higher solubility in methanol than the diamides, which permits their separation by recrystallizations from their solution in hot methanol; the diamide precipitates at room temperature while the monoamide is separated by cooling the filtrate to near 0 ^{o}C.

The reaction of octadecanoic acid (**12**) with DETA **13** gives amidoamines (**1**) and (**2**). (Scheme 4.2).

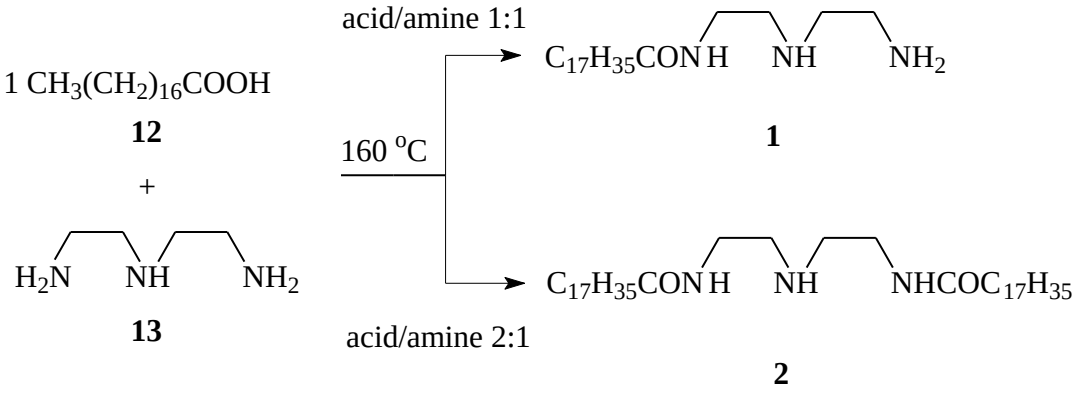

Scheme 4.2

The reaction of dodecanoic acid (**14**) with DETA **13** gives amidoamines (**3**) and (**4**). (Scheme 4.3).

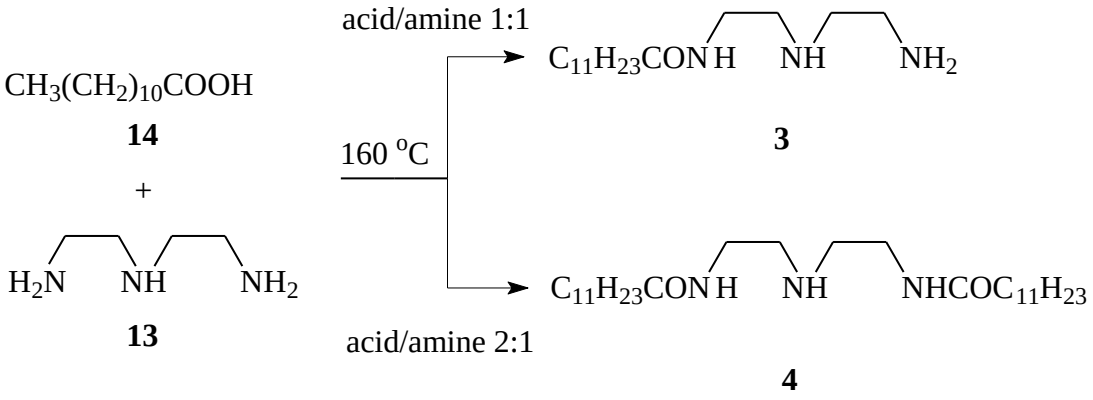

Scheme 4.3

The reaction of octadecanoic acid (**12**) with TEPA **15** gives amidoamines (**5**) and (**6)**. (Scheme 4.4).

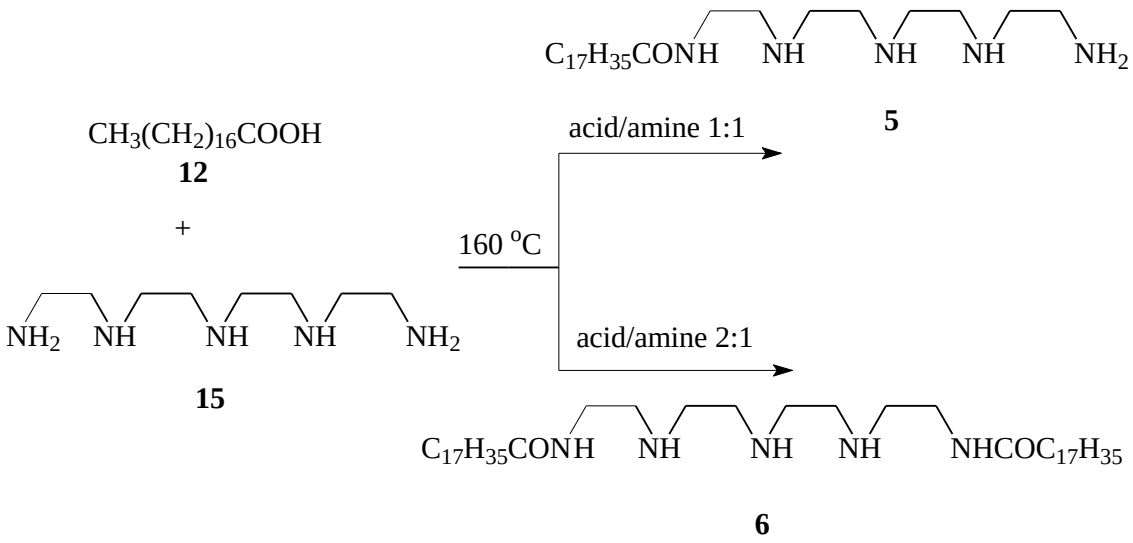

Scheme 4.4

The synthesized amides were identified using spectral analysis including FTIR, ^{1}H NMR and ^{13}C NMR. They have strong IR absorption in the range 3290-3294 cm^{-1} (N-H stretch). Because the IR spectra were taken for neat products, the NH_2 doublet peak overlaps the NH singlet peaks in compounds **1**, **3** and **5** giving a wide apparent singlet, while compounds **2**, **4** and **6** show a sharp singlet peak corresponding to N-H stretch. The amide group is identified by a peak in the range 1637-1635 cm^{-1} (C=O stretch) and a peak in the range 1565-1550 cm^{-1} (N-H bend). C-N stretch can be identified by a peak in the range 1276 -1250 cm^{-1}.

The ^{1}H NMR spectra of **1**, **3** and **5** show N-H peaks for one proton of the amide group in the range 6.29, 6.58 and 6.46 ppm respectively, which confirms that acid attacks the terminal primary amine giving products of type (**a)** rather than **(a_1)** (scheme 4.1). The spectra also show four different types of protons on the poly amine carbon chain, represented by three triplets in the range 2.6-2.9 ppm and one apparent quartet in the range 3.3-3.4 ppm, which conforms to structure (**a**) which lacks symmetry.

The ^{13}C NMR spectra of compounds **1**, **3** and **5** show amide carbonyl peak at 173 ppm. The spectra also show four different types of carbons on the poly amine carbon chain, around 39 ppm, around 41 ppm, around 48 ppm and around 51ppm. This reveals an asymmetric structure for the molecules which conforms to structure (**a**) **(**Scheme 4.1). The more complex peak for **5** at 49 ppm is attributable to the longer polyamine chain.

FIGURE 4.1 and FIGURE 4.2 compare the characteristic area of the ^{1}H NMR and ^{13}C NMR spectra of compounds **1**, **3** and **5** respectively.

The ^{1}H NMR spectra of compounds **2**, **4** and **6** show N-H peaks for two proton of the amide group (5.90, 5.95 and 6.77 ppm respectively) which confirms that the acid attacks the primary amine terminal groups giving products of type **b** rather than $\mathbf{b_1}$ which has one amide proton **(**scheme 4.1). The spectra also show two different types of protons on the polyamine carbon chain**;** a triplet in the range 2.6-2.9 ppm and an apparent quartet in the range 3.3-3.4 ppm which conforms to the symmetric structure (**b**).

The ^{13}C NMR spectra of **2**, **4** and **6** show an amide carbonyl peak at 173 ppm. Also the spectra show only two different types of carbons on the polyamine carbon chain around 39 ppm, and around 48 ppm, this reveals the symmetric structure of the molecule which conforms to symmetric structure (**b**) **(**scheme 4.1). For compound **6** the peak at 48 is more complex because of the longer polyamine chain

FIGURE 4.2 and FIGURE 4.3 compare the characteristic area of the ^{1}H NMR and ^{13}C NMR spectra of compounds **2**, **4** and **6** respectively.

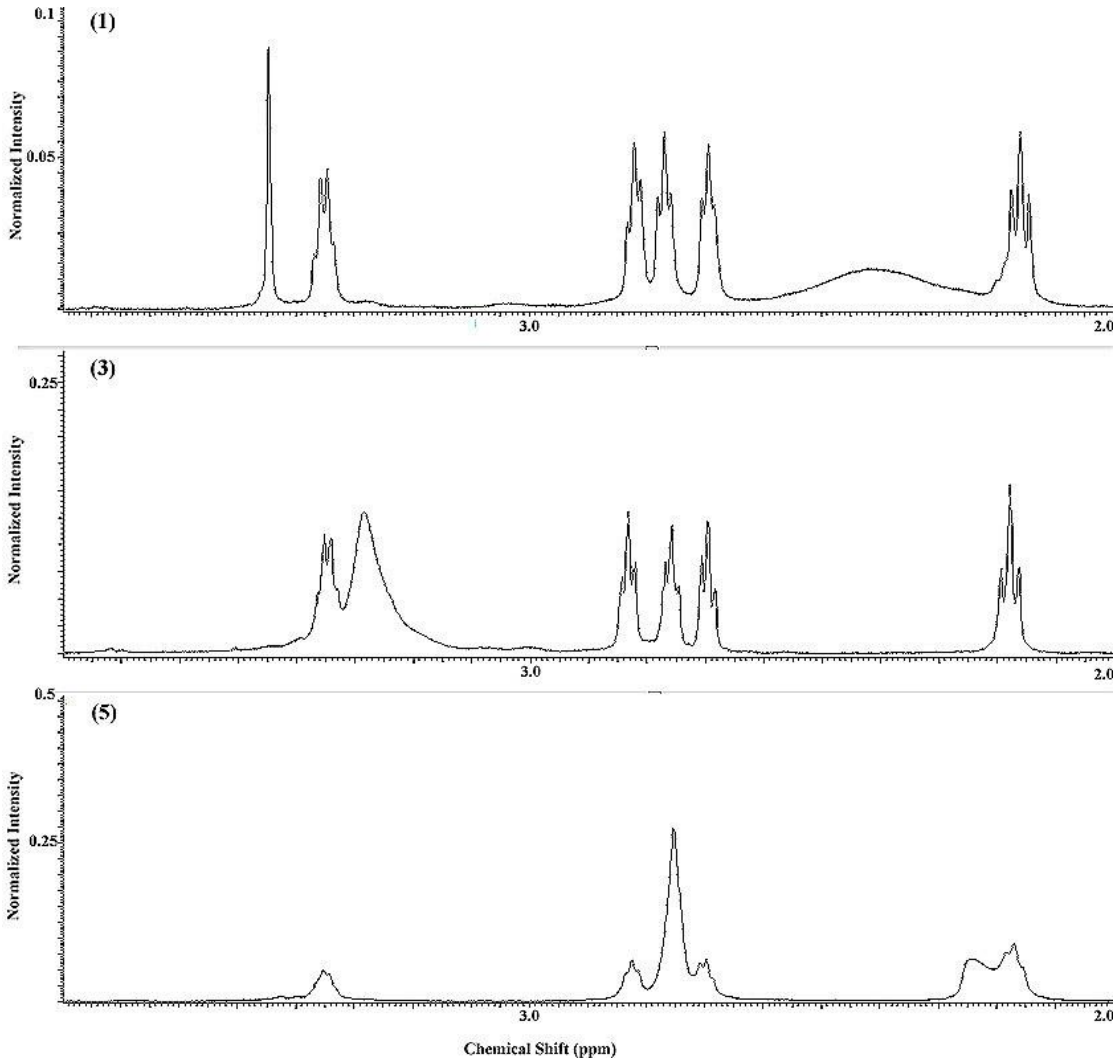

FIGURE 4.1. The Characteristic Area Of ^{1}H NMR Spectra of Compounds **1, 3** and **5**

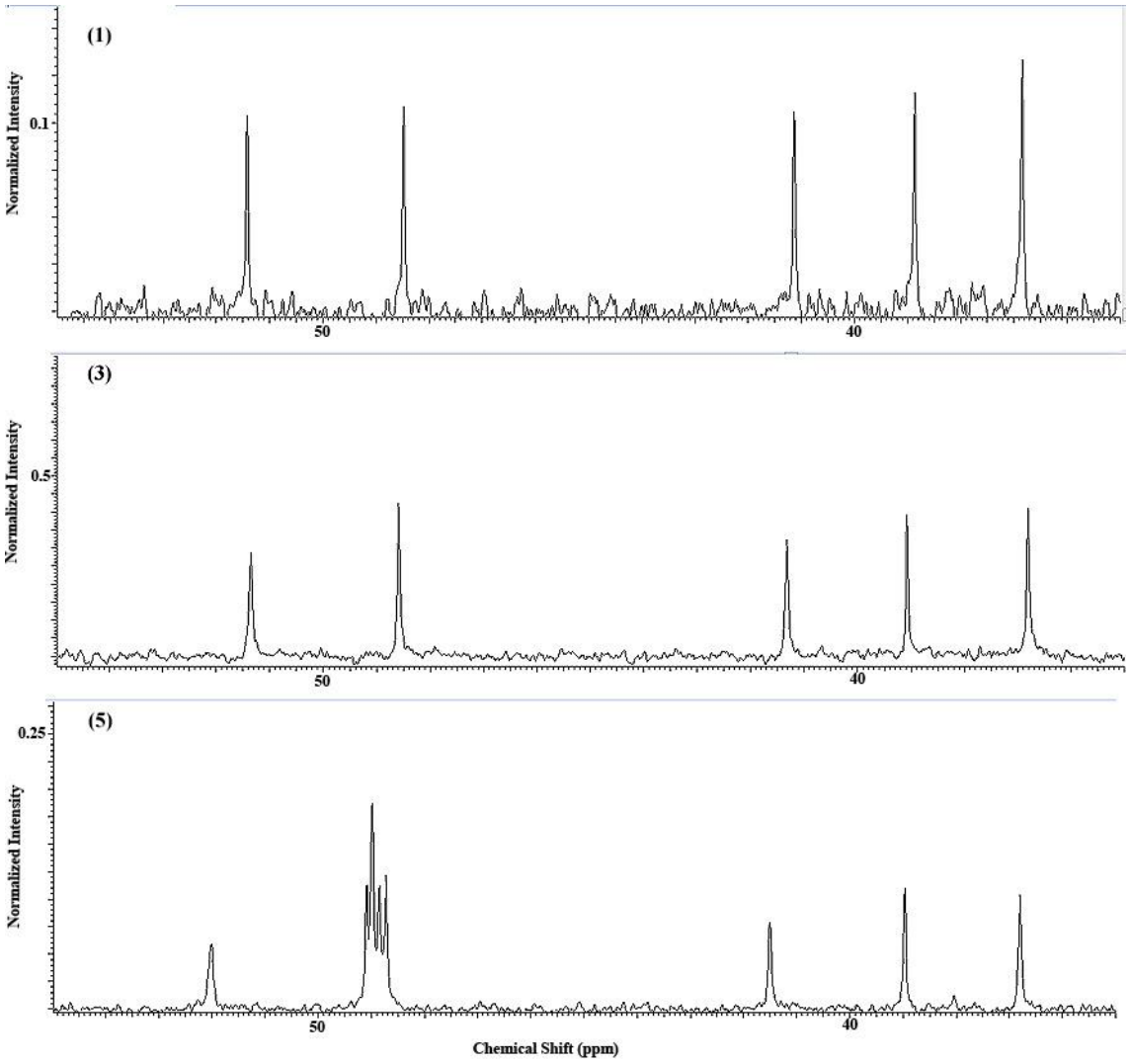

FIGURE 4.2. The Characteristic Area Of ^{13}C NMR Spectra of Compounds **1**, **3** and **5.**

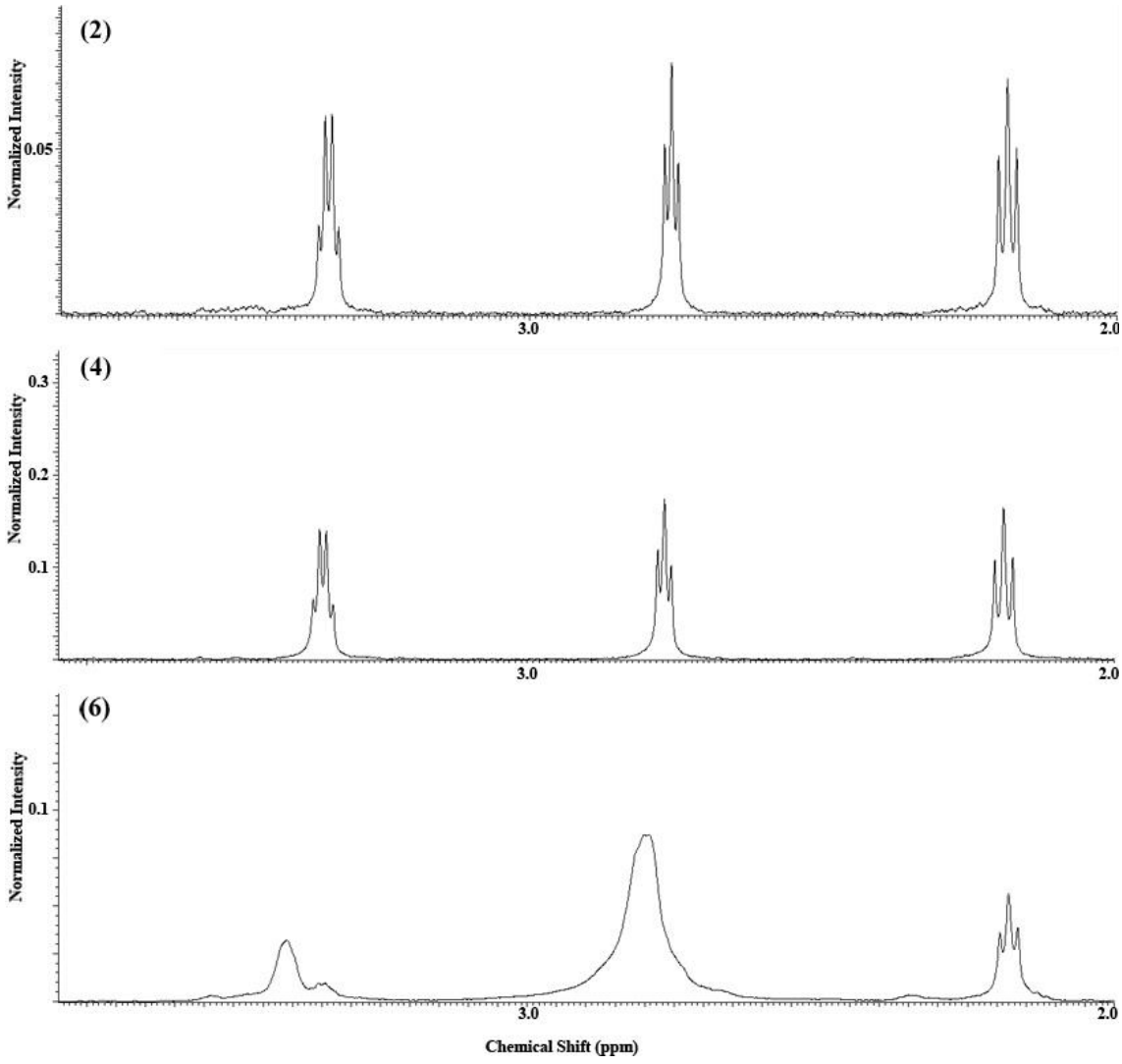

FIGURE 4.3. The Characteristic Area Of ^{1}H NMR Spectra of Compounds **2, 4** and **6.**

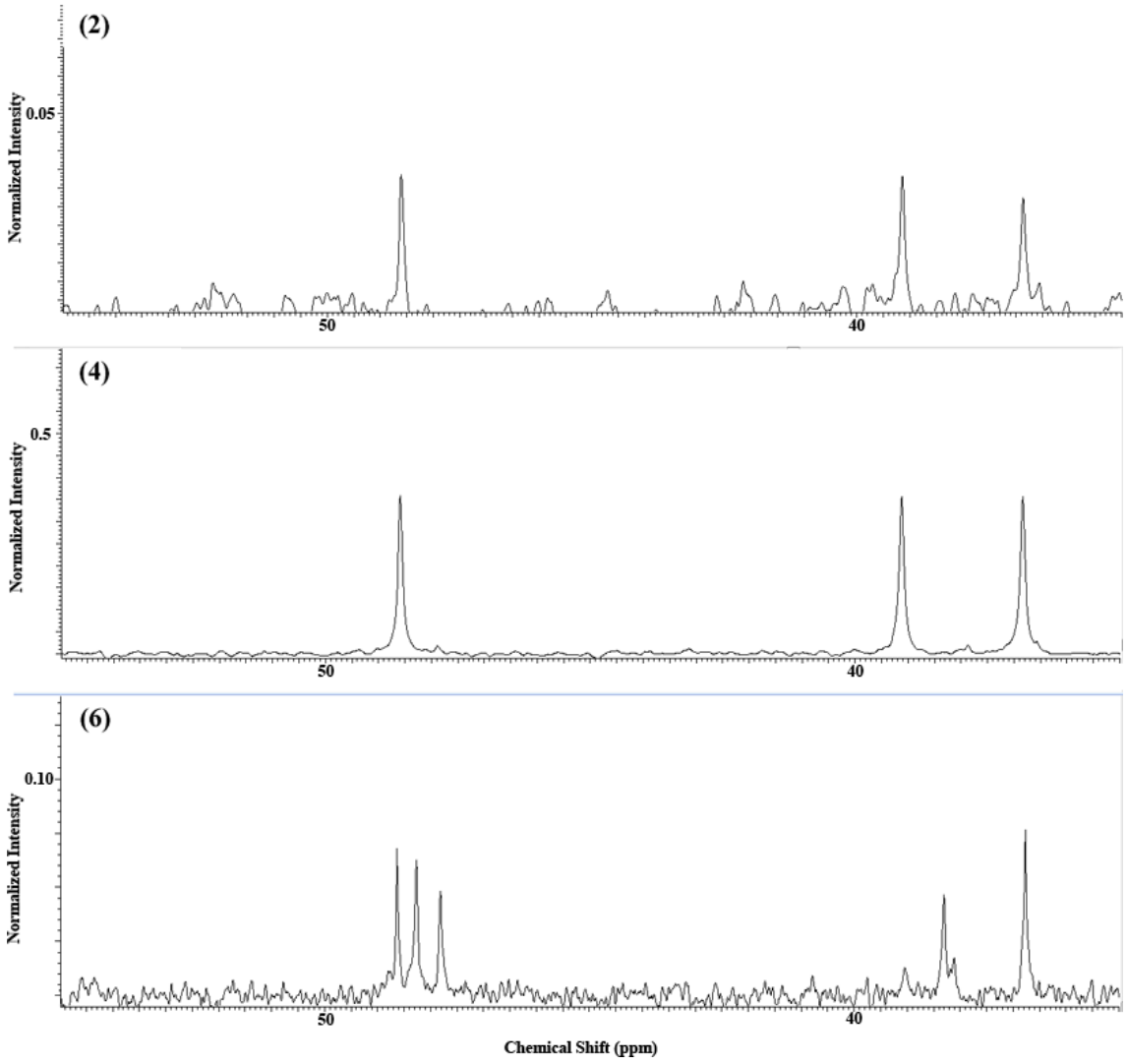

FIGURE 4.4. The Characteristic Area Of ^{13}C NMR Spectra of Compounds **2, 4** and **6.**

4.1.2. PREPARATION OF DIAMIDES OF TWO DIFFERENT FATTY ACIDS.

The synthesized amidoamines have the following general structures

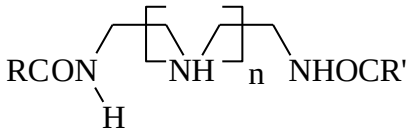

Where R, R′ are for different fatty acids. The starting materials are amidoamine (**1**) prepared according to the procedure described in Chapter 3, and the decanoic and hexanoic acids.

The compounds were prepared by heating the amidoamine (**1**) and the fatty acid to 160 ^{o}C for around 90 minutes, and then the reaction mixture was cooled and recrystallized from hot methanol to remove the remaining reactants.

The reaction product was a mixture of the starting materials, amidoamine (**2**) and the desired diamidoamines. The synthesized diamidoamines have a higher solubility in methanol than amidoamine (**2**), which help in separating the two compounds by recrystallization from hot methanol, when the methanol is cooled to room temperature, the amidoamine (**2**) precipitates, leaving the heterogeneous diamide in the methanol solution.

Cooling the methanol solution gives the diamidoamine as a white precipitate, leaving the remaining start materials in the filtrate.

The reaction of decanoic acid (**16**) with amidoamine (**1**) gives amidoamine (**7**). (Scheme 4.5).

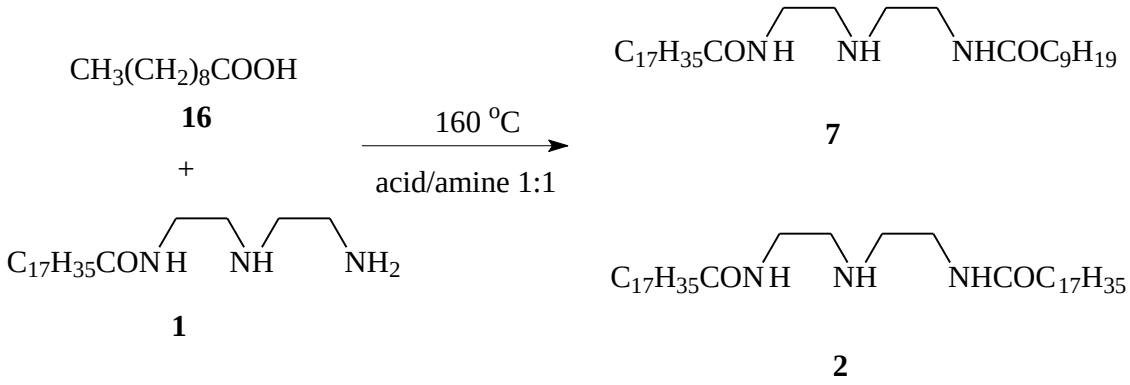

Scheme 4.5

The reaction of hexanoic acid (**17**) with amidoamine (**1**) gives amidoamine (**8**). (Scheme 4.6).

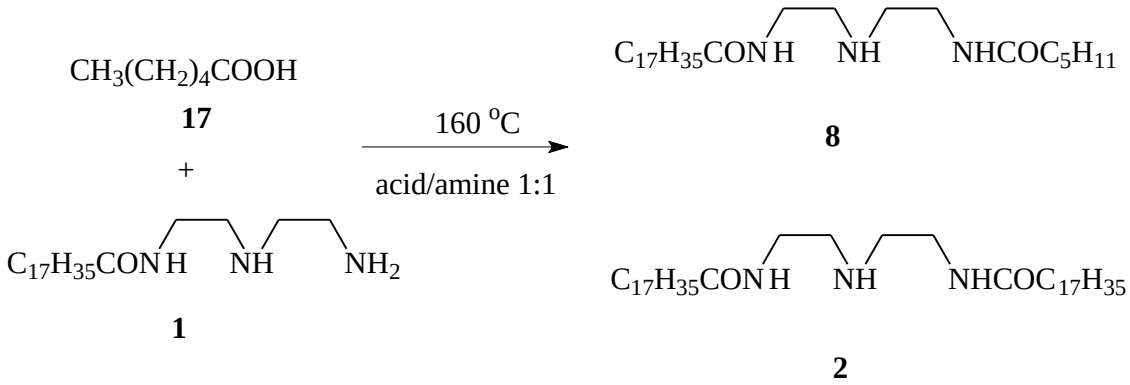

Scheme 4.6

The changes in the length of the hydrocarbon chain on both sides of the diamide is intended to vary the solubility in water and the adsorption behavior of the molecules compared to **2** and thus change the corrosion inhibition efficiency. The synthesized amidoamines were identified using spectral analysis including FTIR, ^{1}H NMR and ^{13}C NMR. They have strong IR absorption in the range 3298-3295 cm^{-1} (N-H stretch for secondary amine). The amide group is identified by a peak in the range 1639-1637 cm^{-1} (C=O stretch) and a peak in the range 1551-1550 cm^{-1} (N-H bend). C-N stretch can be identified by a peak in the range 1276 -1263 cm^{-1}. The peaks in the range 3000-2850 cm^{-1} corresponds to C-H stretching.

The ^{1}H NMR spectra of **7** and **8** show N-H peaks for two proton of the amide group 6.4 ppm which confirms that the second acid attacks the other primary amine terminal giving products of type **b** rather than $\mathbf{b_1}$ which has on amide proton **(S**cheme 3.1). The spectra also show two different types of protons on the polyamine carbon chain, a triplet in the range 2.756-2.85 ppm and apparent quartet in the range 3.3-3.6 ppm, which conforms to the symmetric structure (**b**).

The ^{13}C NMR spectra of 7 and **8** show amide carbonyl peak at 173 ppm. The spectra also show two different types of carbons on the poly amine carbon chain around 38-39 ppm and around 48 ppm. This reveals the symmetric structure of the molecule which conforms to symmetric structure (**b**) (Scheme 4.1).

FIGURE 4.5 compares the characteristic area of the ^{1}H NMR spectra of compounds **7** and **8**. Table 4.1 shows the structures of the synthesized amidoamines.

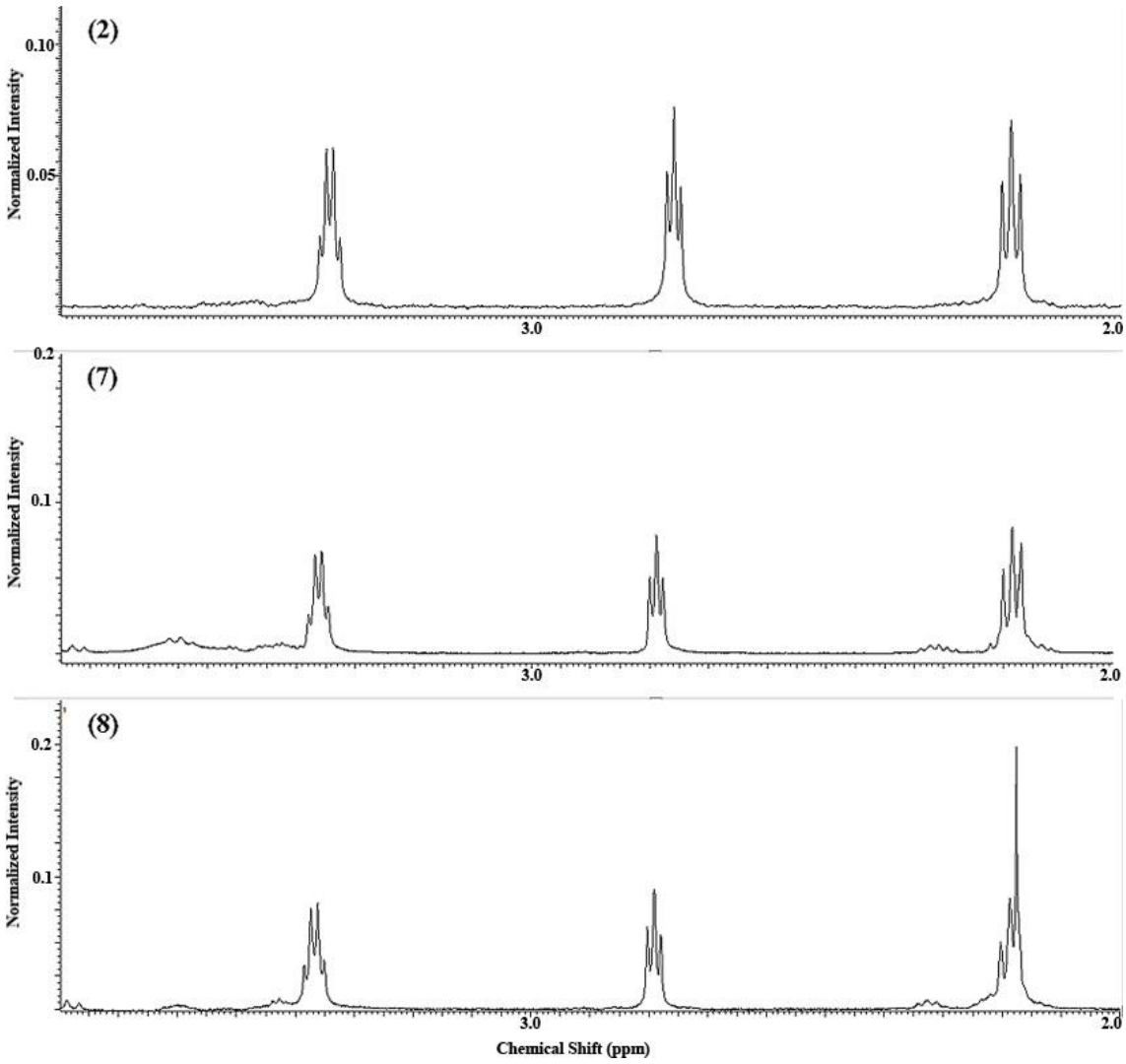

FIGURE 4.5. The Characteristic Area Of ^{1}H NMR Spectra of Compounds 2, 7 and 8.

TABLE 4.1. The Structure of the Synthesized Amidoamines

Compound	Name	Structure
1	N-[2-(2-aminoethylamino)-ethyl]-octadecanamide	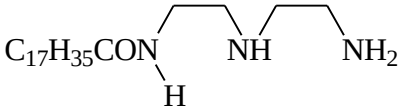
2	N-[2-(2-octadecanoylamino-ethylamino)-ethyl]octadecan	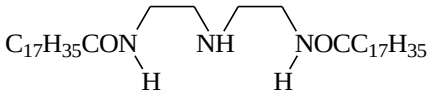
3	N-[2-(2-aminoethyl amino)-ethyl]odecanamide	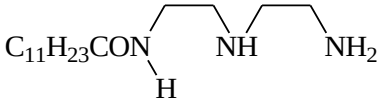
4	N-[2-(2-dodecanoyl amino-ethylamino) -ethyl] dodecan- amide	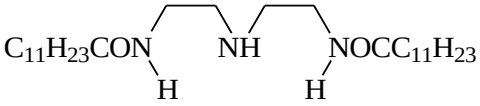
5	2-[2-{2-(2-Aminoethyl amino)-ethylamino}ethyl aminoethyl]octadecanamide	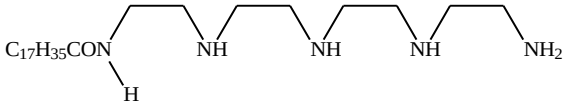
6	2-[2-{2-(2-octadecanoyl amino-ethylamino)-ethyl amino} ethylaminoethyl]-octadecan amide	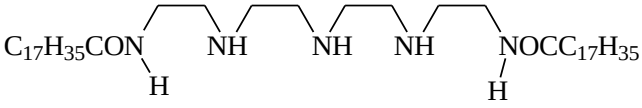
7	N-[2-(2-decanoylamino-ethylamino)-ethyl]octa-decanamide	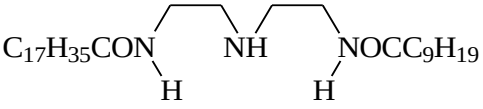
8	N-[2-(2-hexanoylamino-ethylamino)-ethyl]octa-decanamide	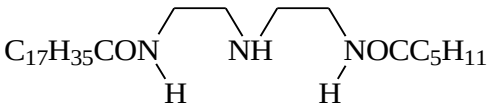

4.1.3. PREPARATION OF IMIDAZOLINE DERIVATIVES.

The start materials are octadecanenitrile, DETA and TEPA. Octadecanonitrile was prepared from octadecanoic acid using an established procedure [75]. 0.1 mol of stearic acid were mixed with 0.27 mol of thionyl chloride. The mixture was dissolved in chloroform and refluxed at 80—83 ^{o}C for about 30 minutes until all the gases are released. The resulting product was a clear brownish solution.

$$CH_3C_{16}H_{32}COOH + SOCl_2 \xrightarrow[80\text{-}83^{o}C,\ reflux]{CHCl_3} CH_3C_{16}H_{32}COCl + SO_2 + HCl$$

0,165 mol of octadecanoyl chloride was reacted with a 30% ammonia solution pre-cooled to around 5 ^{o}C. The reaction mixture was stirred for 30 minutes and then was filtered using a Buchner funnel. The precipitate was re-crystallized in ethyl ether. The yellowish precipitate was dissolved in chloroform and treated with active carbon to remove impurities, then the solvent was removed under vacuum. 0.7 mol of the octadecanoamide were obtained.

$$CH_3C_{16}H_{32}COCl + NH_3 \xrightarrow{5\ ^{o}C} CH_3C_{16}H_{32}CONH_2 + HCl$$

The octadecanoamide was refluxed with 0.7 mol of thionyl chloride in 75mL of benzene at 80-83 ^{o}C for about one hour.

The reaction mixture was extracted with ethyl ether, and then recrystallized from its solution in pentane.

$$CH_3C_{16}H_{32}CONH_2 + SOCl_2 \xrightarrow[80\text{-}83^{o}C,\ reflux]{Benzene} CH_3C_{16}H_{32}CN\ (\mathbf{18}) + SO_2 + 2HCl$$

The imidazolines were prepared by heating the polyamine and octadecanenitrile (**18**) to 150 ^{o}C for around 2 hours, using elemental sulfur as catalyst. The reaction mixture was cooled and dissolved in CH_2Cl_2, washed with water to remove the remaining acid and polyamine, and then the organic layer was separated and dried using Na_2SO_4. The solvent was removed under vacuum to obtain the pure imidazoline (Scheme 4.7 and 4.8).

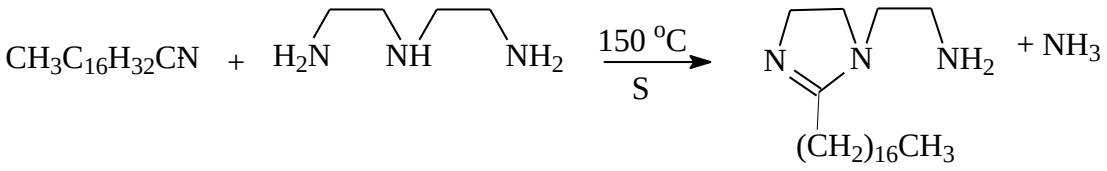

18 **13** **9**

Scheme 4.7

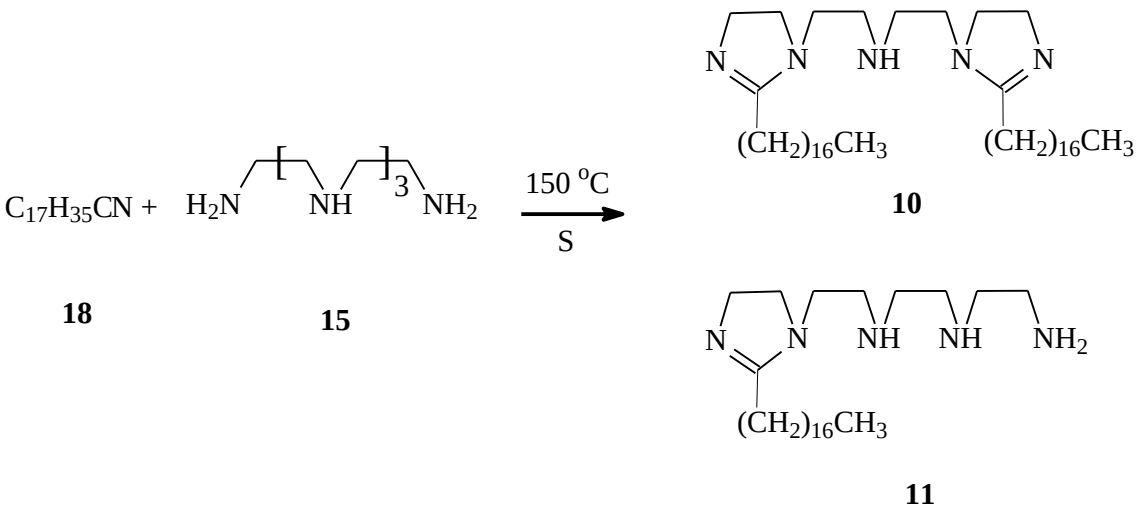

18 **15** **10** **11**

Scheme 4.8

The synthesized imidazolines were identified using spectral analysis including FTIR, ^{1}H NMR and ^{13}C NMR. FTIR was taken for the compounds in solid form. Imidazoline **9** has a doublet peak (3288, 3242) cm^{-1} which corresponds to (N-H stretch) of the primary amine (NH_2), it also has a peak at 1605.0 cm^{-1} which corresponds to primary amine N-H bend. The peak at 1550 cm^{-1} is attributed to the in plane deformation vibration of the N-H bond. The C=N bond is identified by a peak at 1660 cm^{-1} (the ring C=N stretch).

The imidazoline **11** has a doublet peak (3301, 3244) cm^{-1} which corresponds to N-H stretch of the primary amine. The secondary amine N-H stretch adsorption peak is overlapped by the N-H stretch peak for the primary amine which deforms the peak in the range 3300-3240 cm^{-1}. The amine group shows another peak at 1606 cm^{-1} that is due to the primary amine N-H bend. The peak at 1550 cm^{-1} is attributed to the in plane

deformation vibrations of the N-H bond. The ring C=N bond of the imidazoline ring is identified by a peak 1662 cm^{-1} (The ring C=N stretch). This peak is shifted to the high frequency range due to intermolecular the hydrogen bonding in the solid phase of this compound [76].

The imidazoline **10** has a sharp singlet at 3290 cm^{-1} which corresponds to the N-H stretch of the secondary amine group. It is noticed that the peak at 1605 cm^{-1} in **9** and **11** disappears in **10** which is in conformity with the absence of a primary amine in the compound. The peak at 1550 cm-1 is attributed to the in plane deformation vibration of the N-H bond. The C=N ring bond of the imidazoline ring is identified by a peak 1635 cm^{-1} (C=N stretch).

The 1H NMR spectra of compounds **9**, **10** and **11** show triplet in the range 2.8-2.9 ppm and triplet in the range 3.10-3.20 ppm, in the range 3.25-3.35 ppm. Imidazoline **9** exhibits a triplet and each of the imidazolines **10** and **11** exhibits a multiplet. In the range 3.65-3.75 ppm each of imidazolines **10** and **11** exhibits a triplet. These peaks correspond to the four different types of protons on the imidazoline and the polyamine carbon chain.

The ^{13}C NMR spectra of **10** and **11** show four different types of carbons on the polyamine carbon chain and the imidazoline ring, around 33 ppm, 34 ppm, 36 ppm and 38 ppm. The imidazoline **10** molecule shows singlet peaks which reveal its asymmetric structure. Imidazoline **9** shows a doublet with peaks at 36.1, 36.2 ppm and a singlet at 38 ppm.

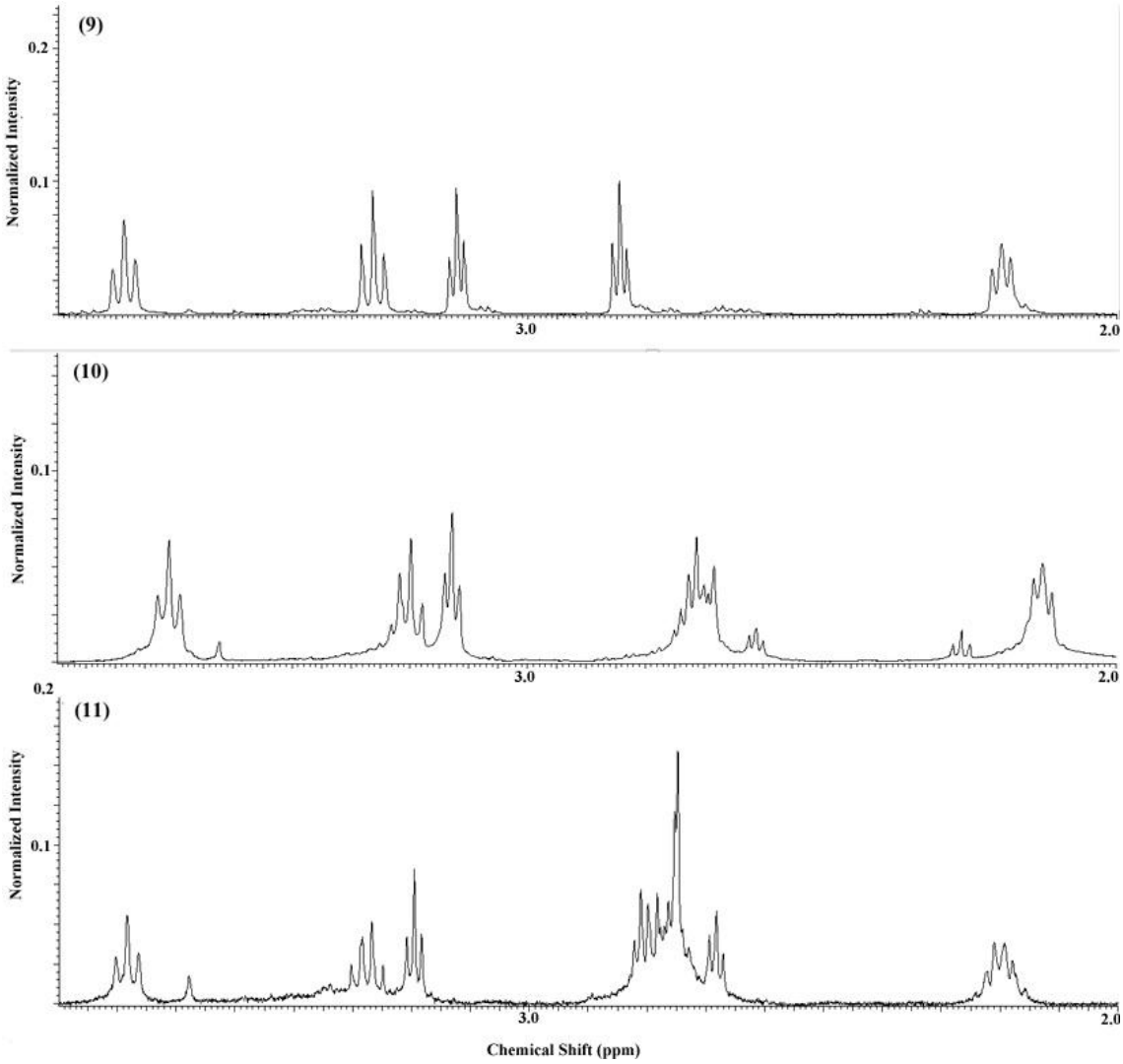

FIGURE 4.6. The Characteristic Area Of ^{1}H NMR Spectra of Compounds 9, 10 and 11.

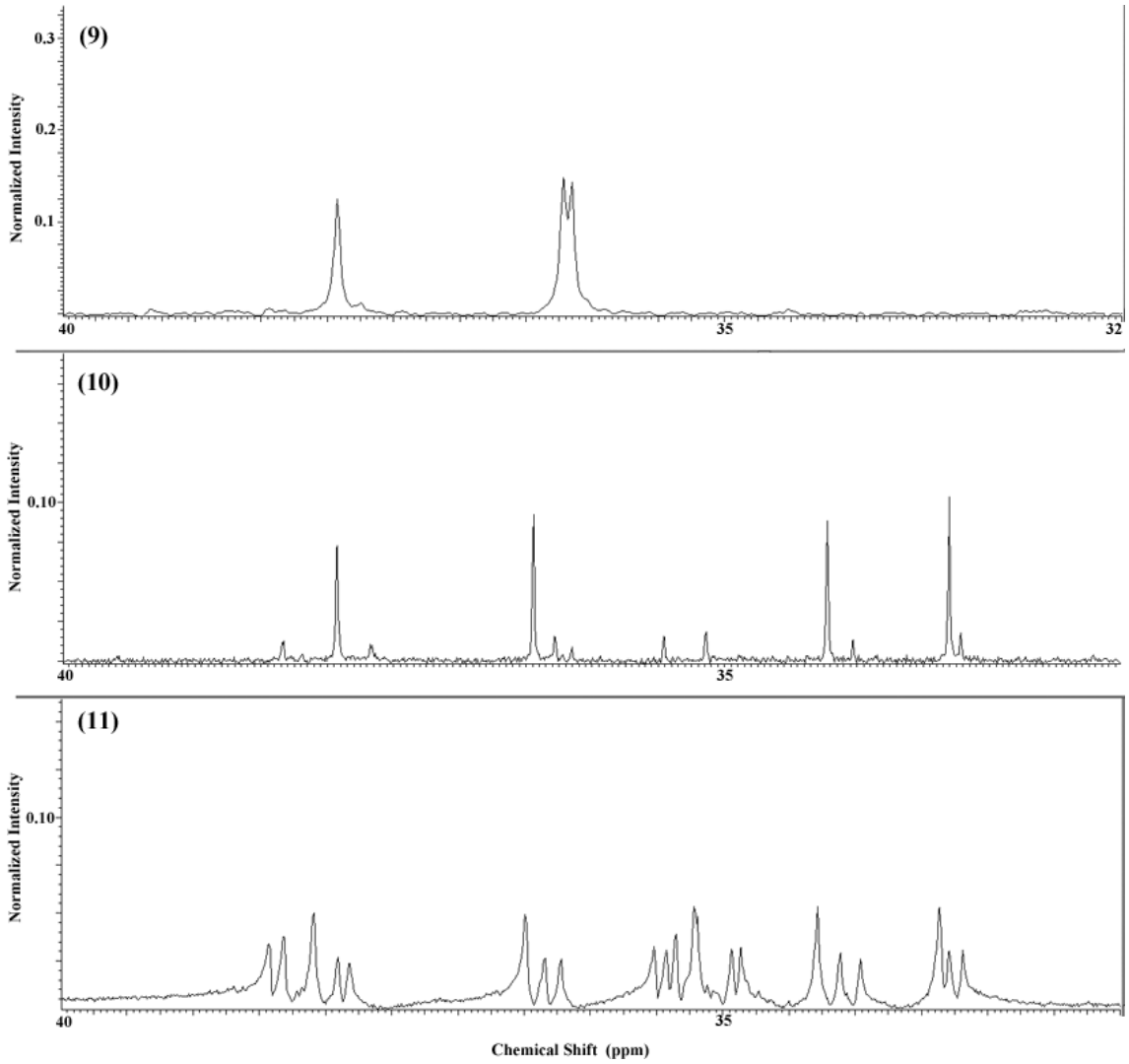

FIGURE 4.7. The Characteristic Area Of ^{13}C NMR Spectra of Compounds 9, 10 and 11.

Table 4.2 shows the structures of the synthesized imidazolines.

TABLE 4.2. The Structure of the Synthesized Imidazolines

Compound	Name	Structure
9	1-(2-aminoethyl)-2-heptadecanyl-2-imidazoline	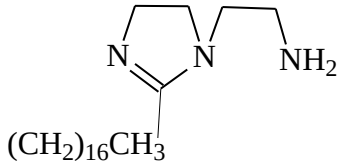
10	N,N'-Di-2,2'-[2-heptadecanyl-2-imidazolinyl]diethylamine	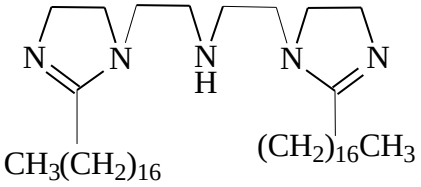
11	1-[2-{2-(2-Aminoethylamino)-ethylamino}ethyl] -2-heptadecanyl-2-imidazolines	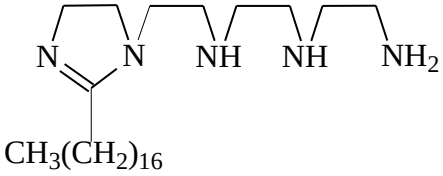

CHAPTER 4

RESULTS AND DISCUSSION

4.1. SYNTHESIS

In this work, thus, 11 polyamine derivates were synthesized by the reaction of polyamines with fatty acids of different chain lengths to obtain the corresponding amido-amines and imidazolines. The polyamines used were N-(2-amino ethyl)-1,2-ethanediamine or and N-(2 amino ethyl)-N´-{2-{(2-aminoethyl)amino}ethyl}-1,2-ethanediamine) or tetra ethylene penta amine (TEPA). The TEPA used for this work was purified to get a pure N-(2-amino -ethyl)-N´-{2-{(2-aminoethyl)amino}ethyl}-1,2-ethanediamine.

4.1.1. PREPARATION OF AMIDES OF THE SAME FATTY ACID.

The synthesized amido-amines have the following general structures

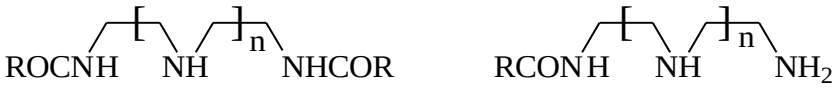

The fatty acids used for the synthesis were octadecanoic acid and dodecanoic acid. The compounds were prepared by heating a polyamine and a fatty acid mixture in the ratio mentioned in chapter 3 to 160 ^{o}C for around 1 hour, and then the reaction mixture

was cooled and re-crystallized in hot methanol to remove the remaining acid and polyamine (Scheme 4.1).

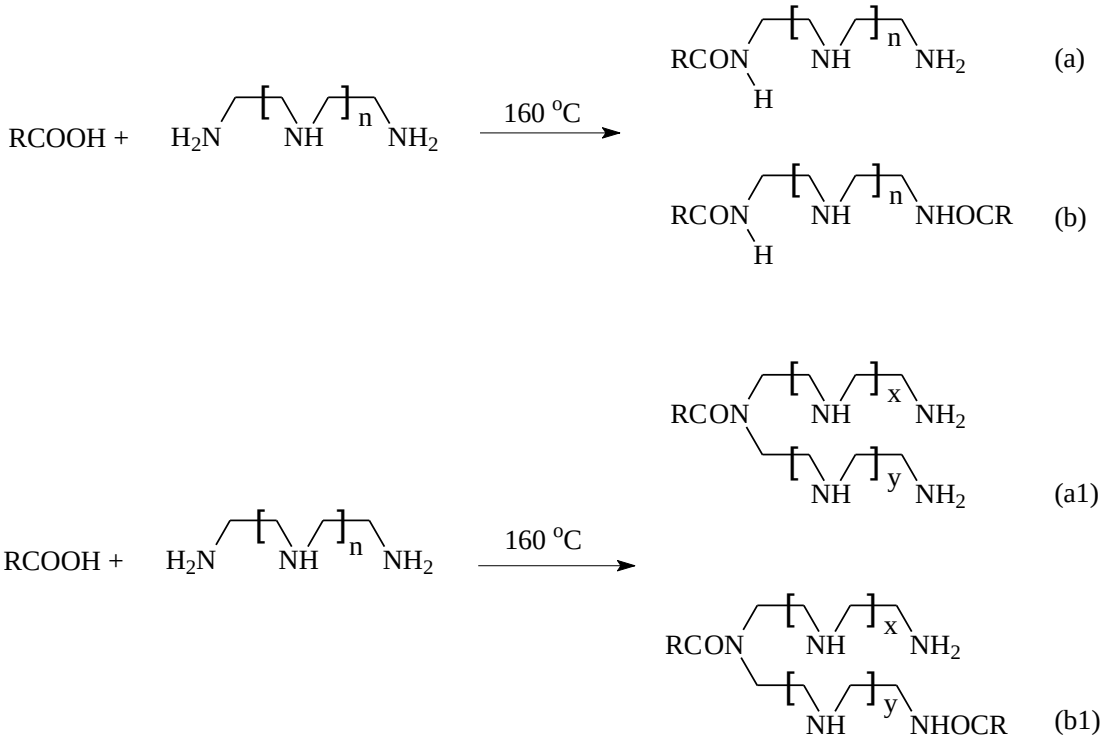

Scheme 4.1

The reaction product is a mixture of mono and diamides. The monoamide could have the structure **a** or $\mathbf{a_1}$ depending on which amine will the acid attack, the primary amine or the secondary amine, consequently the diamide will have the structure **b** or $\mathbf{b_1}$**.**

The use of different polyamines and different polyamine to acid ratios was intended to vary the solubility in water and the adsorption behavior and in turn the corrosion inhibition efficiency of the amide molecules. It also shows which functional group, the

amide group or the terminal amine group, is responsible for corrosion inhibition as compounds of structure (**b**) do not have a terminal amine.

The monoamides have a higher solubility in methanol than the diamides, which permits their separation by recrystallizations from their solution in hot methanol; the diamide precipitates at room temperature while the monoamide is separated by cooling the filtrate to near 0 ^{o}C.

The reaction of octadecanoic acid (**12**) with DETA **13** gives amidoamines (**1**) and (**2**). (Scheme 4.2).

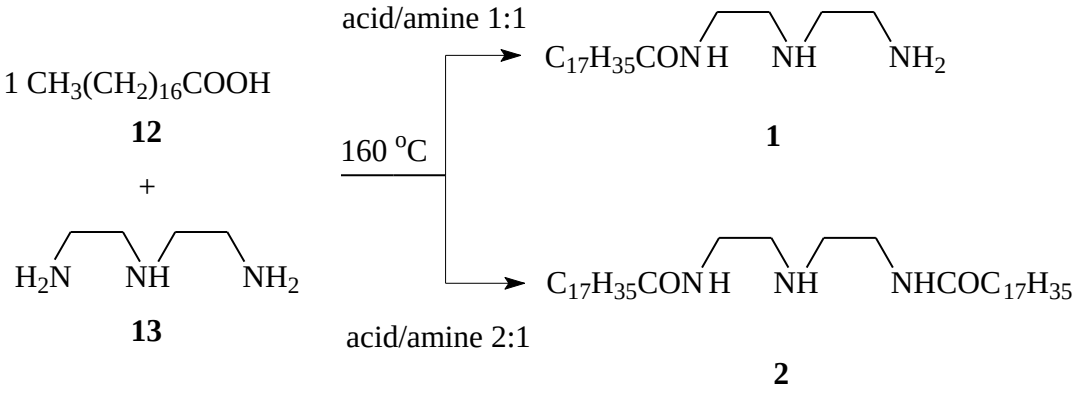

Scheme 4.2

The reaction of dodecanoic acid (**14**) with DETA **13** gives amidoamines (**3**) and (**4**). (Scheme 4.3).

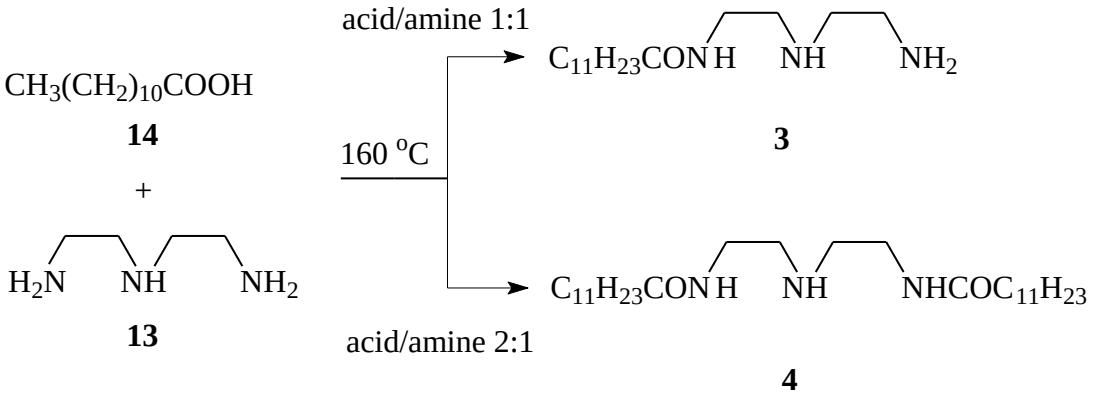

Scheme 4.3

The reaction of octadecanoic acid (**12**) with TEPA **15** gives amidoamines (**5**) and (**6)**. (Scheme 4.4).

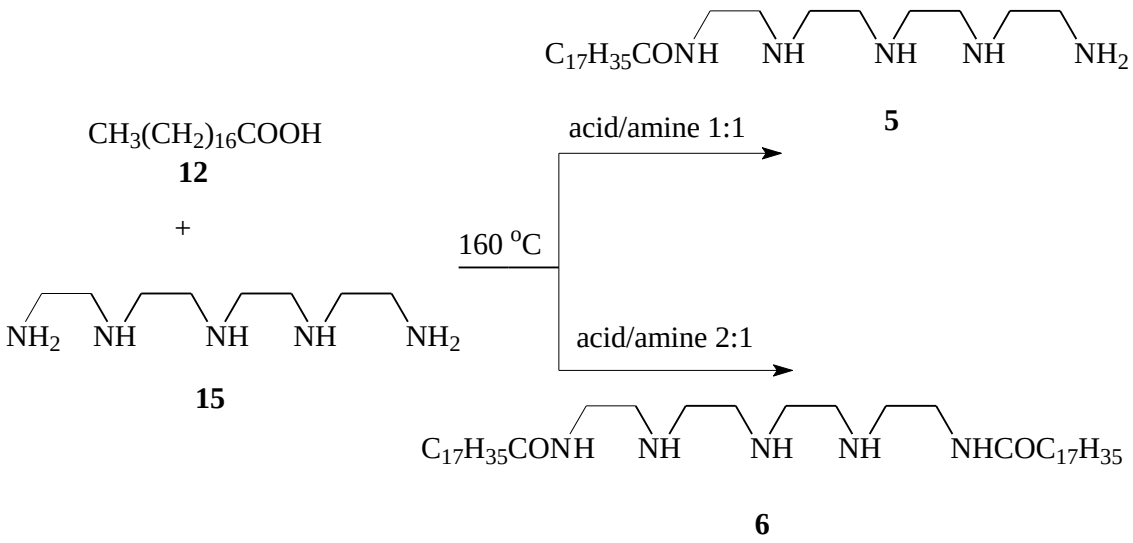

Scheme 4.4

The synthesized amides were identified using spectral analysis including FTIR, ^{1}H NMR and ^{13}C NMR. They have strong IR absorption in the range 3290-3294 cm^{-1} (N-H stretch). Because the IR spectra were taken for neat products, the NH_2 doublet peak overlaps the NH singlet peaks in compounds **1**, **3** and **5** giving a wide apparent singlet, while compounds **2**, **4** and **6** show a sharp singlet peak corresponding to N-H stretch. The amide group is identified by a peak in the range 1637-1635 cm^{-1} (C=O stretch) and a peak in the range 1565-1550 cm^{-1} (N-H bend). C-N stretch can be identified by a peak in the range 1276 -1250 cm^{-1}.

The ^{1}H NMR spectra of **1**, **3** and **5** show N-H peaks for one proton of the amide group in the range 6.29, 6.58 and 6.46 ppm respectively, which confirms that acid attacks the terminal primary amine giving products of type (**a)** rather than **(a_1)** (scheme 4.1). The spectra also show four different types of protons on the poly amine carbon chain, represented by three triplets in the range 2.6-2.9 ppm and one apparent quartet in the range 3.3-3.4 ppm, which conforms to structure (**a**) which lacks symmetry.

The ^{13}C NMR spectra of compounds **1**, **3** and **5** show amide carbonyl peak at 173 ppm. The spectra also show four different types of carbons on the poly amine carbon chain, around 39 ppm, around 41 ppm, around 48 ppm and around 51ppm. This reveals an asymmetric structure for the molecules which conforms to structure (**a**) **(**Scheme 4.1). The more complex peak for **5** at 49 ppm is attributable to the longer polyamine chain.

FIGURE 4.1 and FIGURE 4.2 compare the characteristic area of the ^{1}H NMR and ^{13}C NMR spectra of compounds **1**, **3** and **5** respectively.

The ^{1}H NMR spectra of compounds **2**, **4** and **6** show N-H peaks for two proton of the amide group (5.90, 5.95 and 6.77 ppm respectively) which confirms that the acid attacks the primary amine terminal groups giving products of type **b** rather than $\mathbf{b_1}$ which has one amide proton **(**scheme 4.1). The spectra also show two different types of protons on the polyamine carbon chain**;** a triplet in the range 2.6-2.9 ppm and an apparent quartet in the range 3.3-3.4 ppm which conforms to the symmetric structure (**b**).

The ^{13}C NMR spectra of **2**, **4** and **6** show an amide carbonyl peak at 173 ppm. Also the spectra show only two different types of carbons on the polyamine carbon chain around 39 ppm, and around 48 ppm, this reveals the symmetric structure of the molecule which conforms to symmetric structure (**b**) **(**scheme 4.1). For compound **6** the peak at 48 is more complex because of the longer polyamine chain

FIGURE 4.2 and FIGURE 4.3 compare the characteristic area of the ^{1}H NMR and ^{13}C NMR spectra of compounds **2**, **4** and **6** respectively.

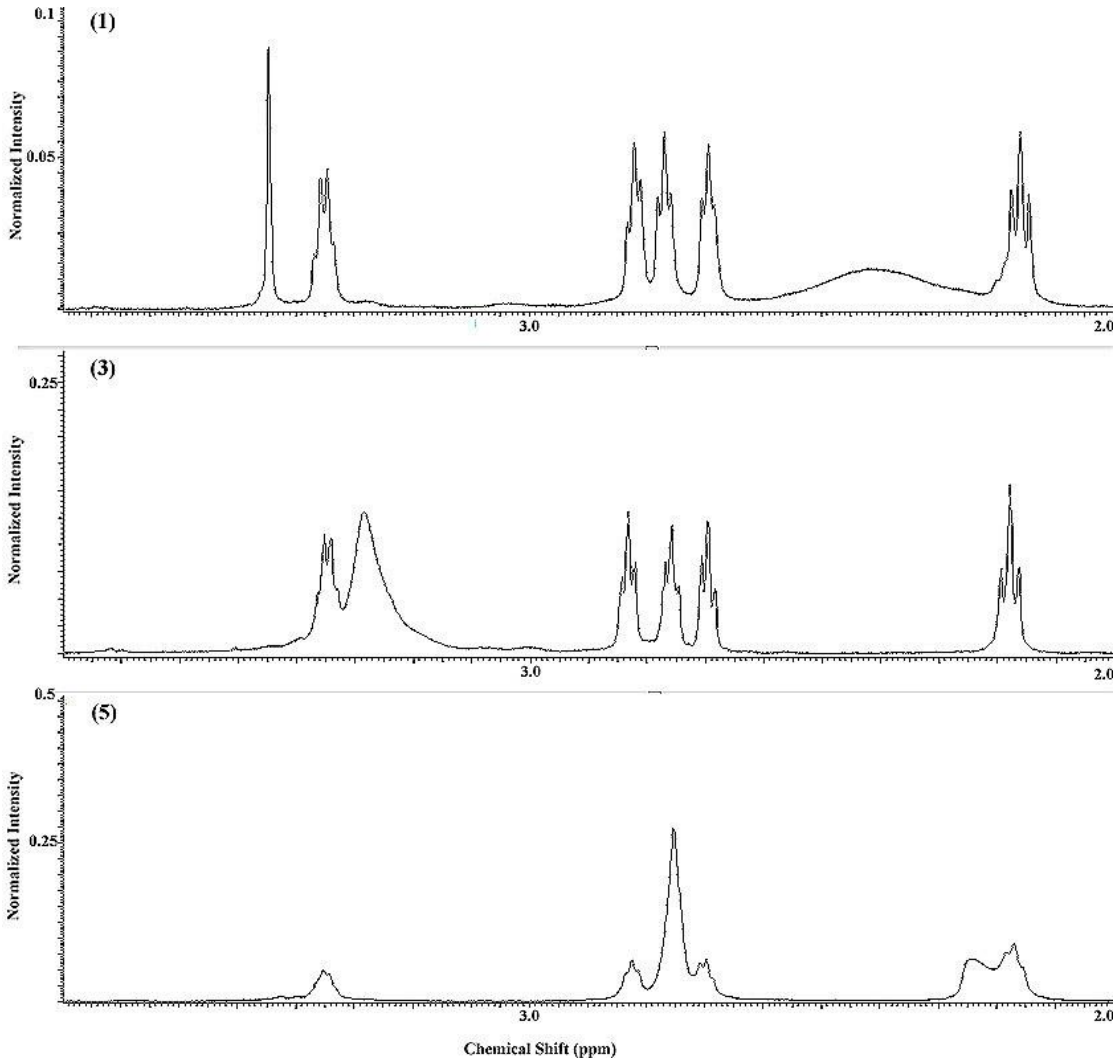

FIGURE 4.1. The Characteristic Area Of ^{1}H NMR Spectra of Compounds **1, 3** and **5**

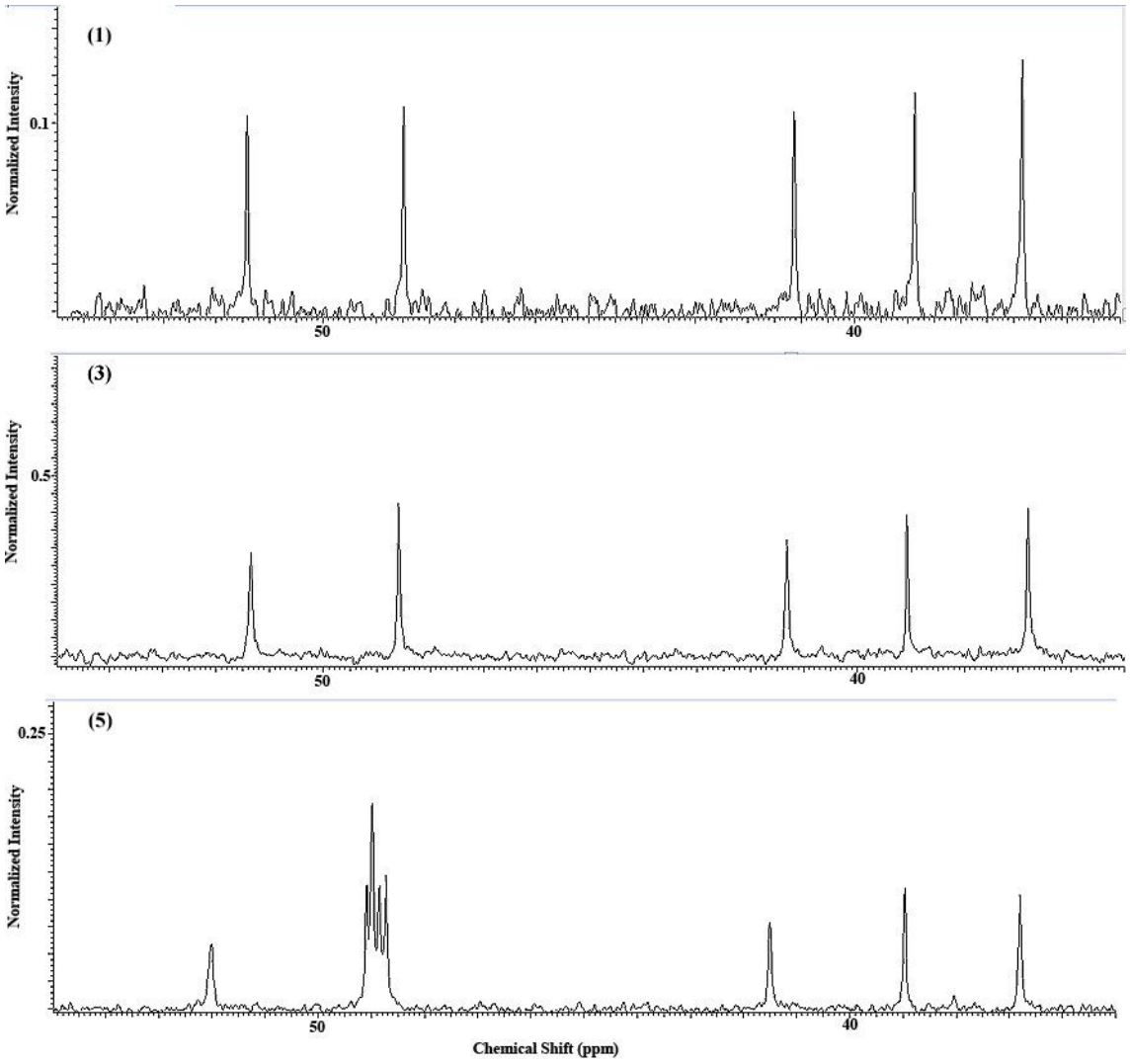

FIGURE 4.2. The Characteristic Area Of ^{13}C NMR Spectra of Compounds **1**, **3** and **5.**

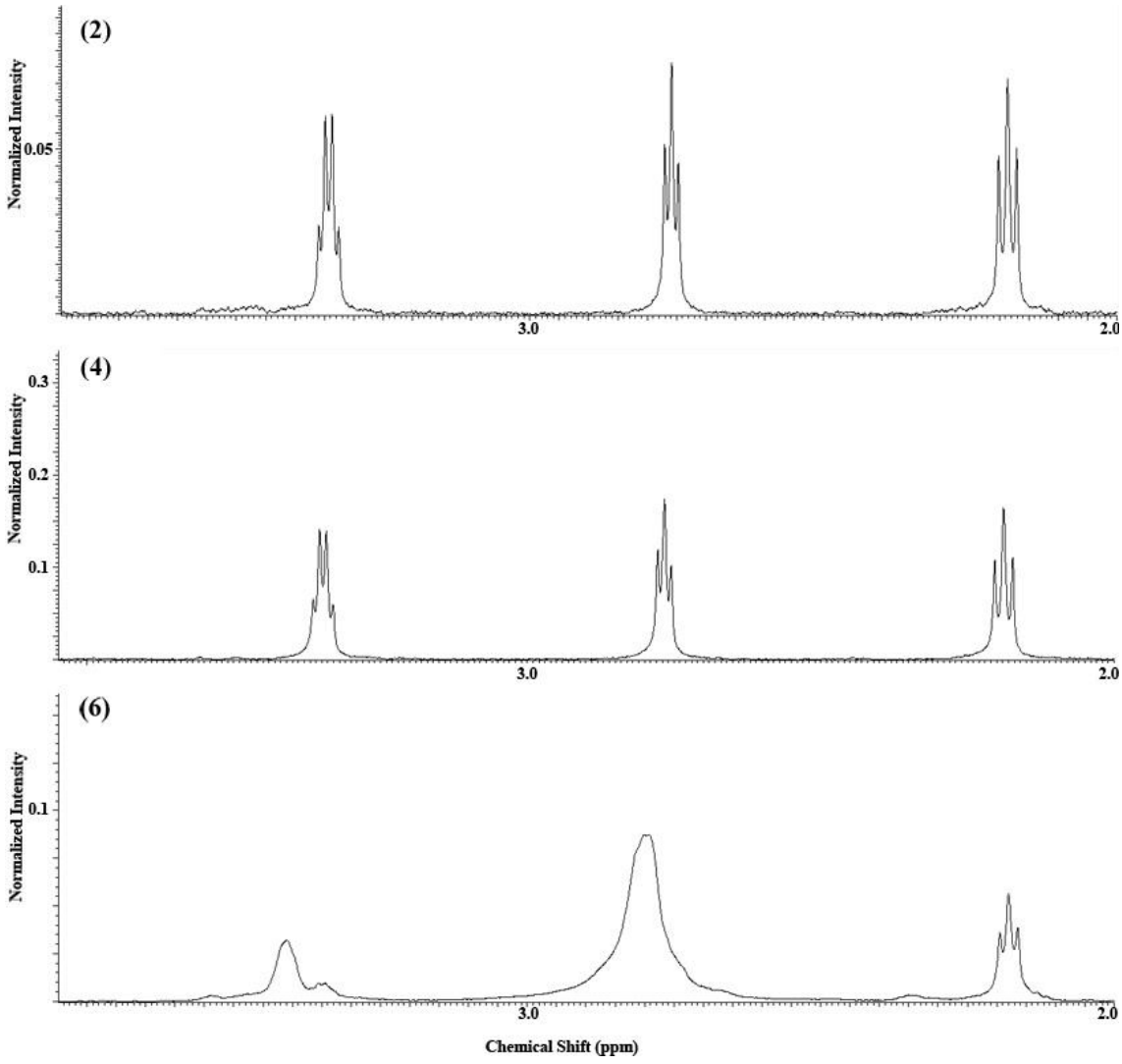

FIGURE 4.3. The Characteristic Area Of ^{1}H NMR Spectra of Compounds **2, 4** and **6.**

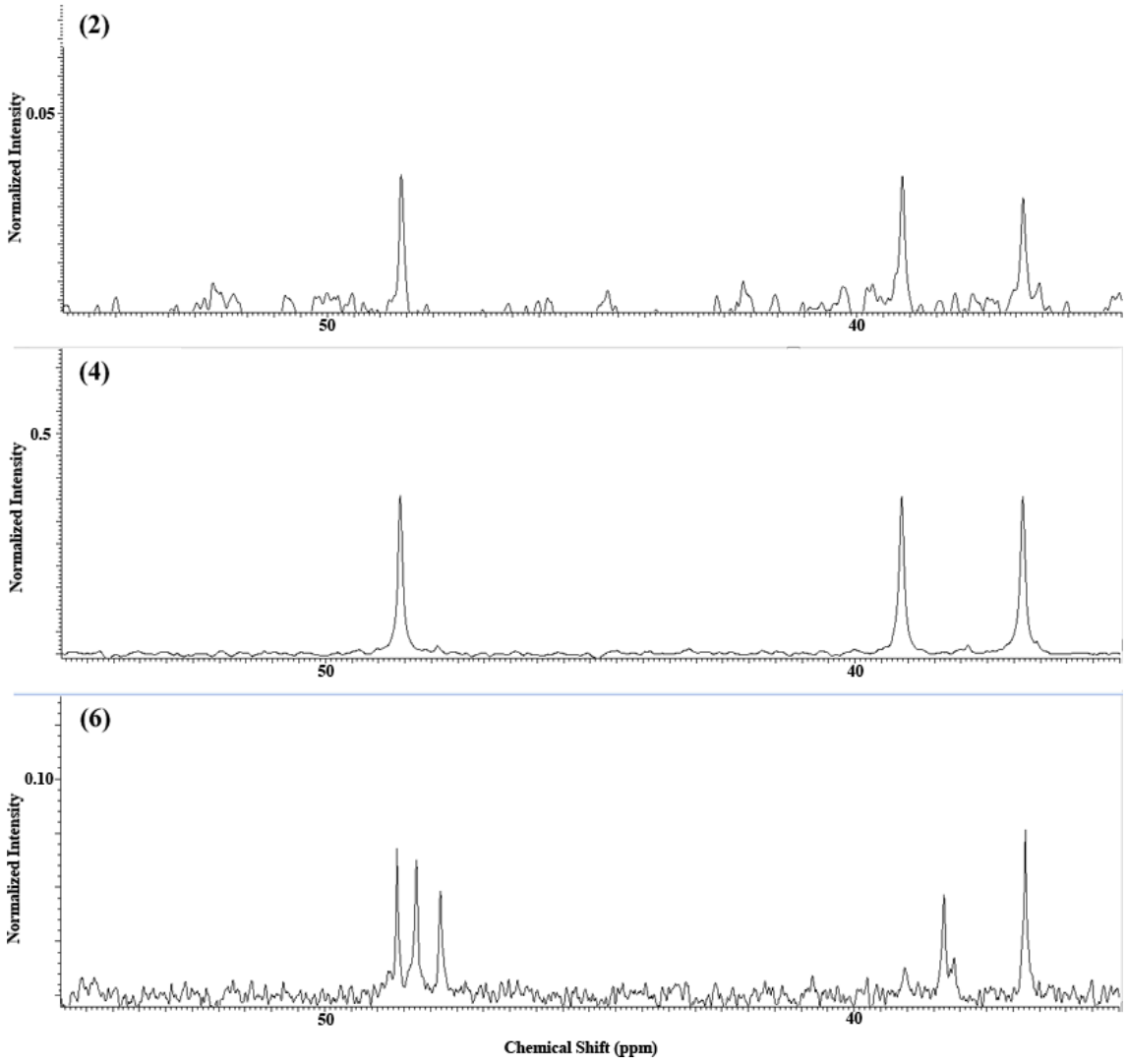

FIGURE 4.4. The Characteristic Area Of ^{13}C NMR Spectra of Compounds **2, 4** and **6.**

4.1.2. PREPARATION OF DIAMIDES OF TWO DIFFERENT FATTY ACIDS.

The synthesized amidoamines have the following general structures

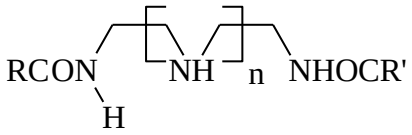

Where R, R′ are for different fatty acids. The starting materials are amidoamine (**1**) prepared according to the procedure described in Chapter 3, and the decanoic and hexanoic acids.

The compounds were prepared by heating the amidoamine (**1**) and the fatty acid to 160 ^{o}C for around 90 minutes, and then the reaction mixture was cooled and recrystallized from hot methanol to remove the remaining reactants.

The reaction product was a mixture of the starting materials, amidoamine (**2**) and the desired diamidoamines. The synthesized diamidoamines have a higher solubility in methanol than amidoamine (**2**), which help in separating the two compounds by recrystallization from hot methanol, when the methanol is cooled to room temperature, the amidoamine (**2**) precipitates, leaving the heterogeneous diamide in the methanol solution.

Cooling the methanol solution gives the diamidoamine as a white precipitate, leaving the remaining start materials in the filtrate.

The reaction of decanoic acid (**16**) with amidoamine (**1**) gives amidoamine (**7**). (Scheme 4.5).

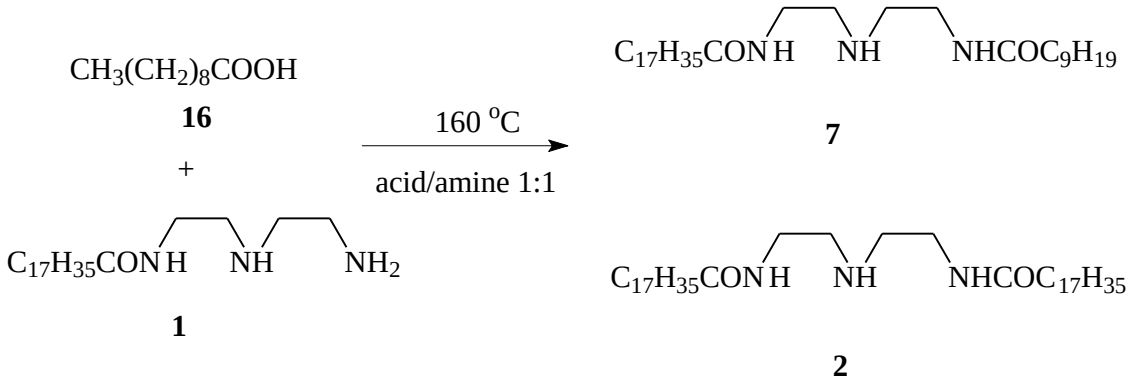

Scheme 4.5

The reaction of hexanoic acid (**17**) with amidoamine (**1**) gives amidoamine (**8**). (Scheme 4.6).

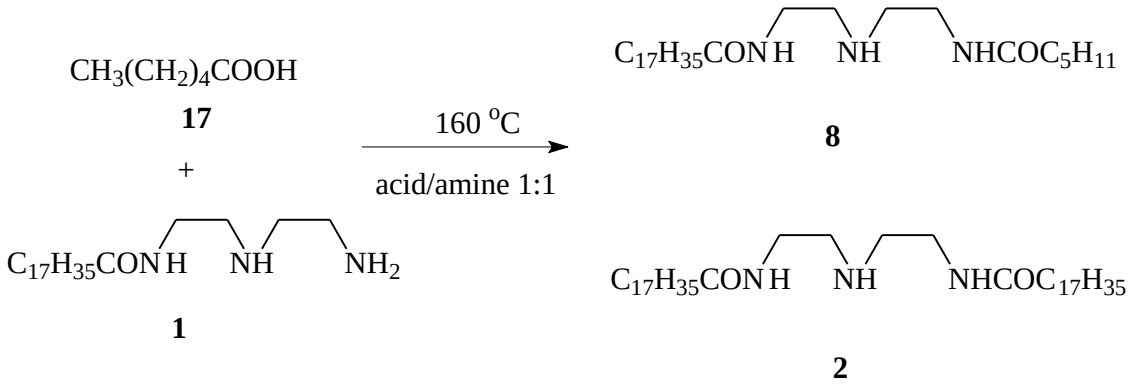

Scheme 4.6

The changes in the length of the hydrocarbon chain on both sides of the diamide is intended to vary the solubility in water and the adsorption behavior of the molecules compared to **2** and thus change the corrosion inhibition efficiency. The synthesized amidoamines were identified using spectral analysis including FTIR, ^{1}H NMR and ^{13}C NMR. They have strong IR absorption in the range 3298-3295 cm^{-1} (N-H stretch for secondary amine). The amide group is identified by a peak in the range 1639-1637 cm^{-1} (C=O stretch) and a peak in the range 1551-1550 cm^{-1} (N-H bend). C-N stretch can be identified by a peak in the range 1276 -1263 cm^{-1}. The peaks in the range 3000-2850 cm^{-1} corresponds to C-H stretching.

The ^{1}H NMR spectra of **7** and **8** show N-H peaks for two proton of the amide group 6.4 ppm which confirms that the second acid attacks the other primary amine terminal giving products of type **b** rather than $\mathbf{b_1}$ which has on amide proton **(S**cheme 3.1). The spectra also show two different types of protons on the polyamine carbon chain, a triplet in the range 2.756-2.85 ppm and apparent quartet in the range 3.3-3.6 ppm, which conforms to the symmetric structure (**b**).

The ^{13}C NMR spectra of 7 and **8** show amide carbonyl peak at 173 ppm. The spectra also show two different types of carbons on the poly amine carbon chain around 38-39 ppm and around 48 ppm. This reveals the symmetric structure of the molecule which conforms to symmetric structure (**b**) (Scheme 4.1).

FIGURE 4.5 compares the characteristic area of the ^{1}H NMR spectra of compounds **7** and **8**. Table 4.1 shows the structures of the synthesized amidoamines.

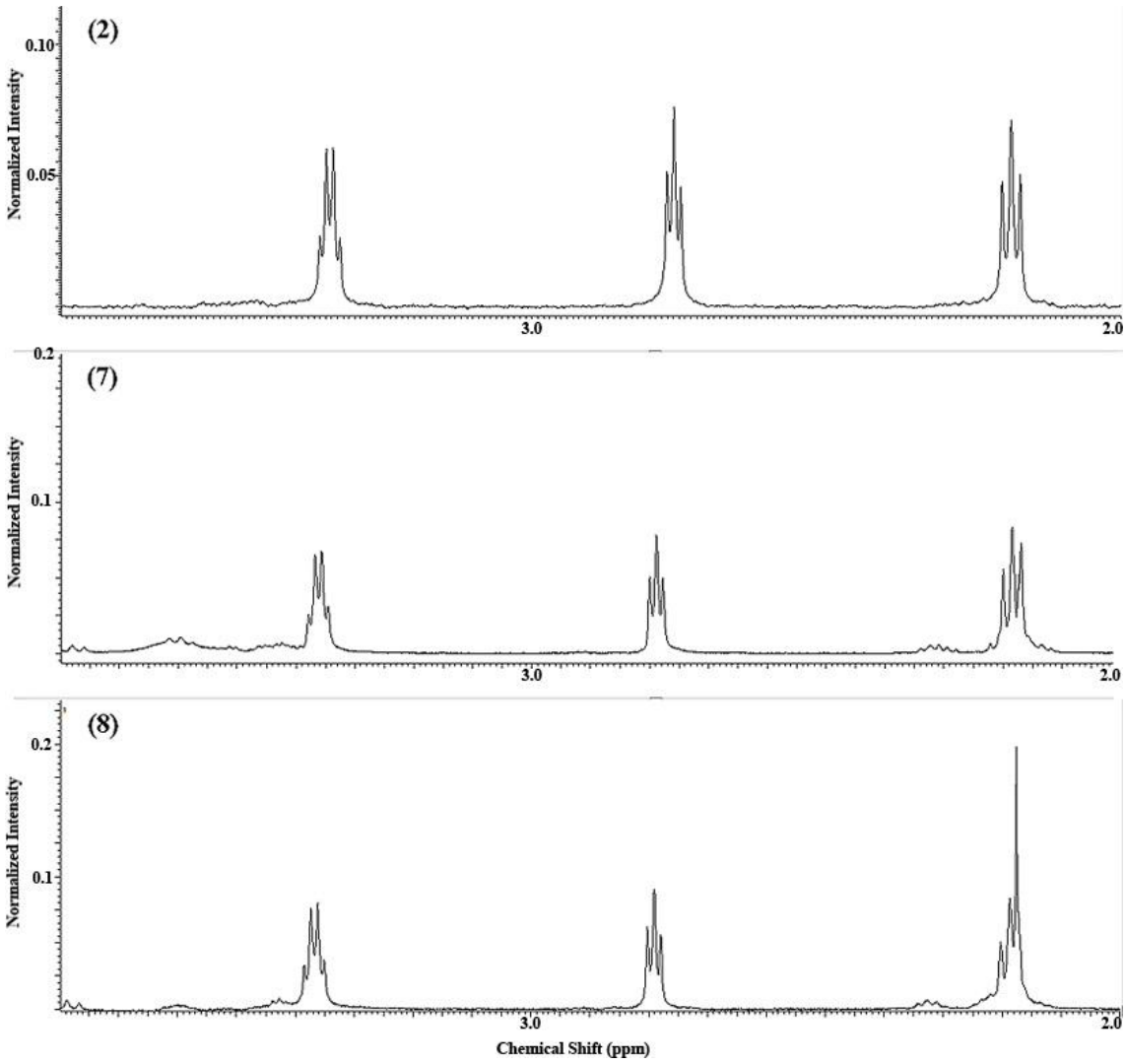

FIGURE 4.5. The Characteristic Area Of ^{1}H NMR Spectra of Compounds 2, 7 and 8.

TABLE 4.1. The Structure of the Synthesized Amidoamines

Compound	Name	Structure
1	N-[2-(2-aminoethylamino)-ethyl]-octadecanamide	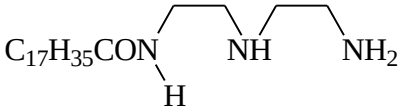
2	N-[2-(2-octadecanoylamino-ethylamino)-ethyl]octadecan	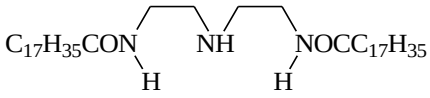
3	N-[2-(2-aminoethyl amino)-ethyl]odecanamide	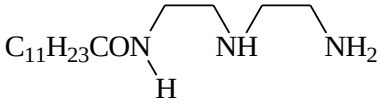
4	N-[2-(2-dodecanoyl amino-ethylamino) -ethyl] dodecan- amide	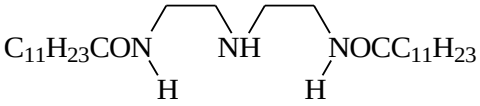
5	2-[2-{2-(2-Aminoethyl amino)-ethylamino}ethyl aminoethyl]octadecanamide	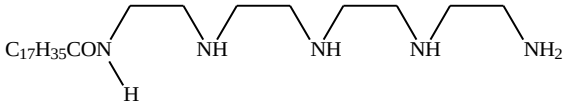
6	2-[2-{2-(2-octadecanoyl amino-ethylamino)-ethyl amino} ethylaminoethyl]-octadecan amide	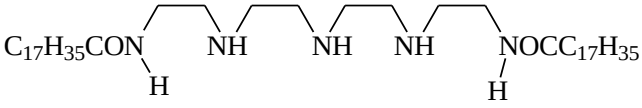
7	N-[2-(2-decanoylamino-ethylamino)-ethyl]octa-decanamide	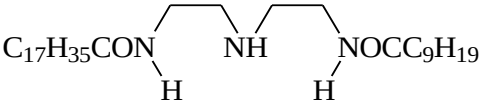
8	N-[2-(2-hexanoylamino-ethylamino)-ethyl]octa-decanamide	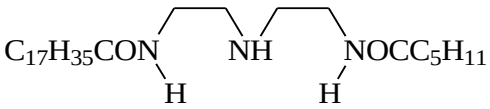

4.1.3. PREPARATION OF IMIDAZOLINE DERIVATIVES.

The start materials are octadecanenitrile, DETA and TEPA. Octadecanonitrile was prepared from octadecanoic acid using an established procedure [75]. 0.1 mol of stearic acid were mixed with 0.27 mol of thionyl chloride. The mixture was dissolved in chloroform and refluxed at 80—83 ^{o}C for about 30 minutes until all the gases are released. The resulting product was a clear brownish solution.

$$CH_3C_{16}H_{32}COOH + SOCl_2 \xrightarrow[80\text{-}83^{o}C,\ reflux]{CHCl_3} CH_3C_{16}H_{32}COCl + SO_2 + HCl$$

0,165 mol of octadecanoyl chloride was reacted with a 30% ammonia solution pre-cooled to around 5 ^{o}C. The reaction mixture was stirred for 30 minutes and then was filtered using a Buchner funnel. The precipitate was re-crystallized in ethyl ether. The yellowish precipitate was dissolved in chloroform and treated with active carbon to remove impurities, then the solvent was removed under vacuum. 0.7 mol of the octadecanoamide were obtained.

$$CH_3C_{16}H_{32}COCl + NH_3 \xrightarrow{5\ ^{o}C} CH_3C_{16}H_{32}CONH_2 + HCl$$

The octadecanoamide was refluxed with 0.7 mol of thionyl chloride in 75mL of benzene at 80-83 ^{o}C for about one hour.

The reaction mixture was extracted with ethyl ether, and then recrystallized from its solution in pentane.

$$CH_3C_{16}H_{32}CONH_2 + SOCl_2 \xrightarrow[80\text{-}83^{o}C,\ reflux]{Benzene} CH_3C_{16}H_{32}CN\ (\mathbf{18}) + SO_2 + 2HCl$$

The imidazolines were prepared by heating the polyamine and octadecanenitrile (**18**) to 150 ^{o}C for around 2 hours, using elemental sulfur as catalyst. The reaction mixture was cooled and dissolved in CH_2Cl_2, washed with water to remove the remaining acid and polyamine, and then the organic layer was separated and dried using Na_2SO_4. The solvent was removed under vacuum to obtain the pure imidazoline (Scheme 4.7 and 4.8).

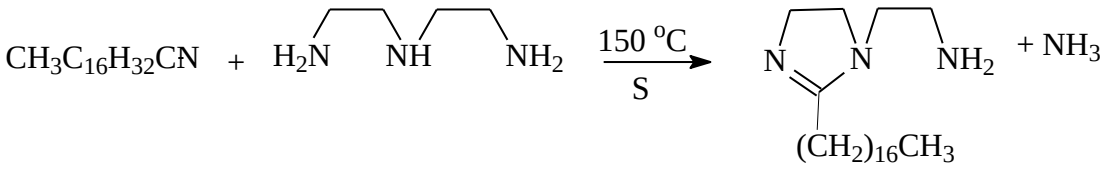

18 **13** **9**

Scheme 4.7

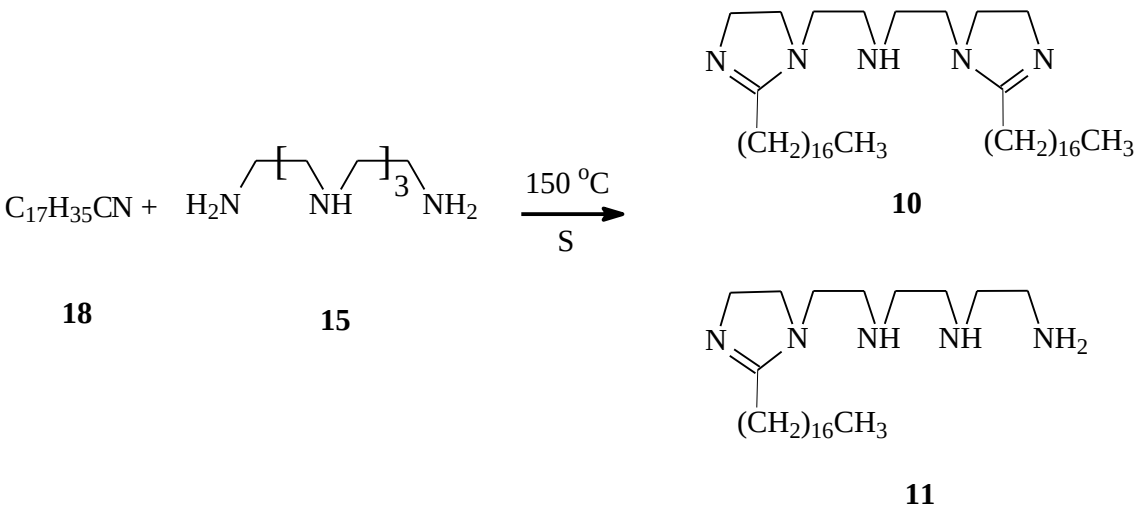

18 **15** **10** **11**

Scheme 4.8

The synthesized imidazolines were identified using spectral analysis including FTIR, ^{1}H NMR and ^{13}C NMR. FTIR was taken for the compounds in solid form. Imidazoline **9** has a doublet peak (3288, 3242) cm^{-1} which corresponds to (N-H stretch) of the primary amine (NH_2), it also has a peak at 1605.0 cm^{-1} which corresponds to primary amine N-H bend. The peak at 1550 cm^{-1} is attributed to the in plane deformation vibration of the N-H bond. The C=N bond is identified by a peak at 1660 cm^{-1} (the ring C=N stretch).

The imidazoline **11** has a doublet peak (3301, 3244) cm^{-1} which corresponds to N-H stretch of the primary amine. The secondary amine N-H stretch adsorption peak is overlapped by the N-H stretch peak for the primary amine which deforms the peak in the range 3300-3240 cm^{-1}. The amine group shows another peak at 1606 cm^{-1} that is due to the primary amine N-H bend. The peak at 1550 cm^{-1} is attributed to the in plane

deformation vibrations of the N-H bond. The ring C=N bond of the imidazoline ring is identified by a peak 1662 cm^{-1} (The ring C=N stretch). This peak is shifted to the high frequency range due to intermolecular the hydrogen bonding in the solid phase of this compound [76].

The imidazoline **10** has a sharp singlet at 3290 cm^{-1} which corresponds to the N-H stretch of the secondary amine group. It is noticed that the peak at 1605 cm^{-1} in **9** and **11** disappears in **10** which is in conformity with the absence of a primary amine in the compound. The peak at 1550 cm-1 is attributed to the in plane deformation vibration of the N-H bond. The C=N ring bond of the imidazoline ring is identified by a peak 1635 cm^{-1} (C=N stretch).

The 1H NMR spectra of compounds **9**, **10** and **11** show triplet in the range 2.8-2.9 ppm and triplet in the range 3.10-3.20 ppm, in the range 3.25-3.35 ppm. Imidazoline **9** exhibits a triplet and each of the imidazolines **10** and **11** exhibits a multiplet. In the range 3.65-3.75 ppm each of imidazolines **10** and **11** exhibits a triplet. These peaks correspond to the four different types of protons on the imidazoline and the polyamine carbon chain.

The ^{13}C NMR spectra of **10** and **11** show four different types of carbons on the polyamine carbon chain and the imidazoline ring, around 33 ppm, 34 ppm, 36 ppm and 38 ppm. The imidazoline **10** molecule shows singlet peaks which reveal its asymmetric structure. Imidazoline **9** shows a doublet with peaks at 36.1, 36.2 ppm and a singlet at 38 ppm.

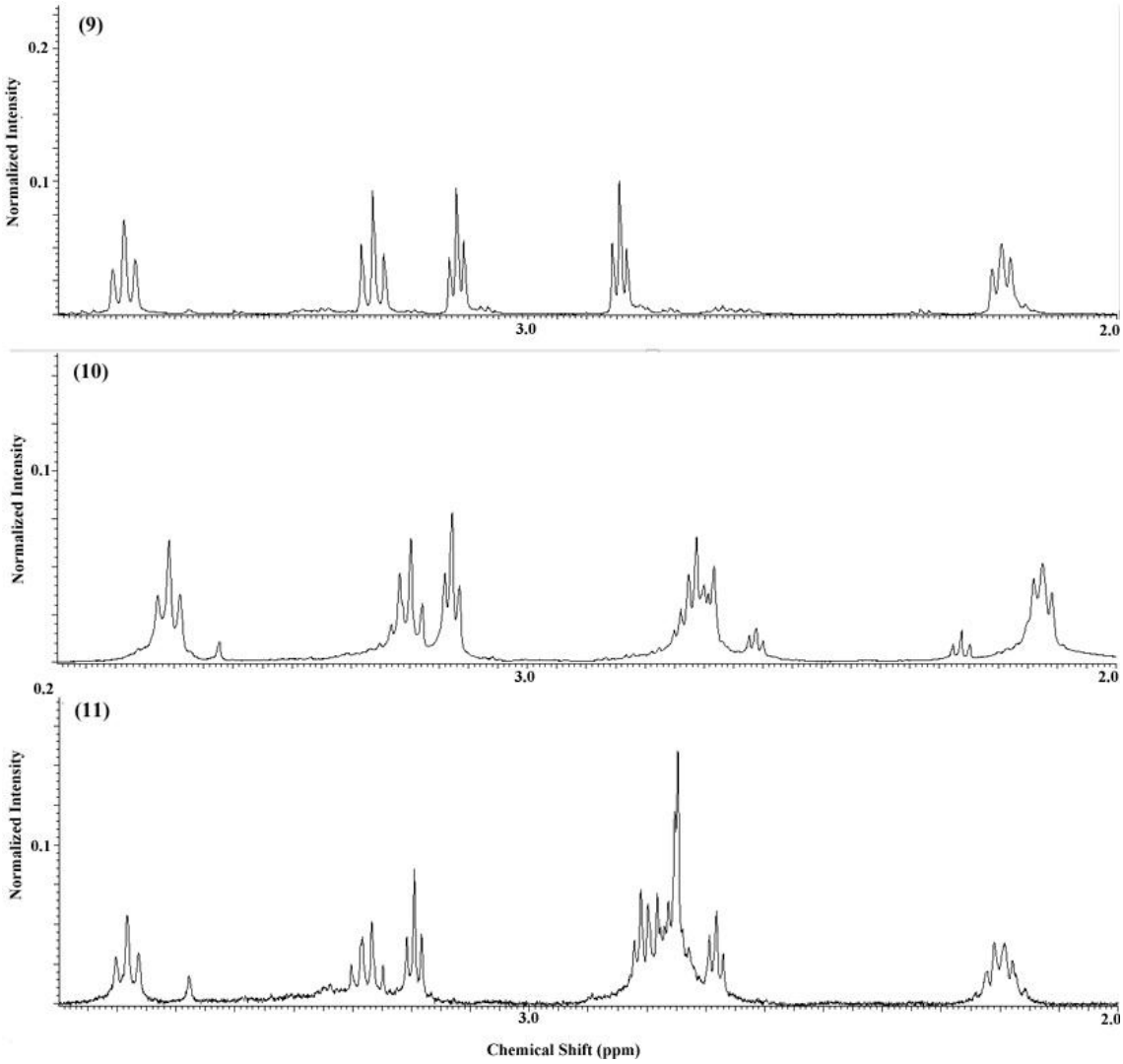

FIGURE 4.6. The Characteristic Area Of ^{1}H NMR Spectra of Compounds 9, 10 and 11.

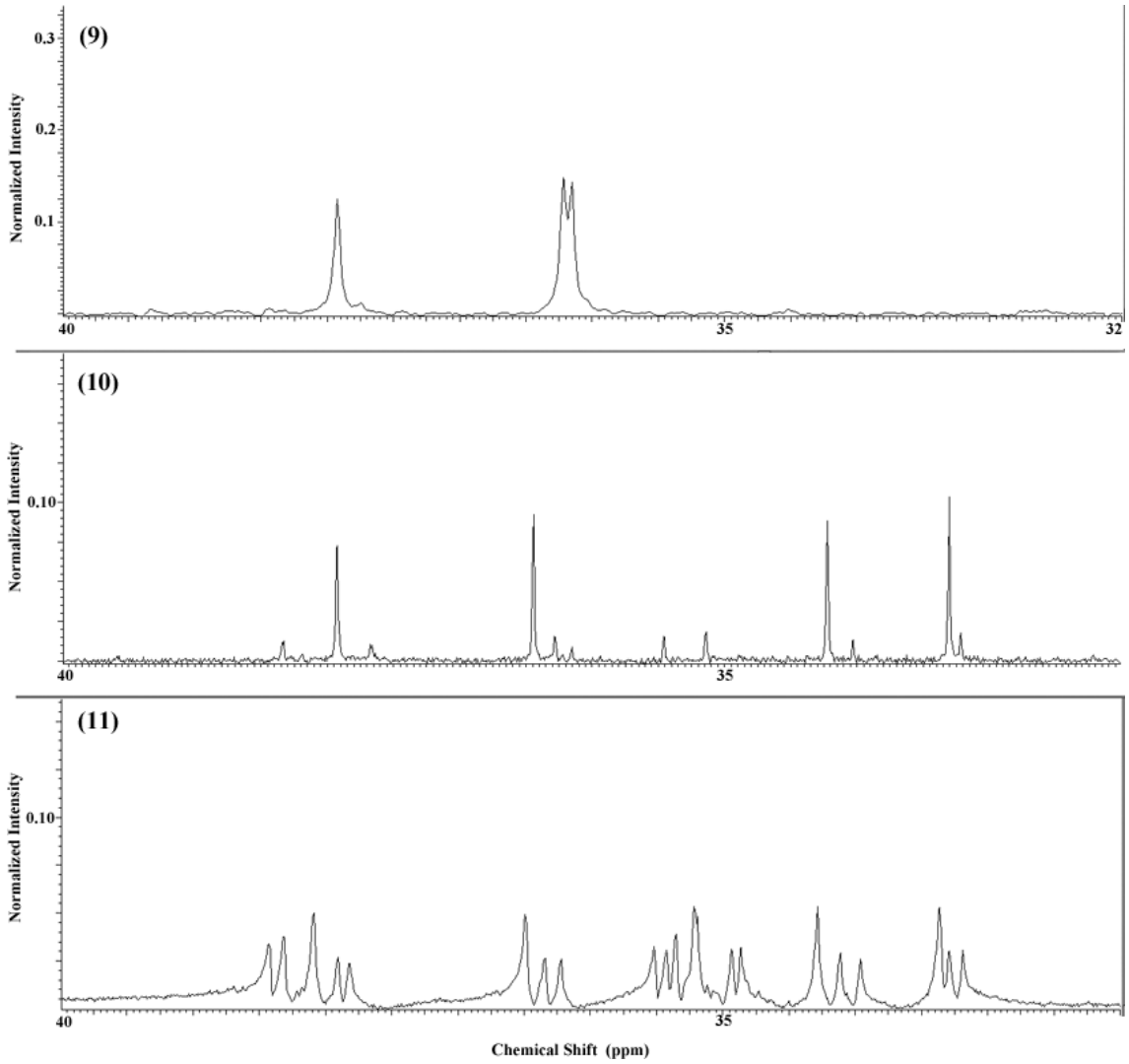

FIGURE 4.7. The Characteristic Area Of ^{13}C NMR Spectra of Compounds 9, 10 and 11.

Table 4.2 shows the structures of the synthesized imidazolines.

TABLE 4.2. The Structure of the Synthesized Imidazolines

Compound	Name	Structure
9	1-(2-aminoethyl)-2-heptadecanyl-2-imidazoline	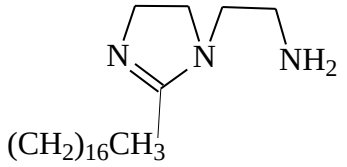
10	N,N'-Di-2,2'-[2-heptadecanyl-2-imidazolinyl]diethylamine	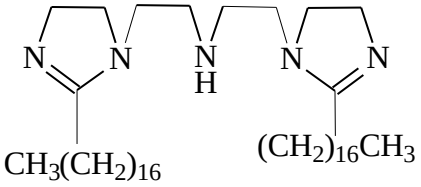
11	1-[2-{2-(2-Aminoethylamino)-ethylamino}ethyl] -2-heptadecanyl-2-imidazolines	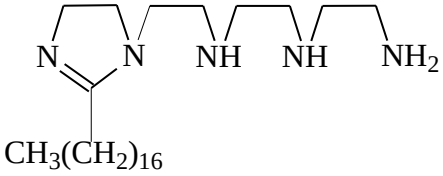

4.2. MEASUREMENTS ON THE INHIBITION EFFICIENCY OF THE SYNTHESIZED COMPOUNDS

4.2.1. THE INHIBITION EFFICIENCY OF AMIDOAMINES

The evaluation of corrosion inhibition of the synthesized compounds was carried out in a 3% NaCl solution saturated with CO_2 gas. Corrosion evaluation was carried out using electrochemical methods (LPR and Tafel) only because the gravimetrical method (NACE 1D182 WHEEL TEST standard method) does not give reproducible readings with pitting corrosion [77, 78].

In CO_2 corrosion systems, when the solution pH is less than 4, the available H^+ ions makes H^+ reduction the dominating cathodic reaction. Also the corrosion rate is found to be flow sensitive at this low pH. Between pH 4 and pH 6, the corrosion rate decreases due to the depletion of H+ in the electrolyte which is required for one of the cathodic reactions in CO_2 corrosion. In addition, another significant cathodic reaction takes place: the direct reduction of H_2CO_3. [34].

To avoid the corrosion caused by oxygen, CO_2 gas purity was selected to be 99.999%. 100 mg/L of $NaHCO_3$ was added to buffer the solution to pH = 5.0-5.5 as measured during the experiment [79].

The experimental setup was designed to maintain oxygen-free (anoxic) conditions, and the solution was purged with CO_2 for 20-30 minutes before the start of the actual

experiment to remove all the dissolved oxygen. The total removal of oxygen and the saturation of the solution with CO_2 is achieved when the open circuit potential is stable. The solution was stirred at a speed around 100 rpm to maintain homogeneity. The solution was maintained at 40 ± 0.5 ^{o}C using a specially designed temperature controlled water bath discussed in the experimental section (3.4.1)

4.2.1.1. ADSORPTION OF THE AMIDOAMINE COMPOUNDS.

Inhibition efficiency values for the synthesized amidoamine as determined by the polarization resistance measurements for various concentrations of the inhibitors at 40 ^{o}C are reported in the Table 4.3

The polarization resistance study showed that not all the synthesized amides were corrosion inhibitors. The effect of the symmetry of the molecule and the hydrocarbon and polyamine chain length can be revealed from the relationship between concentration and prohibition efficiency. The ratio of hydrophobic carbon chain to the hydrophilic polyamine chain affects the micellizasion and solubility of the compounds, with the monoamide amines having better performance than diamidoamines.

The secondary amine group did not give good adsorption on the metal surface as the primary amine group did, which can be attributed to the steric hindrance which prevents dense packing of adsorption layer.

The amidoamine **3** showed a very good solubility in CO_2 saturated brine as well as in an HCl acid solution (pH =5) which is attributed to the formation of the corresponding amine salt.

In a 3% NaCl brine saturated with CO_2, amidoamine **3** achieved a 91% protection at a concentration of 15 ppm. The corresponding diamidoamine **4** showed a maximum efficiency of around 55% at a concentration of 80ppm; close to the limit of its solubility.

On increasing the concentration of amidoamine **4** above 80 ppm the inhibition efficiency decreased. This, as will be discussed later, is attributed to micelle formation in the vicinity of this concentration. This shows that the secondary amine of amidoamine **4** is not strongly adsorbed on the metal surface. The diamide does not dissolve in methanol at room temperature, but partially dissolves in hot methanol which can be attributed to its lower polarity relative to the monoamine. Figure 4.8 illustrates the relationship between inhibitor concentration and the efficiency, or the surface coverage, of amidoamine **3** and amidoamine **4.**

Increasing the hydrocarbon chain length to 18 decreases the efficiency of the molecule, the amidoamine **1,** as a corrosion inhibitor. A concentration of 80 ppm was needed before a protection efficiency of 90% was achieved. The amidoamine **1** has a limited solubility in water, and dissolves in hot methanol. This is attributed to an increase in the size of the hydrophobic portion and in turn a decrease in its polarity.

TABLE 4.3 Corrosion Inhibition Efficiencies of Amidoamines at Different Concentrations for Mild Steel in 3% NaCl Brine saturated with CO_2 As Determined by the Polarization Resistance Method.

Compound									
(1)	C (ppm)	2.5	10	20	30	40	50	70	100
	Eff%	35	57.3	68.1	76	80.6	87.5	89.9	93.4
(3)	C (ppm)	2	5	7	10	15	50		
	Eff%	44.4	65.3	72.5	79.6	90.5	98.2		
(4)	C (ppm)	40	60	80	**90**	**100**			
	Eff%	7.9	29.4	54.9	**45.6**	**27.1**			
(5)	C (ppm)	3	5	10	15	30	**40**	**50**	
	Eff%	25.7	37.1	47.1	48.2	53.3	**45.0**	**30.5**	
(6)	C (ppm)	10	20	30	40	50	**100**		
	Eff%	18.5	33.1	50.4	70.6	79.6	**75.0**		

The diamide **2** did not dissolve in water, methanol, acetone, xylene or aliphatic solvents, thus no corrosion study was done on it. Figure 4.9 illustrates the effect of the hydrophobic chain length on the efficiency of the inhibitors **1** and **3**. On increasing the polar polyamine chain by 2 units (using TEPA instead of DETA); amidoamine **5** reached 53% protection efficiency at a concentration of 30 ppm.

The experiments at the 40 and 50 ppm concentrations gave 45% and 30% protection efficiencies respectively which was found later to be a result of micellization. This shows that increasing the hydrophilic chain reduces the polarity of the molecule and decreases the solubility.

The diamide **6**, which can be viewed as two molecules of amidoamine 1 connected at the terminal amine group, showed an adsorption behavior similar to that of amidoamine **2** and achieved 79% protection at a concentration of 50 ppm, however at 100ppm a slight reduction of protection was noticed. This indicates that due to the greater steric hindrance compound **6** is less adsorbed on the metal surface than amidoamine 1.

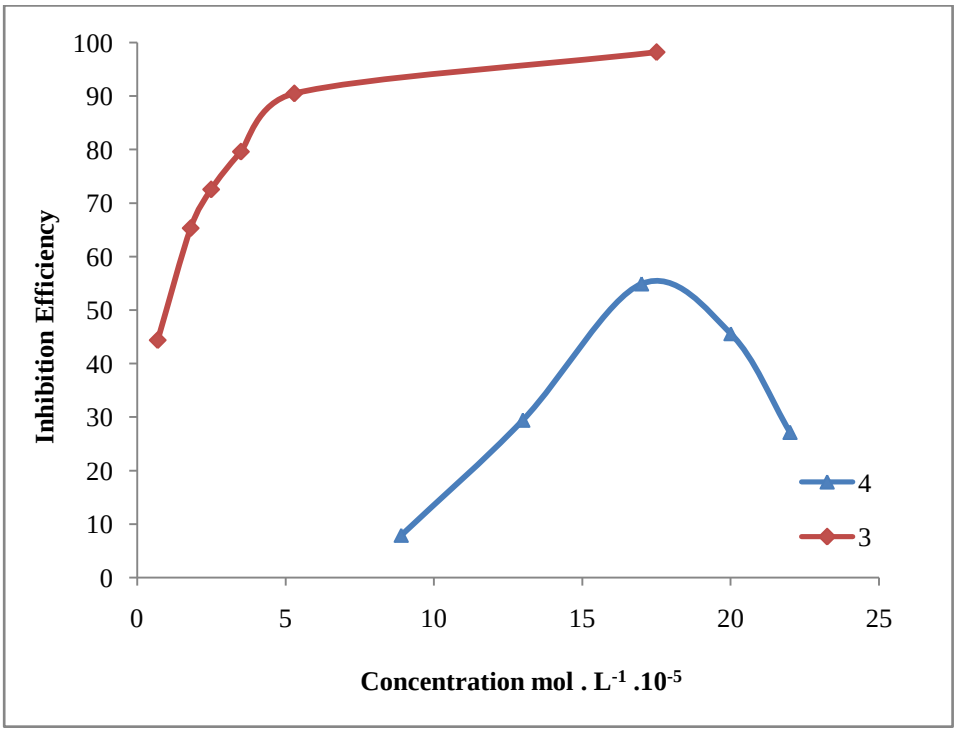

FIGURE 4.8. Inhibition Versus Concentration for Compounds 3 and 4.

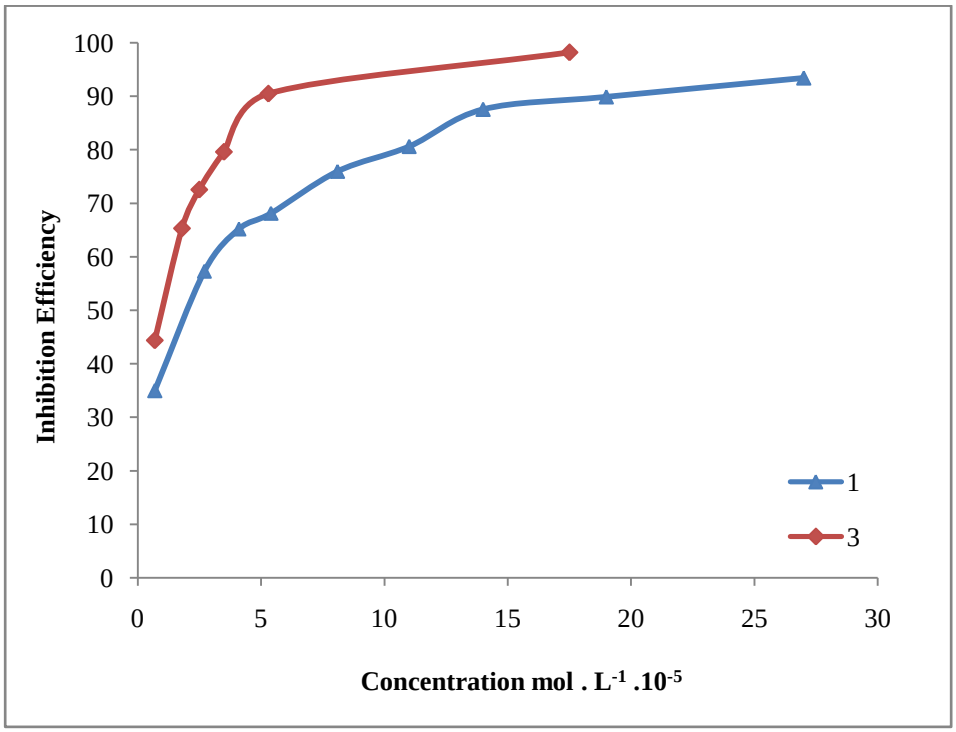

FIGURE 4.9. Inhibition Versus Concentration for Compounds 1 and 3.

Figure 4.10 illustrates the relationships between concentration and corrosion inhibition efficiency for amidoamine **5** and amidoamine 6 and contrasts them with the results for amidoamine 1.

To produce a diamide more polar and more soluble than **2**, acids of different chain lengths were reacted with the amidoamine 1 to obtain amidoamine **7** and **8**. Amidoamine 7 has a limited solubility in water, giving a maximum protection efficiency of 25% at concentrations of 50 ppm and 100 ppm , while amidoamine **8** showed a better solubility than amidoamine **7** and gave 25% protection efficiency at a concentration of 50 ppm and 59 % at a concentration of 200 ppm. Figure 4.11 shows the effect of changing the chain length of the second fatty acid added amidoamine **1**.

The study was limited to 200ppm because solutions of amidoamines **7** and **8** at concentrations higher than 200 ppm were very cloudy and started to precipitate.

Figures 4.12-4.16 show Tafel plots for the synthesized amidoamines. Generally if the inhibitor adsorption shifted the corrosion potential (E_{corr}) in the negative direction with reference to the blank in Tafel plot, it signifies that suppression of the cathodic reaction is the main effect of these corrosion inhibitor. While if the inhibitor adsorption shifted the corrosion potential (E_{corr}) in the noble (less negative) direction with reference to the blank, it signifies that suppression of the anodic reaction is the main effect of these corrosion inhibitor. The slope of a Tafel plot reveals the value of the transfer coefficient; for the given direction of the electrode reaction.

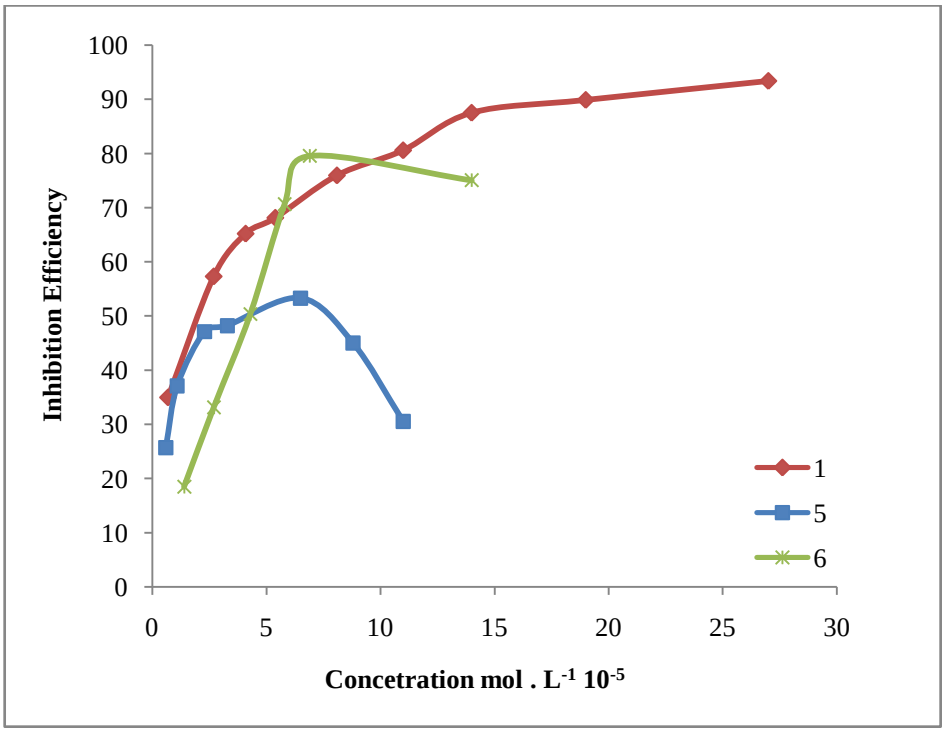

FIGURE 4.10. Inhibition Versus Concentration For Compounds 1, 5 and 6.

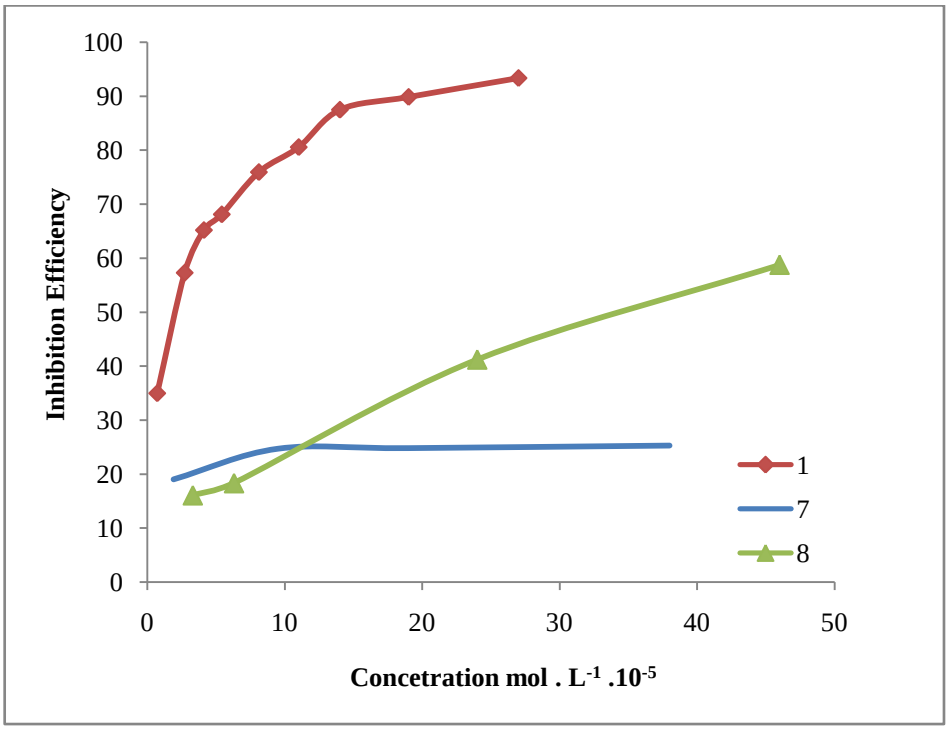

FIGURE 4.11. Inhibition Efficiency Versus Concentration for Compounds 1, 7 and 8.

Table 4.4 shows Tafel constants, corrosion potential and inhibition efficiency of synthesized amidoamines.

A decrease in the values of the anodic and cathodic slopes indicates that the inhibitor did not affect any of the corrosion reactions adversely. Rather, it formed a barrier film, which hindered the diffusion of ions to or from the metal surface. Thus, while the corrosion inhibition by molecules of the first type is predominantly under cathodic control, the inhibition by molecules of the second type (less negative shift) is under anodic control.

TABLE 4.4 Tafel Constants, Corrosion Potential and Inhibition Efficiency of Synthesized Amidoamines.

Compound	C (ppm)	β_A (V/decade)	β_C (V/decade)	E_{corr} (mV)	Eff%
1	2.5	50.60e-3	370.0e-3	-720.0	35.0
	10	116.7e-3	895.9e-3	-698.0	57.3
	20	98.60e-3	447.4e-3	-680.0	68.1
	30	97.90e-3	389.2e-3	-681.0	76.0
	40	93.30e-3	488.7e-3	-694.0	80.6
	50	87.20e-3	251.3e-3	-666.0	87.5
	70	82.80e-3	227.4e-3	-675.0	89.9
3	2	52.20e-3	493.2e-3	-737.0	40.4
	5	49.50e-3	385.6e-3	-731.0	65.3
	7	47.00e-3	314.4e-3	-723.0	72.8
	10	48.80e-3	234.7e-3	-713.0	79.8
	15	63.20e-3	251.4e-3	-689.0	90.5
4	40	54.20e-3	530.6e-3	-746.0	7.9
	60	53.60e-3	575.4e-3	-747.0	29.4
	80	53.50e-3	509.4e-3	-740.0	54.9
	90	53.20e-3	490.3e-3	-744.0	45.6
	100	50.30e-3	597.3e-3	-738.0	15.7
5	3	65.60e-3	596.9e-3	-709.0	25.67
	5	73.80e-3	755.9e-3	-688.0	37.09
	10	41.00e-3	357.1e-3	-673.0	47.13
	15	42.60e-3	411.0e-3	-668.0	48.23
	30	40.10e-3	290.3e-3	-668.0	53.31
	40	42.60e-3	515.9e-3	-673.0	45.01
	50	46.60e-3	547.6e-3	-669.0	30.54
6	10	52.60e-3	532.0e-3	-740.0	18.5
	20	54.80e-3	573.2e-3	-727.0	33.1
	30	67.90e-3	449.7e-3	-730.0	50.4
	40	50.00e-3	243.0e-3	-704.0	70.6
	50	51.30e-3	258.8e-3	-716.0	79.6
	100	50.40e-3	295.7e-3	-722.0	75.1

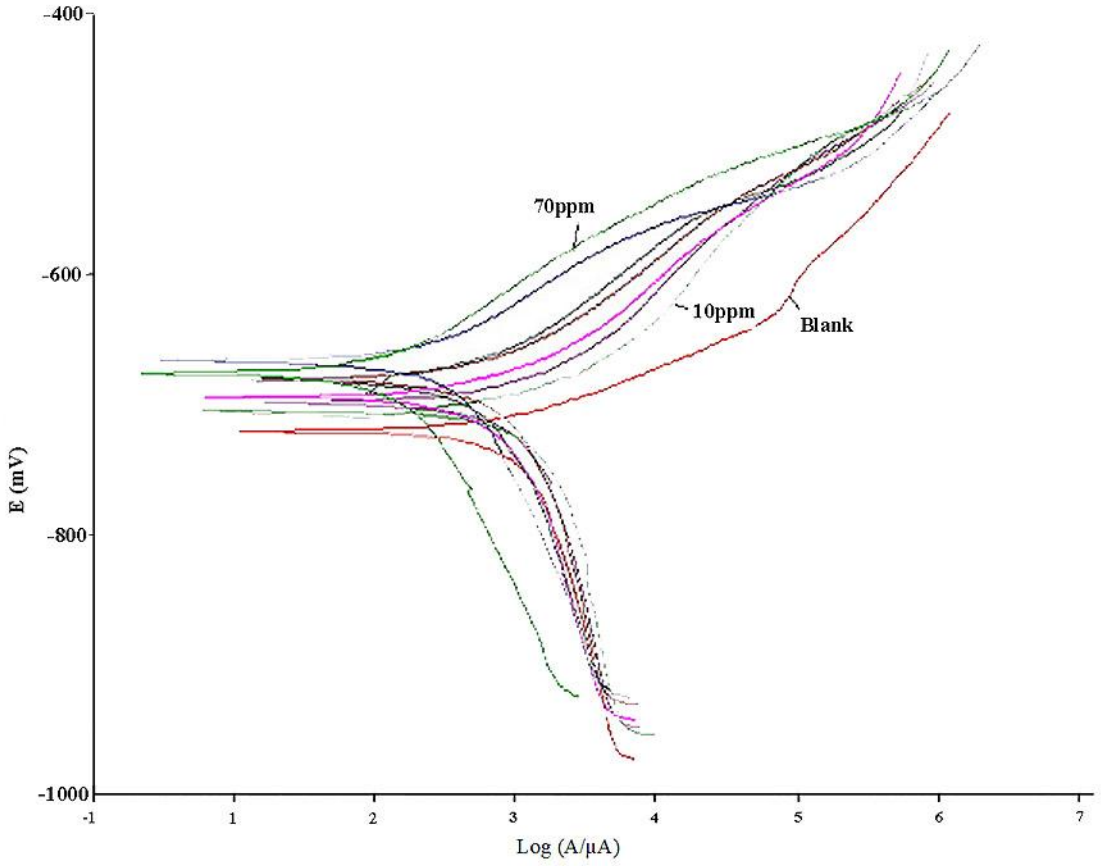

FIGURE 4.12. Tafel Plots for Compound 1 at Different Concentrations.

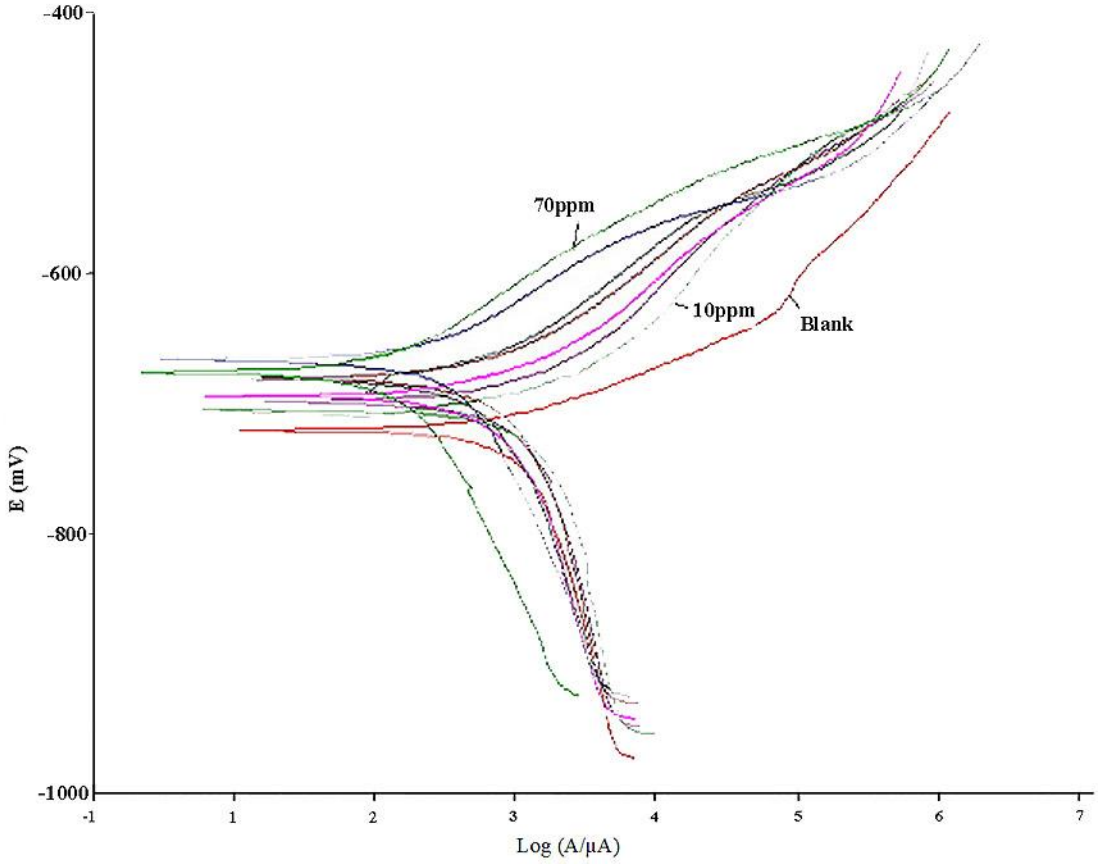

FIGURE 4.13. Tafel Plots for Compound 3 at Different Concentrations.

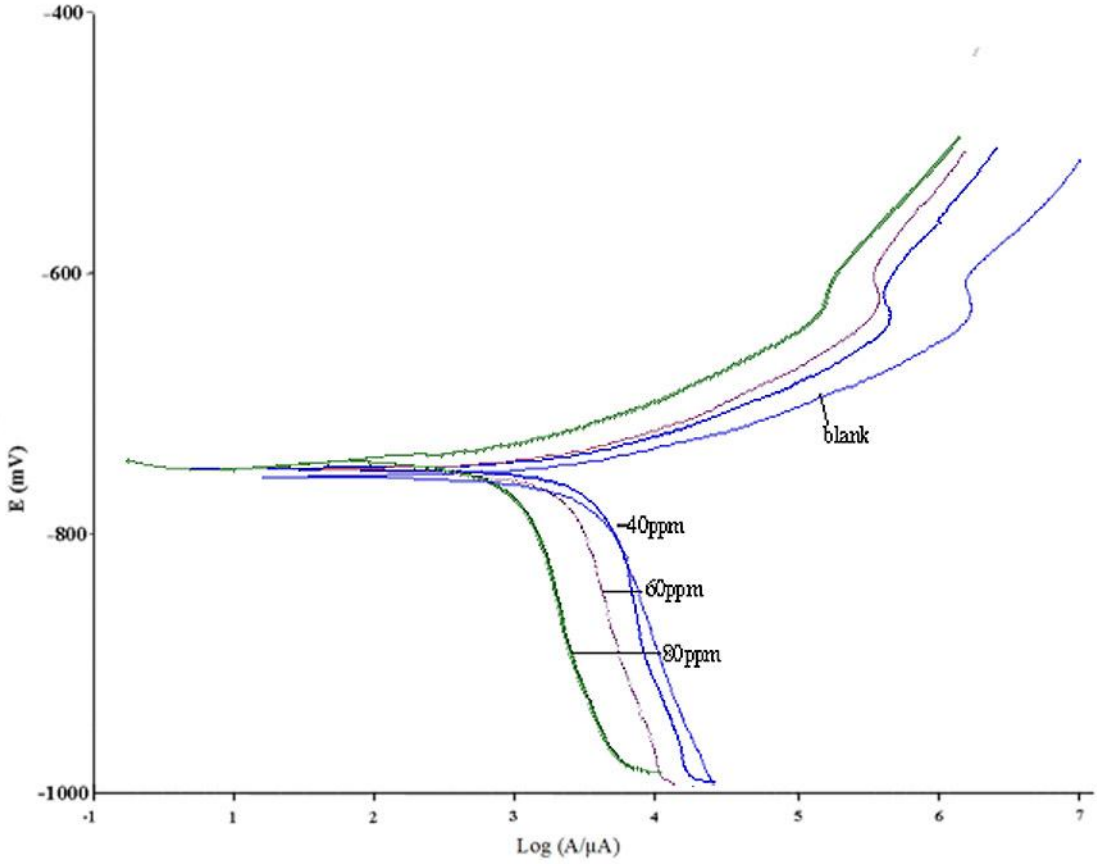

FIGURE 4.14. Tafel Plots for Compound 4 at Different Concentrations.

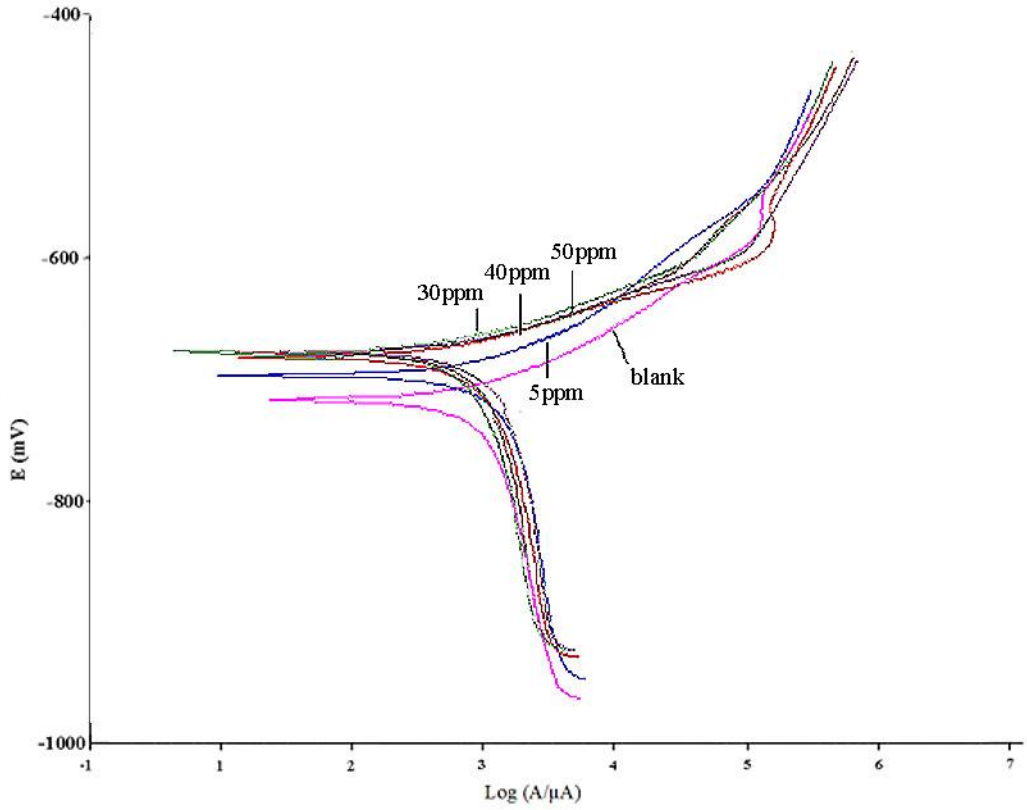

FIGURE 4.15. Tafel Plots for Compound 5 at Different Concentrations.

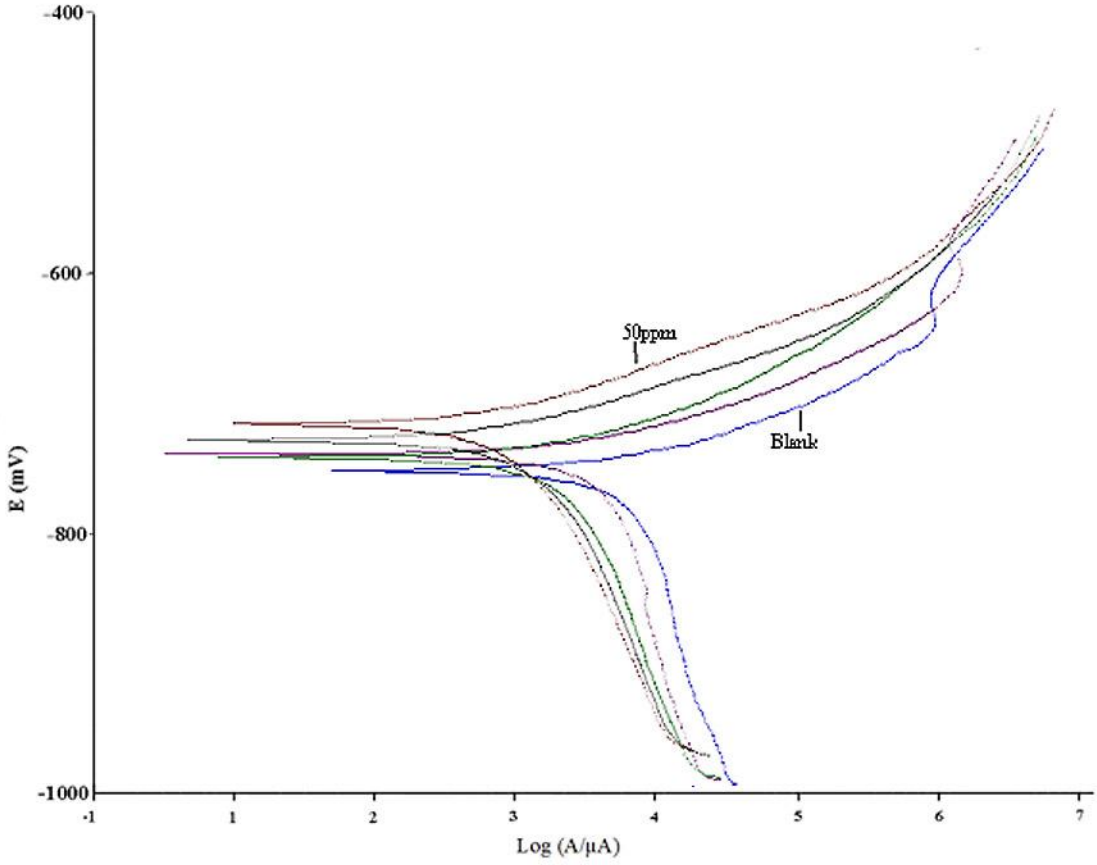

FIGURE 4.16. Tafel Plots for Compound 6 at Different Concentrations.

The Tafel plot of all the inhibitors show that their adsorption shifted the corrosion potential (E_{corr}) in the noble (less negative) direction with reference to the blank, which means that suppression of the anodic reaction is the main effect of these corrosion inhibitors. Amidoamine **4** showed a very slight change in the corrosion potential (E_{corr}) as compared with the other inhibitors, which means it suppressed both the anodic and cathodic reactions. It also showed an increment in the values of the anodic slopes indicating that the inhibitor facilitates the transfer of ions from the surface of the metal to the solution, which can be attributed to micellization at he studied concentration range as will be discussed later.

Amidoamines **1**, **3** and **6** do not affect the Tafel slopes, while amidoamine **5** decreases the value of anodic slope which means it formed a barrier film, which hindered the diffusion of ions from the metal surface to the solution. It is also noted that at the concentration where adsorption reaches its limit, no change is observed in the shape or position of Tafel curve.

As a conclusion, the corrosion inhibition by amidoamines is predominantly under anodic control in CO_2 saturated 3% NaCl brine.

4.2.1.2. ADSORPTION ISOTHERMS OF THE AMIDOAMINE COMPOUNDS.

The surface coverage, θ, (i.e. the fractional inhibition efficiency) values for the synthesized amidoamines are reported in the Table 4.5. The θ values were fitted to the equations for different types of isotherms. The isotherm that fits the data best is the one that gives the highest correlation coefficient.

The thermodynamic parameters of the adsorption process can be calculated from the adsorption isotherm equations. Temkin adsorption isotherm follows the following equation:

$$K_{ads}\, C = e^{f\Theta} \qquad \text{(Eq 4.1)}$$

and Freundluich isotherm follows

$$(\theta = K_{ads}\, C^{\,n}) \qquad \text{(Eq 4.2)}$$

and Frumkin isotherm follows,

$$\frac{\theta}{1-\theta} e^{-2a\theta} = K_{ads}\, C \qquad \text{(Eq 4.3)}$$

and Langumuir isotherm is,

$$\frac{\theta}{1-\theta} = K_{ads}\, C \qquad \text{(Eq 4.4)}$$

where θ is the surface coverage, K_{ads} is the equilibrium constant of the adsorption process and f is a molecular interaction parameter related to the molecular

TABLE 4.5. Surface Coverage *(θ)* versus Concentration (mol. L^{-1}) for Different Amidoamines Tested for the Inhibition of Corrosion of Mild Steel in CO_2 Saturated 3% NaCl Brine.

Compound									
1	C mole × 10^{-5}	0.67	2.71	4.06	5.41	8.12	10.80	13.9	18.90
	Θ	0.35	0.57	0.65	0.68	0.76	0.81	0.88	0.90
3	C mole× 10^{-5}	0.69	1.82	2.48	3.53	5.29			
	Θ	0.44	0.65	0.72	0.79	0.91			
4	C mole× 10^{-5}	8.85	12.80	17.30	**19.90**	**21.70**			
	Θ	0.08	0.29	0.55	**0.46**	**0.27**			
5	C mole× 10^{-5}	0.63	1.06	2.31	3.29	6.52	**8.76**	**11.03**	
	Θ	0.26	0.37	0.47	0.48	0.53	**0.45**	**0.31**	
6	C mole× 10^{-5}	1.42	2.67	4.31	5.82	6.85	**13.98**		
	Θ	0.18	0.33	0.50	0.71	0.80	**0.75**		

interactions in the adsorption layer as well as energetic inhomogeneity of the surface, and *C* is the concentration in mol/L [63].

For Temkin isotherm, the linear fitting slope gave the values of *1/f*, and equilibrium constant K_{ads} is obtained from the intercept ($(1/f)lnK_{ads}$) and for Frumkin isotherms for inhibitors , K_{ads} is the equilibrium constant of the adsorption process, and '*a*' is a constant representing the interaction between adsorbed species. The slopes of the linear fits for the Frumkin's isotherms gave the values of '*2a*'. The concentrations at which surface coverage started to decrease in some of the amines are written in bold. These could not be explained and are not included in our analysis.

(Table 4.6) shows square of coefficient of correlation (R^2) and values of the constants obtained when the data are for different inhibitors in CO_2 saturated 3% NaCl brine are fitted to the adsorption isotherms of Temkin, Frumkin, Langmuir and Freundlich.

The values of the correlation coefficients indicate that except for the data for amidoamine **6** which fitted the Freundlich isotherm best, the Tempkin adsorption isotherm gives the best fit for the data of all the other amides. This may be rationalized in the light of the likely alignment pattern of the molecules on the metal surface (Figure 4.17).

There are two possibilities for adsorption by a monoamide molecule; either via the primary amine group (indicated by the letter A in figure 4.10) or via both the primary amine group and the chain of secondary amine groups (indicated by the letter B

TABLE 4.6. Square of the Correlation Coefficient (R) and Values of the Constants Obtained from Data for Different Amidoamines in CO_2 Saturated 3% NaCl Brine Fitted to the Adsorption Isotherms of Temkin, Frumkin, Langmuir and Freundlich.

Compound	**Temkin (R^2, f)**	**Langmuir (R^2)**	**Frumkin (R^2, a)**	**Freundlich (R^2)**
1	**0.995, 5.94**	0.970	0.458, -0.56	0.981
3	**0.998, 4.47**	0.917	0.315, 0.74	0.993
4	**0.989, 1.43**	0.962	0.969, 0.12	0.979
5	**0.932, 8.67**	0.806	0.725, -0.13	0.880
6	0.954, 2.58	0.891	0.953, 0.24	**0.999**

in figure 4.10). On the other hand the adsorption of a diamide molecule can only occur via the chain of secondary amine groups (indicated by the letter C in Figure 4.17).

Because of this, one diamide molecule occupies the same surface area required by two monoamide molecules which explains the low surface coverage, their apparent high intermolecular interaction, and thus their following Freundluich adsorption pattern. However, amide **4** molecule has shorter hydrophobic and hydrophilic chains, which makes the intermolecular repulsive forces between amide **4** molecule less than those between **6** molecules, and the thus the surface coverage is higher than in **6**, which makes it follow Temkin isotherm.

Amidoamine **5** shows low correlation coefficients for all types of isotherms because of the long hydrophobic and hydrophilic chains, and low molecule polarity, which makes it have lower tendency to adsorb to the metal surface compared to amidoamine **1** and **6**.

The molecular interaction constant f (Eq.4.1) depends on the charge at the hydrophilic nitrogen (N^+) as well as steric factors of the hydrophobic chain [79]. The lower values of f (around 4.468) observed in amidoamine **3** compared to the significantly higher f value of 8.666 for amidoamine **7** indicates that the repulsive forces between adsorbed species and species in solution are greater for molecules of compound **7** than for the molecules of compound **3,** which can also be explained in the light of the special alignment illustrated in Figure 4.17.

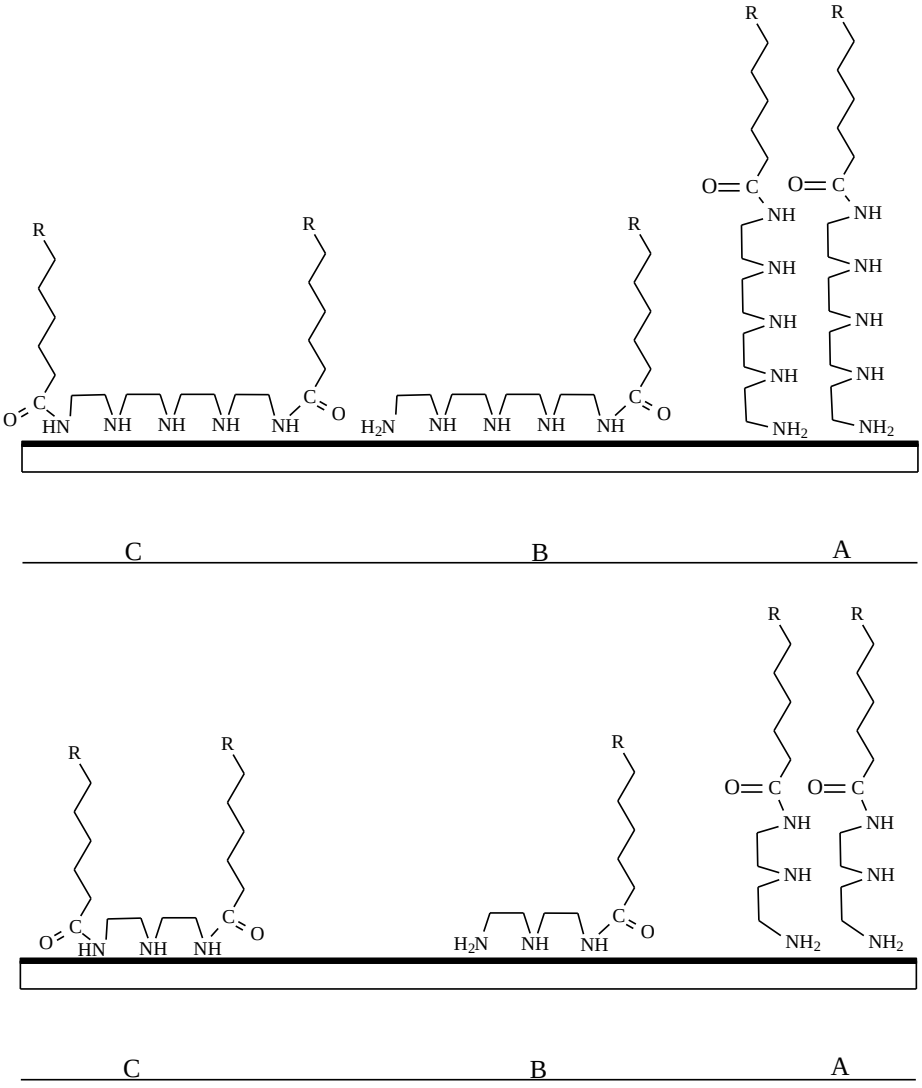

FIGURE 4.17. Adsorption and Surface Alignment of The Synthesized Amidoamines.

The logarithmic form of Temkin isotherm can be written as:

$$\theta = \frac{1}{f} \ln(C) + \frac{1}{f} \ln(K_{ads}) \qquad \text{(Eq 4.5)}$$

The equilibrium constants K_{ads} were obtained from the intercepts of the line obtained from plotting θ against ln (C). In the same manner the logarithmic form of Freundluich isotherms can be written as:

$$\log(\theta) = n \log C + \log(K_{ads}) \quad \text{(Eq 4.6)}$$

The intercepts of the line obtained from plotting log θ against log C is log $K_{ads.}$. The equilibrium constant of the adsorption process K_{ads} is related to the free energy of adsorption (ΔG_{ads}), by:

$$K_{ads} = \frac{1}{C_m} e^{\frac{-\Delta G_{ads}}{RT}} \qquad \text{(Eq 4.7)}$$

where (C_m) is the molar concentration of water in solution which can be obtained from the following relation.

$$C_m = \frac{d_T \times 1000}{Mw} \qquad \text{(Eq 4.8)}$$

Where d_T is the density of water at the experiment temperature (40 ^oC), M is the molar mass of water. The molar concentration of water at 40 ^oC is 55.09. The value of K_{ads} and ΔG^o_{ads} of the inhibitors are given in table 4.5.

The calculated Gibbs free energy of adsorption (ΔG_{ads}) shows that the adsorption of amidoamines is spontaneous.

TABLE 4.7. The Molecular Interaction Parameter f , The Equilibrium Constant Of The Adsorption K_{ads}, and The Free Energy Of Adsorption (ΔG_{ads}) Of The Synthesized Amidoamines.

Compound	**Adsorption Pattern (R^2)**	f	$K_{ads}\,(L\times10^5/mol)$	$\Delta G_{ads}\,(kJ/mol)$
(1)	Temkin , 0.996	5.924	11.30	-46.73
(3)	Temkin, 0.989	4.468	10.35	-46.50
(4)	Temkin , 0.998	1.431	0.124	-34.98
(5)	Temkin , 0.932	8.666	19.32	-48.12
(6)	Freundlich, 0.999	-	0.06	-33.13

4.2.2. THE INHIBITION EFFICIENCY OF IMIDAZOLINE

Inhibition efficiency values for the synthesized imidazolines as determined by the polarization resistance measurements for various concentrations of the inhibitors at 40 ^{o}C are reported in the Table 4.8.

The polarization resistance study showed that all the synthesized imidazolines were corrosion inhibitors. The effect of the symmetry of the molecule and the polyamine chain length can be revealed from the relationship between concentration and prohibition efficiency. The length of hydrophilic polyamine chain affects the number of adsorption sites and thus the adsorption thermodynamics.

4.2.2.1. THE INHIBITION EFFICIENCY OF IMIDAZOLINE

The imidazoline **9** showed a good adsorption on the metal surface, and achieved a 66% protection at a concentration of 15 ppm. On increasing the polar polyamine chain to 2 unites (using TEPA instead of DETA); the imidazoline **11** showed a significant increment in performance, which shows that increasing the hydrophilic chain length increases the solubility of the product and affected the adsorption of the molecule.

TABLE 4.8. Corrosion Inhibition Efficiencies of Imidazolines at Different Concentrations for Mild Steel in 3% NaCl Brine saturated with CO_2 As Determined by the Polarization Resistance Method

Compound									
(9)	C (ppm)	1	2	5	8	10	15	50	100
	C (mol/L $\times 10^{-6}$)	2.84	5.69	14.2	22.8	28.4	42.7	142	284
	Eff%	23.06	30.53	54.03	62.62	64.74	66.09	84.5	88.4
(10)	C (ppm)	1	2	3	5	8	15	50	100
	C (mol/L $\times 10^{-6}$)	1.46	2.91	4.37	7.29	11.7	21.9	72.9	146
	Eff%	15.05	26.17	43.09	65.72	74.86	85.19	95.56	96.04
(11)	C (ppm)	3	7	10	15	20	50	100	
	C (mol/L $\times 10^{-6}$)	6.9	16	23	34	46	110	230	
	Eff%	14.34	49.89	65.37	78.36	87.17	90.2	94.5	

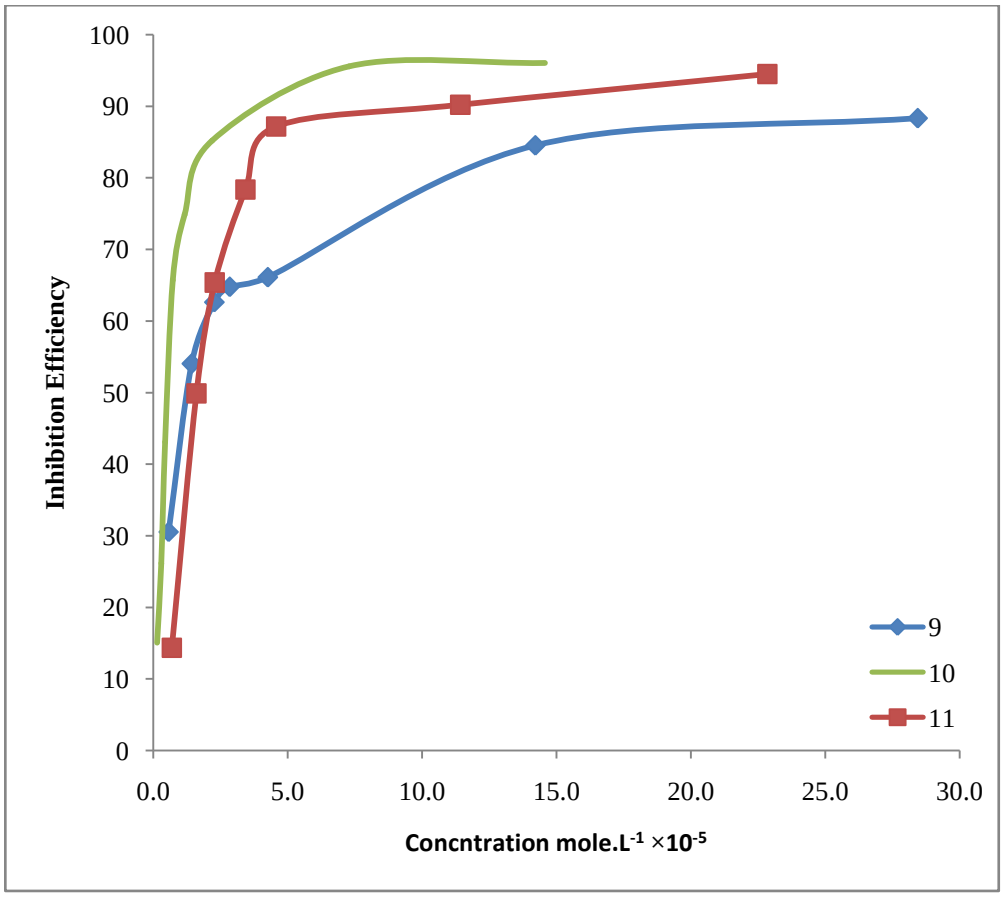

FIGURE 4.18. Inhibition Versus Concentration for Compounds 9 and 10 and 11.

The diimidazoline **10**, which can be also be considered as two molecules of imidazoline **9** connected at the terminal amine group, showed a good adsorption behavior and achieved 66% protection at a concentration of 5 ppm, and 75% at a concentration of 8ppm, however, at higher concentration, a slight increment of protection was noticed, this can be attributed to the presence of two imidazoline rings on the same molecule which increases the electron density on polar end. The concentration (mole) vs. surface coverage relationship (Table 4.9) shows that at high concentrations , imidazoline **10** requires lower molar concentration to reach the same surface coverage compared to imidazoline **9**, which shows that imidazoline **10** behaves as two connected imidazoline **9** molecules.

Figures 4.20-2.22 show Tafel plots for the synthesized imidazolines, and table 4.9 shows the corresponding Tafel constants, corrosion potentials and inhibition efficiencies. The Tafel plot of all the inhibitors show that their adsorption shifted the corrosion potential (E_{corr}) in the noble (less negative) direction with reference to the blank, which means that suppression of the anodic reaction is the main effect of these corrosion inhibitors. Imidazoline **9** and **11** do not significantly affect Tafel slopes, while **10** decreases the values of cathodic slope. This means imidazoline **10** formed a barrier film, which hindered the diffusion of ions from the solution, to the metal surface. As a conclusion, the corrosion inhibition by these molecules is predominantly under anodic control in CO_2 saturated 3%NaCl brine.

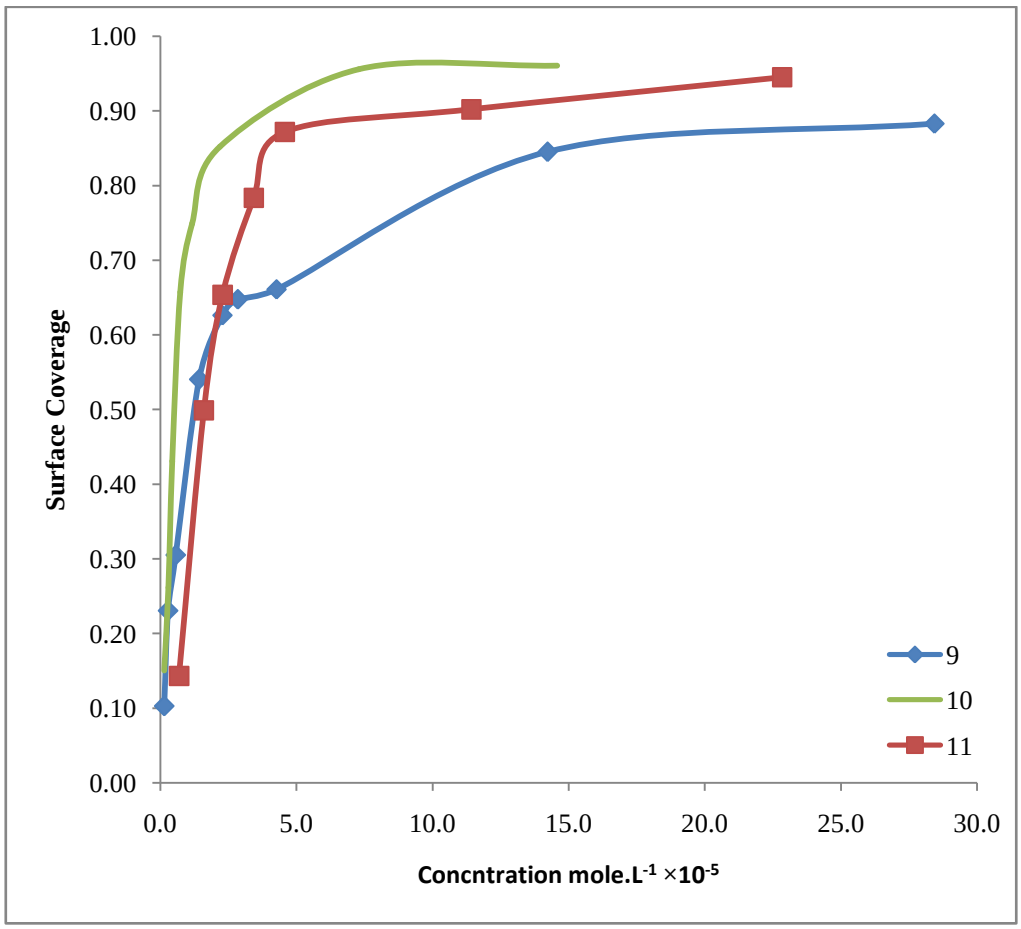

FIGURE 4.19. Surface Coverage Vs concentration for Compounds 9, 10 and 11.

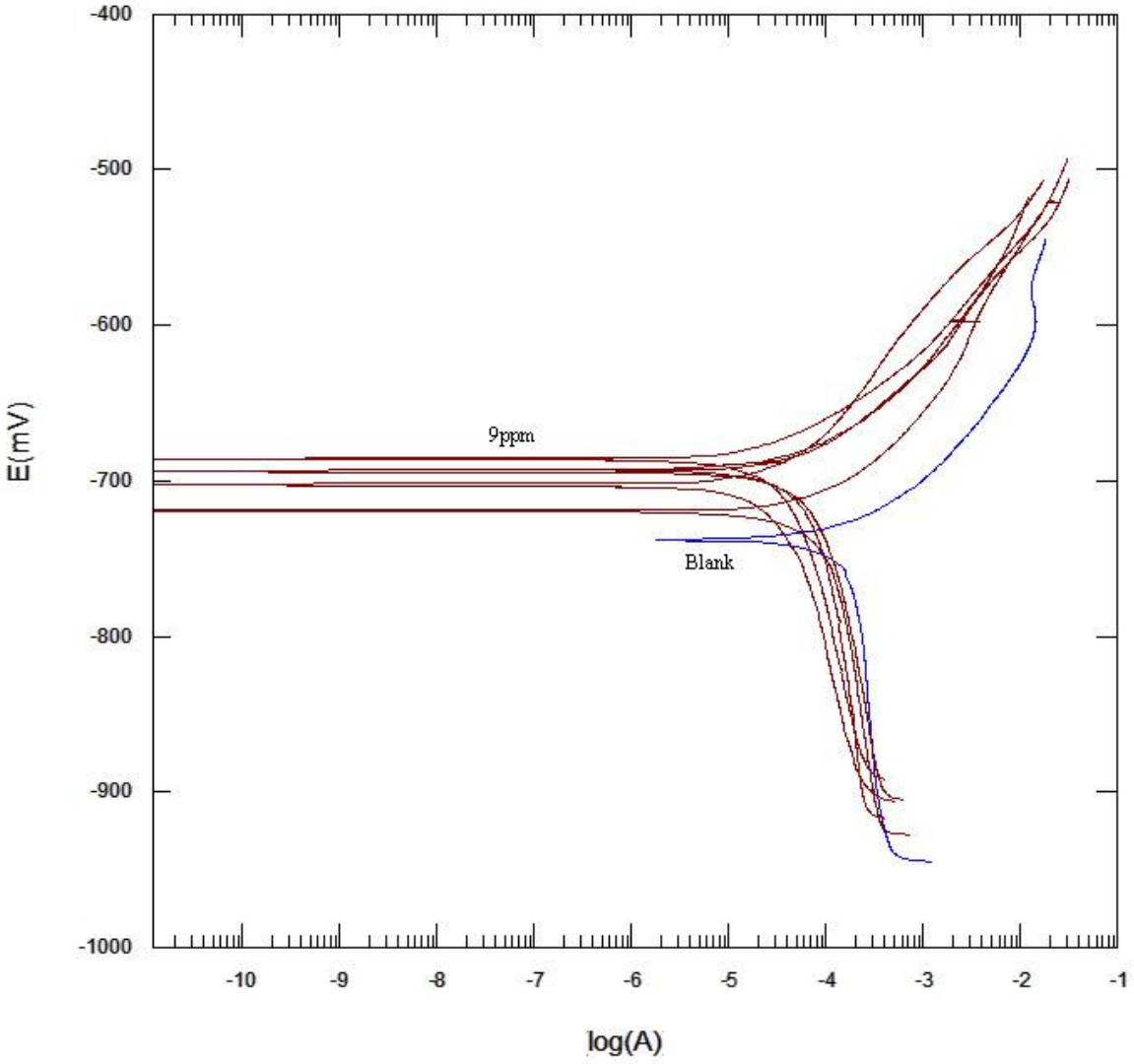

FIGURE 4.20. Tafel Plots for Imidazoline **9** at Different Concentrations.

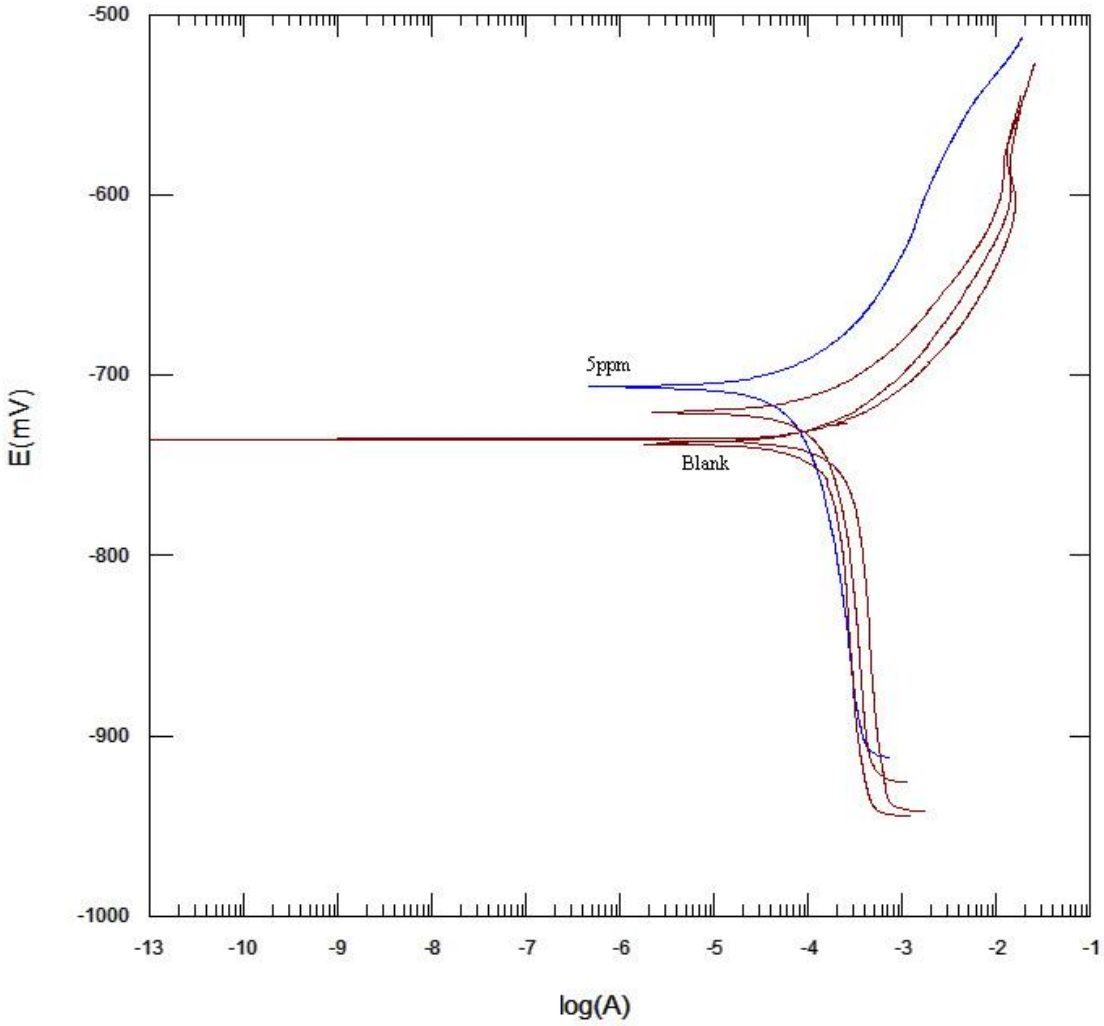

FIGURE 4.21. Tafel Plots for Imidazoline **10** at Different Concentrations.

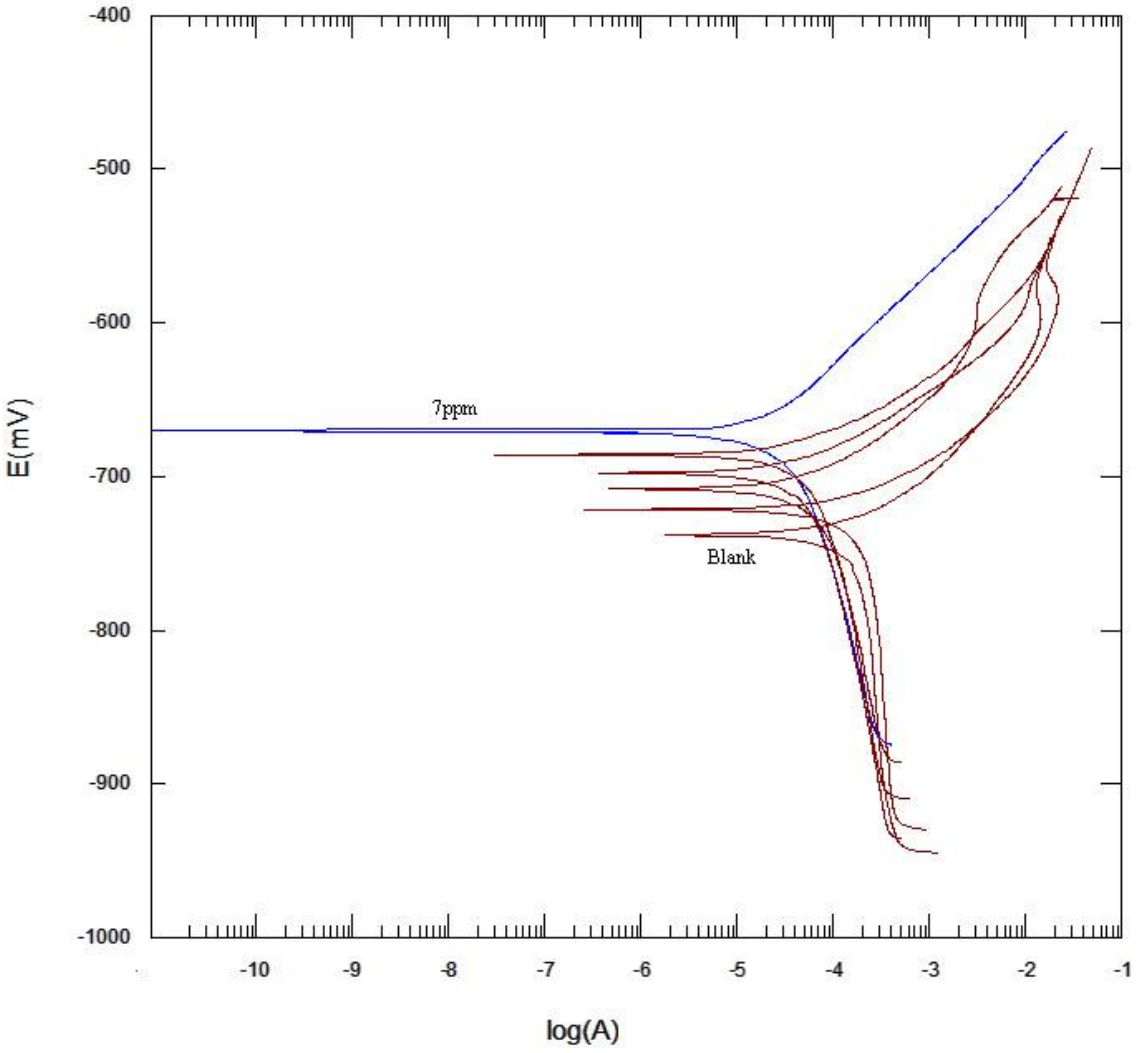

FIGURE 4.22. Tafel Plots for Imidazoline **11** at Different Concentrations.

TABLE 4.9 Tafel Constants, Corrosion Potential and Inhibition Efficiency of Synthesized Imidazolines.

Compound	C (ppm)	β_A (V/decade)	β_C (V/decade)	E_{corr} (mV)	Eff%
9	2	0.0603	0.334	-725.8	49.74
	3	0.0576	0.417	-721.0	60.67
	5	0.0703	0.314	-701.1	70.33
	7	0.0786	0.252	-695.0	79.35
	9	0.0486	0.231	-689.5	82.08
10	1	0.06.55	1.13	-736.0	11.06
	3	0.06.32	0.873	-720.8	35.67
	5	0.07.43	0.413	-706.9	62.48
	8	0.07.60	0.320	-702.3	83.07
11	2	0.04.67	0.2810	-727.6	23.05
	3	0.04.36	0.2870	-700.9	58.68
	5	0.04.22	0.2618	-695.6	75.27
	7	0.04.11	0.2542	-670.8	86.02

4.2.2.2 . ADSORPTION ISOTHERMS OF THE IMIDAZOLINE COMPOUNDS.

Surface coverage (θ, i.e. fractional inhibition efficiency) values for the synthesized imidazolines are reported in the Table 4.10. The θ values were used to find the best adsorption isotherm between those more frequently used, i.e. Temkin, Langmuir, Frumkin and Freundluich.

Table 4.11 shows square of coefficient of correlation (R^2) and values of the constants in the adsorption isotherms of Temkin, Frumkin, Langmuir and Freundlich in the presence of inhibitors in CO_2 saturated 3% NaCl brine at 40 ^oC.

The correlation coefficient indicated the best fit for the Temkin's adsorption isotherm for the imidazolines **9** and **11**, while imidazoline **10** fits for Langmuir. This can be understood in the light of alignment pattern of the molecules on the metal surface (Figure 4.23).

Molecular interaction constant *f* is dependent on the charge at the hydrophilic nitrogen (N^+) as well as steric factors of the hydrophobic chain. The lower values of *f* (2.397) observed in imidazoline **11** compared to the significantly higher *f* value (5.599) of imidazoline **9** indeed signify stronger forces of repulsion between the adsorbed and adsorbing molecules in imidazoline **9** compared to imidazoline **11**, which also can be explained in the light of special alignment illustrated in Figure 4.23.

TABLE 4.10 Surface Coverage (θ) versus Concentration (mol. L^{-1}) for Different Imidazolines Tested for the Inhibition of Corrosion of Mild Steel in CO_2 Saturated 3% NaCl Brine.

Compound									
(9)	C mole× 10^{-5}	0.14	0.28	0.57	1.42	2.28	2.84	4.27	14.2
	θ	0.10	0.23	0.31	0.54	0.63	0.65	0.66	84.5
(10)	C mole× 10^{-5}	0.15	0.29	0.44	0.73	1.17	2.19		
	θ	0.15	0.26	0.43	0.66	0.75	0.85		
(11)	C mole × 10^{-5}	0.69	1.6	2.3	3.4	4.6			
	θ	0.14	0.50	0.65	0.78	0.87			

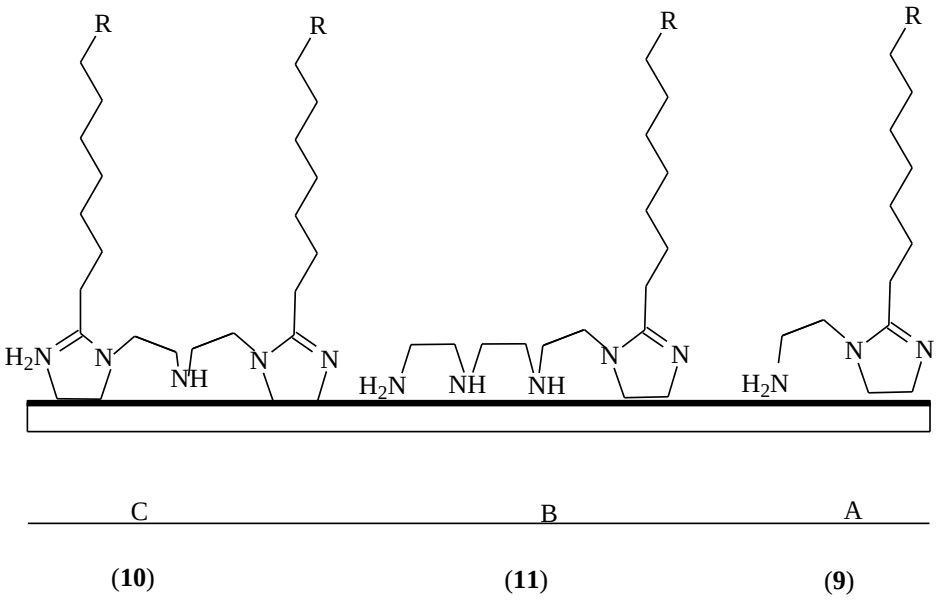

FIGURE 4.23. Adsorption and Surface Alignment of The Synthesized Imidazolines.

TABLE 4.11 Square of the Correlation Coefficient (R) and Values of the Constants Obtained from Data for Different Imidazolines in CO_2 Saturated 3% NaCl Brine Fitted to the Adsorption Isotherms of Temkin, Frumkin, Langmuir and Freundlich.

Compound	Temkin (R^2, f)	Langmuir (R^2)	Frumkin (R^2, a)	Freundlich (R^2)
(9)	**0.9809, 5.627**	0.8914	0.4373, -0.670	0.9369
(10)	0.9676, 3.541	**0.9959**	0.9339, 0.747	0.9257
(11)	**0.9949, 2.581**	0.9533	0.9923, 0.525	0.9214

The equilibrium constants K_{ads} for Temkin isotherms were obtained from the intercepts of the line obtained from plotting Θ against ln(C). In the same manner for Freundluich isotherms, the intercepts of the line obtained from plotting log(Θ) against log(C) is log(K_{ads}). The free energy of adsorption (ΔG_{ads}) was calculated from the equilibrium constant of the adsorption process K_{ads} using (Eq 4.7). The value of K_{ads} and ΔG^{o}_{ads} of the inhibitors are listed in Table 4.12.

4.2.3. ADSORPTION THEROMDYNAMIC PARAMETERS OF THE IMIDAZOLINE COMPOUNDS.

Inhibition efficiency values for the synthesized imidazolines were determined by the polarization resistance measurements for various concentrations of the inhibitors at different temperatures in the range 30-60 ^{o}C .

The relationship between Gibbs free energy of adsorption (ΔG_{ads}) , enthalpy of adsorption (ΔH_{ads}) , entropy of adsorption (ΔS_{ads}) and temperature is:

$$\Delta G_{ads} = \Delta H_{ads} - T\,\Delta S_{ads} \qquad \text{(Eq 4.9)}$$

The relationship of Gibbs free energy with temperature is a linear. The slope of the best fit line is ΔS_{ads} and the intercept is ΔH_{ads}. Figure 4.24 show the Gibbs free energy vs. temperature plots for (**9**), (**10**) and (**11**).

Table 4.13 shows that the values of ΔG_{ads} and ΔH_{ads} for the imidazolines are negative which indicates a spontaneous and exothermic adsorption. ΔG_{ads} for imidazoline **11** does not significantly change with temperature, compared to ΔG_{ads} for imidazoline **9** which decreases significantly with temperature. The value of ΔH_{ads} suggests that the adsorption of the imidazolines is physisorption.

TABLE 4.12 The Molecular Interaction Parameter *f* , The Equilibrium Constant Of The Adsorption K_{ads}, and The Free Energy Of Adsorption (ΔG_{ads}) Of The Synthesized Imidazolines.

Compound	**Adsorption Pattern (R^2)**	***f***	K_{ads} *(L* $\times 10^5$*/mol)*	ΔG_{ads} *(kJ/mol)*
(9)	Temkin, 0.9809	5.627	12.26	-46.96
(10)	Langimur, 0.9959	-	2.80	-43.11
(11)	Temkin, 0.9949	2.581	1.86	-42.05

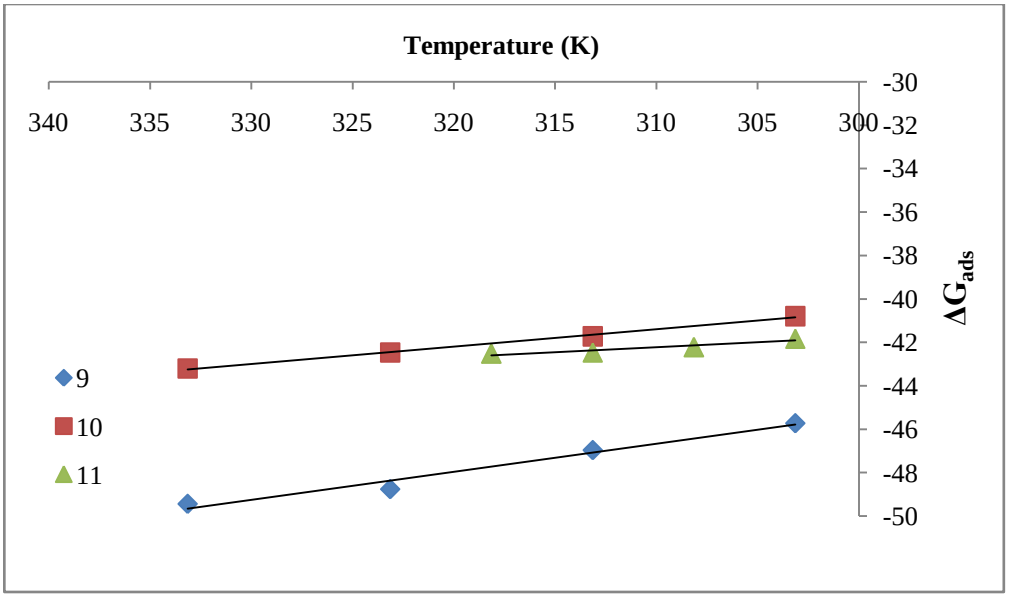

FIGURE 4.24. Gibbs Free Energy Versus. Temperature Plot For The Synthesized Imidazolines.

TABLE 4.13 The Molecular Interaction Parameter f , The Equilibrium Constant Of The Adsorption K_{ads}, And The Thermodynamic Parameters Of The Synthesized Imidazolines At Different Temperatures.

Compound	**T ^{o}C**	**R^2**	***f***	**K_{ads}** *($L\times10^5/mole$)*	**ΔG_{ads}** (kJ/mol)	**ΔH_{ads}** (kJ/mol)	**ΔS_{ads}** (J/mol K)
9	30	0.988	5.96	13.70	-45.73	-6.58	129.3
	40	0.981	5.63	12.38	-46.96		
	50	0.995	4.78	13.89	-48.76		
	60	0.985	4.04	10.34	-49.44		
10	30	0.993	-	1.93	-40.79	- 16.67	79.8
	40	0.997	-	2.80	-41.72		
	50	0.997	-	3.79	-42.47		
	60	0.993	-	5.09	-43.20		
11	30	0.996	3.45	2.92	-41.84	- 28.01	45.9
	35	0.994	2.78	2.60	-42.23		
	40	0.991	2.58	2.20	-42.47		
	45	0.987	2.16	1.74	-42.52		

In typical adsorption systems the surface upon which adsorption occurs does not vary with temperature, and the medium from which the adsorbate molecules come also does not vary. As the following paragraphs clarify this is not the case for the adsorption isotherms obtained by us from electrochemical corrosion measurements.

Dry CO_2 is not corrosive; the corrosiveness of CO_2 comes from the weak carbonic acid H_2CO_3 which undergoes the following solution equilibria.

$$CO_2\,(g) \rightleftharpoons CO_2\,(aq) \qquad (4.1)$$

$$CO_2\,(aq) + H_2O \rightleftharpoons H_3CO^-\,(aq) + H^+ \qquad (4.1)$$

The rate of reaction (4.1) decreases with increasing temperature under isobaric conditions, consequently the rate of the second reaction also decreases, i.e. corrosivity decreases.

The adsorption of these corrosion inhibitors depends on the charge and type of ions on the metal surface, the homogeneity of the surface, and temperature. The adsorption rate is measured by the reduction of the corrosion reaction rate caused by the adsorption of the inhibitor compared to the corrosion reaction rate measured in the absence of the corrosion inhibitor. This method assumes that this change in the coverage is related to the kinetics of the adsorption reactions, but in fact it is also related to the kinetics of the formation of the layer of corrosion products onto the surface of the electrode, the corrosivity of the media and the kinetics of the corrosion reaction itself.

The reactions that might take place on the surface of the metal are:

$$Fe\ (s) + 2\ H_2CO_3\ (aq) \leftrightarrow Fe(HCO_3)_2\ (aq) + H_2\ \ (g) \qquad (4.3)$$

$$Fe\ (s) + 2H^+\ (aq) \leftrightarrow Fe^{2+}(aq) + H_2(g) \qquad (4.4)$$

$$Fe^{2+}\ (aq) + 2H_2O \leftrightarrow Fe(OH)_2\ (s) + 2H^+(aq) \qquad (4.5)$$

$$Fe(OH)_2(s) \leftrightarrow FeO(s) + H_2O \qquad (4.6)$$

As discussed in section (2.1.4.1), reaction (4.4) is the main corrosion reaction that takes place at pH < 4, while when the pH is higher (around 5-6), reaction (4.3) is believed to be the predominant reaction. In the presence of the inhibitor, the amine terminal group is either physically adsorbed or is chemisorbed onto the negatively charged metal surface. The neutral amine group or the imidazoline ring tends to be physically adsorbed, but when the amide is converted to a salt in an acidic medium, the generated amine salt reacts with iron ions to make a complex on the surface of the metal, which promotes chemical adsorption.

In pitting corrosion the surface of the metal is inhomogeneous and includes in addition to areas of exposed metal, areas covered by a mixture of carbonate, hydroxides and oxides. At higher temperatures, the rate of reaction 4.1 is reduced, reducing in turn the rate of reactions 4.2, and 4.3, while the rates of reactions 4.4 and 4.5 increase, and a seventh reaction starts to takes place [22].

$$Fe(HCO_3)_2\ (aq) \leftrightarrow FeCO_3\ (s) + H_2CO_3(aq) \qquad (4.7)$$

Increasing the temperature can either increase or decrease the corrosion rate depending on whether the solubility product of iron carbonate is exceeded or not. However, surface films formed at high temperatures are continuous, compact and more stable than those formed at low temperature [80].

Hunnik et al., developed a mechanistic model that predicts an increase in the growth rate of the iron carbonate layer by several orders when the temperature is increased from room temperature to 50 °C [81]. Nesic et al, proved experimentally that the precipitation rate constant increases with increasing temperature [26].

The adsorption of imidazolines on the inhomogeneous iron carbonate layer is different from its adsorption on the metal surface, because of many factors including the degree of inhomogeneity of the surface and its charge. These differences change as temperature changes, which means the measured ΔG_{ads} at different temperatures are for different adsorption processes.

Table 4.14 shows the corrosion current and potential of mild steel in CO_2 saturated 3%NaCl solution at different temperatures. The decrement in the corrosion potential shows that by increasing temperature the metal surface becomes more vulnerable to the medium attack (less noble), which is acceptable for an endothermic reaction like corrosion. However, the corrosion current (which indicates the corrosion rate) decreases along with increasing cell resistance, which is directly related to the structure of the corrosion layer on the surface of the electrode.

Another factor that affects the thermodynamics of inhibitor adsorption is the fact that CO_2 or H_2CO_3 molecules adsorb onto the surface of the metal before reaction (4.3) takes place. Adsorption of the inhibitor molecules involves the replacement of some of the CO_2 molecules already adsorbed onto the metal surface. The net entropy change, ΔS, of the overall process is positive because the negative entropy change for the adsorption of the inhibitor molecules is smaller in magnitude than the positive entropy change for the desorption of the CO_2 molecules.

In spite of the fact that ΔG_{ads} at different temperatures are for different adsorption processes, ΔH_{ads} and ΔS_{ads} calculated for the ΔG_{ads} values remain useful descriptions of the overall adsorption process.

TABLE 4.14 Linear Polarization Parameters For Mild Steel Electrode In 3%NaCl brine saturated with CO_2 at Different Temperatures.

Temp (^oC)	**pH**	**E (**mV**)**	**I** (μA)	**R (**ohm**)**
30	4.63	-732.4	524.2uA	55.13
35	4.64	-736.4	472.2uA	65.18
40	4.63	-742.2	378.5uA	68.13
45	4.68	-745.5	344.1uA	75.7
50	4.62	-747.8	358.1 uA	72.78
55	4.76	-751.0	388.1 uA	67.01

4.3. THE SURFACE TENSION STUDY OF THE SYNTHESIZED MOLECULES

Neutral amine group in the synthesized molecules in this study have different intermolecular forces and thus different alignment on the metal surface than amine salts (charged amine group), which means their effect on the surface tension is pH dependent. The CO_2 saturated solution has a pH of 4.7-5.2 (experimentally measured in the cell at different temperatures) depending on saturation degree which is temperature dependant. Unlike in HCl solution, the neutralization of the amine group with the week carbonic acid is reversible reaction, and the resulting salt is a week salt that has low dissociation factor. This means the amidoamine or imidazoline might adsorb as a neutral molecule or as a carbonate salt.

Adsorption study showed that amidoamines **4** and **5** showed a low surface coverage of about 50% compared to amidoamines **1**, **3** and **6**. Increasing the concentration of the inhibitor above a certain level either reduced the surface coverage which could be attributed to micelle formation. The micelle formation is expected due to the haziness of the test solution at high concentrations of the amidoamines **4** and **5**.

To investigate micellization, the effect of solution ionic strength and the effect of counter ion on the behavior of the molecules in the solution, a study of the surface tension versus concentration was conducted using Du Nouy platinum ring method.

It was difficult to determine the exact critical micelle concentration for those compounds since it depends on many parameters like the counter ion, ionic strength, pH

and temperature. The neutral amidoamine are expected to have less water solubility than their corresponding salts. In the same manner, the counter ion determines to a large extent the solubility in water. Neutralizing the amidoamine with acetic acid prior to their use enhances their water solubility, and thus it is expected to increase micellization concentration, however, it is not know whether the CO_2 saturated 3% NaCl solution is able to make a carbonate salt of the amidoamine, and if it can, what is the solubility of this salt and how would it affect the CMC value.

4.3.1. SURFACE TENSION MEASUREMENTS OF N-[2-(2-DODECANOYL - AMINOETHYLAMINO)-ETHYL]DODECANAMIDE

A concentrated suspension of amidoamine **4** was prepared by suspending 0.0223 g of the compound in 25 ml of hot distilled water. The solution was kept hot all during the experiment to maintain its homogeneity. Then consequent known volumes of this solution were transferred to a 100 mL volumetric flask filled with 50mL 3% NaCl solution preheated to 40 ^{o}C. The actual concentration of amidoamine **4** in the final solution was calculated depending on the total moles of the compound added and the final volume of the solution after the addition of each aliquot. The temperature of the final solution was maintained at 40 ^{o}C during the measurements. Figure (4.25) shows the plot of surface tension γ against the logarithm of inhibitor concentration.

By the addition of 2×10^{-5} mol . L^{-1} (8.8 ppm) of amidoamine **4**; the surface tension dropped from 7.06 N/m to 4.45 N/m. The addition of further amounts of amidoamine 4 –

up to 150 ppm- didn't change the surface tension, which means critical micelle concentration has already been reached for amidoamine 4 in 3% NaCl in the selected range of concentrations used for corrosion measurements.

At 150 ppm (32×10^{-4} mol . L^{-1}), the solution became very hazy and amidoamine **4** started to precipitate. This means the adsorption of amidoamine **4** is based on adsorption from micelles rather than single molecule adsorption.

.

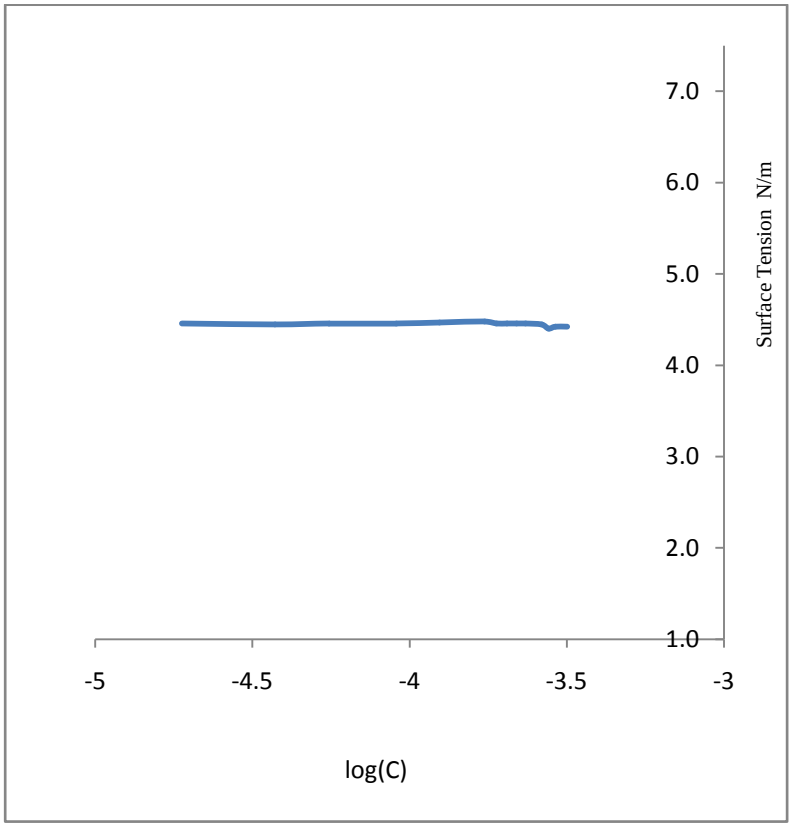

FIGURE 4.25 Surface Tension Vs Log (C) of Amidoamine (4) 3% NaCl Brine

4.3.2. SURFACE TENSION MEASUREMENTS OF 2-[2-{2-(2-AMINOETHYL AMINO)-ETHYL AMINO}ETHYLAMINOETHYL]-OCTADECANAMIDE

A concentrated suspension of amidoamine 5 was prepared by suspending 0.0196 gr of the compound in 25 ml of hot distilled water. The solution was kept hot all during the experiment to maintain its homogeneity. Then consequent known volumes of this solution were transferred to a 100 mL volumetric flask filled with 50mL 3% NaCl solution preheated to 40 ^{o}C. The actual concentration of amidoamine 5 in the final solution was calculated depending on the total moles of the compound and the final volume of the solution after the addition of each aliquot. The temperature of the final solution was kept at 40 ^{o}C during the measurements. An increment in the surface tension for amidoamine 5 in 3% NaCl is noticed around 20 ppm (5×10^{-5} mol . L^{-1}). From the electrochemical study at 40 ^{o}C, amidoamine 5 has also a drop in surface coverage at around 20 ppm. It is believed that this change is because of reaching the solubility limit which causes the precipitation of the compound which in turn decreased its concentration. Figure (4.26) shows the plot of surface tension γ against the logarithm of inhibitor concentration.

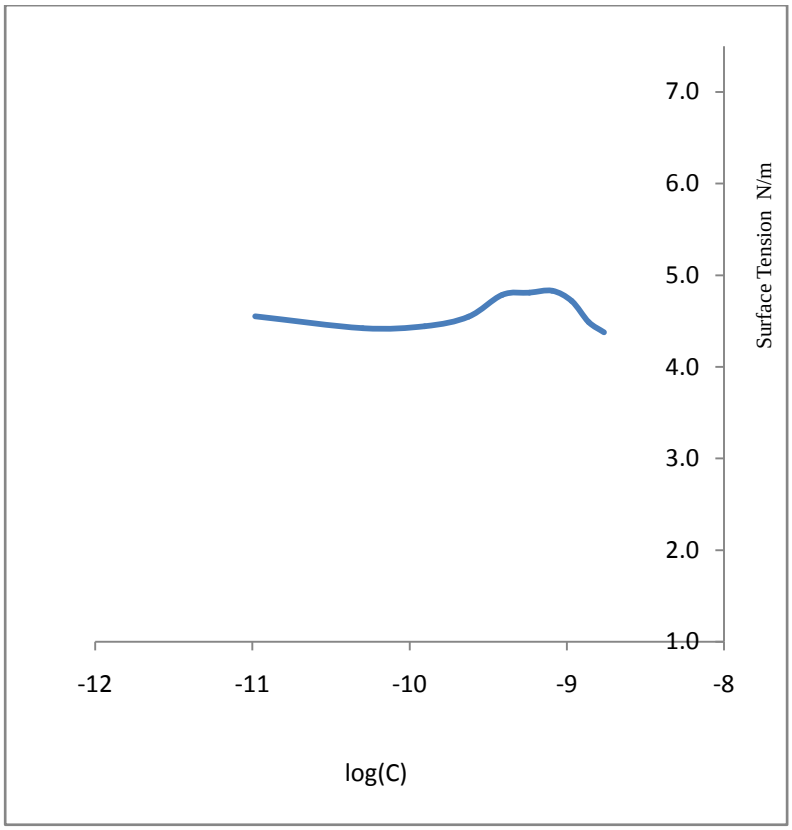

FIGURE 4.26 Surface Tension Vs Log (C) Of Amidoamine (5) in 3% NaCl Brine

4.3.3. SURFACE TENSION MEASUREMENTS OF N-[2-(2-AMINOETHYL AMINO)-ETHYL]-DODECANAMIDE

Amidoamine **3** showed higher surface coverage at low concentration. To investigate the reason a concentrated solution of amidoamine **3** was prepared by dissolving 0.0113 gr of the compound in 25 ml of hot distilled water. The solution was kept hot all during the experiment to maintain its homogeneity. Then consequent known volumes of this solution were transferred to a 100 mL volumetric flask filled with 50mL 3% NaCl solution preheated to 40 ^{o}C. The actual concentration of amidoamine **3** in the final solution was calculated depending on the total moles of the compound and the final volume of the solution after the addition of each aliquot. The temperature of the final solution was kept at 40 ^{o}C during the measurements. Figure (4.27) shows the plot of surface tension γ against the logarithm of inhibitor concentration.

The CMC value for amidoamine **3** in 3% NaCl is around 15-17 ppm (5×10^{-5} mol . L^{-1}). From the electrochemical study at 40 ^{o}C, amidoamine **3** covers 90% of the surface before it reaches its CMC.

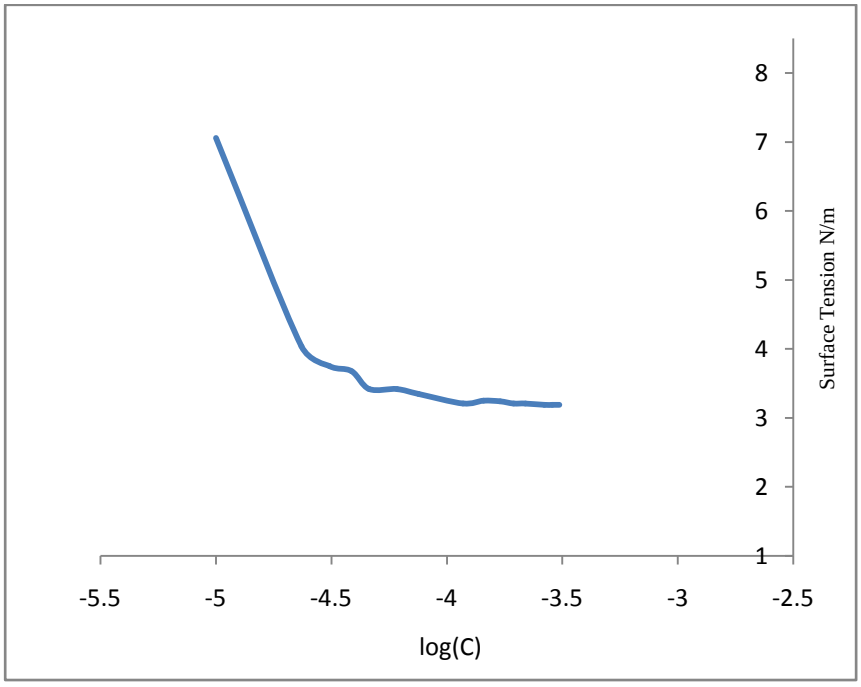

FIGURE 4.27 Surface Tension Vs Log (C) Of Amidoamine (3) in 3% NaCl Brine

4.3.4. SURFACE TENSION MEASUREMENTS OF 1-(2-AMINOETHYL)-2-HEPTADECANYL--2-IMIDAZOLINE .

A concentrated solution of imidazoline **9** was prepared by dissolving 0.0256 g of the compound in 25 ml of hot distilled water. Consequent known volumes of this solution were transferred to a 100 mL volumetric flask filled with 50mL of test solutions preheated to 40 ^{o}C. The temperature of the final solution was kept at 40^{o}C during the measurements. Test solutions used are distillated water and 3% NaCl. The critical micelle concentration of imidazoline **9** in distilled water was in the range 1.1-1.3 $\times 10^{-4}$ mol . L^{-1}. The increment in the ionic strength of the solution decreased the dispersibility of the compound and thus enhanced adsorption, which in turn decreased the surface tension and the CMC value. The CMC value of imidazoline **9** in 3% NaCl solution was about 1.01 $\times$ 10^{-4} mol . L^{-1}.

To investigate the effect of the counterion on the surface activity of this imidazoline, the concentrated solution was neutralized with acetic acid, which converts the imidazoline to imidazoline acetate by the reaction of the terminal amine with acetic acid.

The test solutions are distilled water and 3% NaCl solution. Figure (4.28) shows the plot of surface tension γ against the logarithm of inhibitor concentration of the neutral imidazoline and the imidazoline acetate in both distilled water and 3% NaCl solution.

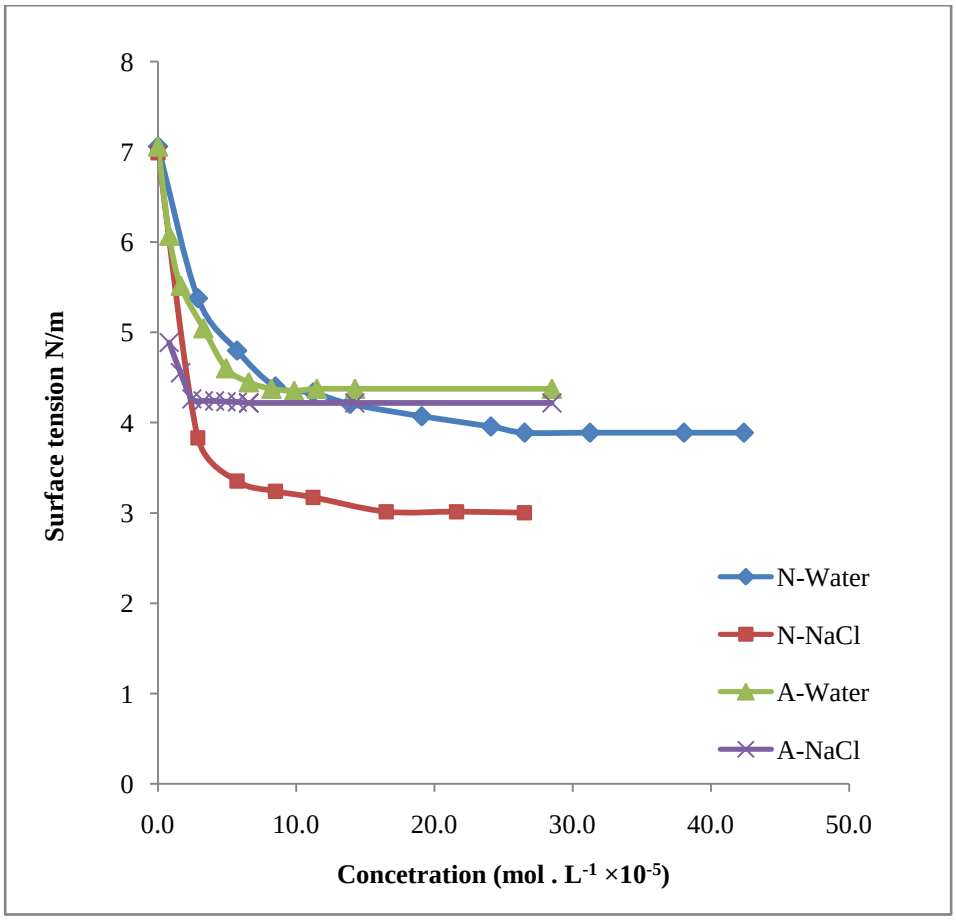

FIGURE 4.28 Surface Tension Versus Concentration Of Imidazoline 9 And Its Acetate Salt In Distilled Water And 3% NaCl Solution

It is noticed that the acetate salt enhances the solubility of the compound in water, which the effect of ionic strength and maintain the lowest surface tension at the CMC similar for the product in both the distilled water and 3% NaCl solution, however the CMC value in 3% NaCl (2.5×10^{-5} mol . L^{-1}) is lower than in distilled water (5.4×10^{-5} mol . L^{-1}).

From the electrochemical study at 40 ^{o}C, compound **9** covers most of the surface before it reaches its CMC in 3% NaCl.

4.3.5. SURFACE TENSION MEASUREMENTS OF OF N,N'-DI-2,2'-[2-HEPTA DECANYL-2-IMIDAZOLINYL]DIETHYLAMINE.

A concentrated solution of imidazoline **10** was prepared by dissolving 0.0442g of the compound in 50 ml of hot distilled water. The volume was adjusted after the solution cooled down. Then consequent known volumes of this solution were transferred to a 100 mL volumetric flask filled with 50mL distilled water preheated to 40^{o}C. The temperature of the final solution was kept at 40 ^{o}C during the measurements.

Test solutions used are distillated water and 3% NaCl. The critical micelle concentration of imidazoline **10** in distilled was in the range 8.8-8.9 $\times 10^{-5}$ mol . L^{-1} (around 60 ppm). The increment in the ionic strength of the solution decreased the dispersibility of the compound and thus enhanced adsorption, which in turn decreased the surface tension and the CMC value. The CMC value of imidazoline **10** in 3% NaCl solution was about 3.7×10^{-5} mol . L^{-1} (around 25 ppm).

To investigate the effect of the counterion on the surface activity of this imidazoline, the concentrated solution was neutralized with acetic acid, which converts the imidazoline to imidazoline acetate by the reaction of the terminal amine with acetic acid.

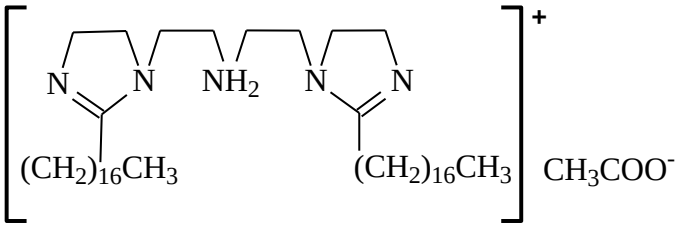

It is noticed that the acetate salt enhances the solubility of the compound in water, which the effect of ionic strength and maintain the lowest surface tension at the CMC similar for the product in both the distilled water and 3% NaCl solution, however the CMC value in 3% NaCl (4.5-4.6 × 10^{-5} mol . L^{-1} or 31 ppm) is lower than in distilled water (4.7-4.8 × 10^{-5} mol . L^{-1} or around 31 ppm)). Figure 4.29 shows the surface tension versus concentration plot of imidazoline **10** and its acetate salt in distilled water and 3% NaCl brine.

From the electrochemical study at 40 ^{o}C, imidazoline **10** covers most of the surface before it reaches its CMC in 3% NaCl.

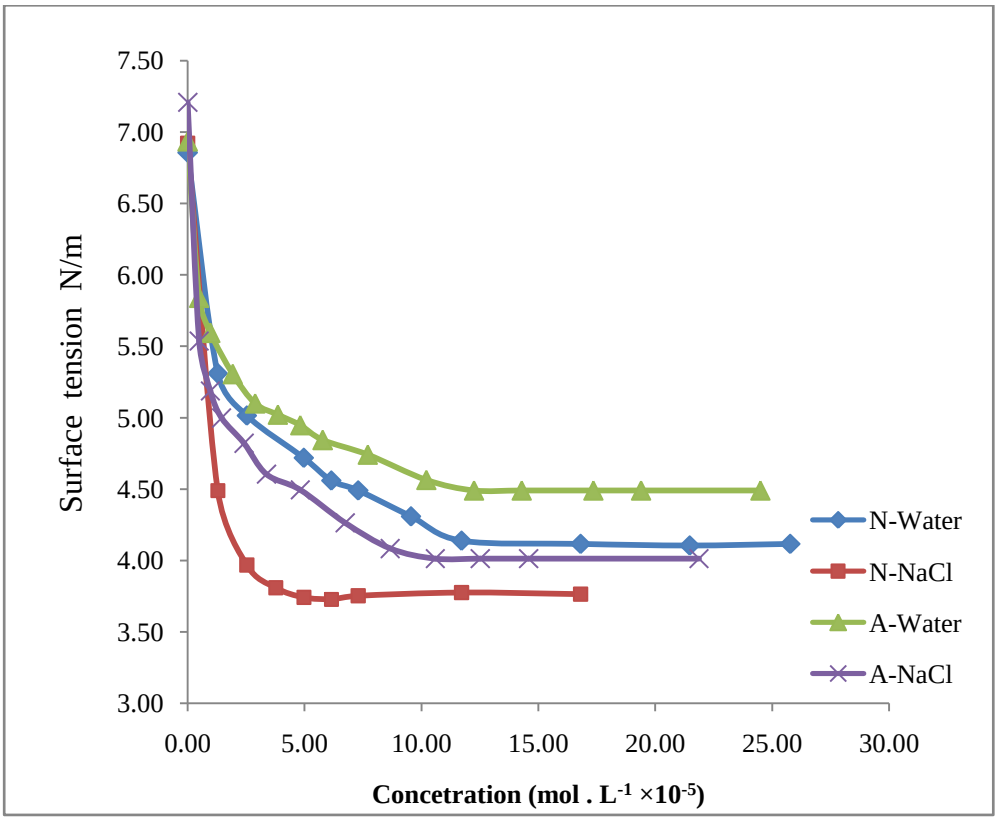

FIGURE 4.29 Surface Tension Versus Concentration of Imidazoline 10 And Its Acetate Salt In Distilled Water And 3% NaCl Solution

4.3.6. SURFACE TENSION MEASUREMENTS OF 1-[2-{2-(2-AMINO ETHYL AMINO)-ETHYLAMINO}ETHYL]-2-HEPTADECANYL-2-IMIDAZOLINES

A concentrated solution of imidazoline **11** was prepared by dissolving 0.0634g of the compound in 50 ml of hot distilled water. The volume was adjusted after the solution cooled down. Then consequent known volumes of this solution were transferred to a 100 mL volumetric flask filled with 50mL distilled water preheated to 40^{o}C. The temperature of the final solution was kept at 40^{o}C during the measurements.

Test solutions used are distillated water, 3% NaCl and a CO_2 saturated 3% NaCl. The critical micelle concentration of compound (**11**) in distilled was in the range 1.56-1.57 × 10^{-4} mol . L^{-1} (around 69 ppm). The increment in the ionic strength of the solution decreased the dispersibility of the compound and thus enhanced adsorption, which in turn decreased the surface tension and the CMC value. The CMC value of (**11**) in 3% NaCl solution was about 7.9-8.0 × 10^{-5} mol . L^{-1} (around 35 ppm).

To investigate the effect of the carbonate counterion on the surface activity of this imidazoline. The salt solution was heated to 40 ^{o}C and saturated with CO_2 before the inhibitor was added. It is noticed that the CO_2 saturated NaCl solution could turn the imidazoline into the carbonate salt, which enhances the solubility of the compound in water, and the CMC value in the same range of imidazoline (**11**) in water (1.56-1.57 × 10^{-4} mol . L^{-1} or 69 ppm).

From the electrochemical study at 40 ^{o}C, compound (**11**) covers most of the surface before it reaches its CMC in CO_2 saturated -3% NaCl solutions.

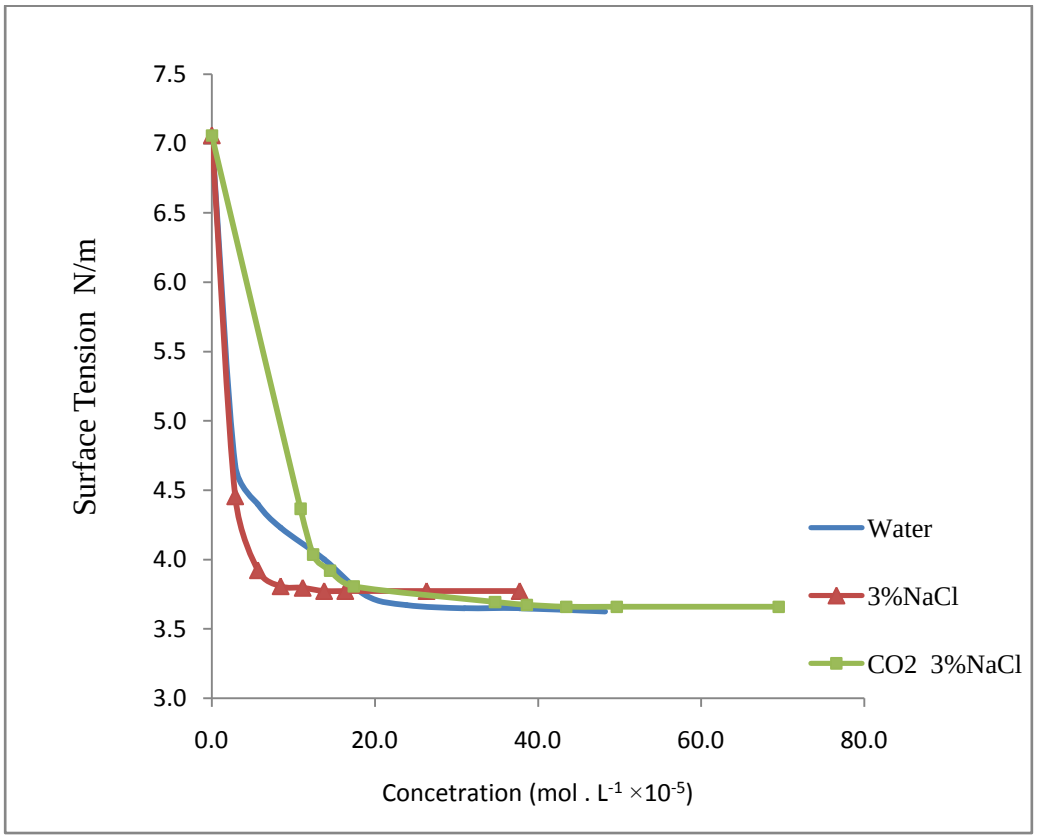

FIGURE 4.30 Surface Tension Vs Concentration of Imidazoline (11) and Its Carbonate Salt In Distilled Water , 3% NaCl Solution and CO_2 3% NaCl Solution

It should be noticed that the micllization of amidoamine is important in introducing more oil to the metal surface in an oil/water system which enhances protection. The ratio of the polyamine to the fatty acid determined whether the amidation reaction will result in a monoamideamine or a diamidoamine, but the length of the polyamine to the hydrocarbon chain of the fatty acid determines the CMC value of the amidoamine.

When a mixed fatty acid– such as tall oil fatty acid-is reacted with a polyamine, some of resulting the amidoamine acts as a corrosion inhibitor, while the others help administering more hydrocarbon phase to built a better inhibitive film.

4.4. CONCLUSIONS AND RECOMMENDATIONS

Nine different amidoamines and three imidazolines were successfully synthesized by the reaction of polyamines with fatty acids or fatty nitriles of different chain lengths. The structures of these compounds were confirmed by their NMR and IR spectra.

The amidoamines can be classified into three main groups: mono diamidoamine, diamidoamine of the same fatty acid, and diamidoamine of different fatty acids. The ratio of the hydrophobic carbon chain to the hydrophilic polyamine chain affects the micellization and solubility of the compounds, with the monoamide amines having better surface coverage than diamidoamines. The monoamides have a higher solubility in water and methanol than the diamidoamines. All the diamidoamines of diethylenetriamine DETA exhibited limited or no solubility in water. The Diamidoamine of octadecanoic acid and triethylenetetraamine TEPA showed better solubility.

The corrosion inhibition efficiencies of the amidoamines was determined by polarization resistance measurements for mild steel alloy C1018 in 3% NaCl saturated with carbon dioxide at 40 ^{o}C. The amidoamine of decanoic acid and diethylenetriamine exhibited the best corrosion inhibition. The amidoamine of octadecanoic acid and diethylene-triamine and the diamidoamine of octadecanoic acid and triethylene-tetraamine exhibited good corrosion inhibition at concentrations higher than that of decanoic amidoamine. The other amidoamines exhibited limited surface coverage and low corrosion inhibition which is attributed to their low critical micelle concentration. The results show that the secondary amine group in the diamidoamine did not give good adsorption on the metal surface as the primary amine group of the monoamidoamine. This may be a result of steric hindrance which prevents a dense packing for the adsorbed layer and the electron withdrawal effect of the neighbor amide groups in diamidoamines.

The Tafel plots of all the amidoamine show that the suppression of the anodic reaction is the main factor behind their inhibition of corrosion. They also show increments in the values of the anodic slopes indicating that the inhibitors facilitate the transfer of ions from the surface of the metal to the solution. This, as will be discussed later on in this thesis, results from the onset of micellization within the studied concentration range. Some amidoamines had a maximum their maximum protection efficiency in the range 20-60%. Above this range the corrosion inhibition was independent of concentration or even decreased. This behavior was found to be related to the reaching of the critical micelle concentration by the inhibitor. In general one can

conclude that in CO_2 saturated 3% NaCl brine the corrosion inhibition by amidoamines is predominantly under anodic control.

Amidoamines 1, 3, 4 and 5 were found to follow the Temkin adsorption equation, while amidoamine 6 followed the Freundlich adsorption equation. The molecular interaction parameter of amidoamines 1 and 8 is higher than those of 3 and 4 due to steric hindrance.

The mono and diimidazoline exhibited a greater solubility in water, higher CMC values and better corrosion inhibition than their amidoamine precursors. All showed very good absorption on the metal surface and were good corrosion inhibitors. Their Tafel plots show that they mainly suppress the anodic reaction. In CO_2 saturated 3% NaCl brine the corrosion inhibition by imidazolines is predominantly under anodic control.

Imidazolines 9 and 11 follow the Temkin adsorption equation, while Imidazoline 10 follows the Langmuir adsorption equation. The lower molecular interaction constant f obtained for imidazoline 11 (2.397) was significantly than that obtained for imidazoline 9 (5.599) signifies stronger repulsive forces between the adsorbed and adsorbing molecules in imidazoline 9 than in imidazoline 11.

The adsorption of imidazolines on the metal surface is exothermic and spontaneous. The Gibbs free energy of adsorption, ΔG_{ads}, for imidazoline 11 does not significantly change with temperature, compared to the ΔG_{ads} values for imidazolines 9 and 10 which decrease significantly with temperature. The value of enthalpy of adsorption, ΔH_{ads}, suggests that the adsorption of the imidazolines is of the physisorption

type. However thermodynamic values obtained from electrochemical measurements reflect the desorption of water and CO_2 molecules alongside the adsorption of the inhibitor molecules. In spite of the fact that at different temperatures the ΔG_{ads} values are for different adsorption processes, the calculated ΔH_{ads} and ΔS_{ads} values remain useful descriptions of the overall adsorption process.

The surface tension studies of imidazolines show that their solubility and surface activity is related to the ionic strength of the solution and the counter ion. The acetate salt of the imidazoline exhibited higher critical micelle concentration and thus it is expected to have better corrosion inhibition properties. The results show that when the corrosion inhibitor is used in a system where hydrolysis does not have a significant effect on the imidazoline concentration such as in transportation pipelines, imidazolines have higher protection efficiencies than their amidoamine precursors. While for applications where hydrolysis plays a significant rule such as during the acid cleaning of the pipelines or during pipeline pressure testing, using amidoamines will be economically a better choice.

A future study that compares the inhibition efficiencies of DETA and TEPA amidoamines and imidazolines of shorter chain fatty acids (such as hexadecanoic, tetradecanoic and dodecanoic acids) with the inhibition efficiencies of their imidazoline derivatives is recommended. It is also recommended to study the effect of the chain length of the fatty acid and the polyamine on the hydrolysis of the imidazoline derivative. This study will help in selecting the chain length distribution of the tall oil fatty acid (TOFA) used for the synthesis.

APENDIX 1.

THE FTIR SPECTRA OF THE SYNTEHSIZED MOLECULES.

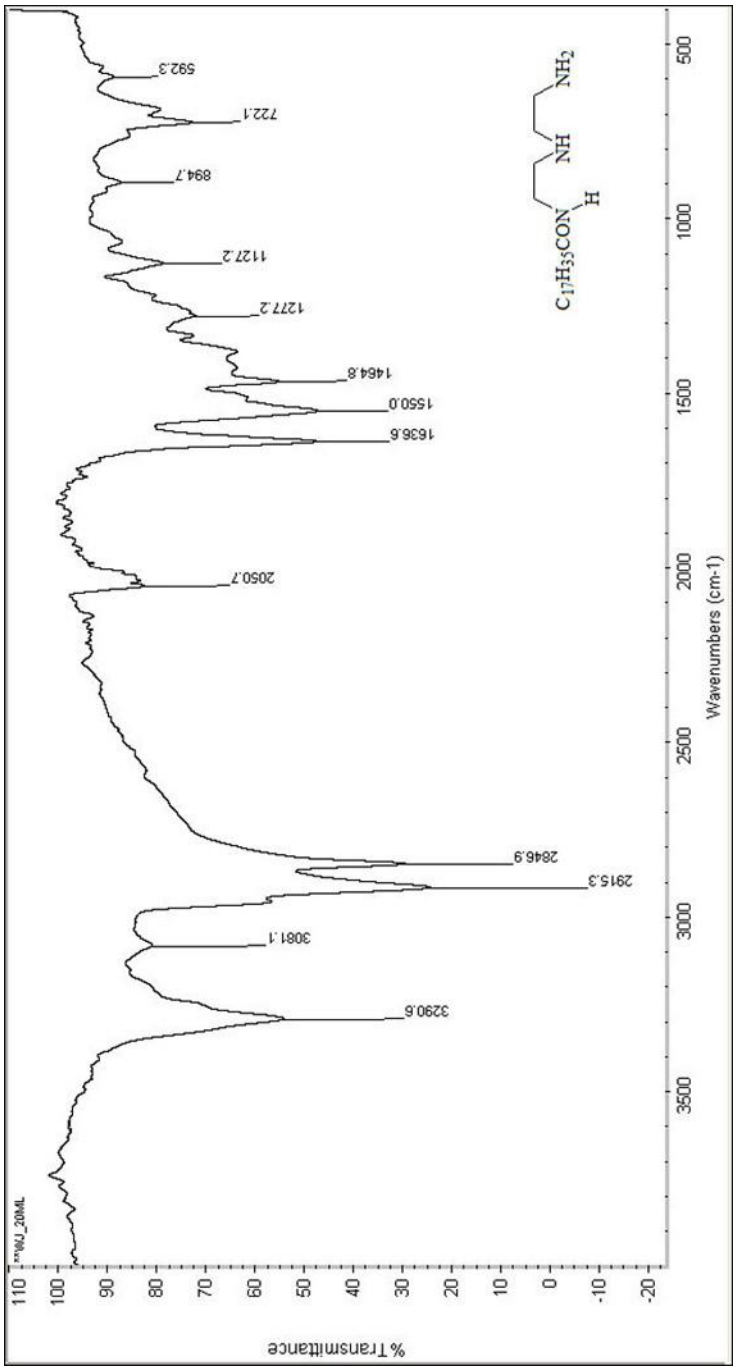

FIGURE A1.1. FTIR Spectrum of Amidoamine (1).

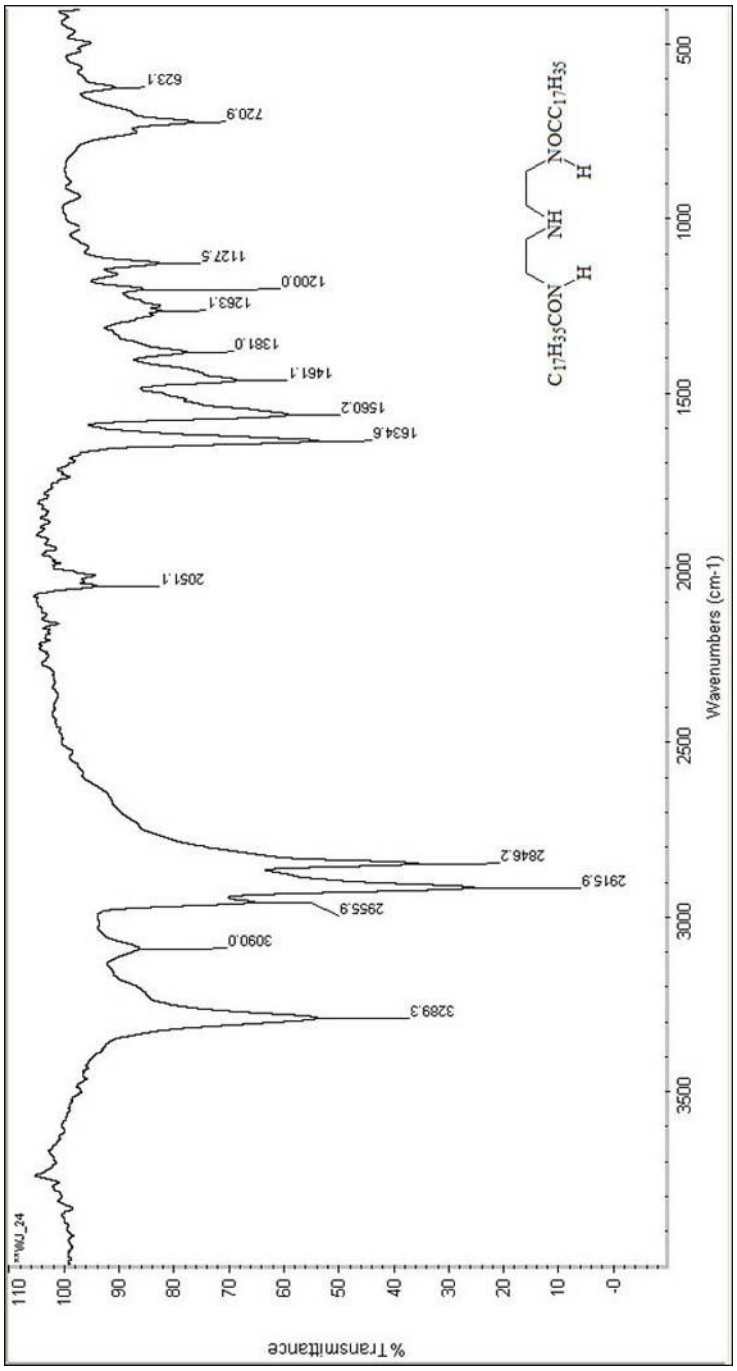

FIGURE A1.2. FTIR Spectrum of Amidoamine (2).

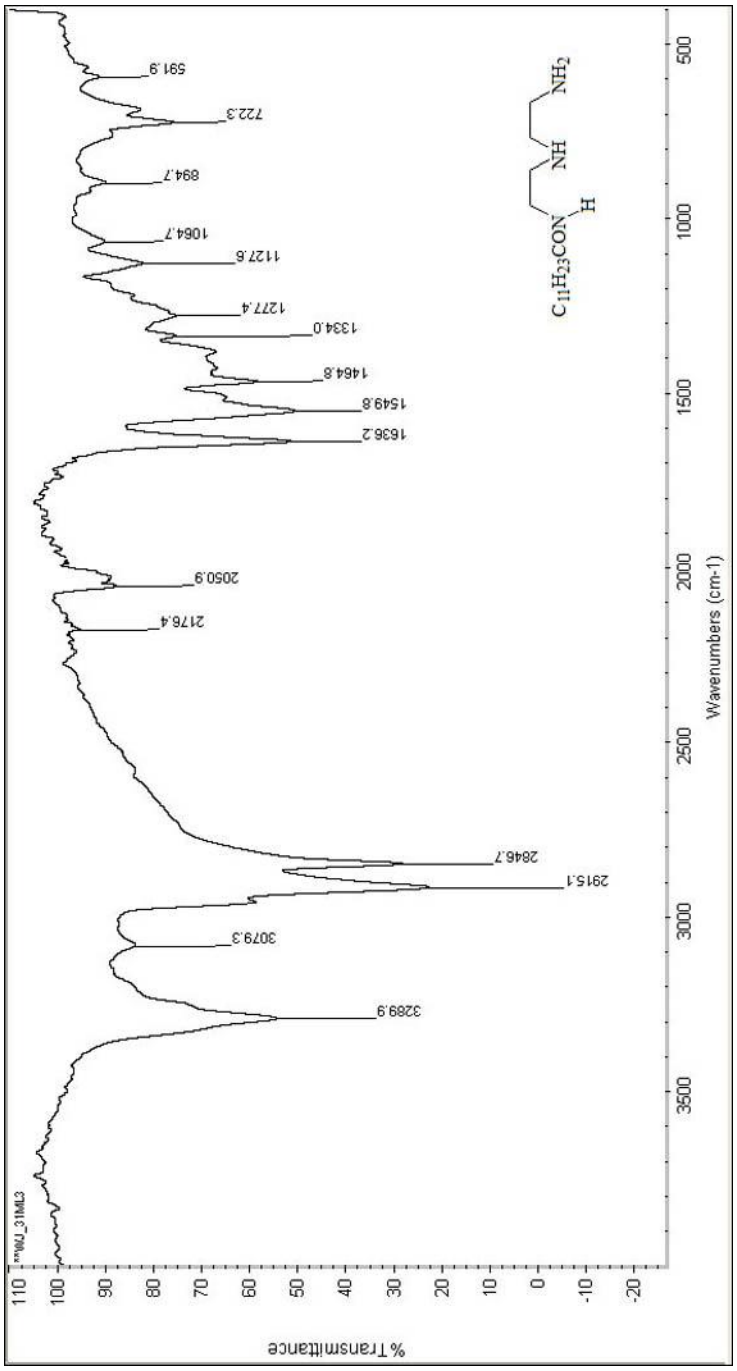

FIGURE A1.3. FTIR Spectrum of Amidoamine (3).

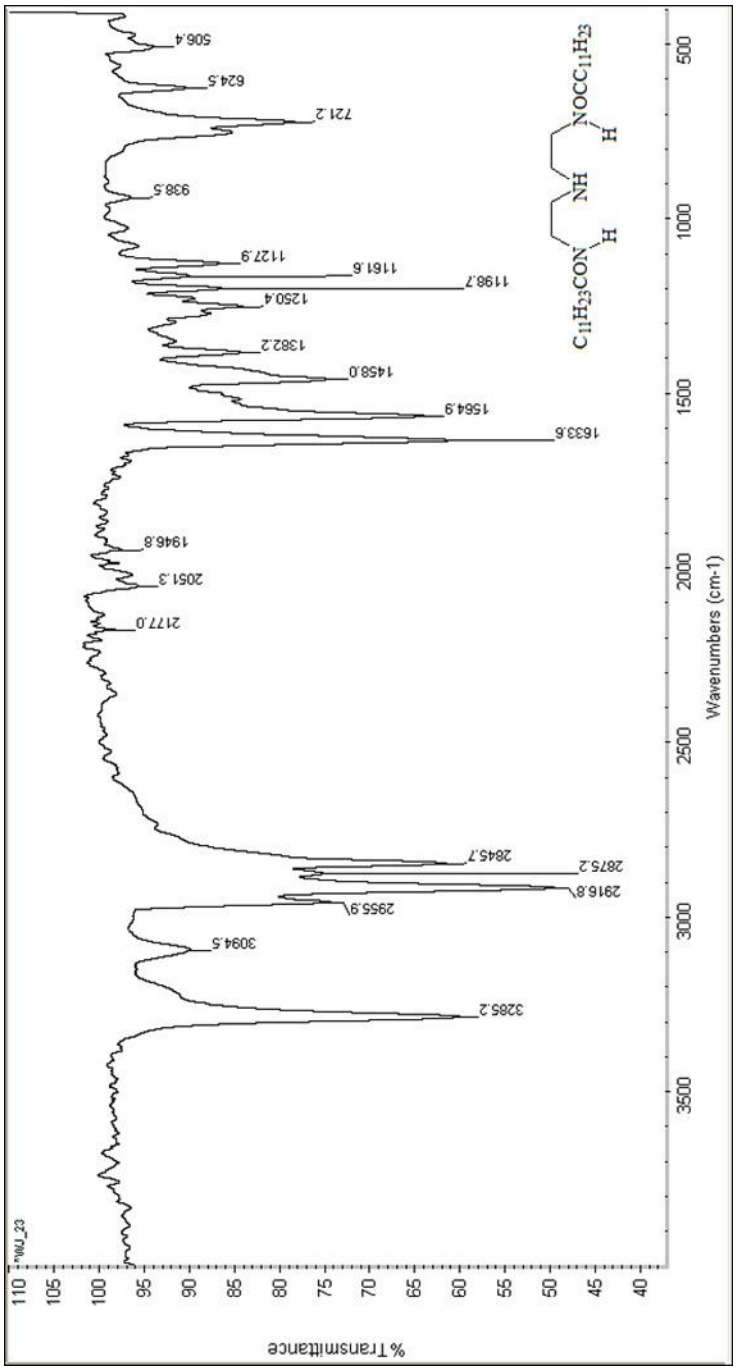

FIGURE A1.4. FTIR Spectrum of Amidoamine (4).

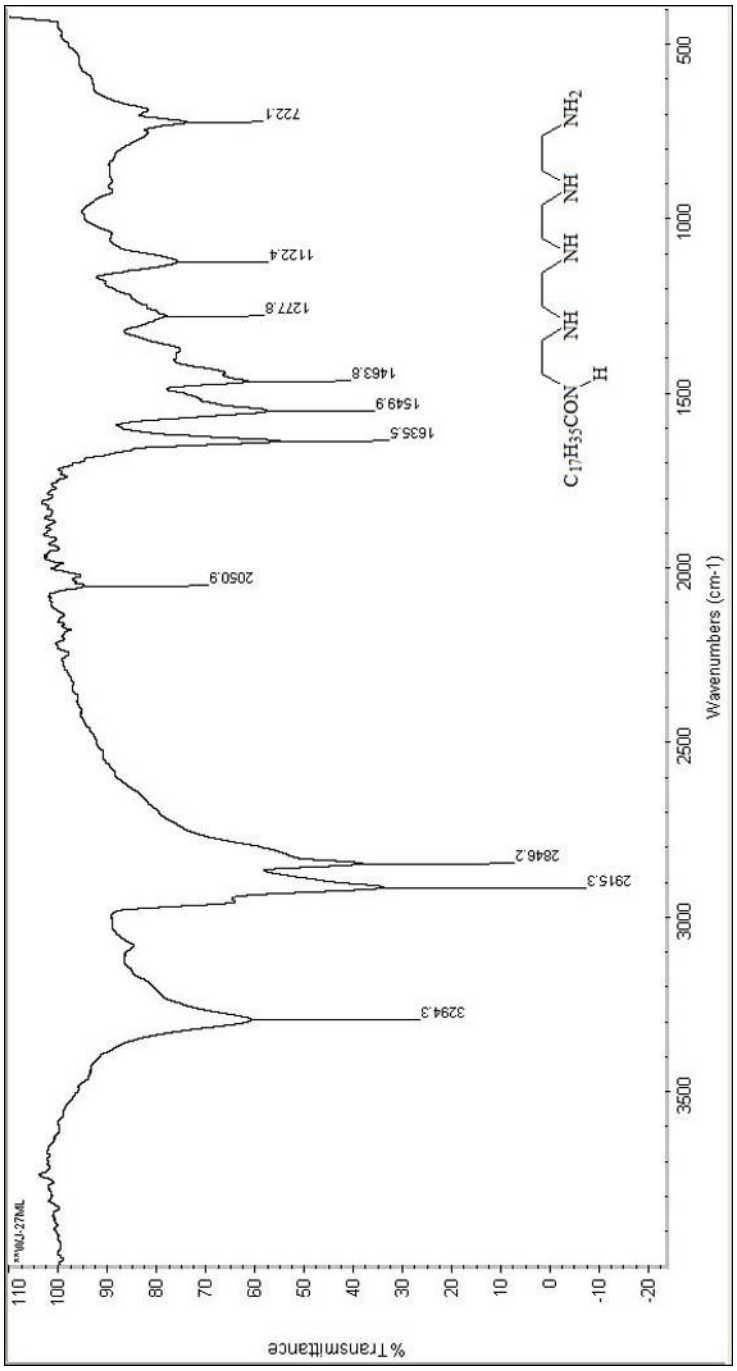

FIGURE A1.5. FTIR Spectrum of Amidoamine (5).

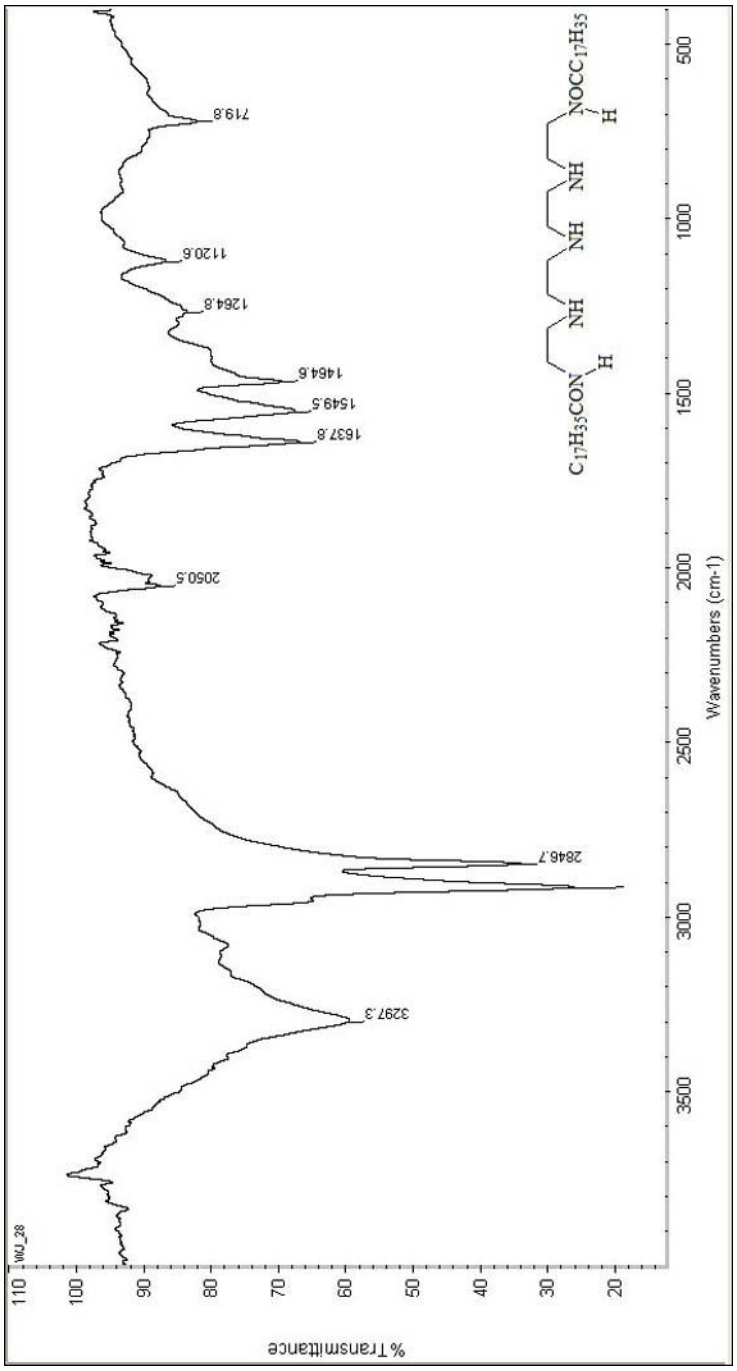

FIGURE A1.6. FTIR Spectrum of Amidoamine (6).

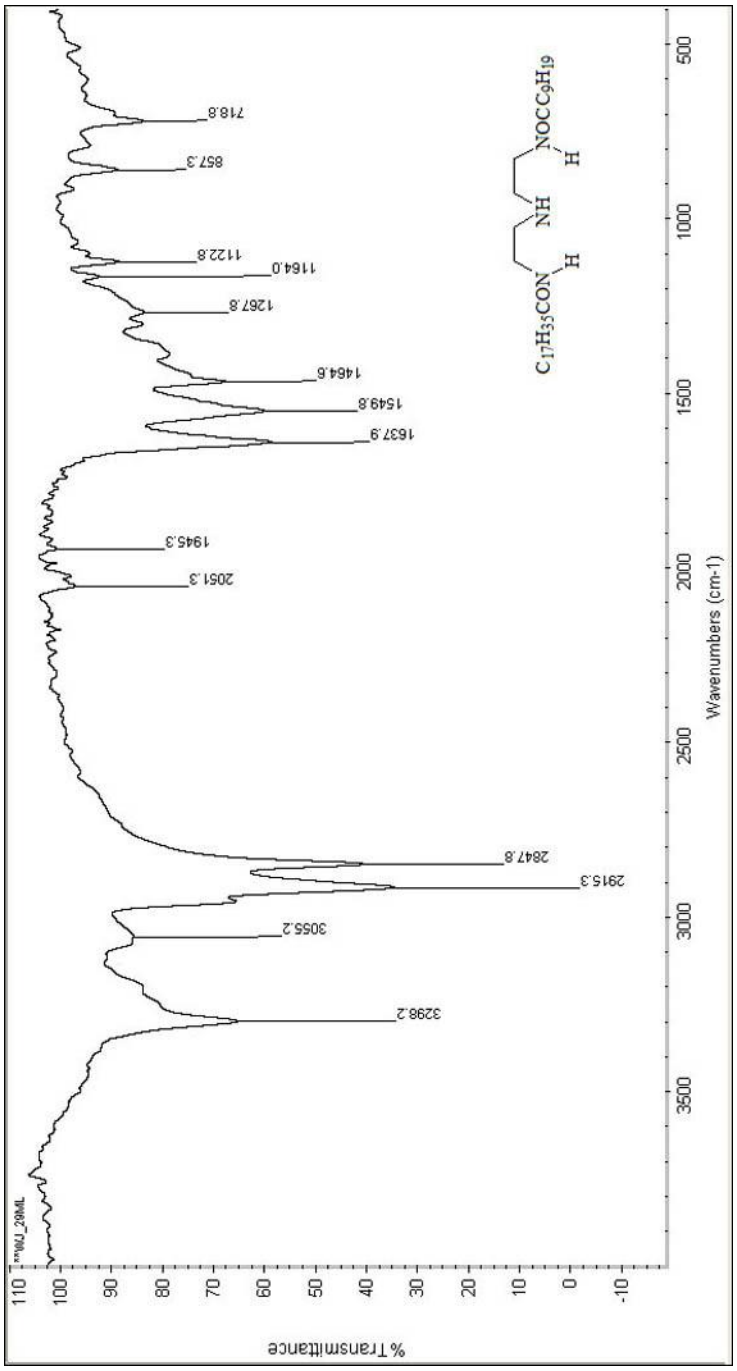

FIGURE A1.7. FTIR Spectrum of Amidoamine (7).

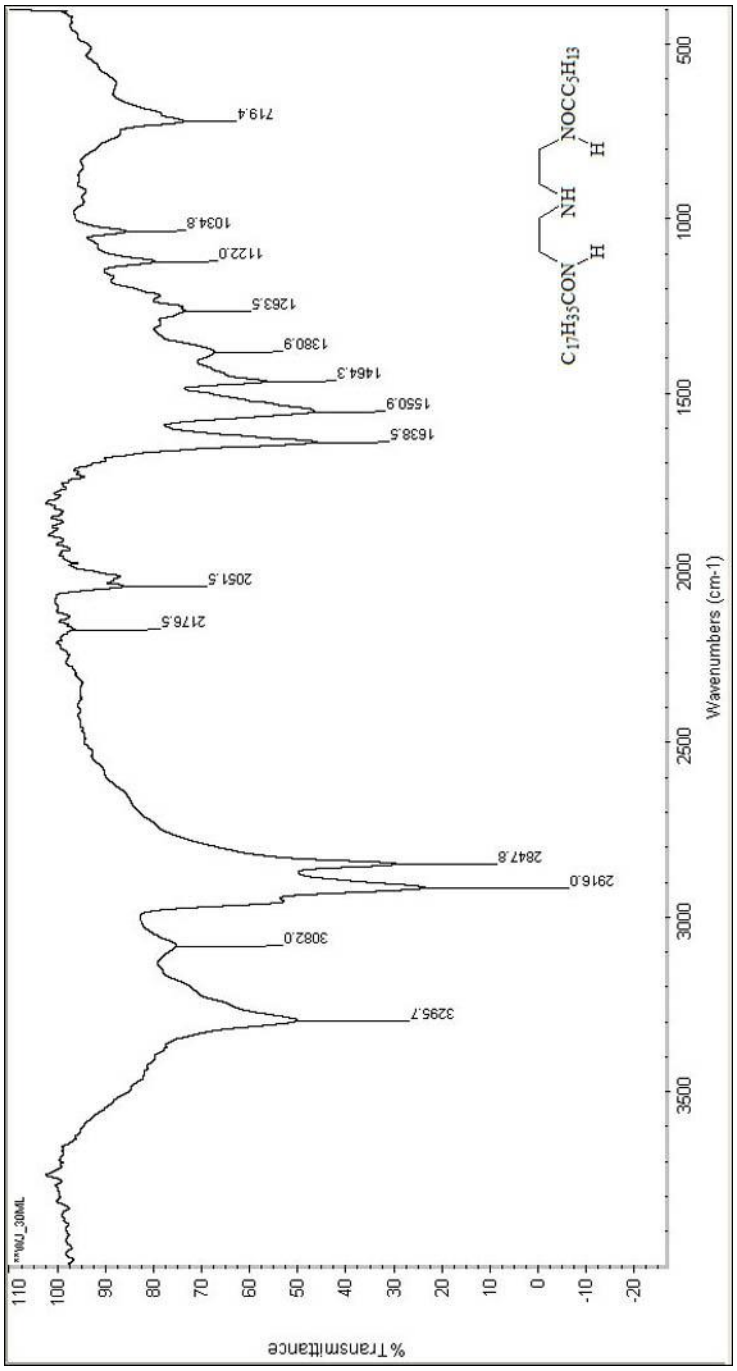

FIGURE A1.8. FTIR Spectrum of Amidoamine (8).

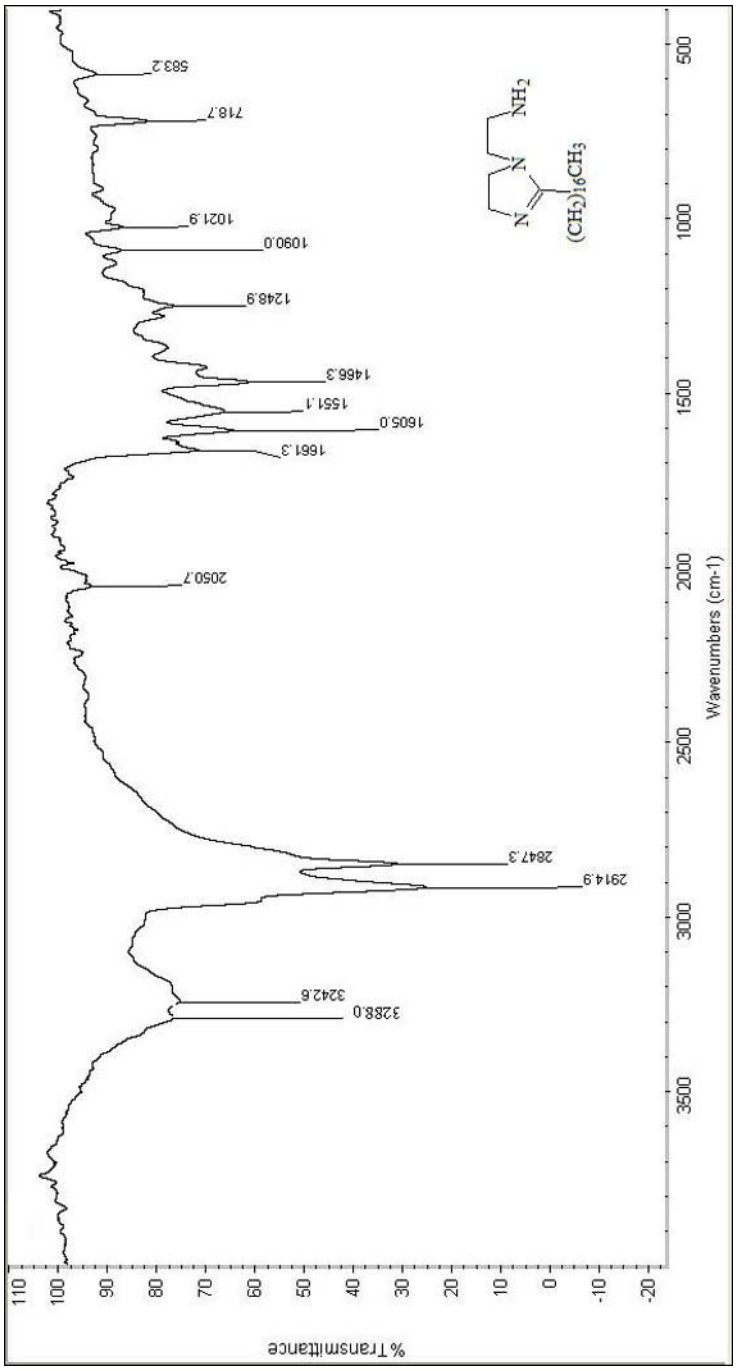

FIGURE A1.9. FTIR Spectrum of Imidazoline (9).

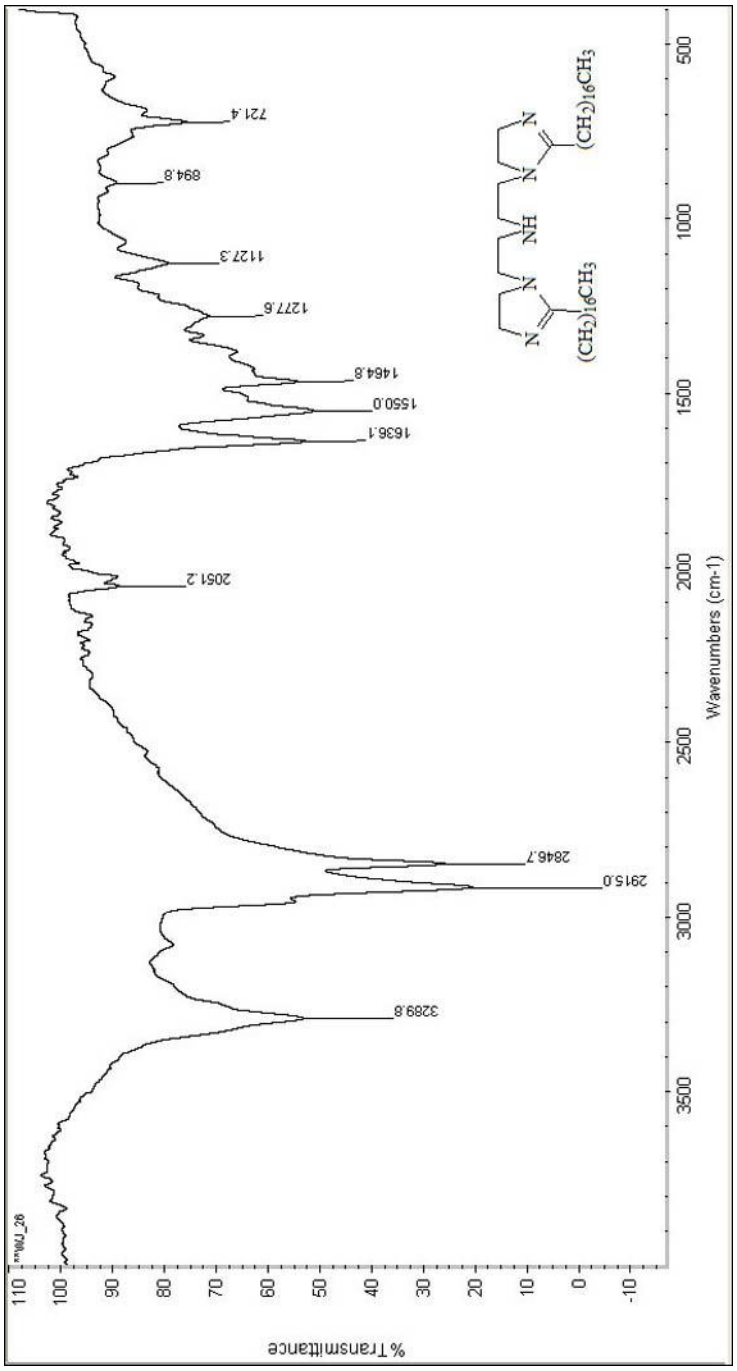

FIGURE A1.10. FTIR Spectrum of Imidazoline (10).

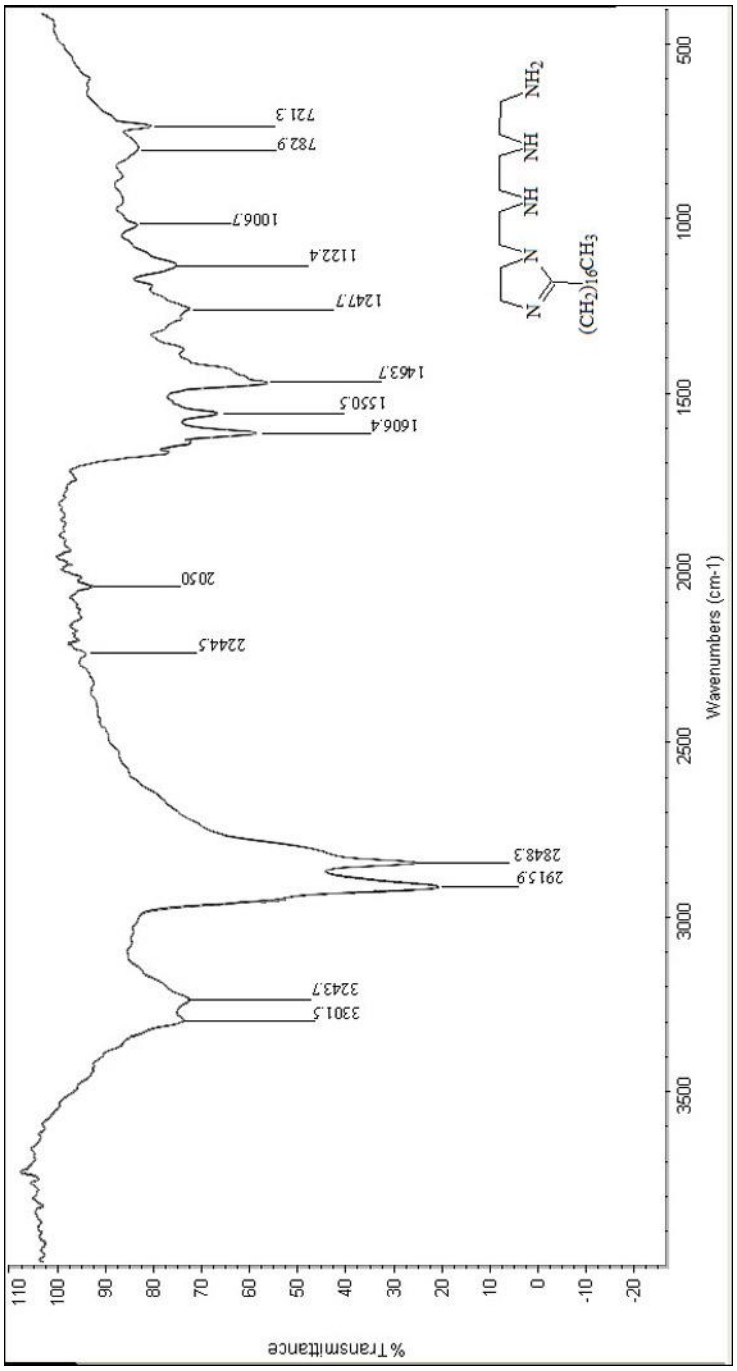

FIGURE A1.11. FTIR Spectrum of Imidazoline (11).

APENDIX 2

THE ^{1}H NMR SPECTRA OF THE SYNTEHSIZED MOLECULES.

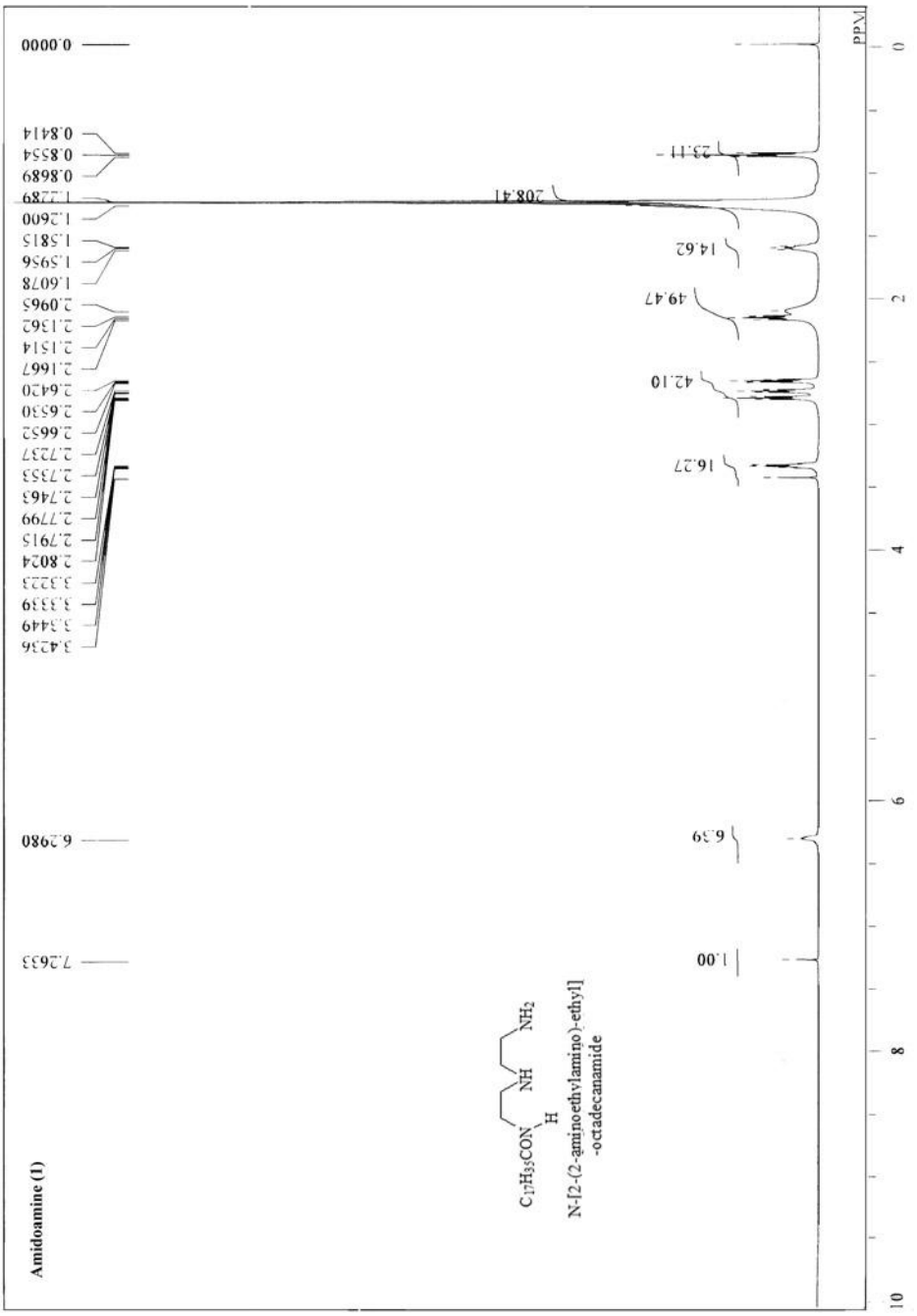

FIGURE A2.1. ^{1}H NMR Spectrum of Amidoamine (1).

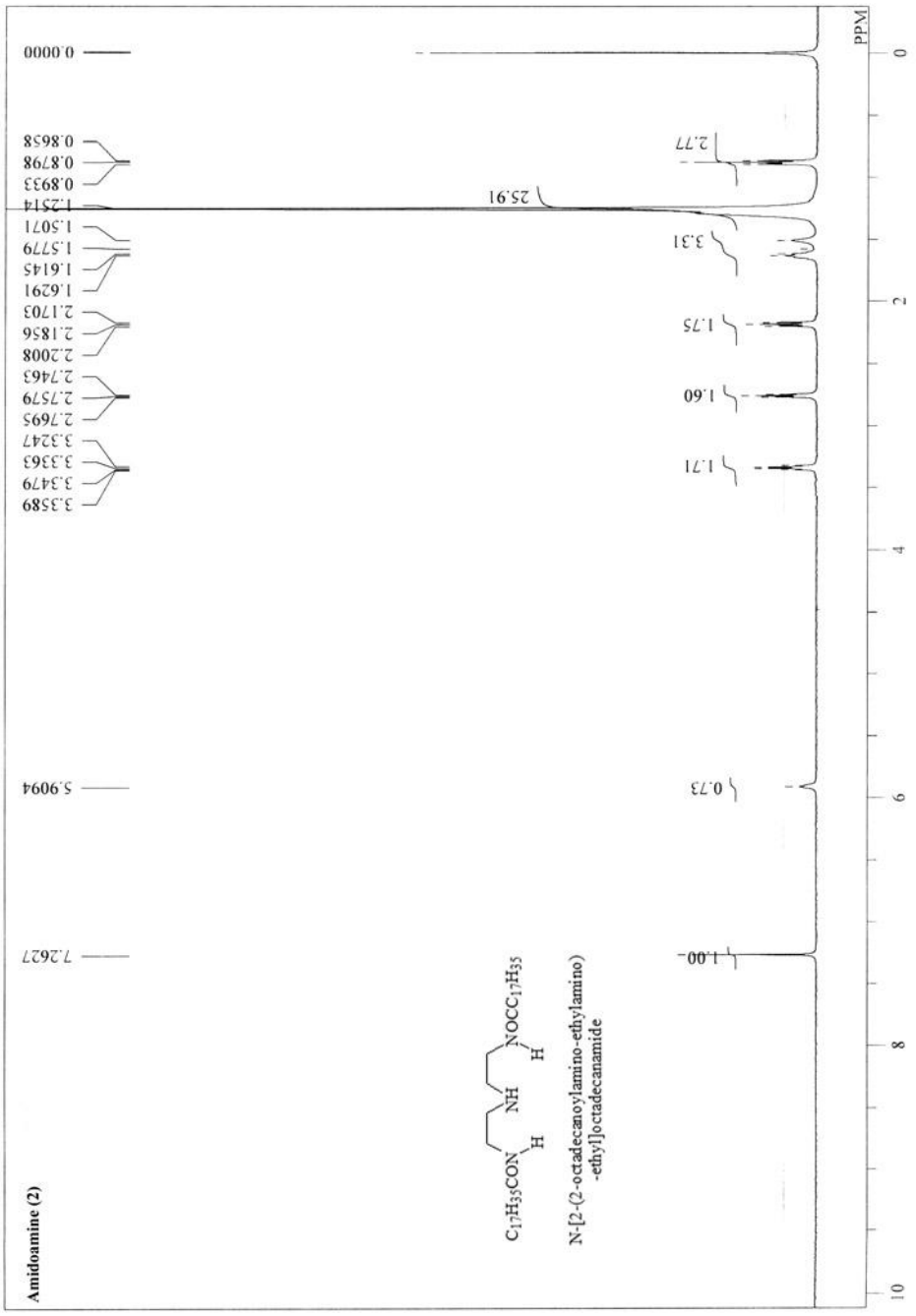

FIGURE A2.2 ^{1}H NMR Spectrum of Amidoamine (2).

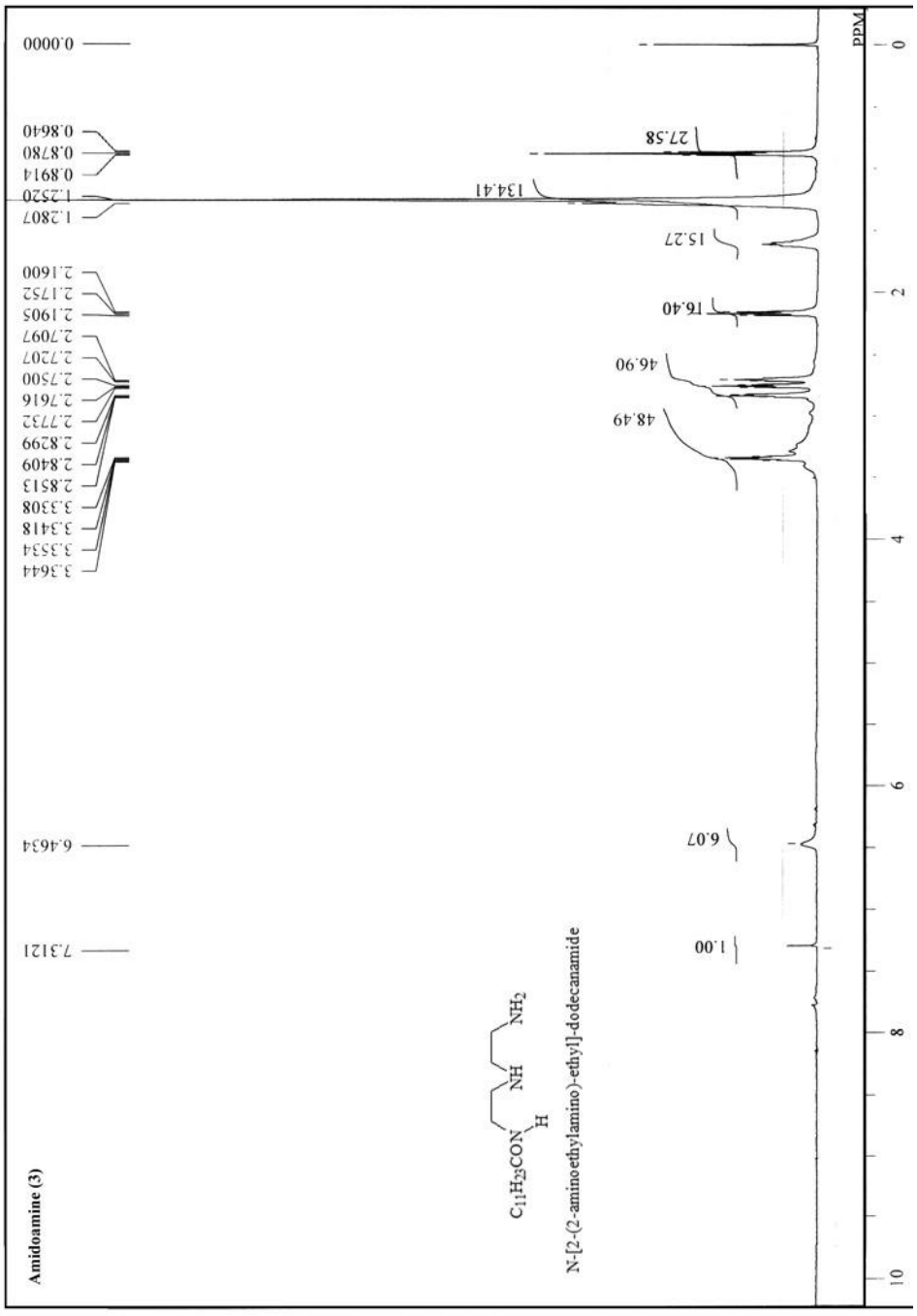

FIGURE A2.3. ^{1}H NMR Spectrum of Amidoamine (3).

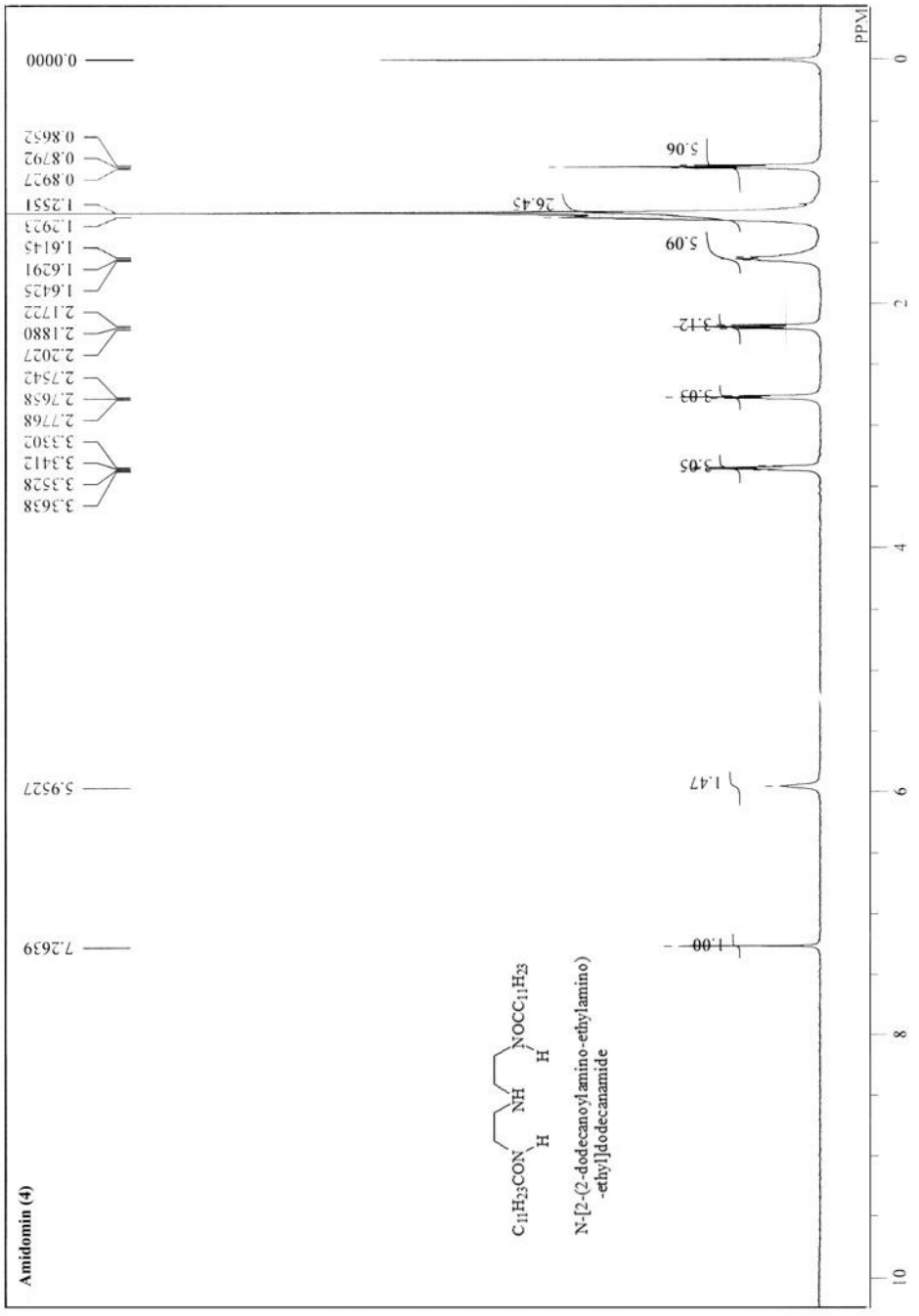

FIGURE A2.4. ^{1}H NMR Spectrum of Amidoamine (4).

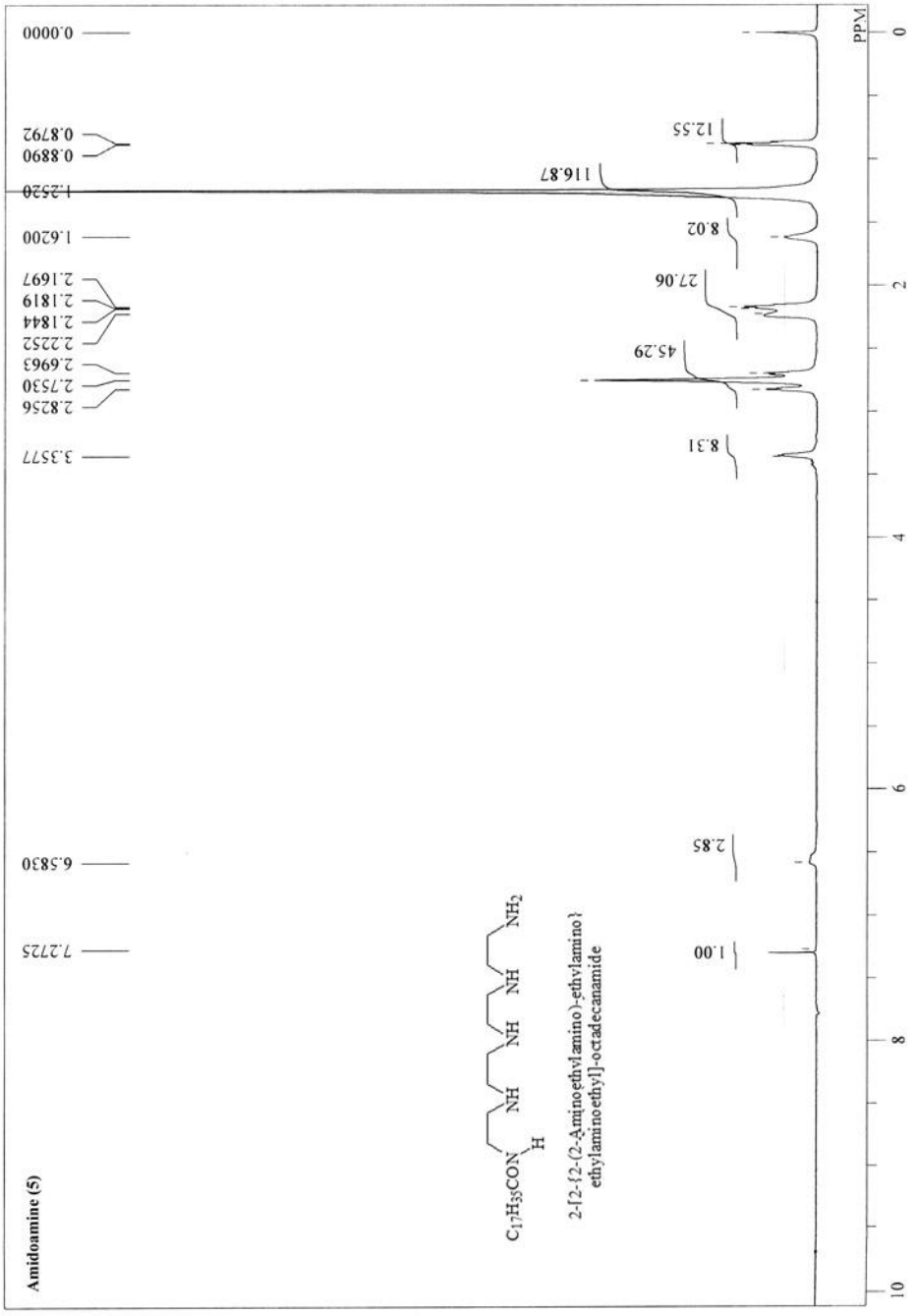

FIGURE A2.5. ^{1}H NMR Spectrum of Amidoamine (5).

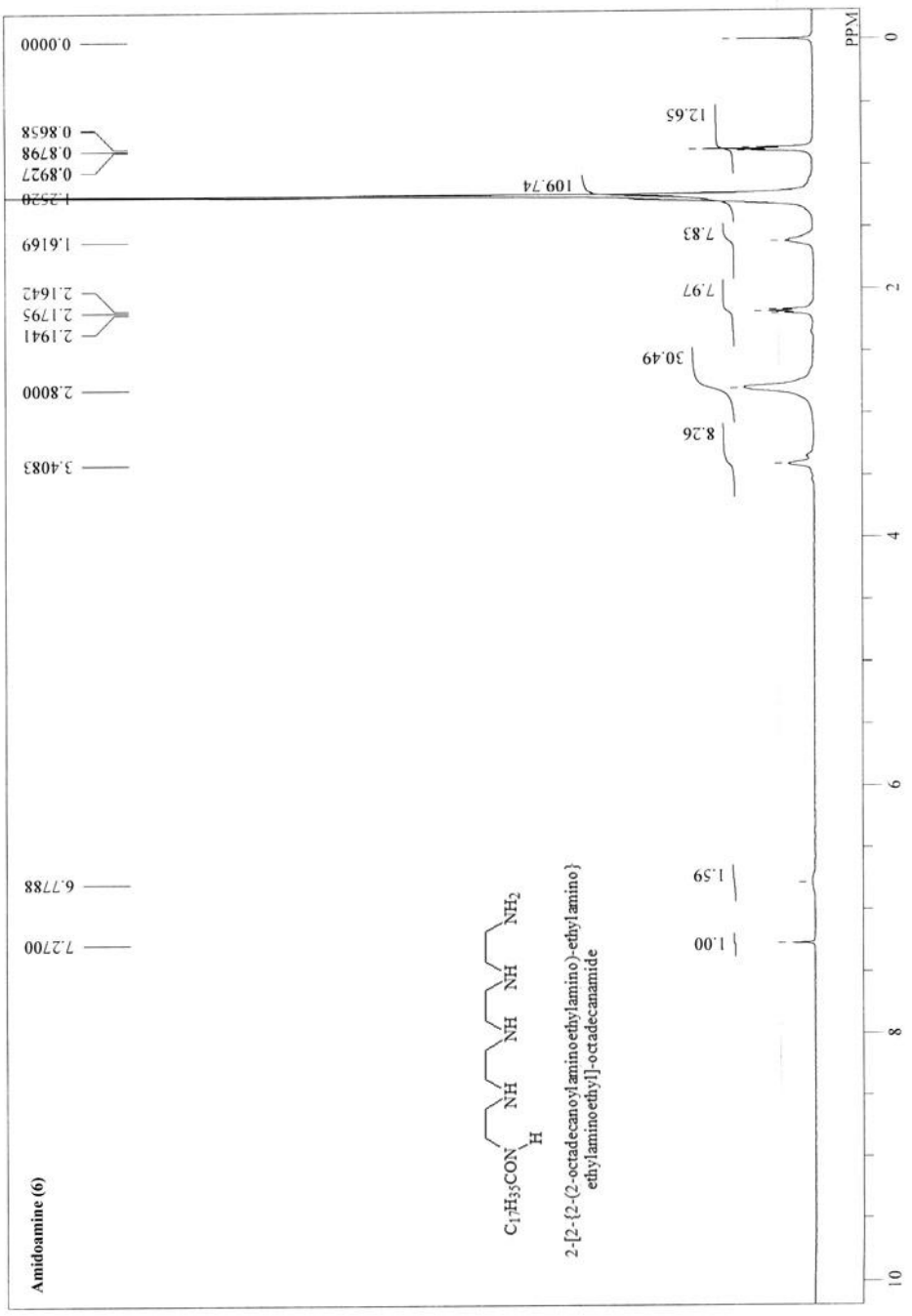

FIGURE A2.6. ^{1}H NMR Spectrum of Amidoamine (6).

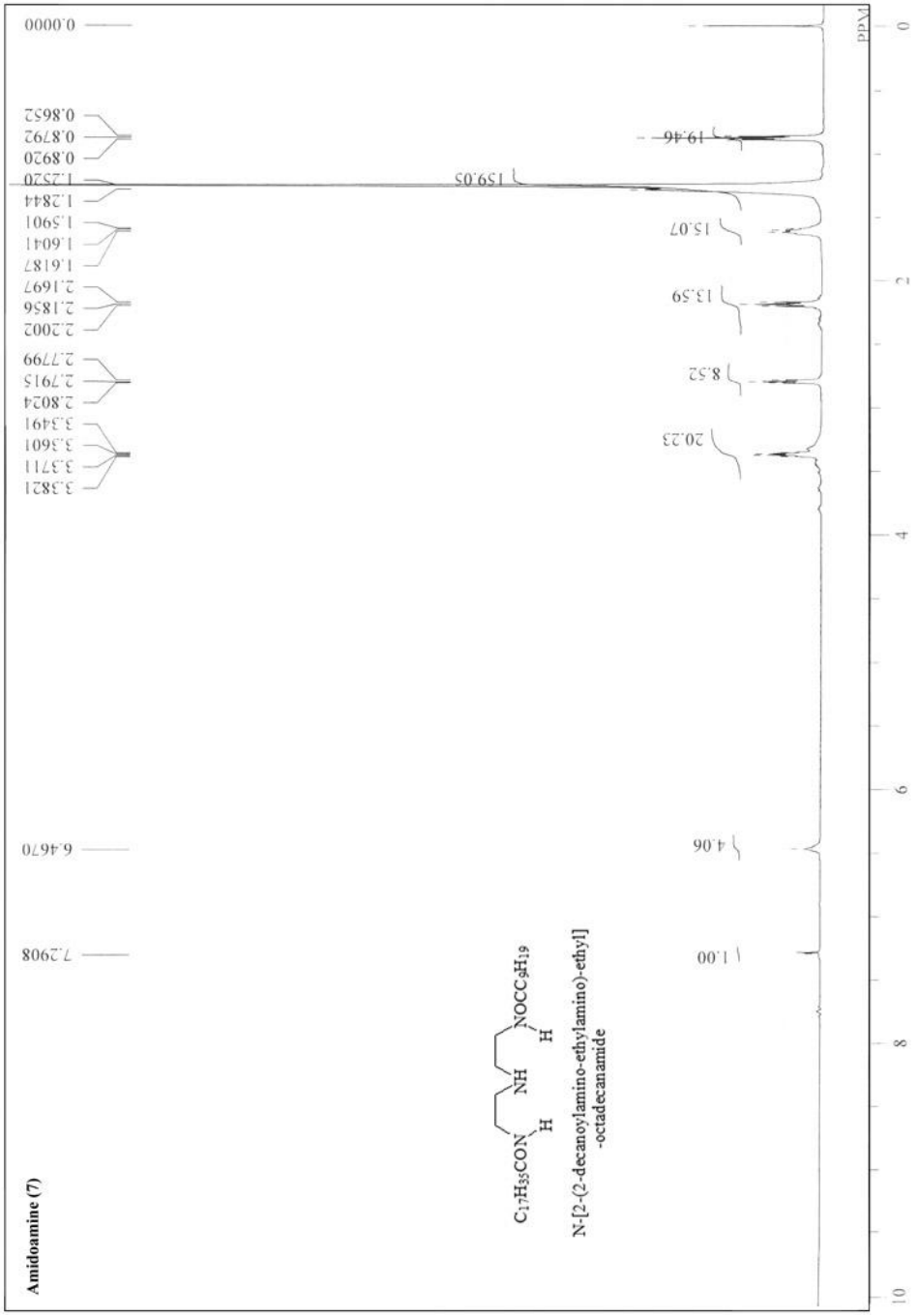

FIGURE A2.7. ^{1}H NMR Spectrum of Amidoamine (7).

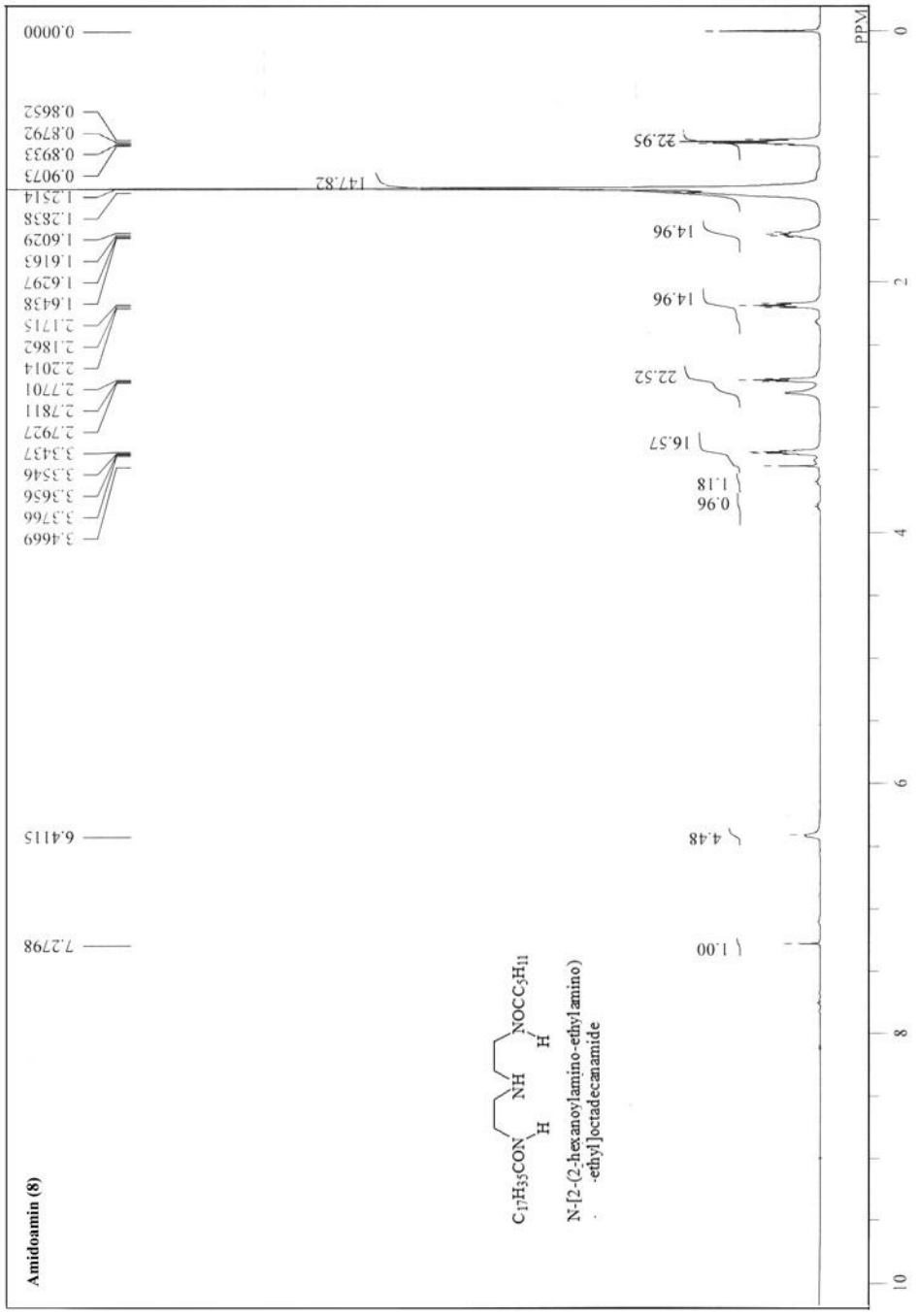

FIGURE A2.8. ^{1}H NMR Spectrum of Amidoamine (8).

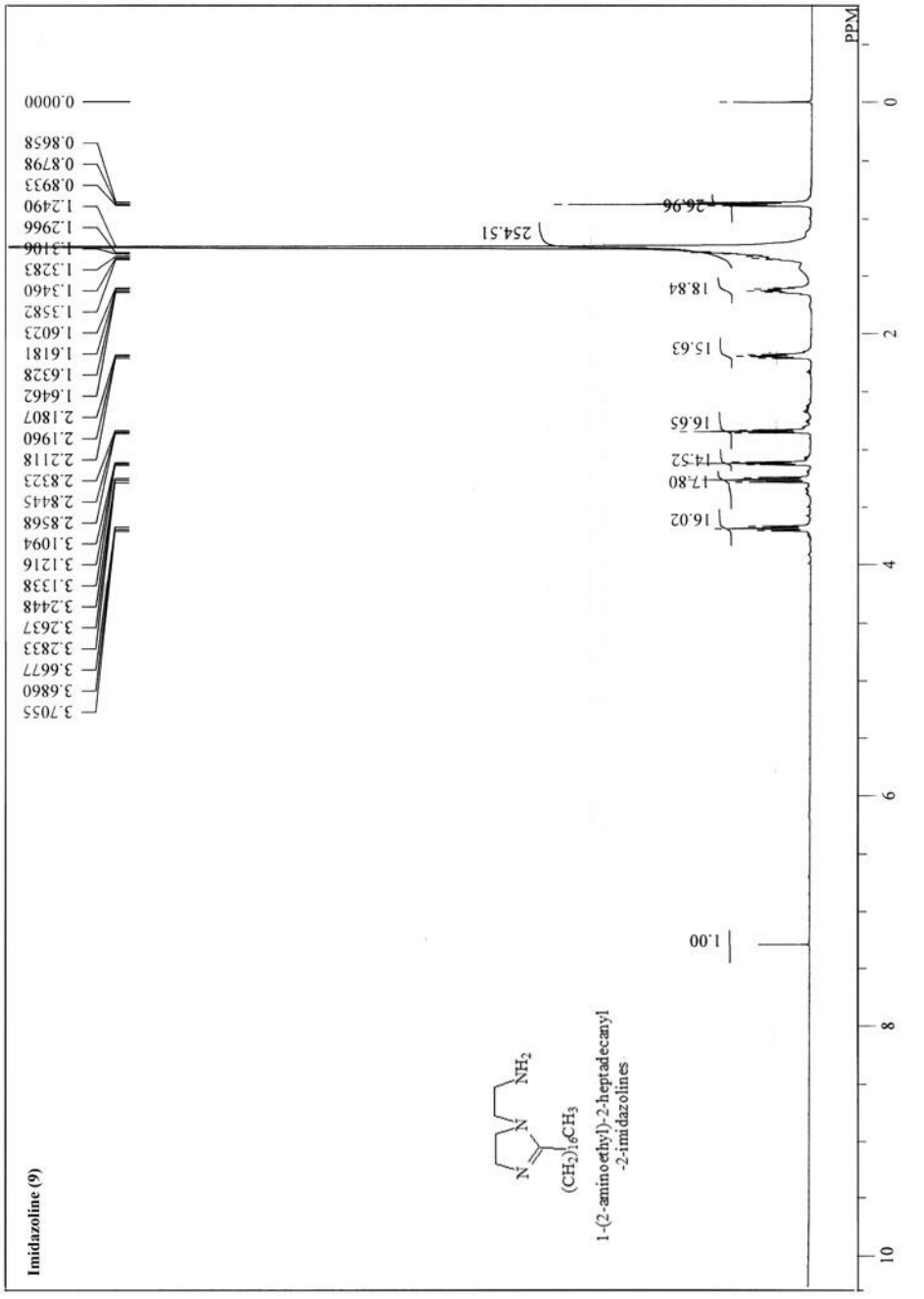

FIGURE A2.9. ^{1}H NMR Spectrum of Imidazoline (9).

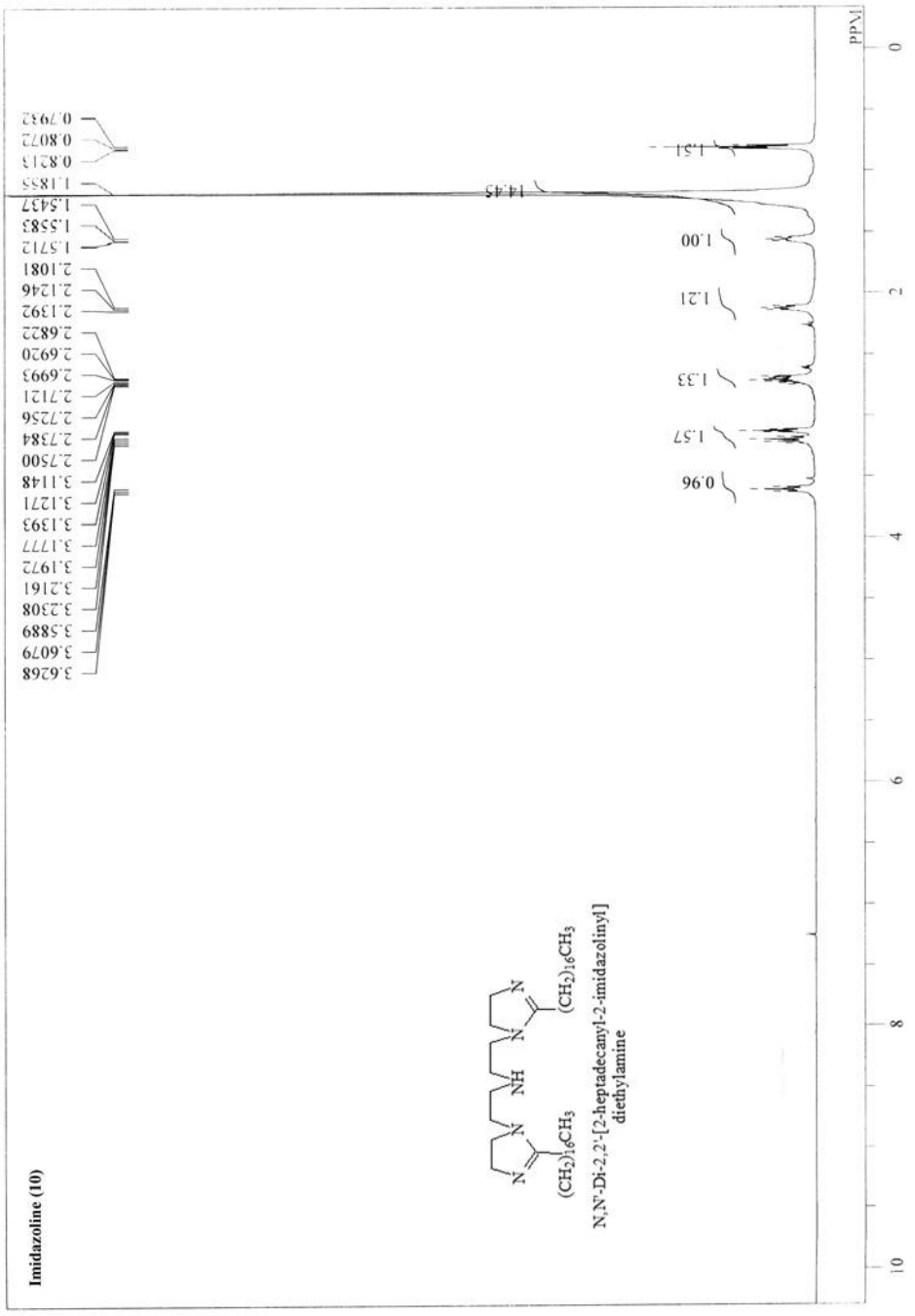

FIGURE A2.10. ^{1}H NMR Spectrum of Imidazoline (10).

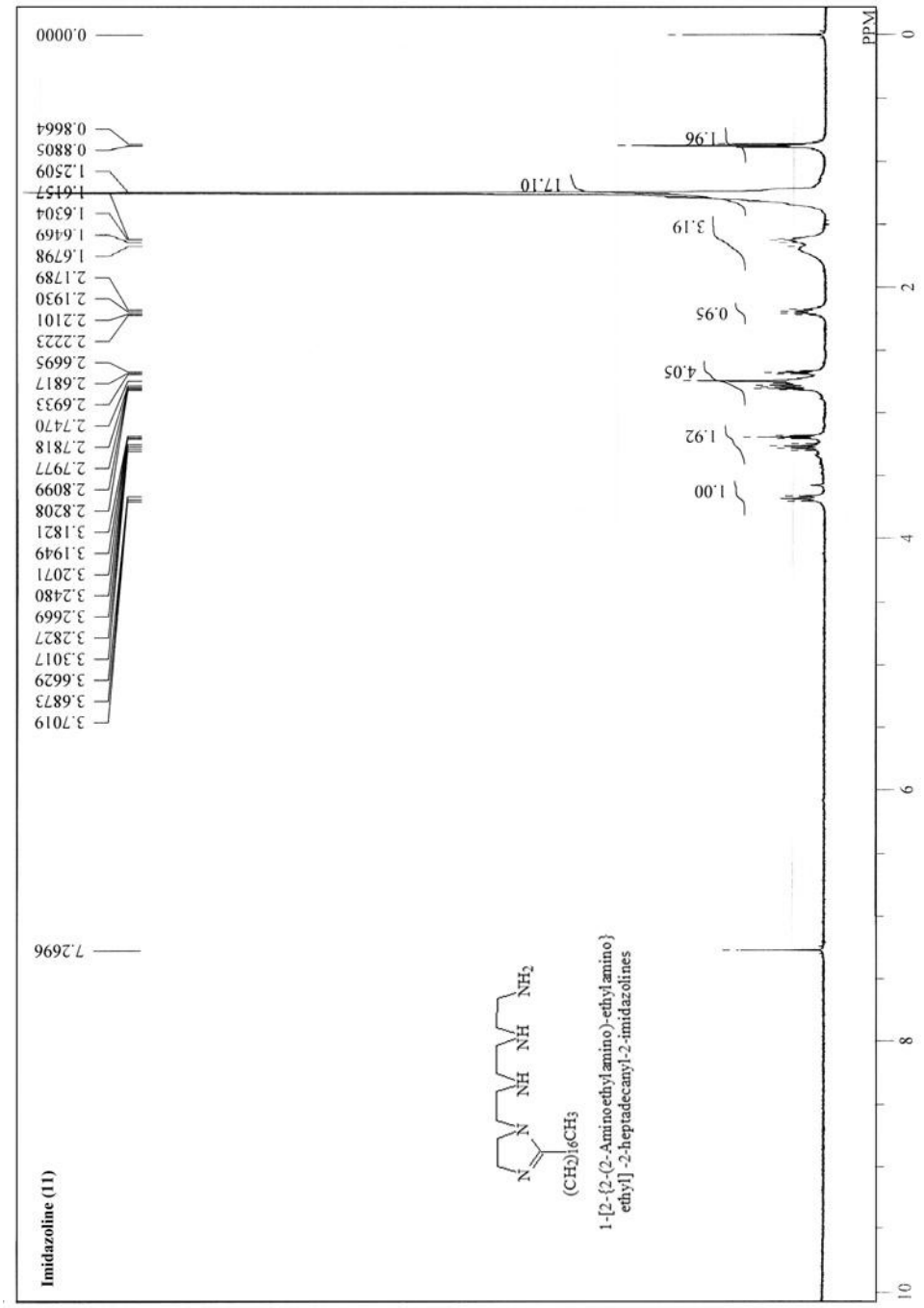

FIGURE A2.11. ^{1}H NMR Spectrum of Imidazoline (11).

APENDIX 3.

THE ^{13}C NMR SPECTRA OF THE SYNTEHSIZED MOLECULES.

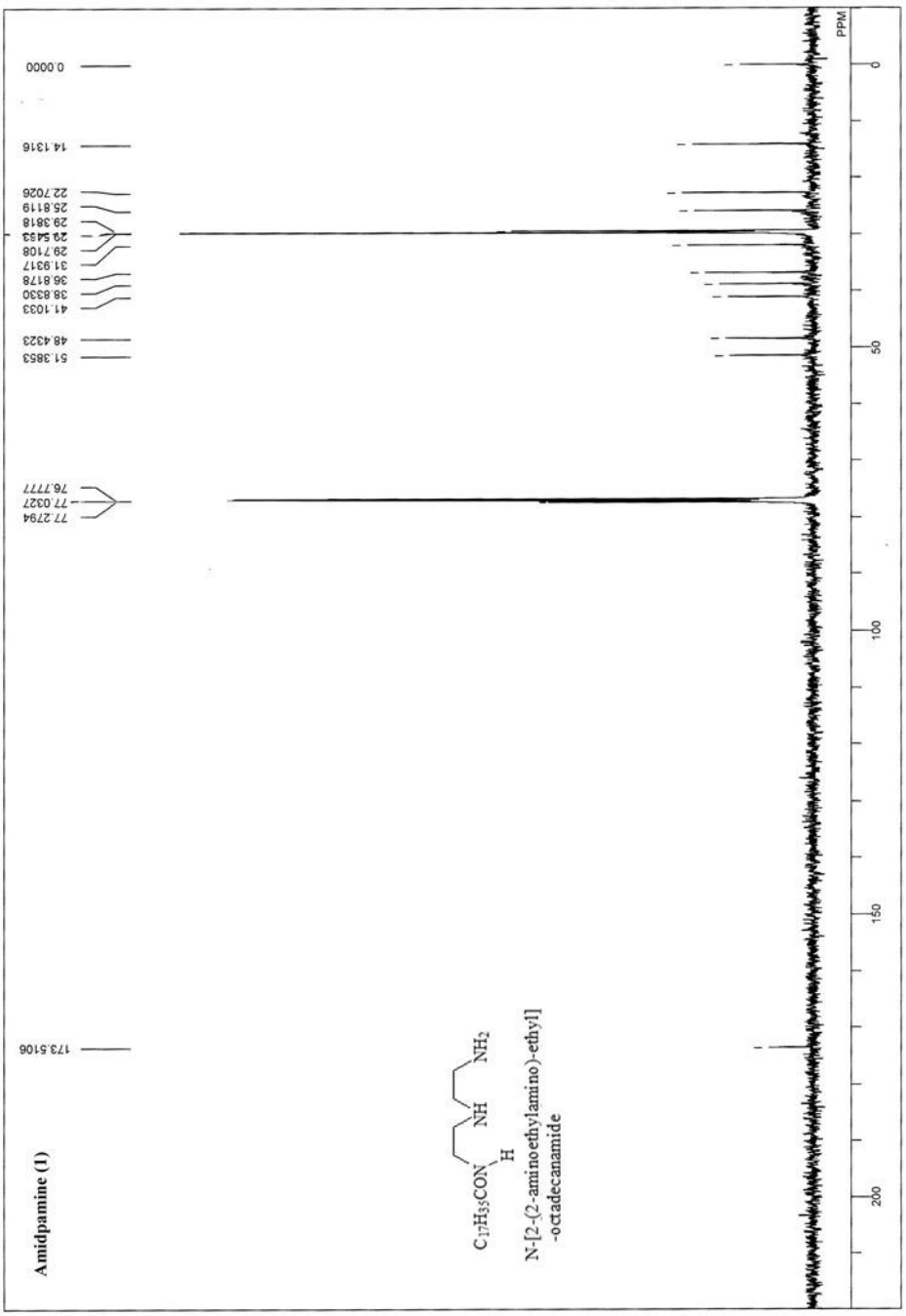

FIGURE A3.1. ^{13}C NMR Spectrum of Amidoamine (1).

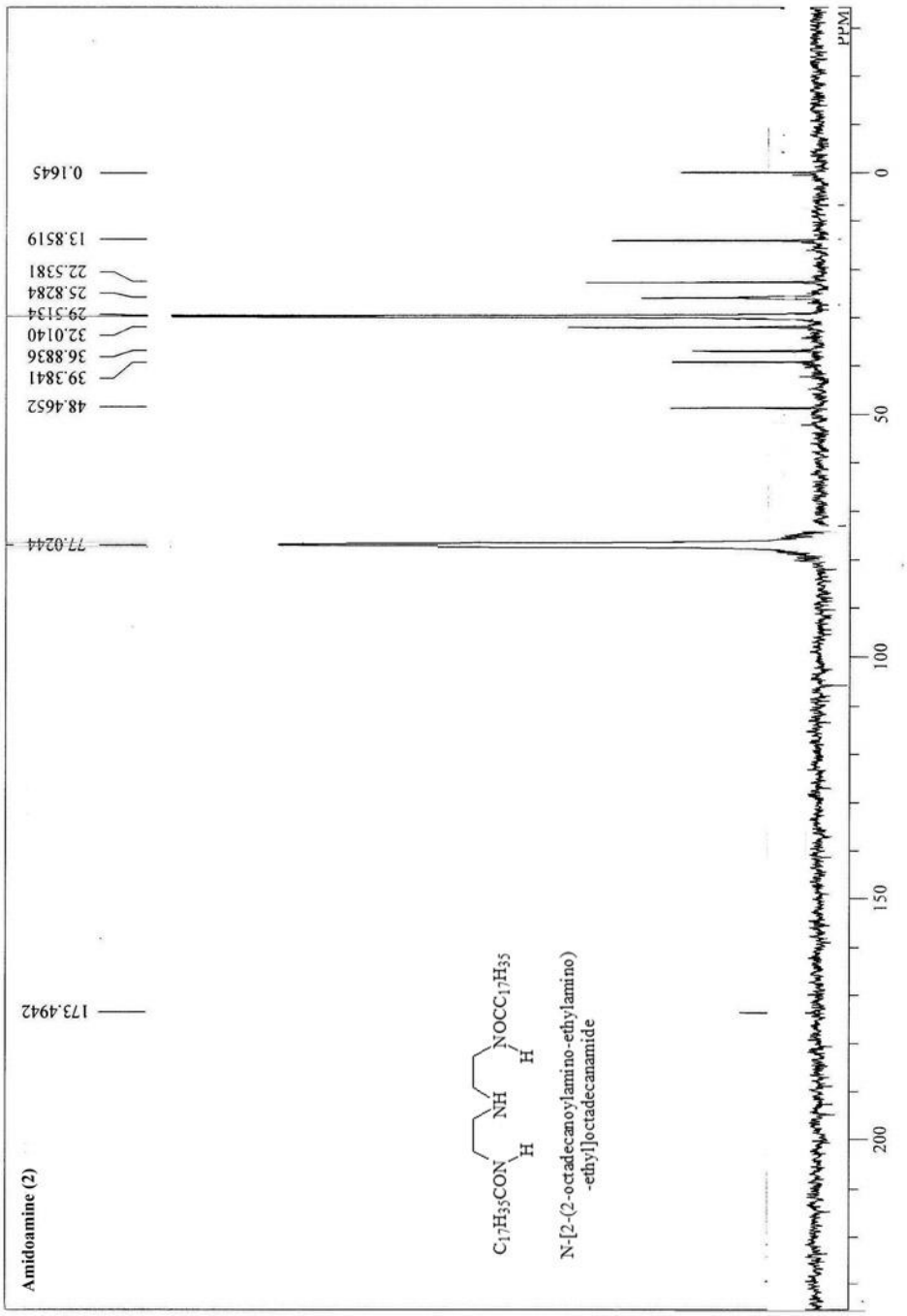

FIGURE A3.2 ^{13}C NMR Spectrum of Amidoamine (2).

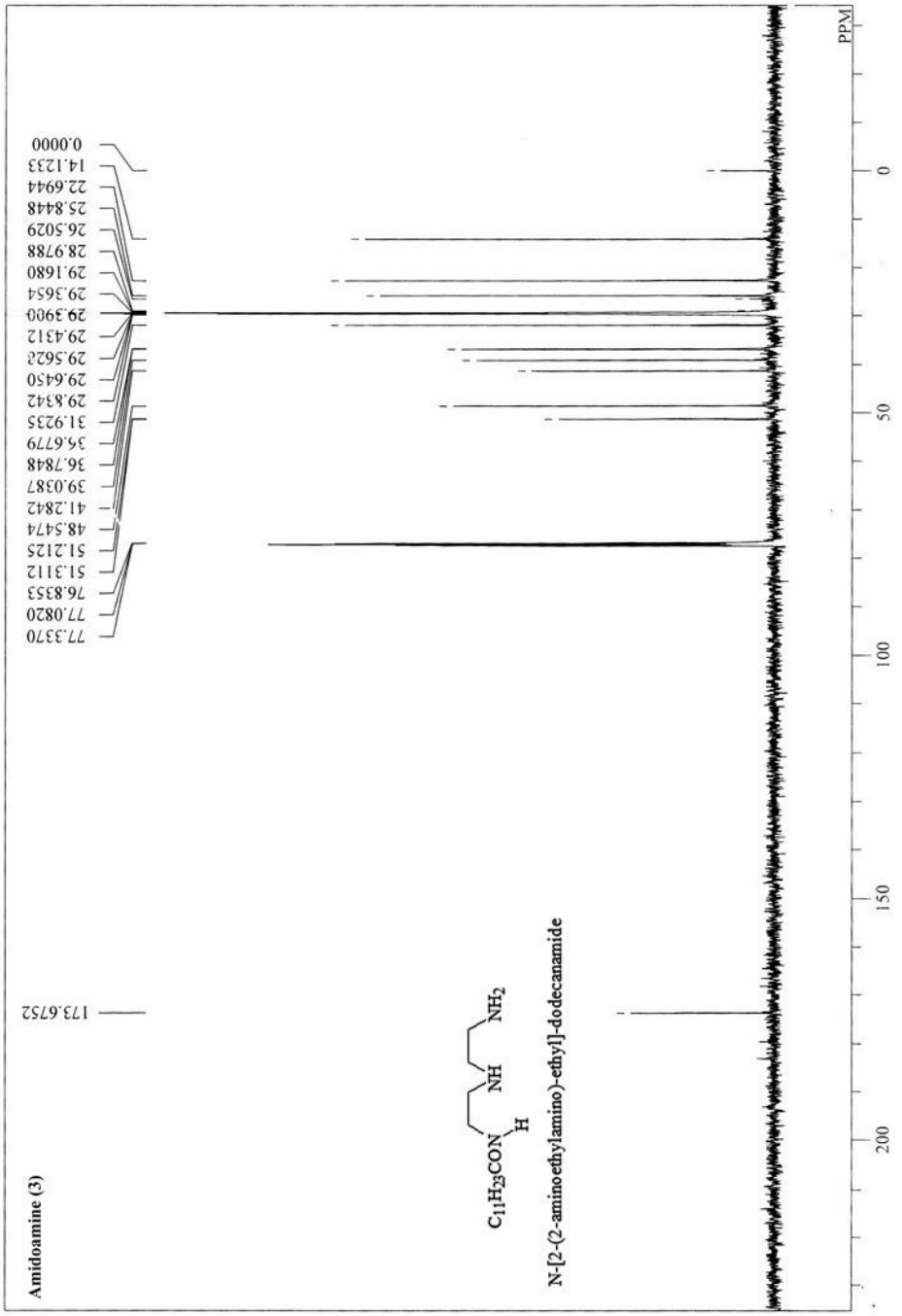

FIGURE A3.3 ^{13}C NMR Spectrum of Amidoamine (3).

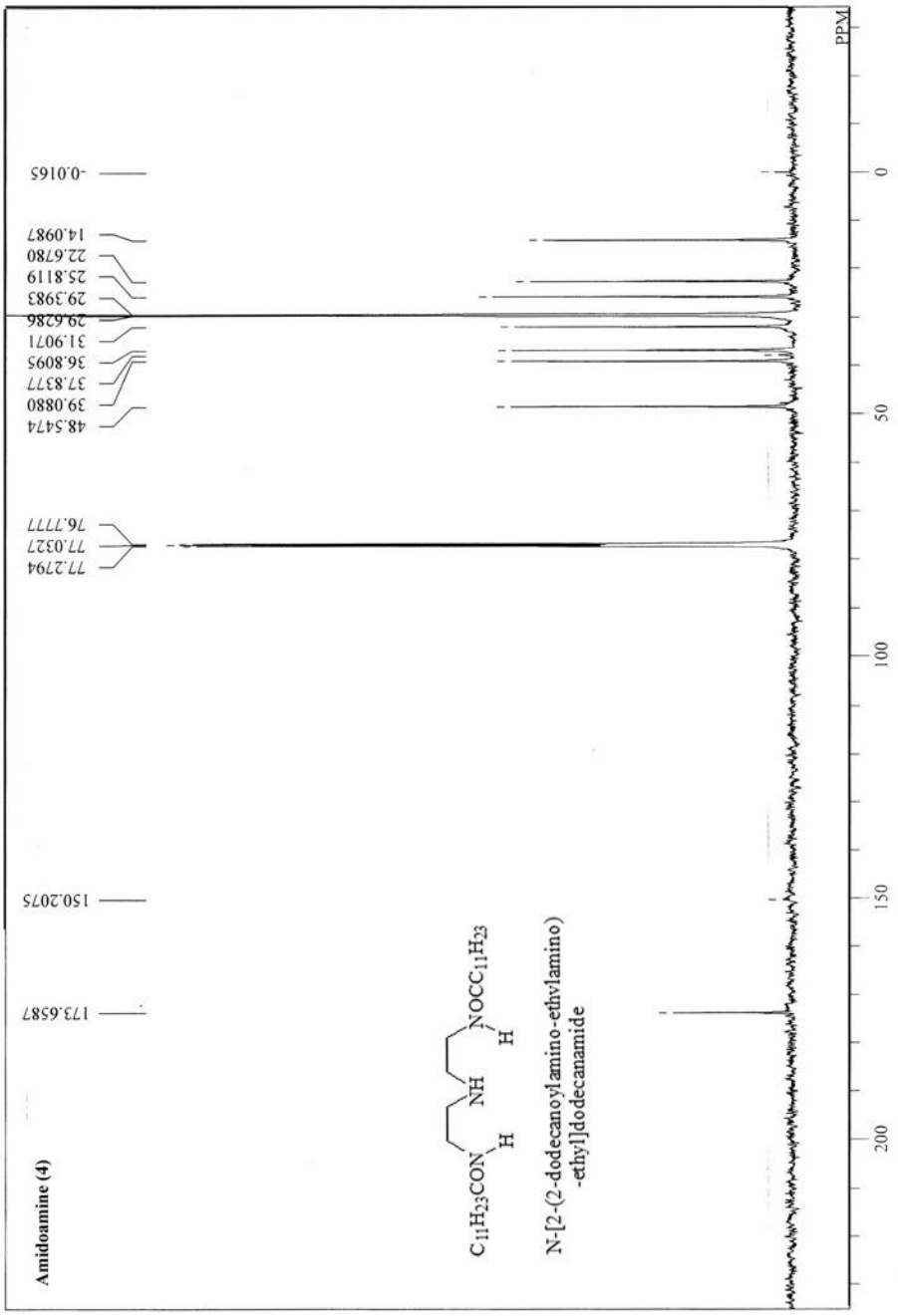

FIGURE A3.4 ^{13}C NMR Spectrum of Amidoamine (4).

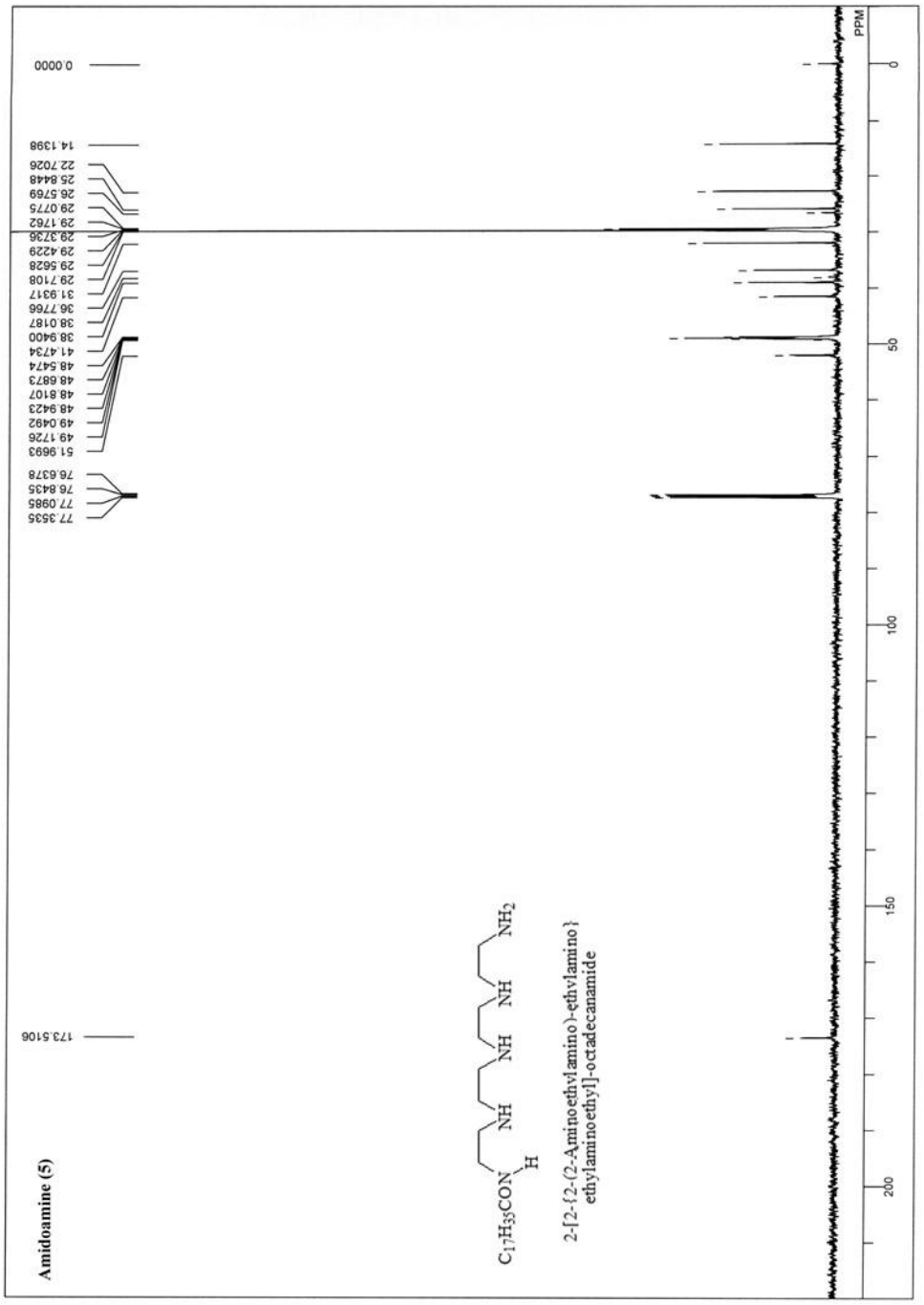

FIGURE A3.5 ^{13}C NMR Spectrum of Amidoamine (5).

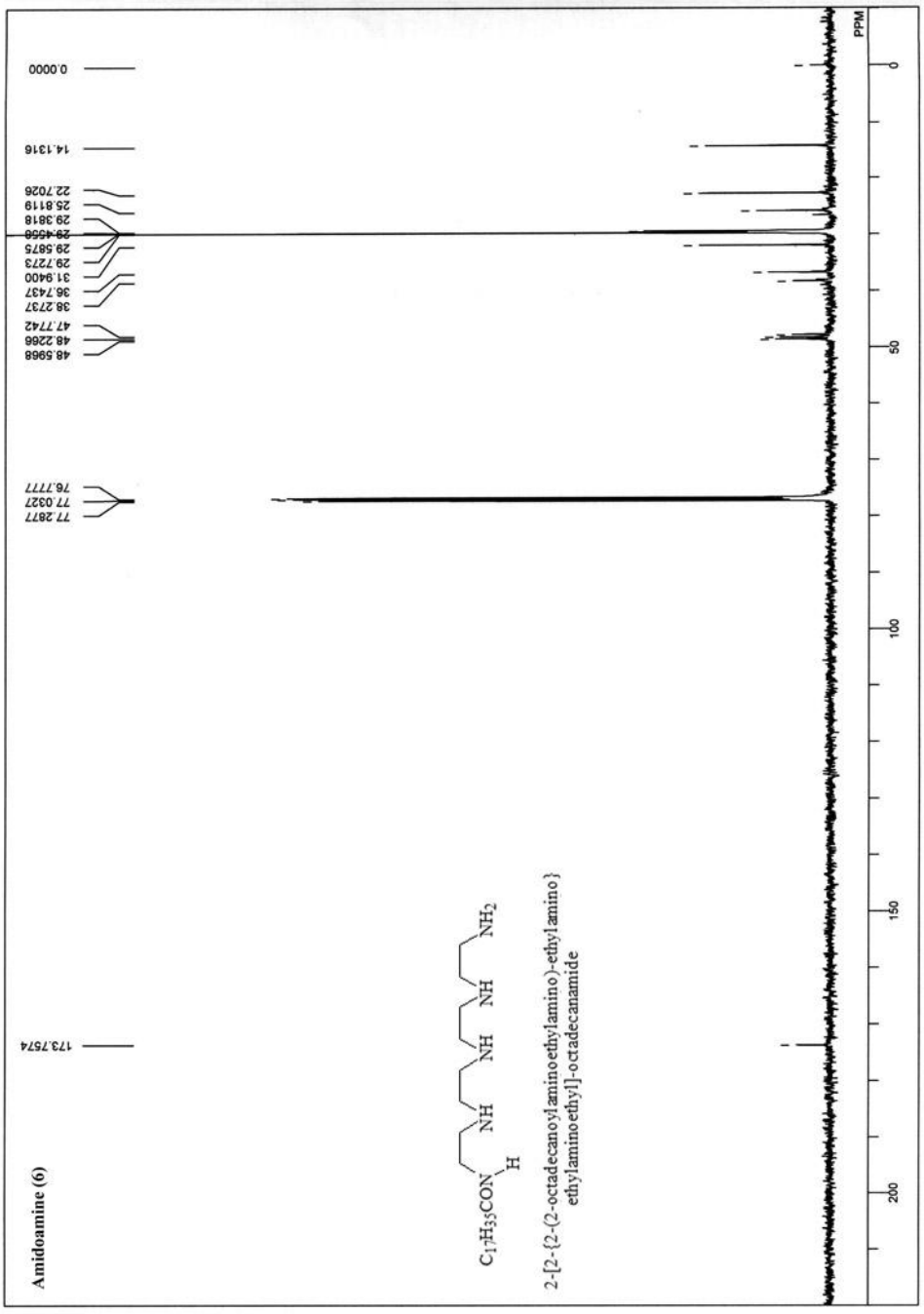

FIGURE A3.6 ^{13}C C NMR Spectrum of Amidoamine (6).

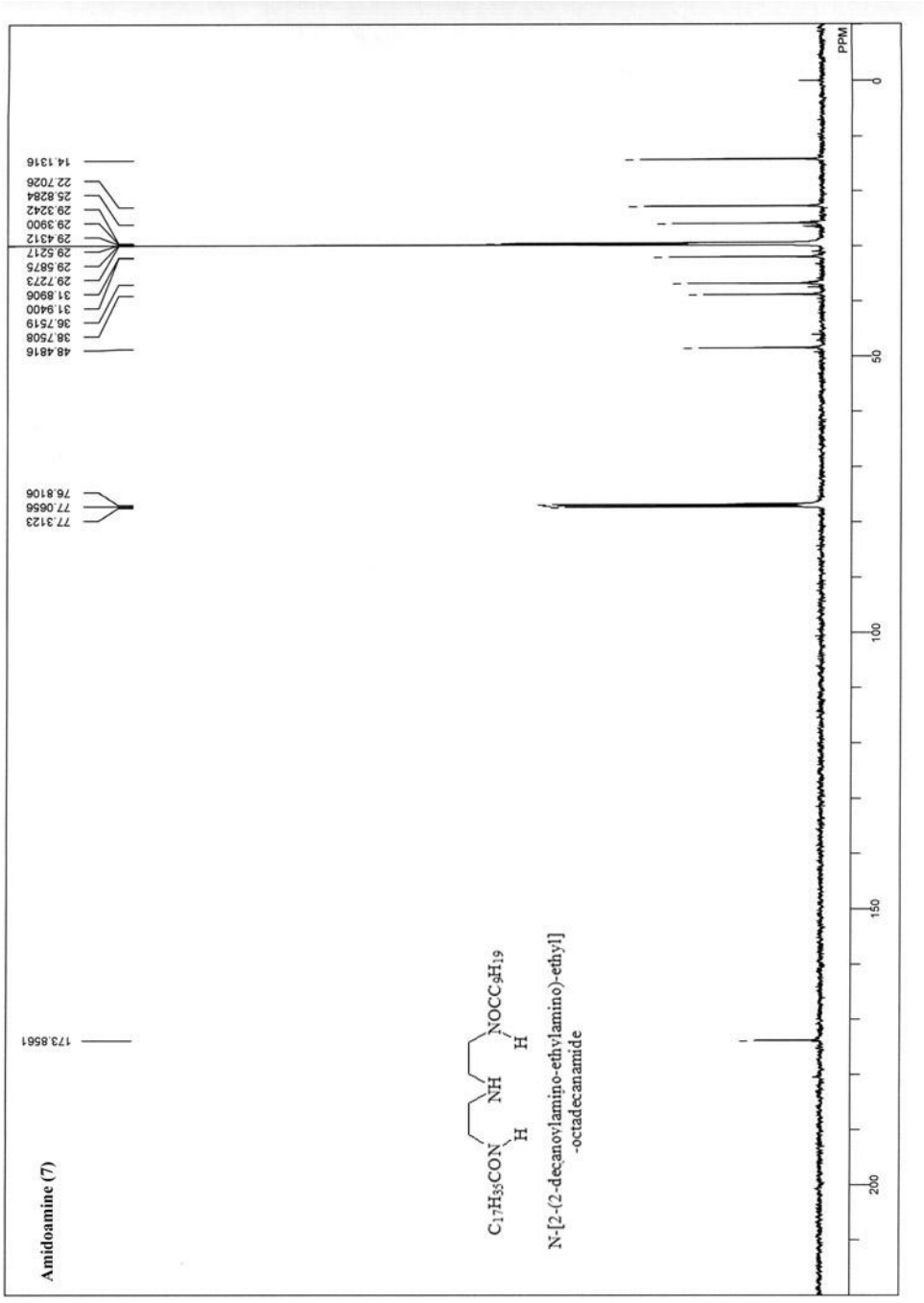

FIGURE A3.7 ^{13}C NMR Spectrum of Amidoamine (7).

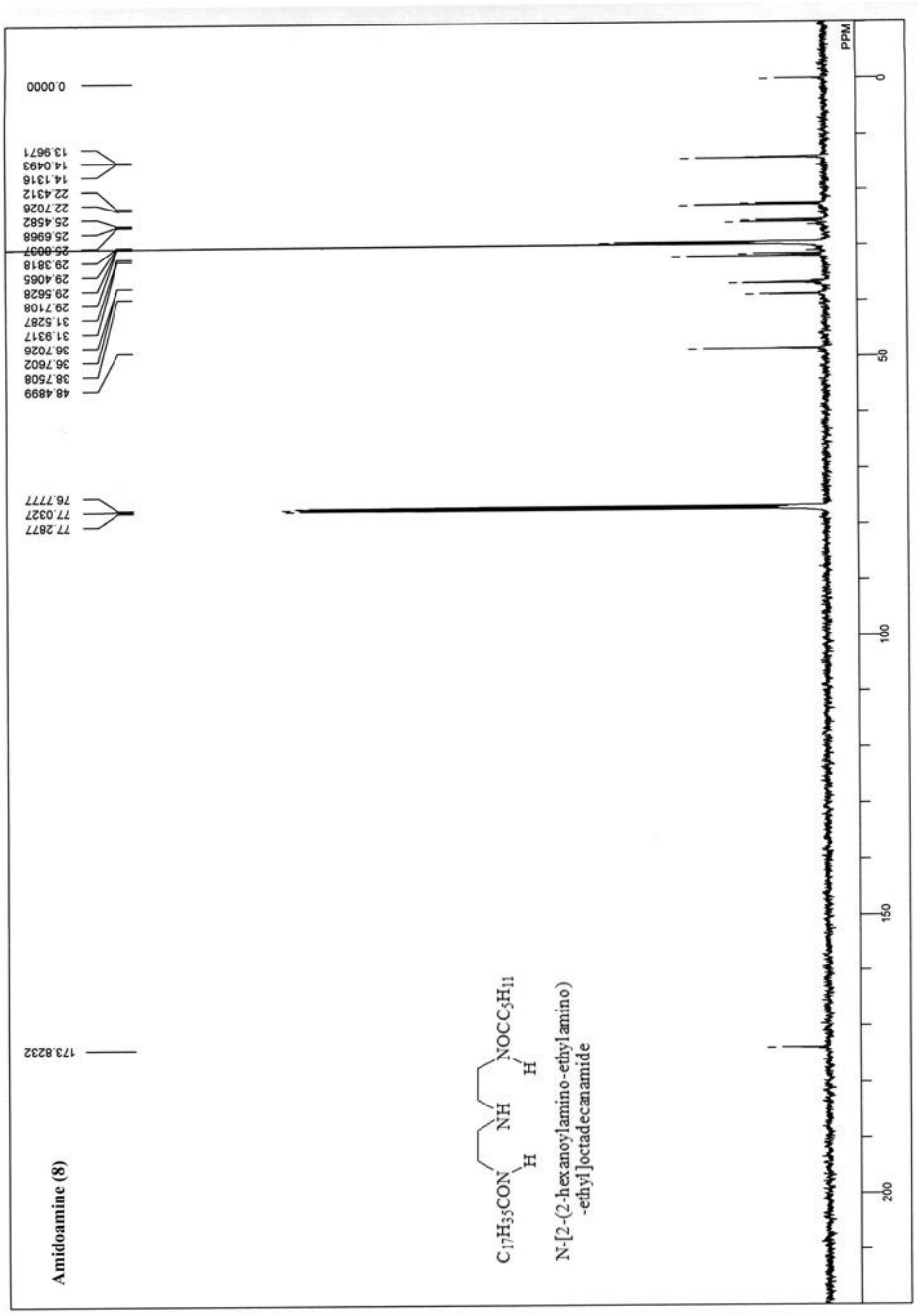

FIGURE A3.8 ^{13}C NMR Spectrum of Amidoamine (8).

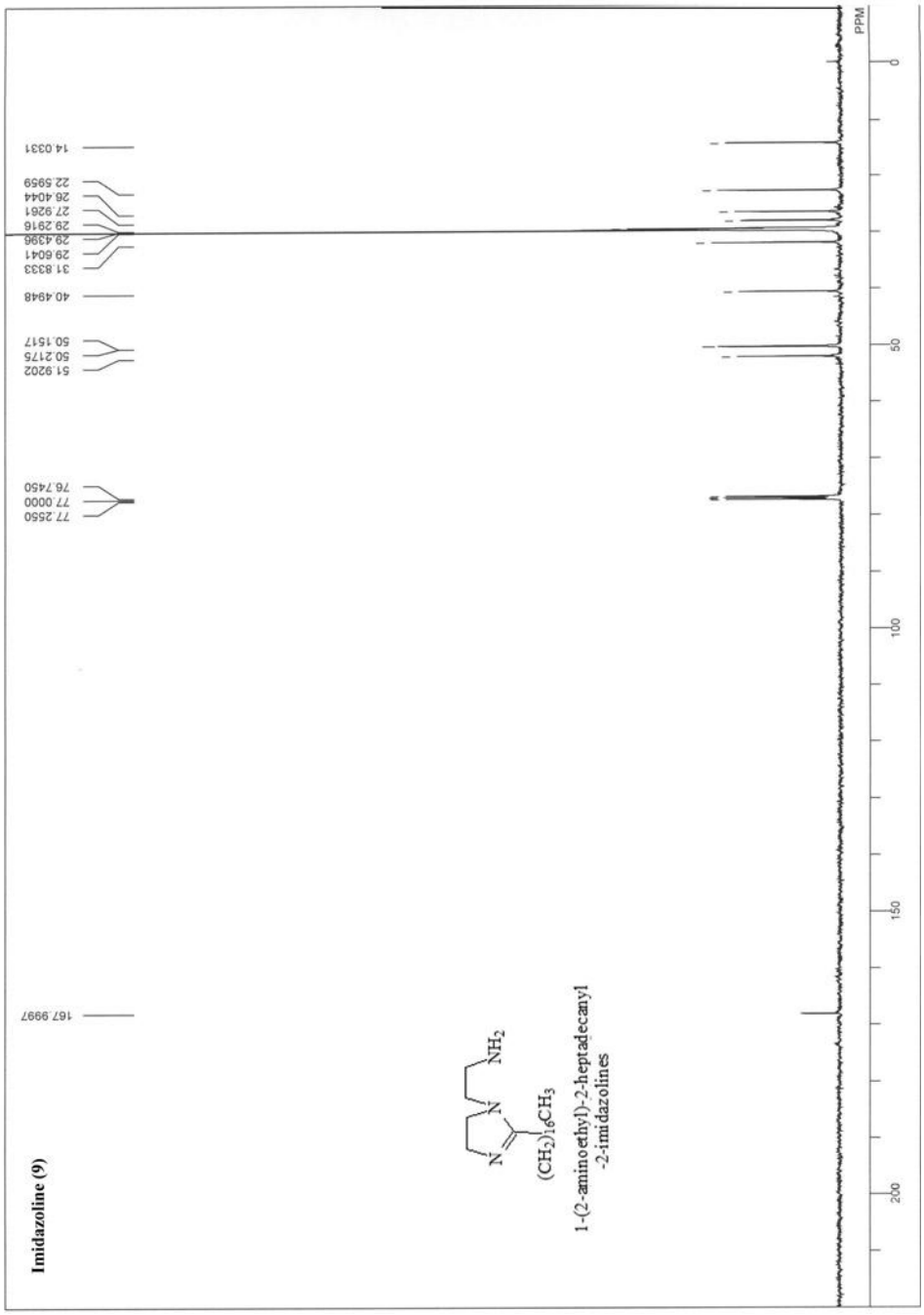

FIGURE A3.9 ^{13}C NMR Spectrum of Imidazoline (9).

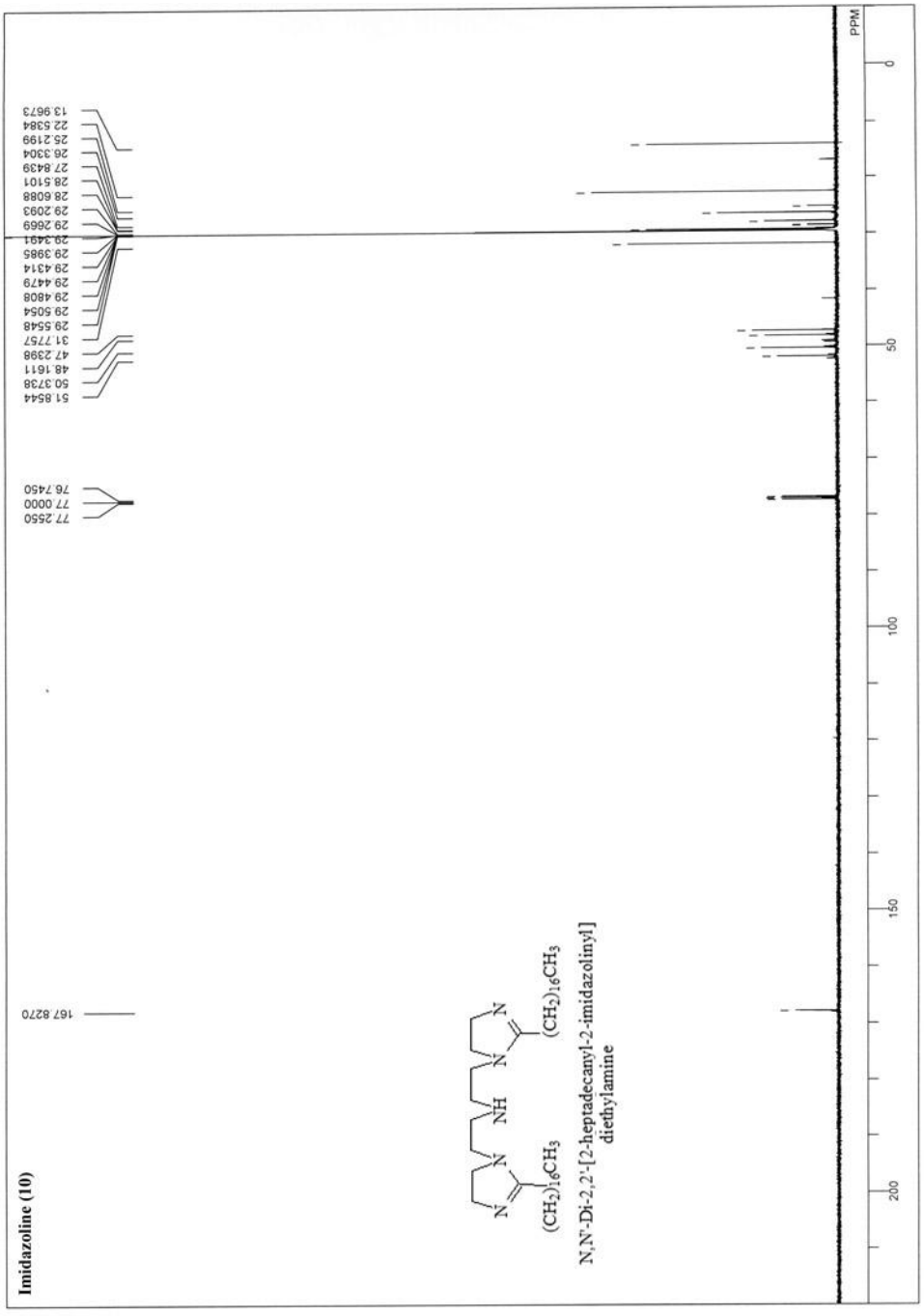

FIGURE A3.10 ^{13}C NMR Spectrum of Imidazoline (1.0).

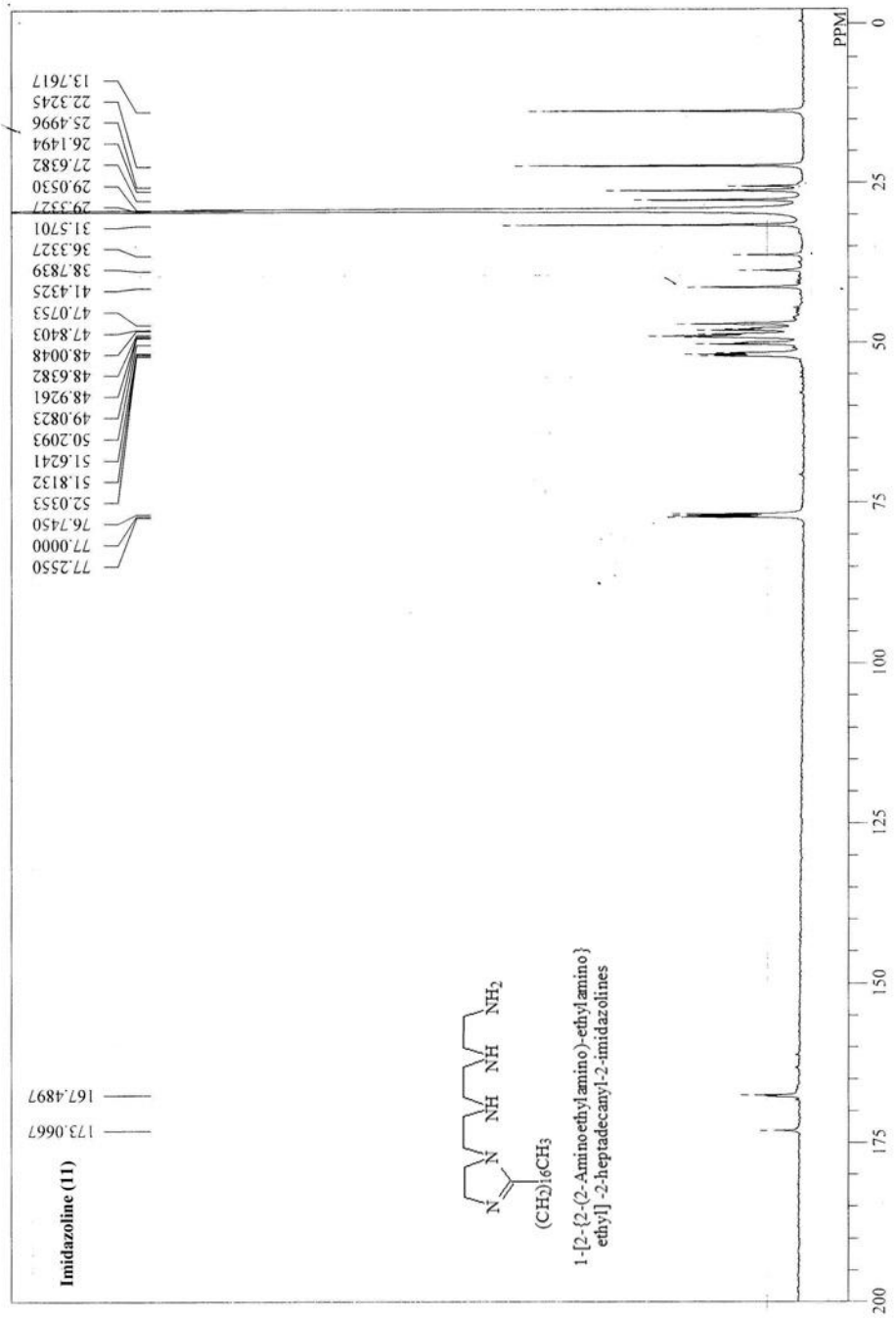

FIGURE A3.11 ^{13}C NMR Spectrum of Imidazoline (1.1.).

REFERENCES

1. Fontana, Mars G. Corrosion Engineering, 1986.

2. Sastri, V. S. Corrosion Inhibitors, Principles And Application, John Wiley & Sons Publication. 1998.

3. Tems, R., Al Zahrani, A.M., Cost Of Corrosion In Oil Production And Refining. . Saudi Aramco Journal Of Technology 2006.

4. Ruschau, G.R., Al-Anezi, M. A., Corrosion Costs And Preventive Strategies In The United States , Appendix 5, Federal Highway Administration (FHWA), Publication No. Fhwa-Rd-01-156.

5. Roberge, P. R., Corrosion Inspection And Monitoring, John Wiley & Sons., Publication , 2007.

6. Bistline, R.G., Jr., J.W. Hampson, And W.M. Linfield, Synthesis And Properties Of Fatty Imidazolines And Their N-(2-Aminoethyl) Derivatives, J. Am. Oil Chem. Soc. 60:823–828 (1983).

7. Linfield, W.M Synnthesis And Surface Active Properties Of Gawafa Fats Based Amphoteric Surfactants. J. Am. Oil Chem. Soc. 54, 371 (1977).

8. Earl G.W. Imidazoline Surfactants, Cationic Surfactants Richmond, J.M.Ed) Marcel Dekker Newyork 1990.

9. Warner, M.L. Bistline, R.Jr.; Hampson, W.J., Synthesis And Properties Of Fatty Imidazolines And Thier N-(2-2aminoethyl)Derivatives. J.Am.Oil Chem. Soc.60 (1983).

10. Butler, R..N.,Thornton, J.D.; Synthesis Of Long Chain 2-Alkyl-2-(2-Hydroxy-ethyl)- 2-Imidazolines Under Microwave In Solvent Free Conditions. J.Chem. Research 34.(1981).

11. Yue, K.F.; Wang, X.F.Journal Ca Section (Surface Active Agent And Detergents) (2000).

12. Welley And Darlene Europe Patent 326222 (1994).

13. Bajpai,D. Tyagi, V.K .” Microwave Synthesis Of Cationic Fatty Imidazolines And Their Characterization”. J Surface Deterg (2008) 11: 79-87.

14. Baltrok, I.M, Alibeik, I,M " Microwave-Assisted Facile And Convenient Synthesis Of Imidazolines" Bull, Korean Chem Soc 2003 Vol 24 No 9.

15. Jovancicevic V; Ramachandran,S ; Inhibition of Carbon Dioxide Corrosion of Mild Steel by Imidazolines and Their Precursors, CORROSION 1999, Vol 55.

16. Zamudio, R, Estrada, A. Benavides, Control of corrosion of carbon steel in hydrogen sulfide environments For 1 - (2-Hydroxyethyl)-2-alkyl-imidazoline and their corresponding amidic precursors , Rev, Soc, Quim, Mex 2002 46, 335.

17. Martin, J. A., Valone, F. W. "The Existence of Imidazoline Corrosion Inhibitors," , Corrosion, 41 (5), May 1985.

18. Desimone, M.P, Grundmeier , G. , Gordillo, G., Simison, S.N. " Amphiphilic amido-amine as an effective corrosion inhibitor for mild steel exposed to CO2saturated solution: Polarization, EIS and PM-IRRAS studies", Elelctrochimica Acta Acta 2011.

19. Atkins,P , De Paula, J. "Physical Chemistry" Oxford University Press; 8 Ed Edition 2006.

20. Duda, Y, Govea-Rueda,R Corrosion Inhibitors, Design Performance And Computer Simulations , J Phys Chem 2005, 109, 22674-22684.

21. De Waard, C, And Milliams, D. E., Carbonic Acid Corrosion Of Carbon Steel, CORROSION 75, Paper No. 177, Vol. 31, No. 5. NACE 1975.

22. Chokshi, K.; Sun, W.; Nesic, S. "Iron Carbonate Scale Growth And The Effect Of Inhibition In CO_2 Corrosion Of Mild Steel", CORROSION 2005, Paper No. 05285, Vol. 61, NACE, 2005.

23. Gao, K.; Yu, F.; Pang, X.; Zhang, G.; Qiao, L.; Chu, W.; Lu, M., "Mechanical Properties Of Co2 Corrosion Product Scales And Their Relationship To Corrosion Rates". Corrosion Science 2008, 50 (10), 2796-2803.

24. Nafday, O. A.; Nesic, S. "Iron Carbonate Scale Formation And CO_2 Corrosion In The Presence Of Acetic Acid", CORROSION 2005, Paper No. 05295, Vol. 61, NACE, 2005.

25. Ruzic, V.; Veidt, M.; Nesic, S., "Protective Iron Carbonate Films- Part 1: Mechanical Removal In Single-Phase Aqueous Flow". CORROSION 2006, Paper No. 06050419, Vol. 62, NACE, 2006.

26. Nesic, S.; Lee, K. L. J., "A Mechanistic Model For Carbon Dioxide Corrosion Of Mild Steel In The Presence Of Protective Iron Carbonate Films - Part 3: Film Growth Model". CORROSION 2003, Paper No. 03070616, Vol. 59, NACE, 2003.

27. Dugstad, A, "The Importance Of Iron Carbonate Super Saturation On The Carbon Dioxide Corrosion Of The Carbon Steels", CORROSION 92, Vol. 48, NACE, 1992.

28. Zhang, R., Gopal, M., Jepson, W. P., Development Of A Mechanical Model For Predicting Corrosion Rate In Multiphase Oil/Water/Gas Flows. CORROSION 97, Paper No 601. NACE 1997.

29. Nesic, S., Postlethwaithe, J., And Olsen, S., An Electrochemical Model For Prediction Of CO_2 Corrosion. CORROSION 95, Paper No 131. NACE 1995.

30. Dayalan, E., Vani G., Shadley, J. R., And Shirazi, S. A., Rybicki, E. F., Modeling CO_2 Corrosion Of Carbon Steel In Pipe Flow, CORROSION 95, Paper No 118. NACE1995.

31. Herce, J. A., Wrighl E. J., Efird, K. D., Boros, J. A., Hailey, T. G., "Effects Of Solution Chemistry And Flow On The Corrosion Of Carbon Steel In Sweet Production", CORROSION 95, Paper No 111. NACE 1995.

32. Nesic, S,. Wang, S., Cai, J., Xiao,Y. Integrated CO_2 Corrosion –Multi Phase Flow Model. CORROSION 2004, Paper No. 4626. NACE 2004.

33. Gray, L. G. S, Anderson, B. G, Danysh, M.J, Tremaine P.R. Effect Of pH And Temperature On The Mechanism Of Carbon Steel Corrosion By Aqueous Carbon Dioxide. CORROSION 90, Paper No 40, NACE 1990.

34. Nesic, S.; Solvi, G. T.; Enerhaug, J., "Comparison Of The Rotating Cylinder And Pipe Flow Tests For Flow-Sensitive Carbon Dioxide Corrosion". CORROSION 1995, 51773-787. (10).

35. Fajardo, V., Canto, C., Brown, B., And Nesic, S. Effect Of Organic Acids On CO_2 Corrosion, CORROSION 2007, Paper No 7319. NACE 2007.

36. Einar Bardal. Corrosion And Protection. Springer (2003), P. 82.

37. Omkar A. Nafday , Srdjan Nesic. Iron Carbonate Scale Formation And CO_2 Corrosion In The Presence Of Acetic Acid. CORROSION 2005 Paper No 05295. NACE 2005.

38. Pisigan, R.A., Singley, J.E. “Evaluation Of Water Corrosivity Using The Langelier Index And Relative Corrosion Rate Models,” CORROSION 84, Paper No.149, NACE 1984.

39. Ferguson, R. J., Developing Corrosion Inhibitor Models. Watertech '93, Houston Tex.

40. David R. Lide, CRC Handbook Of Chemistry And Physics, 71 Ed. Boca Raton, Ann Arbor, Boston: CRC Press, 1990-1991.

41. Physical And Engineering Data, January 1978 Ed. The Hague: Shell Internationale Petroleum Maatschappij Bv, 1978.

42. De Waard C, Lotz U, Dugstad A. Influence Of Liquid Flow Velocity On CO_2 Corrosion: A Semi–Empirical Model. CORROSION 95, Paper No 128, NACE 1995.

43. Pourbiax, M., Atlas Of Electrochemical Equilibria, In Aqueous Solutions” Pergamon Press Oxford, Uk 1966.

44. Jin Koryta , Principles Of Electrochemistry ,Second Edition, John Wiley & Sons Press 1993.

45. Marcus P, “Corrosion Mechanisms in Theory and Practice”, 2nd ED, MARCEL DEKKER, 2002.

46. Freedman Aj, Troscinski Es, And Dravnieks A. An Electrical Resistance Method Of Corrosion Monitoring In Refinery Equipment. CORROSION 1958.

47. Orazem, M. Tribollet, B. Electrochemical Impedance Spectroscopy, A John Wiley & Sons, Inc., Publication, 2008.

48. Perez, N. Electrochemistry And Corrosion Science , Kluwer Academic Publishers 2004.

49. Kelly, R.G And Scully, J.R Electrochemical Techniques In Corrosion Science And Engineering Marcel Dekker, Inc 2002.

50. Corrosion Of Metals And Alloys, Terms And Definitions, ISO 8044 (1986).

51. Turgoose,S., Chemical Inhibitors For Corrosion Control (Clubley, B.G), Royal Society Of Chemistry, U.K.,(1990).

52. McCafferty , E. “Introduction to Corrosion Science” Springer Science ,2010.

53. Hackerman, N., McCafferty, E. “Proceedings of the Fifth International Congress on Metallic Corosion”, p. 542, NACE, Houston, TX (1974).

54. Olivares-Xometl ,O. Surface Analysis Of Inhibitor Films Formed By Imidazolines And Amides On Mild Steel In Acidic Environment. Applied Surface Science 252 (2006) 2139-2152.

55. Lorenze, W.J., Mansfled, F., Electrochem Acta, 31, Pg467 (1986).

56. Mercer, A.D., Material Performance Journal, Vol 29 Pg45 (1990).

57. Deberry, D.W., Viehbeck,A. , CORROSION 88, Paper No.229, NACE 1988.

58. Palmer, J. W., Hedges, W., Dawson, J. L., The Use Of Corrosion Inhibitors In Oil And Gas Production. Maney Publishing 2004.

59. Ferm, R.J., And J.L. Riebsomer, The Chemistry Of The 2-Imidazolines And Imidazolidines, Chem. Rev. 54:593–613 (1954).

60. Linfield, W.M., Fatty Oxazolines And Imidazolines, Ibid. 61:437–441 (1984).

61. Wu, Y., Herrington, P.R, Thermal Reactions Of Fatty Acids With Diethylene Triamine. Journal Of The American Oil Chemists' Society. 1997.

62. Halsey, G.; Advances In Catalysis And Related Subjects, Academic Press . 1952.

63. J. O'.M. Bockris, S. U. M. Khan, Surface Electrochemistry: A Molecular Level Approach, Plenum Press, New York, London, 1993.

64. Yıldırım E.Y "Surface Chemistry Of Solid And Liquid Interfaces", Blackwell Publishing 2006.

65. O'm Bockris, J. Reddy, A. K. N., Gamboa-Aldeco, M. "Modern Electrochemistry". Kluwer Academic Publishers. 2002.

66. A. N. Frumkin, Z. Phys. Chem. 116 (1925) 466-484.

67. Brett C. A, Brett , A .M. O., Electrochemistry Principles, Methods, And Applications Oxford University Press 1994.

68. Duan, S. Z., Tao, Y. L., Interface Chemistry, Higher Education Press, Beijing, 1990, Pg. 124-126.

69. Branzoi, V., Baibarac, M., Branzoi, F., Scientific Bulletin - University Politehnica

Of Bucharest, Series B: Chemistry And Materials Science, 2001, Vol. 63.

70. Esumi. K ,. Ueno. M., Structure Performance Relationships In Surfactants. Marcel Dekker Press, 2003.

71. Myers, Drew. Surfactant Science And Technology. A John Wiley & Sons, Inc., Publication. 3rd Edition 2006.

72. Esumi. K ,. Ueno. M., Structure Performance Relationships In Surfactants. Marcel Dekker Press, 2003.

73. Robert Baboian, Corrosion Tests And Standards: Application And Interpretation, Astm International 2005.

74. Hong, T., Sun, Y.H., Jepson, W.P, Study On Corrosion Inhibitor In Large Pipelines Under Multiphase Flow Using Eis ,Corros. Sci. 44 (2002) 101.

75. John E. Mcmurry (2010). Fundamentals Of Organic Chemistry (7th Ed.). Cengage Learning.

76. Perov, P.A., Infrared Spectra Of Imidazoline And Their Hydrochlorides.

77. NACE Publication 1D182, "Wheel Test Method Used For Evaluation Of Film-Persistent Inhibitors For Oilfield Applications" (Houston, Texas: NACE).

78. Winston, Revie R.W, "Uhlig's Corrosion Handbook" Second Edition, A Wiley Publication, 2000.

79. Durnie, W. De Marco, R. Jefferson, A. Kinsella, B., Development Of A Structure-Activity Relationship For Oil Field Corrosion Inhibitors., J. Electrochem. Soc., 146 (5), 1751-1756, 1999.

80. Wu, S. L.; Cui, Z. D.; He, F.; Bai, Z. Q.; Zhu, S. L.; Yang, X. J., "Characterization Of The Surface Film Formed From Carbon Dioxide Corrosion On N80 Steel". Materials Letters 2004, 58 (6), 1076-1081.

81. Hunnik Van, E. W. J.; Pots, B. F. M.; Hendriksen, E. L. J. A. "The Formation Of Protective $FeCO_3$ Corrosion Product Layers In CO_2 Corrosion", CORROSION 96, Paper No. 6 , NACE, 1996.

VITA

- Muhammad Wadah Saleh Jawich.
- Citizen of the Syrian Arabic Republic.
- Born In Damascus, Syrian on January 30, 1975
- Received Bachelor of Science (B.Sc) in Applied Chemistry from the University of Aleppo, Aleppo, Syria in 1999.
- Received High Diploma of Science in Applied Chemistry from the University of Aleppo, Aleppo, Syria in 2000/
- Joined King Fahd University of Petroleum and Minerals in January 2004.
- Present Address: Badee Str. Dammam City, Kingdum of Saudi Arabia.
- Permanent Address: Al Furqan Str. Aleppo City, Syria.
- E-mail: wadah.jawich@hotmail.com
- Mobile Phone: 00966509401117.
- Home Tel: 0096638303166.